Water Technology and Sciences

Included in Thomson Reuters Science Citation Index® (ISI) • Expanded Thomson Reuters Research Alert® (ISI) • EBSCO • ProQuest

Vol. V, No. 2, March-April, 2014

Water Technology and Sciences

Edit Board

Editorial coordination and careful editing: Helena Rivas-López • **Editorial assistance and editorial layout:** Luisa Guadalupe Ramírez-Martínez • **Figures design:** Luisa Guadalupe Ramírez-Martínez and Rosario Castro-Rivera • **Coordination arbitration:** Elizabeth Peña and Bibiana Bahena • **Proofreading English:** Ellen Weiss • **Logo design and cover:** Oscar Alonso-Barrón • **Design format:** Gema Alín Martínez-Ocampo • **Marketing:** Marco Antonio Bonilla-Rincón.

Editorial Committee

©***Water Technology and Sciences.*** Vol. V, No. 2, March-April, 2014, is a bimonthly publication edited by the Instituto Mexicano de Tecnología del Agua, Paseo Cuauhnáhuac 8532, Colonia Progreso, Jiutepec, Morelos, C.P. 62550, telephone +52 (777) 3 29 36 00, extension 474, www.imta.gob.mx/tyca, fsalinas@tlaloc.imta.mx. Responsible editor, Nahún Hamed García Villanueva; Copyright No. 04-2013-121014514100-203, granted by the Instituto Nacional de Derechos de Autor. ISSN pending. Responsible for the latest update of this issue: Sub-Department of Dissemination and Circulation, Francisco José Salinas Estrada, Paseo Cuauhnáhuac 8532, Colonia Progreso, Jiutepec, Morelos, C.P. 62550.

Water Technology and Sciences is the traslation of *Tecnología y Ciencias del Agua*, which is the continuation of the following journals: *Irrigación en México* (1930-1946); *Ingeniería hidráulica en México* (1947-1971); *Recursos hidráulicos* (1972-1978), and *Ingeniería hidráulica en México*, second period (1985-2009).

For subscriptions, click here

Water Technology and Sciences

Vol. V, No. 2, March-April, 2014

Coordination for editorial comments, click here give

Portada: Home: Water Quality Laboratory of the Institute Mexican Water Technology. Box, count aerobic mesophilic over medium SPC water sample the ECA7 bottled brand.

In recent years, the consumption of bottled water has increased considerably not only in quantity but in variety. Many people rely more on it than the tap water, among other reasons to come in a container closed; in in developing countries, consumption may be related to the lack of potable water in some populations. Given the lack of information in this field in Colombia, the article "Approaching the presence SPD and microorganisms in bottled water "Elisa C. Arevalo-Perez *et al*. (pp. 5-18) aimed to make a first approach to chemical and microbiological quality of Bottled water from THM content and AHA as SPD main chlorination generated, and the presence mesophilic microorganisms, enterobacteria, fungi and yeasts as indicators of microbiological quality. Furthermore, From these results, observe the relationship between SPD and microorganisms in bottled water.

Photos: Laboratory of Water Quality, Nayely Cortez Sánchez; inset, Elisa Arévalo y Juliana Martínez.

Water Quality Laboratory, Mexican Institute of Water Technology, Cuernavaca, Morelos, Mexico.

Photo: Nayely Cortez Sánchez.

Contents

Technical articles

Contenido

Artículos técnicos

Study of the Presence of DBP and Microorganisms in Bottled Water

• Elisa C. Arévalo-Pérez* • Aida J. Martínez-León • Mildred F. Lemus-Pérez •
• Manuel S. Rodríguez-Susa •
Universidad de los Andes, Colombia
*Corresponding Author

Abstract

ARÉVALO-PÉREZ, E.C., MARTÍNEZ-LEÓN, A.J., LEMUS-PÉREZ, M.F. & RODRÍGUEZ-SUSA, M.S. Study of the Presence of DBP and Microorganisms in Bottled Water. *Water Technology and Sciences* (in Spanish). Vol. V, No. 2, March-April, 2014, pp. 5-18.

Little information exists in the literature about the chemical quality of disinfection by-products (DBP) and their relationship with the microbiological quality of bottled water. Therefore, trihalomethanes (THM) and haloacetic acids (HAA) —the main DBP— were assessed in seven brands of bottled water available on the Colombian market. The presence of microbiological indicators, enterobacteria, mesophilic aerobes, fungi and yeast were also measured as microbiological indicators. Results showed maximum values of 135 for total THM and 140 μg/L for total HAA, and 28% of samples did not comply with FDA regulations. At least one microbiological indicator was found in 69% of samples and 30% did not comply with Colombian norms for drinking water. The association between DBP and microbiological quality varied. A recommended scenario of low DBP concentration and microorganisms was observed in two of the brands evaluated. Finally, more information is needed to analyze yeast as an indicator of organoleptic changes in water and its possible relationship with the proliferation of other types of microorganisms.

Keywords: Bottled water, disinfection byproducts, enterobacteria, fungi, mesophiles, yeast.

Resumen

ARÉVALO-PÉREZ, E.C., MARTÍNEZ-LEÓN, A.J., LEMUS-PÉREZ, M.F. & RODRÍGUEZ-SUSA, M.S. Aproximación a la presencia de SPD y microorganismos en agua embotellada. Tecnología y Ciencias del Agua. *Vol. V, núm. 2, marzo-abril de 2014, pp. 5-18.*

Poca información existe en la literatura acerca de la calidad química referente a subproductos de desinfección (SPD) y su relación con la microbiología del agua embotellada. Por tanto, se evaluó el contenido de trihalometanos (THM) y de ácidos haloacéticos (AHA) como principales SPD en siete marcas de agua embotellada del mercado colombiano, al igual que la presencia de indicadores microbiológicos, enterobacterias, aerobios mesófilos, hongos y levaduras. Los resultados mostraron valores máximos de 135 y 140 μg/l de THM y AHA totales, así como incumplimiento del 28% de la norma propuesta por la FDA. Se encontró la presencia de alguno de los indicadores microbiológicos en el 69% de las muestras e incumplimiento de la norma colombiana de agua potable en el 30%. La relación entre la cantidad de SPD y la calidad microbiológica fue diversa, observándose un escenario recomendable de baja concentración de SPD y microorganismos en dos de las marcas evaluadas. Finalmente, se requiere mayor información para analizar el efecto de la presencia de levaduras como indicador de cambios organolépticos en el agua y su posible relación con la proliferación de otro tipo de microorganismos.

***Palabras clave**: agua embotellada, subproductos de desinfección, enterobacterias, hongos, levaduras, mesófilos.*

Introduction

The consumption of bottled water has increased considerably over recent years, not only in quantity but also variety. Many people trust this water more than tap water, in part because it comes in a sealed container. In developing countries, its consumption may be related to the lack of drinking water for certain populations. By 2004, Columbia was 52 among 71 countries in per capita consumption of drinking water, with a total of 13.6 liters per year; Italy and Mexico were among the countries with the highest indices —184 and

169 liters per person per year (Gleick, 2006). In spite of its widespread consumption, little information exists about the presence of disinfection byproducts (DBP) such a trihalomethanes (THM) and haloacetic acids (HAA), as well as the microbiological quality of the product. Monitoring of drinking water supplied by distribution networks is regulated differently than bottled water since the latter is considered a food product (WHO, 2007). Thus, internationally, bottled water standards can be found only for THM in the case of the European Community, or for THM and HAA in Japan and the United States. In terms of microbiological quality, parameters that are controlled for drinking water are not required for bottled water —such as *Giardia* or *Cryptosporidium* (Graff *et al*., 2011). In addition, measurements are less frequent than for water supplied by a distribution network and there are fewer consequences resulting from a lack of compliance (Olson, 1999).

Bottled water is defined by the *Codex Alimentarius* Commission as water used to fill hermetically sealed containers, which is innocuous and suitable for immediate human consumption (WHO, 2001). Nevertheless, in Colombia not all the companies that sell this water comply with the norms and requirements, which leads to the possible presence of pathogens or high concentrations of other substances that present a risk to health. To decrease the concentrations of pathogenic microorganisms, chlorination or the use of ozone is permitted in accordance with the 1991 Resolution 12186. Nevertheless, these treatments can lead to the generation of DBP (INVIMA, 1991). According to the World Health Organization (WHO, 2008), the most common byproducts are THM and HAA, halogenated acetonitriles and chlorinated phenols, of which THM and HAA are the primary groups found in chlorinated water.

THM and HAA are formed when organic matter reacts with free residual chlorine present in the water. According to Garrido (2003), the speed of formation and final concentration of these compounds depend on factors such as temperature, pH, residual chlorine concentration, the organic precursors present, concentration of bromine in the water and contact time with chlorine. The general formula for THM is CHX3, where X can be any halogen, or the combination of several. Generally, it refers only to chlorine or bromine compounds —mainly chloroform (CF), bromodichloromethane (BDCM), dibromochloromethane (DBCM) and bromoform (BF)— which compose what is known as total THM (TTHM), which are regulated because of their association with effects due to chronic exposure. Because of their volatility, it is presumed that most of the THM are transferred to the air (WHO, 2008). Meanwhile, HAA are weak acids, non-polar and are less stable than the THM in the network. Therefore, their concentration at the ends of the system tends to be less, even though they are less volatile. Compounds with more prevalence in the distribution networks are chloride monochloroacetic acids (MCAA), dichloroacetic acids (DCAA) and trichloroacetic acids (TCAA), of which TCAA has the highest concentrations due to increased free chlorine (Duarte, 2011). As with THM, because of their impact on health there are 5 HAA that are regulated by the United States Environmental Protection Agency (EPA): MCAA, DCAA, TCAA, monobromoacetic acid (MBAA) and dibromoacetic acid (DBAA).

Chronic exposure to treated water with high concentrations of DBP —such as THM and HAA, nitrosamines, furanones–has been associated with problems related to embryonic development as well as liver, bladder, kidney and colon cancers, according to toxicological trials and epidemiological evi-

dence (Villanueva *et al*., 2004; Richardson *et al*., 2007; Nieuwenhuijsen *et al*., 2009). The International Agency for Research on Cancer (IARC) has classified different compounds according to their carcinogenic potential in humans. CF, BDCM and DCAA are classified as group 2B, as possibly carcinogenic for humans since there is sufficient evidence in animals but not in humans. On the other hand, BF, DBCM and TCAA are in group 3, which is not classified as carcinogenic for humans because of the limited evidence from animal experiments. MCAA has not been classified by IARC and, therefore, is not considered a carcinogenic risk to humans. The EPA (2003) suggests that a potential relationship exists between the DBP present in chlorinated water and colon, rectum and bladder cancer, which has been analyzed by epidemiological trails, with statistically significant results for colon cancer (Villanueva *et al*., 2004), rectum cancer (Hildesheim *et al*., 1998) and some evidence between exposure to DBP and the development of bladder cancer (Koivusalo *et al*., 1998).

Due to the possible effects on the health of consumers, several studies have been carried out internationally to determined the concentrations of DBP in bottled water. Ikem (2010) evaluated the contents of volatile organic compounds, including THM, in different types of drinking water, finding that in all the samples of bottled water (19 brands, including flavored water), CF, BDCM, DBCM and BF were lower than the maximum concentration allowable by the United States Food and Drug Administration (FDA) of 80 μg/L for TTHM. In Egypt, Saleh *et al.* (2001) analyzed the concentration of CF, BDCM and DBCM in five brands of bottled water available on the market. Concentrations of these three compounds were found to be lower than the guidelines established by WHO in one brand, and in another brand only concentrations of CF and DBCM were observed to be lower than those reported for the former brand. In addition, Leivadara *et al*. (2008), in Greece, and Al-Mudhaf *et al*. (2009) in Kuwait evaluated 13 and 71 brands of bottled water, respectively, showing the presence of THM and HAA in concentrations lower than the maximum limit established by the FDA (80 μg/L for TTHM and 60 μg/L for total HAA). The presence of HAA in bottled water was also analyzed in Beijing by Liu and Mou (2004), in which 5 of the 10 brands of water were found to have DCAA concentrations between 0.4 and 0.6 μg/L, while MCAA and TCAA were not detected in any of the samples.

On the other hand, reducing the concentration of disinfectants to control the presence of DBP can lead to renewed growth of microorganisms in bottled water, where storage time can be relevant to their proliferation. Based on the microbiological characterization conducted by Varga (2011) of bottled water in Hungary, with indicators such as *Clostridium*, total chloroform, *E. coli*, *Enterococcus* spp. and *Pseudomonas aeruginosa*, positive results for at least one of the indicators were observed in 5.3% of the carbonated water and 10.2% of the non-carbonated water evaluated. Fungi have also been isolated in bottled mineral water on the Argentine market in 33% of samples that complied with regulations for total chloroform, *E. coli, Enterococcus* spp. and *Pseudomonas aeruginosa* (Cabral and Fernández-Pinto, 2002).

In Colombia, few studies have been conducted on the quality of bottled water. In Sincelejo, Vidal *et al.* (2009) analyzed the microbiological quality of water in bags distributed in that city, and although the study mentions the formation of THM in tap water, its presence in bottled water was not evaluated. The lack of this information is connected to the 1991 Resolution 12186 which does not establish limits for DBP.

Meanwhile, the maximum concentration of TTHM in water distribution networks has been set at 0.2 mg/L, while no concentration limit exists for HAA (MAVDT, 2007). In terms of microbiological quality, Resolution 12186 sets maximum values for total and fecal coliforms and *Pseudomonas aeruginosa* at 2 MPN/100 mL, and for drinking water, at 0 UFC/100 mL for total coliforms and 100 UFC/100 mL for mesophilic microorganisms (MAVDT, 2007). The presence of fungi was not found to be regulated, nevertheless they are important from a health perspective since many of these organisms can cause infectious diseases and irritation of the mucous membranes, which are particularly harmful to persons with immune deficiencies. In addition, although yeasts do not have an effect on the health of the exposed population, they can cause organoleptic changes in the water and generate an environment conducive to the growth of other organisms by changing the pH (Ancasi *et al*., 2006).

Given the lack of information in this field in this country, the objective of the present work was to conduct a preliminary study of the chemical and microbiological quality of bottled water in terms of THM and HAA contents —the main DBP generated by chlorination— and the presence of mesophilic microorganisms, enterobacteria, fungi and yeasts as indicators of microbiological quality. In addition, the relationship was observed between DBP and the microorganisms present in bottled water, according to these results.

Materials and Methods

Sampling

Samples from seven brands of bottled water available on the Colombian market were collected at different points of sale chosen at random. Three belonged to two large drinks companies, two were brands belonging to large hypermarkets, one belonged to a known national store and one was a brand with little market share. The main reason for conducting the study with these samples was the high consumption of the first six brands, where the last brand was used to compare quality with the large companies.

Table 1 shows some of the characteristics of the samples collected. All the labels, with the exception of the first, indicated "treated drinking water." The treatment process before bottling the water for each brand was not known, since this information is restricted by the manufacturers. With the exception of the ECA1 brand, two samples were used from different lots —one for each DBP group (*i.e.* THM and HAA), since the analysis was not conducted in parallel and preservation did not allow for using the same sample.

Analysis of THM

To quantify the THM, the samples were transferred to a 250 mL glass amber container, to which 25 mg of sodium **thiosulfate pentahydrate** were added (Sharlau®, Spain) to obtain a final concentration of 100 mg/L to eliminate residual chlorine, up to a concentration of 15 mg/L, in order to prevent the additional formation of THM when analyzing the samples (USEPA, 1981). The containers were completely filled and covered with aluminum foil to prevent the reaction of THM with oxygen or light. The samples were kept covered and refrigerated until analysis. The analysis was repeated with 5 of the 7 samples.

Solid phase microextraction (SPME) was conducted after gas chromatography with electron capture detector using the reference method ASTM D 6520-06 (2006), USEPA 551-1 (1995), with a Hewlett Packard® (GC) 5890 Series II chromatograph (United States).

Table 1. Type, Expiration Date and Bottling of the Samples of Bottle Water Analyzed.

Sample		Type		Expiration date	Packaging	Net Contents
ECA1	T	PSW	FS	14/08/2012	PET	500 ml
	H			14/08/2012		
ECA2	T	TDW	DP	15/02/2012	PET	600 ml
	H			10/03/2012		
ECA3	T	TDW	DP	12/02/2012	PET	600 ml
	H			04/03/2012		
ECA4	T	TDW	DP	31/01/2012	PET	600 ml
	H			12/02/2012		
ECA5	T	TDW	LB	30/02/2012	PET	600 ml
	H			19/03/2012		
ECA6	T	TDW	SC	05/12/2011	PET	600 ml
	H			15/01/2012		
ECA7	T	TDW	SC	11/02/2012	PET	600 ml
	H			06/03/2012		

PSW: pure spring water; TDW: treated drinking water; FS: food store; DP: drink producer; SC: Storage chain; LB: little known brand; T: sample used to analyze THM; H: sample used to analyze HAA.

Table 2. Operating Conditions for THM and HAA Detection Methods.

Parámetro	THM Condition	HAA Condition
Columna	HP-5	HP-5
Injection	Splitless	Splitless
Gas Carrier	Nitrogen	Nitrogen
Gas *Make up*	Helium	Helium
Temperature ramping	40 °C (2 min) to 50 °C @ 3 °C/min (10 min); 50 °C to 75 °C @ 8 °C/min (10 min); 75 °C to 250 °C @ 10 °C/min (0 min)	40 °C (2 min) to 50 °C @ 3 °C/min (10 min); 50 °C to 75 °C @ 5 °C/min (10 min); 75 °C to 250 °C @ 8 °C/min (8 min)
Injector temperature	250 ºC	250 ºC
Detector temperature	300 ºC	250 ºC

The operating conditions for the methods are shown in Table 2. Microextraction was performed as follows: 3 grams of NaCl (analytic grade, Merck®, United States) were added to a graphable vial (30% p/v of the sample); 10 mL of the bottled water sample were added to the vial; the pH was adjusted to 2 with 0.5M H_2SO_4 (analytic grade, CarloErba®, France) and the closed vial was submerged in an oil bath at 50° C for 20 minutes; the fiber was then exposed for 10 minutes, followed by exposure in the injection port of the chromatograph.

Analysis of HAA

SPME with head-space was used to measure HAA, which consisted of derivatization of the acids into their respective esters to reduce their boiling point and thereby enable recuperation by adsorption with a 75 µm carboxen/polydimethylsiloxane

(CAR-PDMS) fiber for exposure in the gas chromatograph. The Agilent Technologies® 7890A GC System (United States) was used (See Table 2 for conditions). The procedure was quantified based on the proposal by Perez (2010) as described as follows. In a 30 mL glass amber jar, 2.25 mL of H_2SO_4 and sodium sulphate (Na_2SO_4, JTBaker®, United States) in a 40% p/v proportion were added to a 10 mL sample of bottled water. The salt was dissolved and 30% v/v of HPLC grade methanol (3 mL) (Panreac®, Spain) added to perform the derivatization of HAA. The closed jar was submerged in mineral oil bath at a temperature of 55° C, immediately exposing the fiber for 15 minutes with constant agitation at 750 rpm, retracting and exposing in the injection port, and immediately initiating the run. The bottled water samples were kept sealed and refrigerated until analysis.

The detection and quantification limits were 0.5 and 1 µg/L for chloroform (CF), bromodichloromethane (BDCM), dibromochloromethane (DBCM), bromoform (BF) and trichloroacetic acid (TCAA), and 1.5 and 3 µg/L for monochloroacetic acid (MCAA) and dichloroacetic acid (DCAA).

Microorganism Cultures

Three culture media were used to isolate the microorganisms: agar (SPC) plate count Agar (Oxoid®, England); Eosin Methylene Blue agar (EMB) (Sharlau®, Spain); and Potato Dextrose agar (PDA) (Pronadisa®, Spain). Agar (SPC) is a non-selective media used to count and detect mesophilic aerobic microorganisms (ICMSF, 1978). Plate count agar is a selective and differential medium used to isolate gram-negative bacilli which enables the development of species of the *Enterobacteriaceae* family. It is used to confirm total coliforms (Oranusi *et al.*, 2003; Ngwai *et al.*, 2010) and its use has also been reported for *E. coli* recount in bottled water (Ramalho *et al.*, 2001). PDA is one of the most commonly used media for growing fungi and yeast (Hurtado, 2011). Plate count was the technique used for all three cases. Negative controls without inoculation were applied for isolation in all media.

The samples used to analyze THM as well as those used to analyze HAA were cultured in the three media. Bottom seeding of 0.1 mL of the samples was performed and they were incubated at a temperature of 37° C for 36 hours for the first two media. For PDA, the samples were seeded at the surface and incubated at a temperature of 25 °C for six days. The count was based on SPC and PDA total counts with EMB differential (coliforms (lactose positive fermentation) presenting as purple or black colonies). Although the EMB count was conducted only for coliform colonies, the results were reported as enterobacteria since the presumptive test (MPN count) and membrane filtration were not conducted (FDA, 2002).

Results and Discussion

Chloroform was found in all brands except the first, in a range of 1.8 to 132.8 µg/L. While the concentration of chloroform in bottled water is not regulated (Table 2), 2 brands exceeded the FDA norm for TTHM. Bromodichloromethane was found to be above the quantification limit (1 µg/L) in only 4 brands, while the other two compounds — dibromochloromethane and bromoform— were below the detection limit (0.5 µg/L). In terms of HAA, MCAA was found in 3 of the brands (between 3 and 7.1 µg/L) while the other two acids were detected in 4 of the 7 brands (5.6 and 73 µg/L). TCAA had the highest concentrations, between 9 and 73 µg/L. Unlike the THM, no significant concentrations of any acid were quantified in 3 brands (Figure 1).

Table 3. International Standards for Drinking and Bottled Water.

Parameter (µg/l)	WHO (DW)	Japan (DW)	Australia (DW)	ICBWA (BW)	US (BW)	Colombia (DW)	Argentina (BW)	South Africa (BW)	EC (BW)	UK (BW)
MCAA	20	20	150	-	-	-	-	-	-	-
DCAA	50	40	100	50	-	-	-	-	-	-
TCCA	200	200	100	100	-	-	-	-	-	-
HAA5	-	-	-	-	60	-	-	-	-	-
BDCM	60	30	-	60	-	-	-	-	-	-
BF	100	90	-	100	-	-	-	-	-	-
DCM	100	100	-	100	-	-	-	-	-	-
CF	300	60	-	200	-	-	-	-	-	-
TTHM	-	100	250	-	80	200	100	200	100	100

ICBWA: International Council of Bottled Water Associations; US; United States; EC: European Community; UK: United Kingdom; DW: normal for drinking water; BW: normal for bottled water.

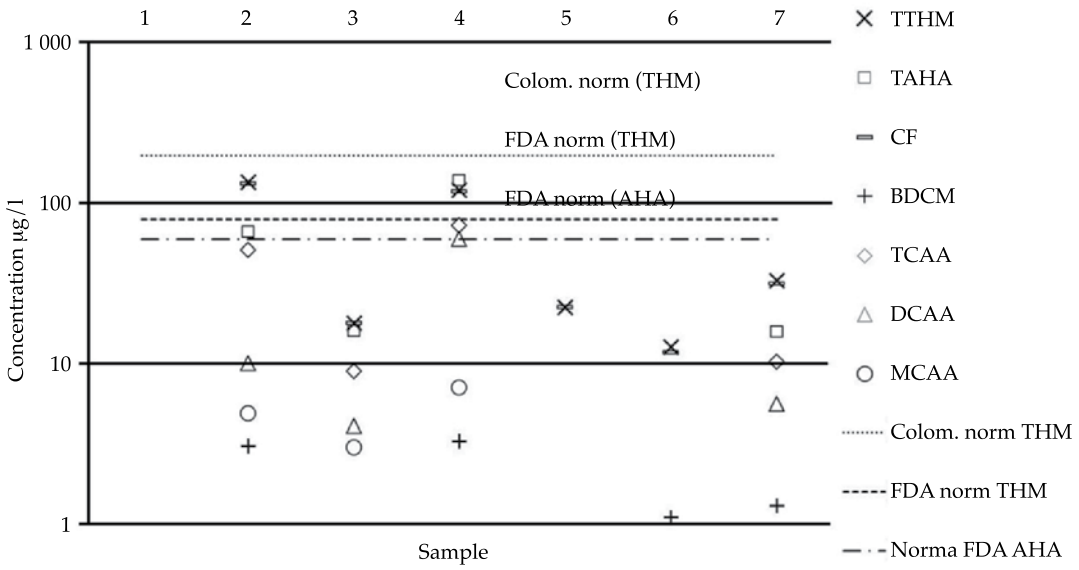

Figure 1. THM and HAA Contents in Bottled Water in Relation to Colombian Norms for Drinking Water and FDA Regulations for Bottled Water.

Furthermore, the microorganism cultures also provided important results. Of the 7 brands studied, only 2 did not present growth in bacteria, enterobacteria or mesophiles (ECA6 and ECA4). There were growth of mesophilic aerobes in 3 (ECA1, ECA5, ECA7) and brands ECA5 and ECA7 were found to have growth of both mesophilic aerobic microorganisms and enterobacteria. None of the samples presented colonies with metallic sheen typical of *E. coli*. In the case of fungi and yeast, only brand ECA5 showed no

growth (Figures 2 and 3), 3 brands presented growth of yeast and another 3 presented growth of fungi.

The analysis of the data showed that brands ECA2 and ECA4 had the highest DBP contents, with TTHM concentrations of 135.9 µg/L and 122.2 µg/L, respectively, and HAA concentrations of 66.9 µg/L for brand ECA2 and 140.4 µg/L for brand ECA4. This may be due to the re-chlorination of drinking water to ensure a residual concentration between the 0.5 and 1 mg/L as required by the 1991 Resolution 12186, and the presence of natural organic matter in the process. In general, the

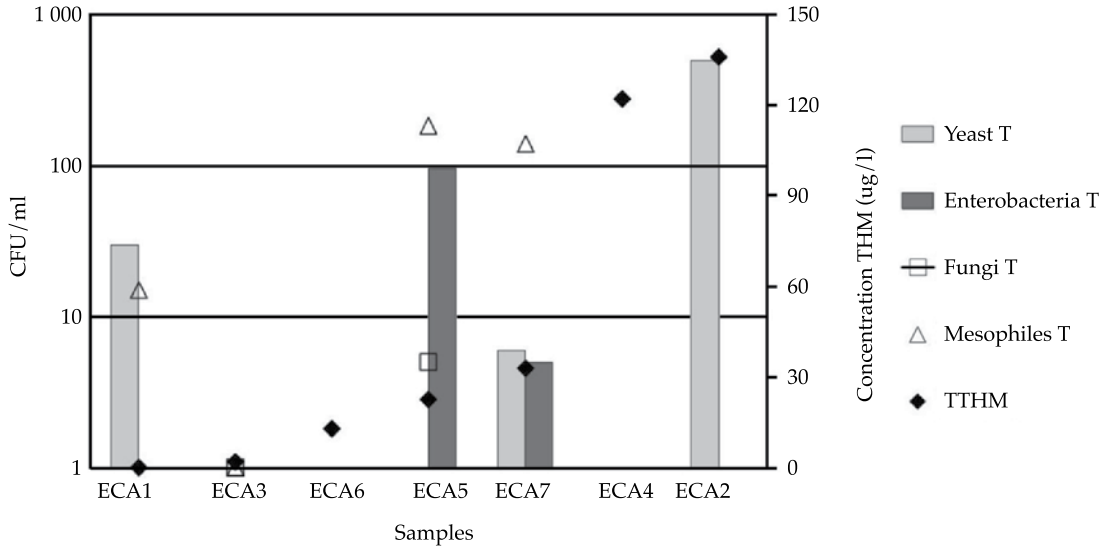

Figure 2. Relationship Between THM Contents in Bottled Water and the Presence of Mesophiles, Enterobacteria, Fungi and Yeast.

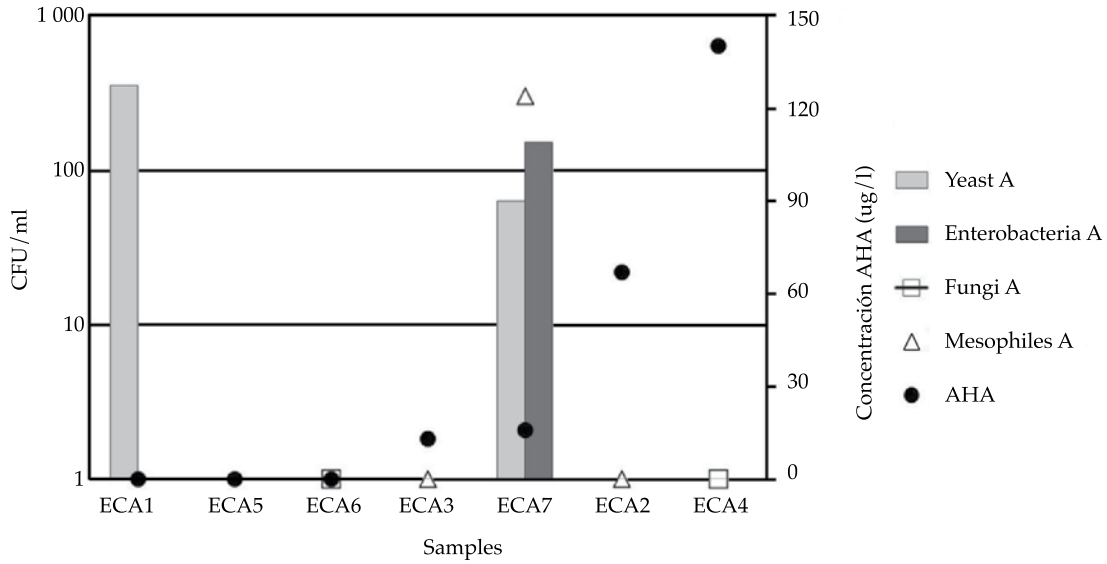

Figure 3. Relationship between HAA Contents in Bottled Water and the Presence of Mesophiles, Enterobacteria, Fungi and Yeast.

compounds that were predominant were chloroform and TCAA, similar to drinking water networks, in which chloroform values can be as high as 95% of TTHM (Gang *et al*., 2003) and TCAA is 49 to 66% of regulated total HAA (Uyak *et al*., 2007). The concentration of chloroform was greater than that of TCAA in 5 of the 7 samples, possibly because of its abiotic transformation in the water (which has been studied by Xiang *et al*. (2005), among others) or due to the differential effect of chlorine on THM and HAA (Rodriguez *et al*., 2004).

Figure 1 shows that the results for THM comply with the 2007 Resolution 2115, in which the maximum allowable limit is 200 μg/L; nevertheless, 2 of the brands analyzed —ECA2 and ECA4— do not comply with the United States norm of 80 μg/L. The same is true for HAA. And while Colombian regulations do not establish maximum allowable limits, these 2 samples do not comply with United States norms of 60 μg/L, which are the most restrictive internationally, as can be seen in Table 3 which presents the standards for DBP in drinking and bottled water for different countries.

Although it is not possible to find a correspondence between the THM and HAA concentrations found, since they were evaluated in different samples, the THM/HAA ratio in brands 2 and 7 were in the same range (2.04 and 2.14). In addition, THM and HAA concentrations were found to be similar in the same brand (ECA4 and ECA7), a trend that could be associated with the maintenance of factors that affect the formation of these byproducts —such as organic matter and the disinfectant dosage— during each of the production processes. Also important to take into account is the stability of components, which is greater for THM than for HAA (Rodriguez *et al*., 2004), which can be biodegraded by microorganisms found in the drinking water networks (Pérez, 2010).

Even though these samples comply with Colombian legislation, because this is lower than international limits consumers may be exposed to significant levels of chloroform, BDCM, DCAA and TCAA, primarily. Chloroform, BDCM and DCAA are considered to be possible carcinogens according to results found in animal studies, while there is not enough evidence related to TCAA. Furthermore, high concentrations of chloroform, the primary component in THM, can have depressing effects on the central nervous system as well as toxic effects on the kidney and liver, as was observed in beagle dogs exposed to doses of 15 mg per kg body weight (WHO, 2004). In addition, chloroform is metabolically activated, forming phosgene, where toxicity begins when reacting with macromolecules (Fang *et al*., 2008). BDCM can interfere in gonadotropic hormone activity which is vital to embryonic development. Chloroacetic acids (MCAA, DCAA, TCAA) also can create developmental problems because of the production of free radicals during their metabolism, which act on the cellular lipid membrane (Nieuwenhuijsen *et al*., 2009).

Figures 2 and 3 show the concentrations of the DBP evaluated and the presence of microbiological indicators in the 7 brands of bottled water, in which a relationship is observed. Based on the results, four scenarios were identified: high concentration of DBP, low presence of microorganisms (MO); medium concentration of DBP, high presence of MO; low concentration of DBP, low presence of MO; absence of DBP and high presence of MO. In the first case, low growth of bacteria and fungi in brands ECA4 and ECA2 is an indicator of the use of high concentrations of chlorine in the disinfection process. Nevertheless, a more in-depth study that takes into account this aspect would be needed in order to corroborate the results. In the second group, the largest growth of enterobacteria and mesophile aerobes

was produced in brand ECA7, which were detected in the sample used to analyze HAA as well as the one used to analyze THM and for which medium concentrations (33.1 and 15.9 μg/L) of these DBP were reported. This would indicate that re-chlorination of treated water may not have occurred and that natural organic matter and the DBP from the network could have been a source of carbon for these microorganisms. Also observed in the brand was a high growth of yeast due to conditions favorable to its proliferation in water with low disinfectant contents and assimilable organic matter. In the third scenario, for samples of brands ECA3 and ECA6, low growth in microorganisms was identified —1 UFC/mL and zero, respectively— as well as the lowest concentrations of THM and HAA (1.8 and 13 μg/L in ECA3; and 13 μg/L and not detectable in ECA6). This suggests that the disinfection process used adequate dosages, or that it was performed using techniques other than classic chlorination, that low contents of natural organic matter existed in drinking water and/or an organic matter removal system was used before disinfection, such as activated carbon, which in turn reduces the concentration of DBP from the network. For the fourth group, which includes the mineral water sample, the absence of these DBP would indicate that disinfection with chlorine was not used or the dosages were very low, in which case the lack of residual action would favor the presence of microorganisms such as yeast and mesophiles. Controls of treatment and packaging processes must ensure a quality similar to that of scenario three, with low contents of DBP and microorganisms.

In addition, Figures 2 and 3 make it possible to identify relationships among the growth of different microorganisms. First, it is important to mention that enterobacteria are found among mesophilic organisms, which is consistent with that observed in Figures 2 and 3. In sample ECA5, most of the mesophilic organisms were enterobacteria, and there was growth of these microorganisms in ECA7, but in lesser proportions. This result is similar to that shown in Figure 3, in which most of the mesophiles contained in ECA7 corresponded to enterobacteria.

As in other studies of bottled water, no relationship was observed between the presence of yeast and other indicators of contamination (Yamaguchi *et al*., 2007). On the other hand, yeasts can be an indicator of a change in the characteristics of the medium, which could lead to the appearance of other microorganisms and, eventually, the disappearance of yeasts due to less competition. Therefore, a second relationship could be considered in terms of the behavior of the yeasts seen in Figure 2. In the samples of bottled water analyzed, differences in the presence of yeasts were identified, which could be associated not only with the concentration of disinfectant but also with the proliferation phase of the microorganisms during which the recount was performed. This corresponds to the first phase in sample ECA2, in which there was a large amount of yeasts and no mesophiles, indicating a possible change in the characteristics of the water, but not as needed for the growth of these microorganisms. Sample ECA1 would indicate the next state, with less yeasts and the appearance of mesophiles. A more advanced state would correspond to ECA7, which presented a growth of yeast, although to a lesser degree, and a higher recount of mesophiles along with the appearance of enterobacteria. Finally, in sample ECA5 there was no evidence of yeast growth while there was evidence of mesophile growth —specifically, enterobacteria— which had the highest concentration of all the samples and could indicate evidence of the absence of yeast due to competition. Figure 3 also shows this trend in samples

ECA1 and ECA7. In addition, other studies have observed the effect of storage time on the release of phthalates —additives in PET— which would serve as substrates for fungi spores such as *Penicillium citrinum* and *Alternaria alternata* (Criado *et al.*, 2005). This indicates that the time between bottling and consumption can modify bacteria diversity. An indicator of the first states could be useful to determine whether conditions exist that lead to proliferation of other regulated microorganisms during storage, such as coliforms which are included in enterobacteria. More information is needed about the relationships among microbiological indicators.

When comparing the results obtained with the Colombian norms for mesophilic microorganisms (100 UFC/100 mL for drinking water) it was determined that brands ECA2, ECA3, ECA4 and ECA6 fully complied with the maximum limits. One sample from brand ECA1 exceeded the maximum value for mesophile aerobes. For brand ECA5, the sample used for HAA was within the regulations, while the sample used for THM presented growth of mesophilic aerobes above the maximum value. None of the samples from brand ECA7 complied with the maximum allowable limits. Brands ECA5 and ECA7 may not have complied with the limit of 0 UFC/100 mL for total coliforms according to the recount of enterobacteria in the EMB medium. Meanwhile, brands ECA1, ECA2, ECA5 and ECA7 did not present fungi growth and the recount of samples ECA3, ECA4 and ECA6 resulted in 1 UFC/mL.

The data observed suggest that microbiological quality can vary among samples obtained from the same process (brands ECA2, ECA3 and ECA5) but from different lots. Therefore, it is important to enforce Resolution 12186, which indicates that 5 samples per lot must be analyzed (3 for microbiological quality, 2 for physiochemical quality and 1 additional counter sample). Compliance with the norm for mesophiles in samples ECA3, ECA4 and ECA6 would not indicate microbiological safety since the presence of certain unregulated fungi —such as *A. alternata* and *P. citrinum* which have been isolated in bottled water— can generate mycotoxins (Criado *et al.*, 2005). Significant differences exist in the microbiological quality between the popular brands and the brand most recently introduced on the market; the latter was positive for three of the four indicators and, therefore, more restrictive controls should be placed on new products.

Since this study provides important results concerning the quality of bottled water and its possible effect on human health, the continuation of this research is critical, including more in-depth and detailed studies with a larger number of samples, an analysis of chlorine contents and a more specific microbiological analysis. Another key factor to consider is legislation. Compliance with norms by the majority of bottled water companies needs to be evaluated in order to justify and enforce a more restrictive DBP guideline since, as can be observed, Colombia has one of the most lax norms on this subject.

Conclusions

The results obtained identified high concentrations of THM and HAA in two of the most common brands of bottled water which, along with regulations that do not limit the presence of DBP in Colombia, constitutes a potential risk to the health of consumers. This study determined that the water in these brands have low growth of microorganisms which could be related to the use of high concentrations of chlorine as a disinfection mechanism. All of the other samples had concentrations of TTHM and

HAA below the limits required by United States norms. In terms of microbiological quality, 2 of the brands with medium concentrations of DBP presented growth of enterobacteria, in addition to a high recount of mesophile aerobes, which could suggest the use of low concentrations of chlorine, with which adequate disinfection is not possible. In the other brands, low concentrations of DBP and weak growth of microorganisms was found, which could be due to the use of alternative disinfection mechanisms and/or the removal of natural organic matter. With regard to mesophiles, 3 brands did not comply with drinking water standards. Lastly, it was found that the presence of yeast can act as an indicator of the possible generation of mesophile microorganisms, enterobacteria and probably total coliforms.

Acknowledgements

This project was financed by the Department of Civil and Environmental Engineering and the Environmental Engineering Research Center of the University of the Andes. The authors would like to particularly thank the team of professionals at the Environmental Engineering Laboratories of the University of the Andes.

Received: 16/01/2013
Accepted: 31/05/2013

References

AL-MUDHAF, H. and ALSHARIFI F ABU-SHADY, A. A survey of organic contaminants in household and bottled drinking waters in Kuwait. *Sci. Total Environ*. Vol. 407, 2009, pp. 1658-1668.

ANCASI, E., CARRILLO, L. y BENÍTEZ, M. Mohos y levaduras en agua embotellada y bebidas sin alcohol. *Rev. Argent. Microbiol*. Vol. 38, 2006, pp. 93-96.

ASTM. *Standard Practice for the Solid Phase Microextraction (SPME) of Water and its Headspace for the Analysis of Volatile and Semi-Volatile Organic Compounds*. D 6520-06. Pennsylvania, USA: American Society for Testing and Materials International, 2006, 6 pp.

CABRAL, D. and FERNÁNDEZ-PINTO, V.E. Fungal spoilage of bottled mineral water. *Int. J. Food Microbiol*. Vol. 72, 2002, pp. 73-76.

CRIADO, M.V., FERNÁNDEZ-PINTO, V.E., BADESSARI. A., and CABRAL, D. Conditions that regulate the growth of moulds inoculated into bottled mineral water. *Int. J. Food Microbiol*. Vol. 99, 2005, pp. 343-349.

DUARTE, C. *Formación química de ácidos haloacéticos (AHAs) a partir de la reacción de las fracciones hidrófila e hidrófoba de la materia orgánica natural (MON) del agua cruda.* Tesis de Maestría en Ingeniería Civil. Bogotá: Universidad de los Andes, 2011, 52 pp.

FANG, C., BEHR, M., XIE, F., LU, S., DORET, M., LUO, H., YANG, W., ALDOUS, K., DING, X., and GU, J. Mechanism of chloroform-induced renal toxicity: Non-involvement of hepatic cytochrome P450-dependent metabolism. *Toxicol. Appl. Pharmacol*. Vol. 227, 2008, pp. 48-55.

FDA. *Bacteriological Analytical Manual Online. Chapter 4: Escherichia coli and the Coliform Bacteria.* Feng, P., Weagant, S.D., Michael, A., Grant, M.A., and Burkhardt, W (editors). Online: 2002 [citado el 24 de mayo de 2013]. Disponible para *World Wide Web*: http://www.fda.gov/Food/FoodScienceResearch/LaboratoryMethods/ucm064948.htm.

GANG, D., CLEVENGER, T.E., and BANERJI, S.K. Relationship of chlorine decay and THMs formation to MON size. *J. Hazard Mater.* Vol. A96, 2003, pp. 1-12.

GARRIDO, S.E. Consideraciones sobre los subproductos de la desinfección. En: *Agua potable para comunidades rurales, reuso y tratamientos avanzados de aguas residuales domésticas*. Delgado, C.D., Fall, C., Quentin, E., Jiménez, M.C., Esteller, M.V., Garrido, S.E., López, C.M. y García, D. (editores). México, D.F.: Red Iberoamericana de Potabilización y Depuración del Agua, CYTED Press, 2003, pp. 172-174.

GLEICK, P.H. Per capita bottled water consumption by country 1999 to 2004. In: *The World's Water 2006-2007*. Cooley, H., Katz, D, Lee E., Morrison, J., and Palaniappan, M. (editors). Washington, D.C.: Island Press, 2006, pp. 284-286.

GRAFF, J., NEIDELL, M., and SCHLENKER, W. Water quality violations and avoidance behavior: evidence from bottled water consumption. *Americ Economic Rev.: Papers Proceed.* Vol. 101, 2011, pp. 448-453.

HILDESHEIM, M.E., CANTOR, K.P., LYNCH, C.F., DOSEMECI, M., LUBIN, J., ALAVANJA, M., and CRAUN, G.F. Drinking water source and chlorination byproducts: risk of colon and rectal cancers. *Epidemiology*. Vol. 9, 1998, pp 29-35.

HURTADO, S. *Caracterización de la diversidad de los hongos presentes en las biopelículas de las redes de distribución de agua potable en la ciudad de Bogotá.* Tesis de Grado en Ingeniería Ambiental. Bogotá: Universidad de los Andes, 2011, 125 pp.

ICMSF. *Microorganisms in Foods. I. Their Significance and Methods of Enumeration*. Second edition. Toronto, Canada: University of Toronto Press, 1978, 452 pp.

IKEM, A. Measurement of volatile organic compounds in bottled and tap waters by purge and trap GC–MS: Are

drinking water types different? *J. Food Composition Anal.* Vol. 23, 2010, pp. 70-77.

INVIMA. *Resolución 12186 de 1991. Por la cual se fijan las condiciones para los procesos de obtención, envasado y comercialización de agua potable tratada con destino al consumo humano.* Bogotá, D.C.: Instituto Nacional de Vigilancia de Medicamentos y Alimentos, 1991, 7 pp.

KOIVUSALO, M., HAKULINEN, T,. VARTIAINEN, T., PUKKALA, E., JAAKKOLA, J.J.K., and TUOMIST, J. Drinking water mutagenicity and urinary tract cancers: a population-based case-control study in Finland. *Amer. J. Epidemiol.* Vol. 148, 1998, pp. 704-712.

LEIVADARA, S., NIKOLAOU, A., and LEKKAS, T. Determination of organic compounds in bottled waters. *Food Chem.* Vol. 108, 2008, pp. 277-286.

LIU, Y. and MOU, S. Determination of bromate and chlorinated haloacetic acids in bottled drinking water with chromatographic methods. *Chemosphere.* Vol. 55, 2004, pp. 1253-1258.

MAVDT. *Resolución 2115 de 2007. Por medio de la cual se señalan las características, instrumentos básicos y frecuencias del sistema de control y vigilancia para la calidad del agua para consumo humano*. Bogotá D.C.: Ministerio de Ambiente, Vivienda y Desarrollo Territorial, 2007, 32 pp.

NGWAI, Y.B., SOUNYO, A.A., FIABEMA, S.M., AGADAH, G.A., and IBEAKUZIE, T.O. Bacteriological safety of plastic-bagged sachet drinking water sold in Amassoma, Nigeria. *Asian Pacific J. Tropic Med.* Vol. 3, 2010, pp. 555-559.

NIEUWENHUIJSEN, M.J., GRELLIER, J., SMITH, R., ISZATT, N., BENNETT, J., BEST, N., and TOLEDANO, M. The epidemiology and possible mechanisms of disinfection by-products in drinking water. *Philos. Trans. R. Soc. A*. Vol. 367, 2009, pp. 4043-4076.

OLSON, E. (editor). *Bottled water: Pure drink or pure hype?* Report In: Natural Resources Defense Council. (Online): 1999 [citado el 10 de septiembre de 2011]. Disponible para *World Wide Web*: http://www.nrdc.org/water/drinking/bw/chap4.asp#table6.

OMS. Organización Mundial de la Salud (editor), 2008. *Guidelines for Drinking-Water Quality*. WHO Press. (Online) [citado el 10 de septiembre de 2011]. Disponible para *World Wide Web*: http://www.who.int/water_sanitation_health/dwq/fulltext.pdf, pp. 179-180.

OMS. *Codex Alimentarius. Waters*. Rome: FAO/WHO, 2007, pp 16.

OMS. *Trihalomethanes in drinking-water: background document for development of WHO guidelines for drinking-water quality* HO/SDE/WSH/03.04/64. Ginebra, Suiza: Organización Mundial de la Salud, 2004, 49 pp.

OMS. *Codex Alimentarius. Código de prácticas de higiene para las aguas potables embotelladas distintas de las aguas minerales naturales ALINORM 01/20*. Ginebra. Suiza.: Organización Mundial de la Salud, 2001, 31 pp.

ORANUSI, S.U., UMOH, V.J., and KWAGA, J.K.P. Hazards and critical control points of kunun-zaki, a non-alcoholic beverage in Northern Nigeria. *Food Microbiol.* Vol. 20, 2003, pp. 127-132.

PÉREZ, A. *Degradación de ácidos haloacéticos (AHA) clorados por medio de microorganismos presentes en biopelículas de redes de distribución de agua potable*. Tesis de Maestría en Ingeniería Civil. Bogotá: Universidad de los Andes, 2010, 38 pp.

RAMALHO, R., AFONSO, A., CUNHA, J., TEIXEIRA, P., and GIBBS, P.A. Survival characteristics of pathogens inoculated into bottled mineral water. *Food Control*. Vol. 12, 2001, pp. 311-316.

RICHARDSON, S.D., PLEWA, M.J., WAGNER, E.D., SCHOENY, R., and DEMARINI, D.M. Occurrence, genotoxicity, and carcinogenicity of regulated and emerging disinfection by-products in drinking water: A review and roadmap for research. *Mutat. Res.* Vol. 636, 2007, pp. 178-242.

RODRIGUEZ, M.J., SÉRODES, J.B., and LEVALLOIS, P. Behavior of trihalomethanes and haloacetic acids in a drinking water distribution system. *Water Res.* Vol. 38, 2004, pp. 4367-4382.

SALEH, M., EWANE, E., JONES, J., and WILSON, B. Chemical evaluation of commercial bottled drinking water from Egypt. *J. Food Composition Anal.* Vol. 14, 2001, pp. 127-152.

USEPA. *Treatment Techniques for Controlling Trihalomethanes in Drinking Water, EPA/600/2-81/156*. Washington, D.C.: US Environmental Protection Agency, 1981, 302 pp.

USEPA. *Method 551.1. Determination of chlorination disinfection by-products, chlorinated solvents, and halogenated pesticides/herbicides in drinking water by liquid-liquid extraction and gas chromatograph with electron-capture detection,* Cincinnati, USA: US Environmental Protection Agency, Office of Research and Development, 1995, 61 pp.

USEPA. *National Primary Drinking Water Regulations: Stage 2 Disinfectants and Disinfection Byproducts Rule, EPA 815Z03005*. Washington, D.C.: US Environmental Protection Agency, 2003, 135 pp.

UYAK, V., OZDEMIR, K., and TOROZ, I. Multiple linear regression modeling of disinfection by-products formation in Istanbul drinking water reservoirs. *Sci. Total Environ.* Vol. 378, 2007, pp. 269-280.

VARGA, L. Bacteriological quality of bottled natural mineral waters commercialized in Hungary. *Food Control*. Vol. 22, 2011, pp. 591-595.

VIDAL, J., CONSUEGRA, A., GOMESCASERES, L. y MARRUGO, J. Evaluación de la calidad microbiológica del agua embotellada en bolsas producida en Sincelejo-Colombia. *Rev. MVZ Córdoba*. Vol. 14, 2009, pp. 1736-1744.

VILLANUEVA, C.M., CANTOR, K.P., CORDIER, S., JAAKKOLA, J.J.K., KING, W.D., LYNCH, C.F., PORRU, S., and KOGEVINAS, M. Disinfection byproducts and

bladder cancer. A Pooled Analysis. *Epidemiology*. Vol. 15, 2004, pp. 357-367.

XIANG, W., XIANG, J., ZHANG, J., WU, F., and TANG, J. Geochemical transformation of trichloroacetic acid to chloroform in freshwaters – The results based upong laboratory experiments. *Water Air Soil Pol*. Vol. 168, 2005, pp. 289-312.

YAMAGUCHI, M.U., PONTELLO-RAMPAZZO, R., YAMADA-OGATTA, S.F., NAKAMURA, C.V., UEDA-NAKAMURA, T., and PRADO DIAS-FILHO, B. Yeasts and filamentous fungi in bottled mineral water and tap water from municipal supplies. *Braz Archiv. Biol. Tech.* Vol. 50, 2007, pp. 1-9.

Institutional Address of the Authors

Ing. Elisa C. Arévalo Pérez
M.C. Aida J. Martínez León
M.C. Mildred F. Lemus Pérez
Dr. Manuel S. Rodríguez Susa

Universidad de los Andes, Colombia
Carrera Primera # 18A-12,
Bogotá, D.C., Colombia
Teléfono: +57 (1) 3394 949
ec.arevalo114@uniandes.edu.co
ai-marti@uniandes.edu.co
mf.lemus39@uniandes.edu.co
manuel-r@uniandes.edu.co

Click here to write the autor

Potential Influences of Climate Change on Pluvial Floods in an Andean Watershed

• Miguel Ángel Lagos-Zúñiga* • Ximena Vargas-Mesa •
Universidad de Chile
*Corresponding Author

Abstract

LAGOS-ZÚÑIGA, M.A. & VARGAS-MESA, X. Potential Influences of Climate Change on Pluvial Floods in an Andean Watershed. *Water Technology and Sciences* (in Spanish). Vol. V, No. 2, March-April, 2014, pp. 19-38.

In studies of floods in basins with a snow regime, the role of temperature has been found to be as important as precipitation to determine the magnitude of the floods, since it defines the contributing catchment area bounded by snow lines (H_{LN}). Therefore, the hypsometry of the basin is also relevant since it determines the percentage of additional catchment area resulting from small variations in H_{LN}. This study analyzes the effects of different combinations of snow line elevations and precipitation, different probabilities of exceedance, for pluvial floods with return periods of 1 000 and 10 000 years (T) in a Chilean Andean basin with a snow regime. The results obtained were compared with previous studies in which the contributing catchment area was taken as constant, finding a significant variation of up to 20% with respect to the mean peak flow of floods with T = 1 000 years. This suggests that future designs of large hydraulic works in basins with similar hydrological regimes should take into account these combinations. In addition, the possible effects of climate change, based on future scenarios A2 and B1 (2045-2065), on the magnitude of these floods were examined. In the study zone, an increase in the magnitude of daily precipitation is projected for T = 1 000 years, up to 70% on average, for scenario B1 and an average increase in temperature of +1.8 °C and +1.3 °C is projected for scenarios A2 and B1, respectively. This will lead to increases in peak flow and direct runoff volumes of up to 72 and 84%, respectively, for the period 2045 – 2065, variations that could exceed the confidence interval for extreme floods calculated for the historical period and result in the vulnerability of the dam located at the outlet of the study basin to floods under climate change scenarios.

Keywords: Climate change, contributing area, floods, mixed regime.

Resumen

LAGOS-ZÚÑIGA, M.A. & VARGAS-MESA, X. Potenciales influencias del cambio climático en crecidas pluviales en una cuenca andina. Tecnología y Ciencias del Agua. *Vol. V, núm. 2, marzo-abril de 2014, pp. 19-38.*

En los estudios de crecida en cuencas de régimen nival, la temperatura juega un rol tan importante como la precipitación en la determinación de la magnitud de las mismas, pues define el área pluvial aportante delimitada por la línea de nieves (H_{LN}). *En este mismo sentido, la hipsometría de la cuenca es también relevante debido a que determina cuánto porcentaje de área pluvial adicional se tendrá como resultado de pequeñas variaciones de la* H_{LN}. *En este estudio se analizan los efectos de considerar diferentes combinaciones de elevación de línea de nieves y precipitación, de distinta probabilidad de excedencia, en las crecidas de origen pluvial de 1 000 y 10 000 años de periodo de retorno* (T), *en una cuenca cordillerana chilena de régimen nival. Se comparan los resultados obtenidos con estudios previos, donde el área pluvial aportante era considerada constante, encontrando una importante dispersión que alcanza variaciones de hasta un 20% respecto a la media del caudal máximo en crecidas de* T = *1 000 años, sugiriendo que se incorporen a futuro estas combinaciones para el diseño de grandes obras hidráulicas en cuencas de régimen hidrológico similar. Se examinan además los posibles efectos del cambio climático bajo los escenarios futuros A2 y B1 (2045-2065) en las magnitudes de estas crecidas. En la zona en estudio, en términos de precipitación diaria, se proyecta un incremento de las magnitudes para el evento de* T = *1 000 años de hasta un 70% promedio en el escenario B1, y un aumento promedio en la temperatura de +1.8 °C y +1.3 °C en los escenarios A2 y B1, respectivamente. Esto conduciría a incrementos del caudal máximo y del volumen de escorrentía directa de hasta 72 y 84%, respectivamente, para el periodo 2045-2065, variaciones que podrían escapar de un intervalo de confianza de crecidas extremas estimadas en el periodo histórico y dejar al embalse situado a la salida de la cuenca analizada, vulnerable frente a inundaciones en los escenarios de cambio climático.*

Palabras clave: *crecidas, área contribuyente, régimen mixto, cambio climático.*

Introduction

Studies of floods have been conducted widely and floods are a common problem in the design of hydraulic engineering projects. In basins where snow plays an important role, these studies are more complex than normal since temperature plays as important a role as precipitation, given that the size of floods will vary depending on the coldness or warmth of the storm. Thus, the frequency of pluvial floods in basins with snow regimes is not necessarily related only to the return period of the storms, since temperature will (primarily) determine the elevation of the snow line (H_{LN}), which corresponds to the elevation at which solid versus liquid precipitation is differentiated and, therefore, defines the contributing catchment area of the storm.

The return period for a pluvial flood in basins with mixed hydrological regimes is therefore related to the frequency of precipitation events and the temperature at which they occur, as mentioned by Seguel and Stowhas (1985). Historically, most engineering studies simplify the problem, taking H_{LN} as a constant equal to the average condition or in a range given by the mean condition. Nevertheless, these hydrometeorological phenomena are actually much more complex and their H_{LN} vary with each storm. The same assumption is made when developing unit hydrographs (UH) in uncontrolled basins (MOP, 1995) to evaluate severe precipitation conditions, for which considering a constant catchment area for all storms only makes sense in basins with rainfall regimes.

Monitoring of snow in the Chilean Andes has not yet attained international standards (250 km^2/station, according to WMO, 1994) primarily due to the complex topography in these areas, which makes it difficult to access them and maintain instruments. Therefore, existing records focus on determining maximum accumulation and snow water equivalent, and are registered occasionally through snow routes between June and December. Thus, the contributing catchment area of floods is currently calculated using good correlations between snow cover and temperature observations (Carrasco *et al*., 2008).

The elevation of the snow line in unmonitored zones is currently calculated in Chile using thermal gradients on days with precipitation, with a threshold temperature to distinguish between solid and liquid rainfall (US Army Corp of Engineers, 1956). In Chile, these methodologies may use a temperature index of around 1° C for the occurrence of solid precipitation (Seguel and Stowhas, 1985; Vargas *et al*., 1988), as well as a linear relationship between H_{LN} and zero isotherm elevation (Garreaud, 1993).

Worldwide, remote sensing techniques are the methods most commonly used in areas with little monitoring and complex topography, such as the Chilean Andes, but they have not yet been adequately validated for winter precipitation events because of a lack of monitoring. In Chile, by comparing MODIS and LANDSAT images, MOP (2008) determined the dynamic of the snow cover for a large portion of the national territory between the years 2000 to 2007. While MODIS provides snow cover products with a precision of roughly 93% (Hall and Riggs, 2007), the presence of clouds is a key obstacle for these techniques, which results in large uncertainty precisely on rainy days when the sky is covered, making its use difficult for specific storms.

Historically, the Chilean climatology has been studied by Carrasco *et al*. (2005)using a large amount of records from different latitudes in the central territory, showing a decrease in annual precipitation and an increase in maximum and minimum

temperatures, which agree with the study by Rösenbluth *et al*. (1997) who found evidence of warming rates at 33 ° S latitude over the last century?, de aproximadamente por siglo. Likewise, during recent decades a positive increase in the zero isotherm elevation has been observed throughout Chile (Carrasco *et al*., 2008), reducing glacial areas in Chile (Cassasa, 1995) and Argentina (Leiva, 1999). These trends could continue given climate change projections (IPCC, 2007), according to which less water resources will be available during the dry season and, in the context of this study, the contributing catchment areas during floods will increase (DGF, 2006).

The different projections by the Intergovernmental Panel on Climate Change (IPCC, 2007) show wide ranges in precipitation, while there is greater agreement with regard to temperature. Ruosteenoja *et al*. (2003) show a range in precipitation from -12 to +10%, and an increase in temperature from +1.0 to +2.9 °C for the winter period in South America, which is the most critical period in Chile, during which roughly 85% of the annual precipitation occurs (DMC, 2001). Recent studies of precipitation events show a possible increase in the magnitude of infrequent storms (Kharin *et al*., 2007; Sugiyama *et al*., 2010). In addition, the IPCC (2007) indicates the possibility of an increase in the intensity of precipitation even in zones where annual rainfall is expected to decrease. This fact, added to the projections of increased temperatures, reflects a change in the concept behind historical flood studies and suggests the need to quantify the effects of these projections on the hydrological safety of works.

To determine the effects of the projections developed by diverse IPCC models, global circulation models (GCM) need to be scaled. These are climate models on the macro scale aimed at physically or statistically reproducing the global atmospheric behavior. Many statistical and dynamic scaling techniques are used for Regional Climate Models (RCM) (Wood *et al*., 2004). In Chile, PRECIS-DGF (DGF, 2006) was the only regional model available when the study was conducted, which adequately represents the seasonal variability of the climate. This model, nonetheless, does not contain projections for the mid 21st century and tends to overestimate maximum precipitations in the Andes (DGF, 2006). Thus it is impossible to perform dynamic scaling and therefore a specific statistical process is required in order to analyze the different weather stations.

Climate change will be analyzed for A2 scenarios, which describe a very heterogeneous world with large population growth, slow economic development and slow technological change, as well as for B1 scenarios which describe a convergent world with a maximum worldwide population in the mid 21st century and a more rapid evolution towards a service and information economy (IPCC, 2007). These scenarios were chosen since they include one of the most unfavorable scenarios, A2, and one which projects the smallest increases in temperature, B1; thereby obtaining a wide range of possible futures.

The main objective of this study is to show the importance of including the return period for both H_{LN} as well as precipitation in studies of floods in basins with mixed regimes, to demonstrate the range of floods that can result from different combinations of precipitation and snow line elevations, as compared to floods obtained by the design study for the Puclaro dam in Chile (30.6° S, 70.7° O) using a constant H_{LN} with the same return periods and probable peak floods.

Another main objective of this study is to quantify the possible effects of A2 and B1 climate change scenarios (2045-2065) on floods with return periods of 1 000 and 10 000 years under warmer conditions and with rainfalls that could be more intense.

Methodology

Study Zone

The Puclaro basin is located in the Coquimbo Region (Figure 1), with an area of 6 582 km^2 and an elevation ranging from 580 to 6 200 masl. Its climate is semi-arid or steppe, with an average annual rainfall of 100 mm at the Rivadavia station at 820 masl and mean temperatures ranging from 14.5° C in winter to 20.1 °C in summer. This study included seven weather stations located in the basin with over 30 years of information. These are listed in Table 1, where *Pp* indicates precipitation records and *Temp* indicates temperature.

The Elqui River is the main river in the Puclaro Basin, where there is a mostly snowy hydrological regime, mean annual flow of 9.5 m^3/s and average flow of 31.2 m^3/s during the melting period. The instantaneous peak flow of the Elquit River is 108 m^3/s in winter with a return period of 10 years. The Puclaro Basin also contains two dams: the Puclaro which bounds the study basin with a capacity

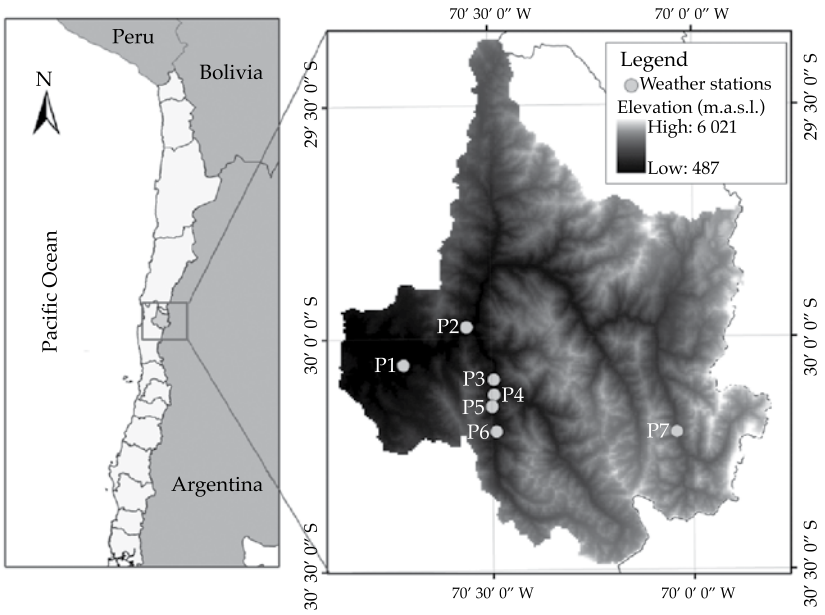

Figure 1. General Location of the Puclaro Basin (left), Digital Elevation Model and Location of Weather Stations (right).

Table 1. Weather Stations in the Study Zone.

Code	Name	UTM N (m)	UTM E (m)	Altitude (masl)	Years of Records	Variable
P1	Vicuña INIA	6 673 645	334 506	730	40	*Pp*
P2	Rivadavia	6 682 825	349 469	820	57	*Pp* and *Temp*
P3	Monte Grande	6 670 313	356 032	1 120	50	*Pp*
P4	Pisco Elqui DMC	6 666 743	356 133	1 250	32	*Pp*
P5	Los Nichos	6 663 904	355 688	1 330	32	*Pp*
P6	La Ortiga	6 657 957	356 723	1 560	32	*Pp* and *Temp*
P7	Laguna Embalse	6 658 116	399 735	3 160	47	*Pp* and *Temp*

of 200 hm^3, and the Laguna, with 15 hm^3. The discharge capacity of each dam is 2 500 m^3/s and 50 m^3/s, respectively.

Evaluation of Floods in Basins with Mixed Regimes

Seguel and Stowhas (1985) suggested that the frequency of a flood in a basin with a mixed regime is not necessarily related to the return period of a given storm, but rather to the aggregate exceedance probability of the snow line elevation (H_{LN}) and precipitation. In this case, considering that these variables are independent and integrating any other variable into them, the return period (T) for a flood event is given by (1). Therefore, to determine the magnitude of a pluvial flood in basins with mixed regimes, various combinations of return periods for H_{LN} and Pp should be taken into account.

$$T_{\text{crecidas}} = T_{\text{Líneas de nieves}} \cdot T_{\text{Precipitación}} \qquad (1)$$

This study analyzed the effects of different combinations of H_{LN} and winter Pp for floods with return periods of 1 000 and 10 000 years, as shown by the sample in Table 2. The magnitude of floods was evaluated using a Snyder synthetic unit hydrograph (SUH), calibrated for Chilean regions according to MOP (1995), similar to the UH for historical floods in the same basin (MOP, 1994).

All the floods generated with the combinations listed in Table 2 were calculated for the historical baseline (BL: 1961 – 1999) and A2 and B1 scenarios (2045-2065), taking into account climate change projections for precipitation and temperature, with the corresponding effect on the determination of H_{LN}, the contributing area and SUH.

Precipitation Data and Scaling Process

The maximum annual daily precipitation series was evaluated using a frequency analysis for each station listed in Table 1 for the BL period, calculating the return period events shown in Table 2.

Because of the large range in precipitation projections, 15 MCG models by IPCC (2007) were compared to the NCEP/NCAR (Kalnay *et al*., 1996) re-analysis, which corresponds to a global forced atmospheric model with climatological measurements from stations around the world. Considering this re-analysis to be a reliable model, it was used as a reference comparison for each MCG. Therefore, an MCG with a high degree of correlation with the re-analysis in the study zone will be considered a model capable of satisfactorily reproducing the climate process of interest. Another criteria used was comparing ΔT versus ΔP graphs for projections generated by Maurer *et al*. (2007) for the mid 21st century for 15 MCG, choosing those closest to the average ranges in temperature and precipitation during the winter period. Ten MCG were selected according to these comparison criteria (see Table 3).

The scaling process used by this study was an adaptation of the bias-correction and

Table 2. H_{LN} and Pp Combinations for Floods with 1 000- and 10 000-year return periods.

Floods with T = 1 000 years		**Floods with T = 10 000 Years**	
T Pp (years)	**T H_{LN} (years)**	**T Pp (years)**	**T H_{LN} (years)**
1 000	1	10 000	1
500	2	5 000	2
100	10	1 000	10
20	50	200	50

Table 3. MCG Filtered Models Compared to NCEP/NCAR Re-analysis and ΔT *vs.* ΔP graphs.

Center	Center acronym	Model	Spatial resolution (lat-lon)
Australia's Commonwealth Scientific and Industrial Research Organization **Australia**	CSIRO	*Mk*3.0 *Mk*3.5	1.9 x 1.9º
Canadian Center for Climate Modeling and Analysis **Canadá**	CCCma	*CGCM*3	1.9 x 1.9º
Centre National de Recherches Meteorologiques **Francia**	CNRM	*CM*3	1.9 x 1.9º
Max-Planck-Institut for Meteorology **Alemania**	MPI-M	*ECHAM*5_*OM*	1.9 x 1.9º
Meteorological Institute, University of Bonn, **Alemania** Meteorological Research Institute of KMA, **Corea** Model and Data Groupe at MPI-M, **Alemania**	MIUB METRI M&D	*ECHO-G*	3.9 x 3.9º
Geophysical Fluid Dynamics Laboratory **Estados Unidos de América**	GFDL	*CM*2.0 *CM*2.1	2.0 x 2.5º 2.0 x 2.5º
National Institute for Environmental Studies **Japón**	NIES	*MIROC*3.2 *medres*	2.8 x 2.8º
Meteorological Research Institute **Japón**	MRI	*CGCM*2.3.2	2.8 x 2.8º

spatial scaling method formulated by Wood *et al*. (2004), applied to the station scale, using two key steps: spatial scaling (SS) and temporal scaling (TS).

The SS consisted of fitting each MCG selected to the local station scale, weighting each of the MCG nodes in the sector of interest by the inverse distance, thereby considering the four closest climatologies modeled. TS involved fitting the series to which the SS was applied to local observations using statistical correlations so they coincide with the same T, resulting in a scaled series with a unit slope fitting and an error less than 1 mm, in order to minimize the variation in the results to the greatest extent possible.

Other widely used scaling processes (Li *et al*., 2010; Ternik *et al*., 2009, among others) fit the MCG to observations with good precision, but considerable errors persist for extreme events, as noted by Perkins (2011). Since in this study the extreme precipitation values are those that need to be correctly represented, several statistical fits to the resulting spatial scaling series are needed.

Assuming independence among the maximum annual daily precipitation series for scenarios BL, A2 and B1, a particular frequency analysis was conducted for each station with each series, thereby determining the values associated with the return periods listed in Table 2. The projected changes in precipitation are expressed as a percentage of change with respect to BL.

Temporal Precipitation Distribution

Since daily precipitation from different MCG models are analyzed, these models must be distributed over the duration of the storm in order to apply the SUH. This is performed using Varas(1985) distributions, similar to Huff (1967), which classifies four stations into four groups, from I to IV, according to

the time interval during which the instant of greatest precipitation is recorded, associating the intervals with the greatest intensity between the first and fourth segment of the storm's duration. A probability of exceedance of the temporal distribution for each group is associated with these groups.

According to the study by Varas (1985), for the Embalse Paloma station located in the same region, the instant with the greatest *Pp* occurred during the second quarter of the storm's duration and, therefore, the Group II distribution was selected for all the stations analyzed in this study.

Mean Precipitation in the Basin

Given H_{LN}, the average liquid precipitation in the basin is calculated using the Thiessen polygon method, for simplicity. The low density of weather stations in the basin does not allow for using more sophisticated interpolation methods, such as co-kriging for precipitation with elevation, isohyet lines or methods by Teegavarapu *et al*. (2006) (inverse distance, weighting according to the correlation coefficient and genetic algorithms).

Since the Coquimbo region is strongly influenced by the orographic effect of the Andes mountain range, where the slope increases from the coast to the range and from north to south (Falvey and Garreaud, 2007; Viale *et al*., 2008), for frontal storms coming off the ocean an increase in H_{LN} will mean an increase in mean liquid precipitation in the basin and, therefore, larger flood magnitudes.

Calculation of $\mathbf{H_{LN}}$ *Based on Temperature Analysis*

To calculate the average H_{LN} that could have occurred during a storm, formulas by Garreaud (1993) and Vargas *et al.* (1988) are used. These methods take into account mean temperature on a rainy day (equation 2) and its variation with altitude (equation 3):

$$H_{LNG} = H_{\text{Temp}=0} - 300 \quad (2)$$

$$H_{LNV} = H_{\text{Station}} - \left(Temp_{\text{Index}} - Temp_{\text{threshold}}\right) * 1\,000 / G \quad (3)$$

Where:

H_{LNG}, H_{LNV}: snow line elevation (masl).
$H_{Temp=0}$: zero isotherm elevation (masl).
$H_{Station}$: elevation of the reference weather station (masl).
$Temp_{\text{Umbral}}$: threshold temperature of precipitation solid liquid at 1 °C.
G: observed thermal gradient (°C/km).
$Temp_{\text{Index}}$: temperature index (Seguel and Stowhas, 1985) calculated according to (4):

$$Temp_{\text{Index}} = \left(Temp_{max} + \left(k-1\right)Temp_{min}\right)/k \quad (4)$$

Where k is a number between 4 and 7 and $Temp_{\text{max}}$ and $Temp_{\text{min}}$ correspond to maximum and minimum daily temperatures. Seguel and Stowhas (1985) showed a good correlation between the calculated $Temp_{\text{index}}$ when k = 7 and the occurrence of solid precipitation for Chilean stations. To calculate $H_{T=0}$ and G, mean daily temperatures from the Rivadavia, La Ortiga and La Laguna Embalse stations were correlated with their respective elevations on stormy days, establishing a linear relation among them for each event.

The main problem with the formulation of H_{LNV} is that it depends on one single weather station and not a series of records from several stations, leaving it up to the hydrologist to arbitrarily determine which station to use. In this case La Ortiga station was used mainly because of the amount and quality of its records. H_{LNG} was formulated based on observations of radiosondes in

central Chile, finding a difference of 300 m with $H_{T=0}$ due to the possibility of occurrence of snow at temperatures over 0° C (US Army Corp of Engineers, 1956).

In order to validate these methodologies, MOD10A images from the Terra satellite were used, with a temporal resolution of 8 days (Hall *et al*., 2000), assuming an approximate precision of 93% for measurements with little cloud cover (Hall and Riggs, 2007). This product was coupled with an Aster Digital Elevation Model (DEM) with a spatial resolution of 30 m to calculate the lowest elevation of a snow pixel, which determines the "observed" H_{LN} for each event, subject to possible error due to cloudiness.

The changes in H_{LN} were quantified considering the changes in temperature in the study zone projected by Maurer *et al*. (2007) for the winter period for A2 and B1 scenarios. The new zero isotherm elevation during the period 2045-2065 was determined considering that for altitude $H_{Temp=0}$ during the BL period, the future temperature would be positive, the same as the temperature changes projected by Maurer *et al*. (2007) for the winter period. Thus, since the future thermal gradients will be equal to the average for the BL period, a new $H_{Temp=0}$ can be obtained for the future period. All future H_{LN} projections generate new geomorphological parameters for the pluvial basin, along with new concentration times and SUH for each A2 and B1 scenario.

Another method to validate the indirect calculations of H_{LN} is to compare the results with H_{LN} calculations reported in the literature (see Table 4).

Sub-scenarios to Evaluate Pluvial Floods Considering Climate Change

To evaluate future pluvial flood conditions, average precipitation projections are considered for the 10 MCG selected for scenarios A2 and B1. The temperature changes used are based on the average increase in temperature projected by Maurer *et al*. (2007) for the winter in the study zone and the standard error for the 15 MCG used in the analysis. The calculated floods are based on the separate and joint occurrence of temperature and precipitation projections for probable occurrence scenarios, according to the combinations listed in Table 5. Thus, historical or future SUH are obtained according to the temperature conditions reported in the section "Study Zone."

Results

Thermal Gradients and Calculation and Validation of $\mathbf{H_{LN}}$

The thermal gradients obtained from 58 days of rainfall with daily precipitation over 10 mm indicated an average of -5.55 °C/km, as shown in Figure 2, which is in the range for the moist-adiabatic gradient characteristic of rainy days during the BL period.

Table 6 shows the calculations of snow lines using La Ortiga station as a basis for the H_{LNV} method for these same independent precipitation events. Overall, the H_{LNG} method is observed to be more conservative, since the resulting elevation is 13% higher than H_{LNV}, which indicates larger catchment areas.

Table 4. Calculations of H_{LN} Reported in the Literature.

Study	Range for H_{LN} in winter	Methodology
Zavala and Trigo (2008)	3 000 a 3 500 (masl) Minimum 1 700 (masl)	$H_{LN} = H_{Temp=0}$. Snow routes
MOP (2008)	De 1 600 a 3 600 (masl)	LANDAST and MODIS images
MOP (1991)	De 2 500 a 3 000 (masl)	Snow routes

Table 5. Sub-scenarios Considered to Evaluate Variations in Pluvial Floods in the Puclaro Basin.

Sub-scenario	Projections considered for A2 and B1 Scenarios
1	Average variation in precipitation considering H_{LN} for the BL period
2	Maximum temperature variation considering observations of *Pp* for the BL period
3	Mean temperature variation considering observations of *Pp* for the BL period
4	Minimum temperature variation considering observations of *Pp* for the BL period
5	Maximum temperature variation considering the mean variation of projections of *Pp*
6	Mean temperature variation considering the mean variation of projections of *Pp*
7	Minimum temperature variation considering the mean variation of projections of *Pp*

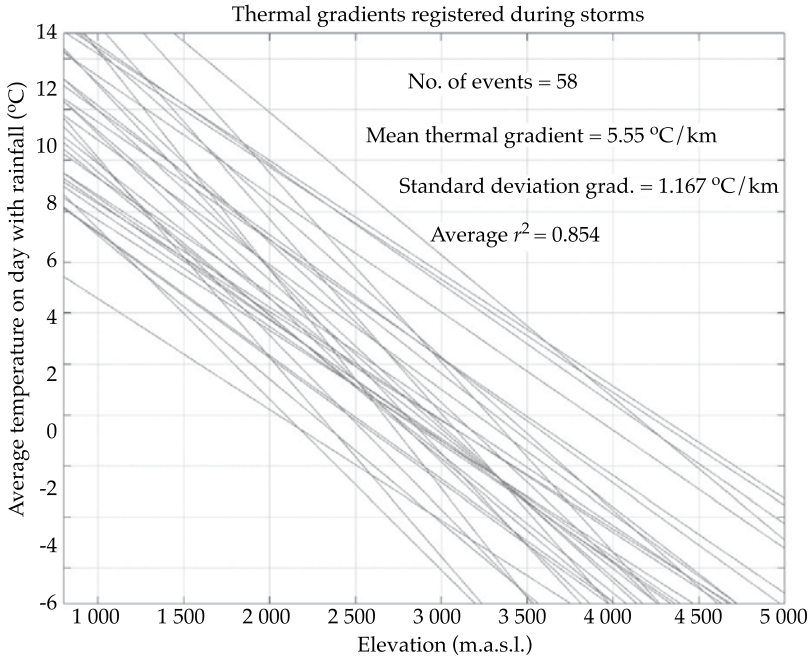

Figure 2. Thermal Gradients Calculated for 58 Precipitation Events over 10 mm.

Table 6. Main Statistics to Calculate Snow Line Elevation for the BL Period.

Statistic	H_{LNV} (masl)	H_{LNG} (masl)
Average	2 400	2 700
Median	2 400	2 600
Standard Deviation	500	600
Maximum	3 300	4 000
Minimum	1 400	1 800

By comparing the results obtained from both indirect methodologies with those from the analysis of 30 MOD10A images (Hall *et al*., 2000) from the period 2001-2010, as shown in Figure 3, an acceptable degree of correlation is seen between these calculations, though there is a large spread for each storm.

According to the values shown in Figure 3, if the slope of the linear fit between $H_{LN\text{-MODIS10A}}$ and each calculation analyzed is

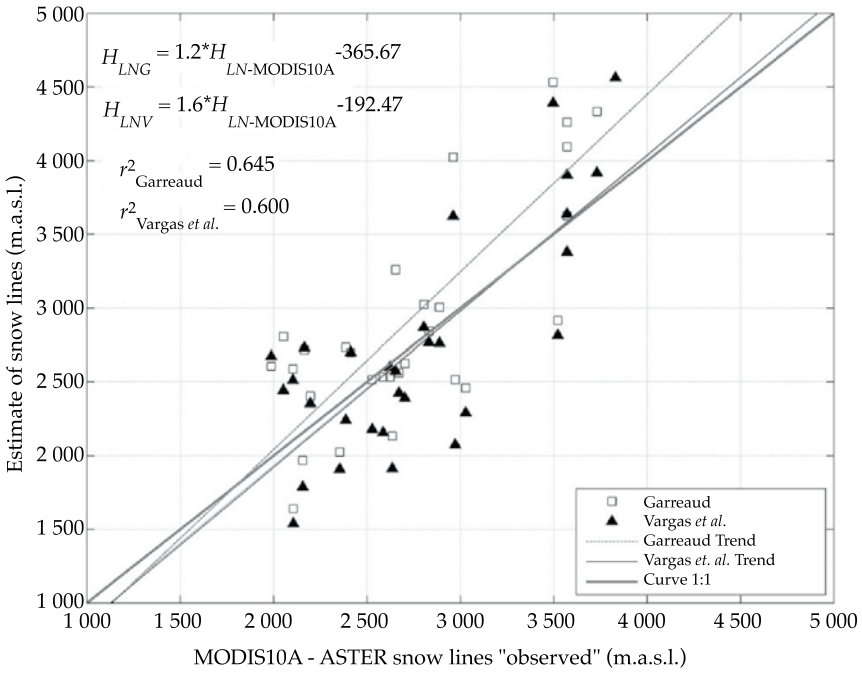

Figure 3. Validating H_{LN} Calculations from the Proposed Methodologies with MOD10A.

compared to the efficiency criteria proposed by Krause *et al*. (2005), weighted correlation values of 0.774 and 0.636 will be obtained, corresponding to the weighting of the r^2 coefficient for the indirect calculations of H_{LNG} and H_{LNV} resulting from the calculations of H_{LN} obtained based on the MODIS10A images. This criterion shows that neither methodology exactly represents the phenomenon studied and that, if considered correct, remote observations are underestimated by 22.6 and 36.4% on average for H_{LNG} and H_{LNV}, respectively.

Considering the range in H_{LN} calculated by the studies in Table 4 and that the zero isotherm range calculated by Carrasco *et al*. (2005), using historical radiosondes information (1975-2001), fluctuates in winter in central Chile at around 3 000 masl, it is possible to infer that the values are similar to other calculations. Therefore, the H_{LNG} methodology is adopted as the most suitable method to calculate future H_{LN} for BL, A2 and B1 scenarios.

Results from Scaling of Precipitation and its Projections

An example of the result from the scaling process applied is shown in Figure 4, which shows correlation coefficients and weighted r^2 near one for each case.

For 1 000 and 10 000 years, maximum annual daily precipitation and changes with respect to BL for the 10 MCG listed in Table 3 are shown in Figure 5 for the six stations in the study, along with the mean precipitation in the basin for A2 and B1 scenarios, considering an H_{LN} elevation with a high frequency (T = 1.02 years), resulting in a large spread.

In terms of mean precipitation projections for the basin, the increase in the frequency of these events was greater for scenario B1

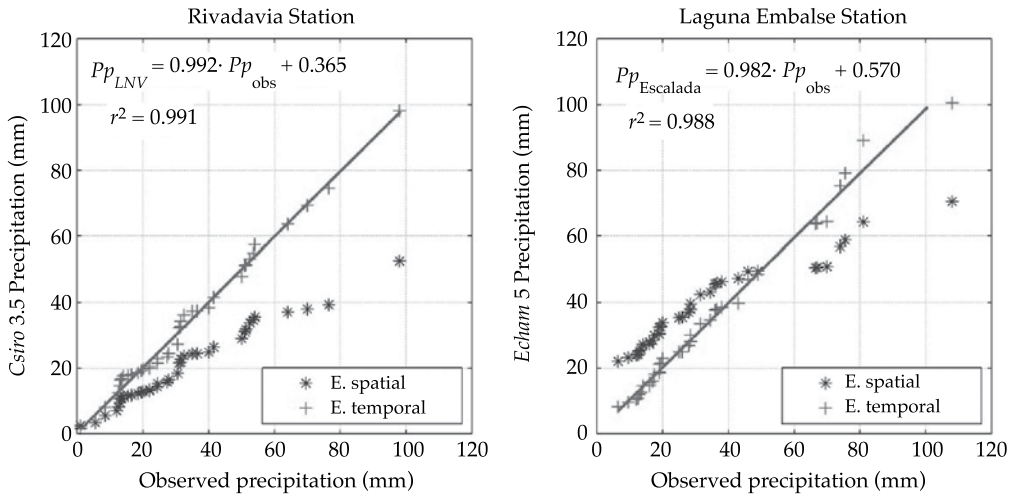

Figure 4. Result of the Fit Obtained with the Downscaling Proposed for the Rivadavia Station with the csiro 3.5 model (left) and for La Laguna Embalse Station with the *echam*5 model (right).

than for A2; on the order of 1.56 and 1.03 for T = 1 000 and 10 000 years. For all cases, an increase over 4.6% is projected for the 25th percentile and 120% for the 75th percentile for events with T = 10 000 years, with respect to the BL scenario. Table 7 shows the median, first and third quartiles and range of change with respect to BL in the basin.

Temperature and Snow Line Elevation Projections

Table 8 shows winter temperature projections for the Puclaro Basin for the mid 21st century according to scaling by Maurer *et al.* (2007) for scenarios A2 and B1. When applied to the H_{LN} series obtained for BL, these variations show an increase given by the standard maximum projections of up to 300 m, as shown in Figure 6 (left).

Small changes in H_{LN} could result in significant increases in the contributing catchment area depending on the hypsometry of the basin, as shown in Figure 6 (right). This is extremely important under climate change projections, as shown in Table 9, where the effect of these changes on the percentage increase in the contributing catchment area is as high as 33% for scenarios A2 and B1, when considering the projected higher standard error for temperature for each scenario. This sensitivity is especially significant at mean altitudes around 3 000 masl.

Flood Study

In order to verify the hypothesis about the independence between precipitation and the mean daily temperature at which it occurs, the student-t test was performed, finding independence between the two variables for different precipitation thresholds, and therefore based on logical transitivity equation (1) can be considered valid at a confidence level of 95%. Figure 7 shows the degree of correlation between the two variables at the La Ortiga station for different thresholds, with R correlation coefficients remaining under the absolute value of 0.4.

The floods obtained for return periods of 1 000 and 10 000 years were calculated using the SUH generated based on the sub-

Table 7. Projections of Mean Precipitation in the Puclaro Basin for A2 and B1 Scenarios.

Quartile	% Δ*Pp* for *T* = 1 000 years		% Δ*Pp* for *T* = 10 000 years	
	A2	B1	A2	B1
25%	4.6	12.4	19.6	16.3
Median	24.5	62.9	39.3	80.0
75%	85.5	93.8	89.2	120.3
Range	80.9	81.4	69.6	104

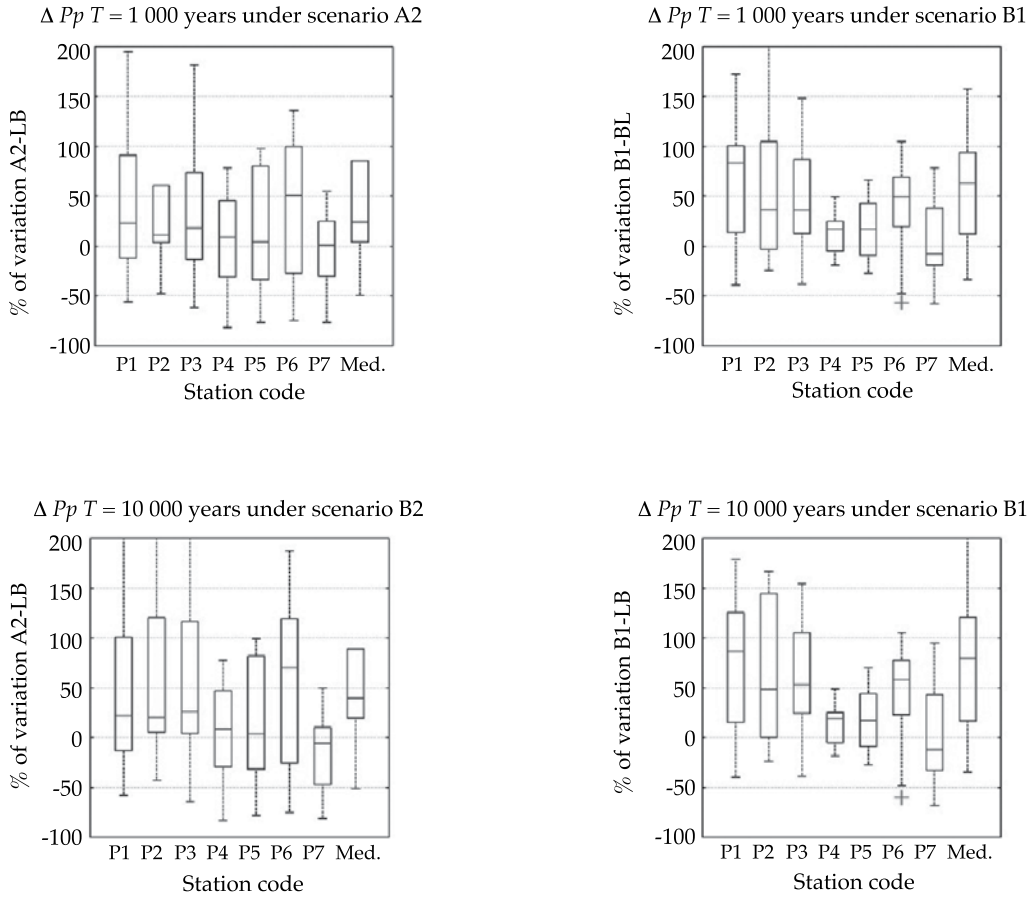

Figure 5. Δ*Pp* de *T* = 1 000 and 10 000 Years for Scenario A2 (left) and B1 (right) at Puclaro Basin Stations and Average (middle) in the Basin for H_{LN} with a High Frequency (1.02-year Return Period).

scenarios studied, which are listed in Table 5. Figure 8 shows the most critical hydrographs for floods with *T* = 1 000 and 10 000 years for scenarios BL, A2 and B1, taking into account the greater temperature increases projected by Maurer *et al.* (2007) listed in Table 8. It is worth noting that it is difficult to distinguish between A2 and B1 floods because they are superimposed in most of the cases.

As seen in Figure 8, for the Varas II distribution with a 10% probability of exceedance, the largest increases in instantaneous peak flows generally occur in scenario A2, up to 61% for floods with *T*

Table 8. Changes in Temperature Projected by Maurer *et al.* (2007) in the Puclaro Basin.

ΔTemp °C	Scenario	
	B1	**A2**
Average	1.3	1.8
Standard Deviation	0.38	0.33
Error +	1.7	2.1
Error -	1.0	1.5

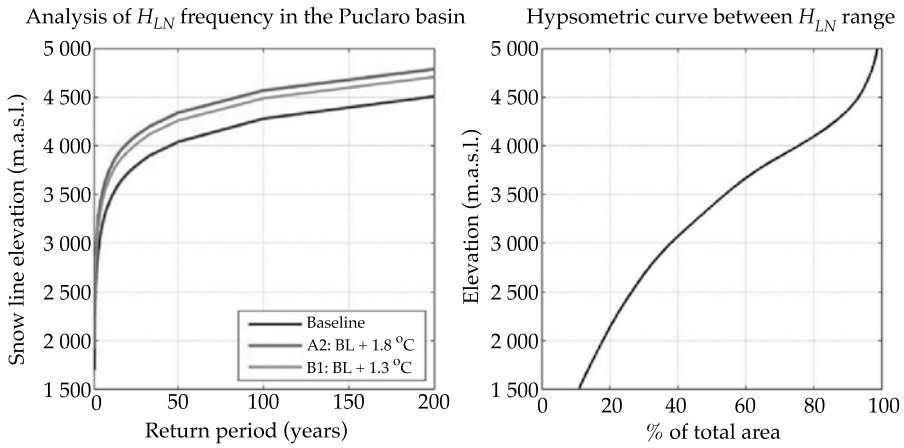

Figure 6. Analysis of the Frequency of H_{LN} for BL scenarios, Average Changes in Temperature for Scenarios A2 and B1 (left), and Hypsometric Curve for H_{LN} ranges (right).

Table 9. H_{LN} for Scenarios BL, A2 and B1 (Average Changes) and Increase in Catchment Area.

T (years)	H_{LN} (masl)			Increase in Catchment Area	
	BL	**B1: BL + 1.3 °C**	**A2: BL + 1.8 °C**	**B1: BL + 1.3 °C**	**A2: BL + 1.8 °C**
1.02	1 700	1 900	2 000	20.2%	31.0%
2	2 600	2 900	3 000	23.5%	33.1%
10	3 400	3 700	3 800	20.7%	29.1%
50	4 000	4 300	4 300	16.4%	16.4%

= 10 000 years. In scenario B1, increases of up to 56% occurred for events with the same frequency. If considering only an increase in precipitation (A2-1 and B1-1), scenario B1 produced the largest peak increase, although the difference is negligible (~ 2%). The effects of the increase in temperature are more important, since they produce as much as 29% more floods than baseline. Floods in B1-6 are slightly more severe than those in scenarios A2-6 for 1 000 and 10 000 years only in the case of the combined effect of precipitation and temperature for an H_{LN} with T = 50 years.

Comparing the results for instantaneous peak flow in Figure 8 for the BL scenario, it can be observed that taking into account various snow line elevations results in notable dif-

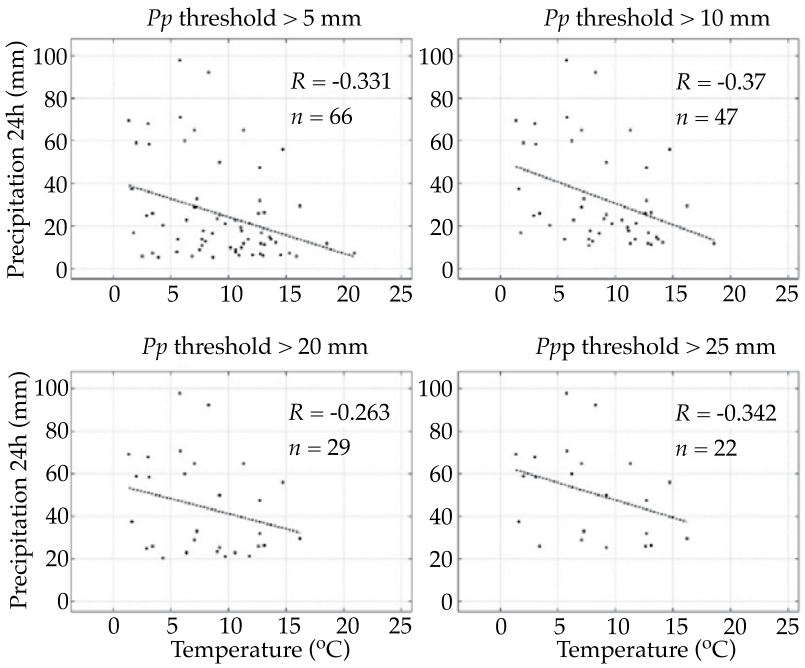

Figure 7. Correlation (*R*) between Mean Daily Temperature and Precipitation Registered at the La Ortiga station and number (*n*) of Events Exceeding the Precipitation Threshold (*Pp*).

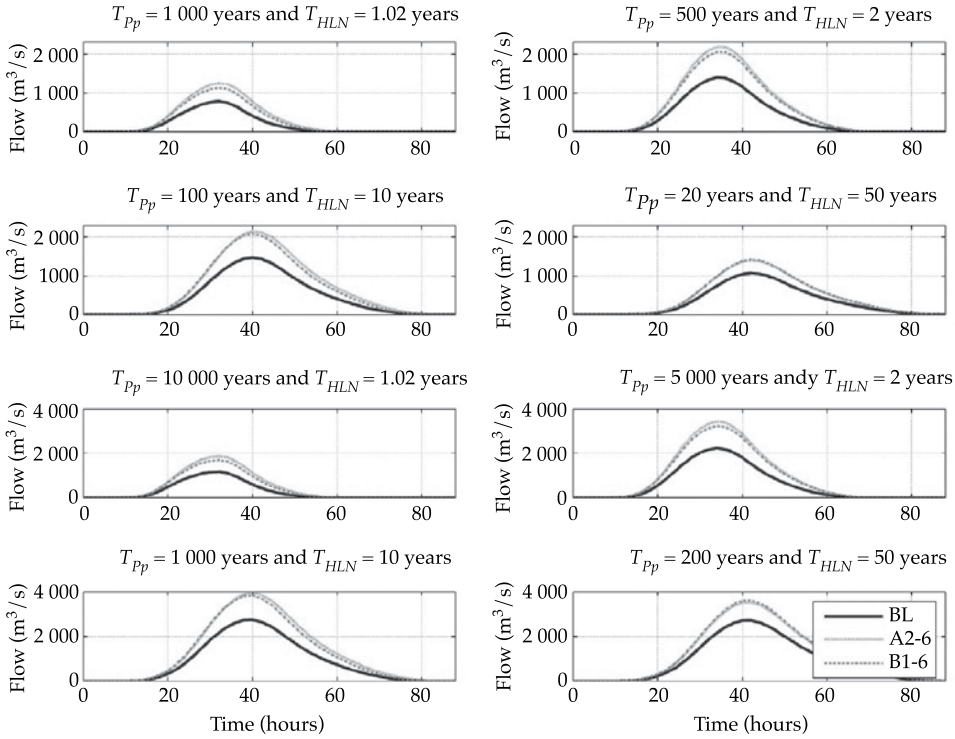

Figure 8. Floods with T = 1 000 and 10 000 years for Different Combinations of Scenarios and H_{LN}, for a 10% Varas (1985) Group II Distribution. Thick line: BL. Dashed line: sub-scenario A2-6. Dotted line: sub-scenario B1-6.

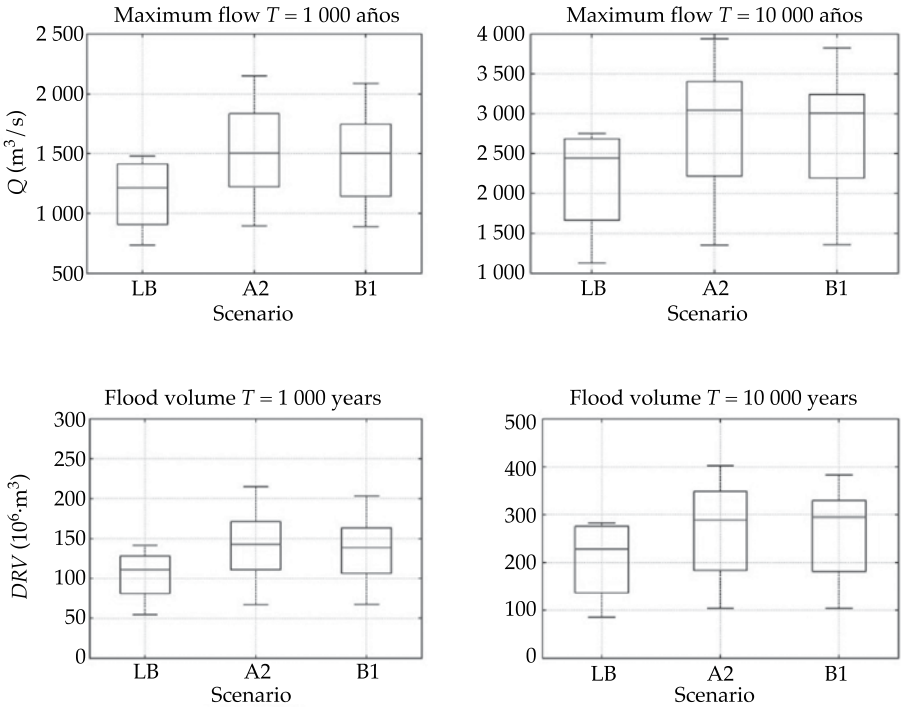

Figure 9. Maximum Flow (*Q*) and Direct Runoff Volume (*DRV*) for Floods with *T* = 1 000 and 10 000 years for each Scenario Analyzed.

Table 10. Instantaneous Peak Flows Obtained according to Different Criteria. Baseline Period.

***T* for floods (years)**	***Q* MOP (1994) (m^3/s)**	***T* for H_{LN} (years)**				**ΔQ with respect to *Q* MOP (1994)**
		1.02	**2**	**10**	**50**	
1 000	1 750	785	1 399	1 478	1 074	De -56.7% a -15.5%
10 000	2 500	1 185	2 231	2 747	2 720	De -52.6% a +9.9%

ferences in the hydrographs. Table 10 shows the calculations obtained during that period and those from the MOP study (1994), which included an H_{LN} of approximately two years and daily precipitation for T = 1 000 and 10 000 years. As shown, precipitation with T = 1 000 years combined with an H_{LN} with a 10-year return period can produce a peak flow of T = 10 000 years, 10% higher than the MOP study with a 20 000-year return period. In addition, precipitation for T = 10 000 years combined with an H_{LN} with a high frequency (~1 year) results in maximum flows that are 56.8% less than those calculated for precipitation with T = 1 000 years and H_{LN} with a return period of 10 years. In addition, values for a 10 000-year flood may be as much as 26% less than the calculated likely maximum capacity (LMC) of 3 700 m^3/s for the dam.

Figure 9 shows the variability in peak flow and volume resulting from different temporal precipitation distributions, as well as from the combination of precipitation and H_{LN} for return periods of 1 000 and 10 000 years, for floods corresponding to scenarios BL, A2 and B1. Floods that are 13% greater than the median of those generated can be obtained for the BL scenario, and 38 and

32% greater than the median for A2 and B1 scenarios, respectively.

A large spread can be seen in the magnitudes of the variables for all the scenarios, since they are dependent on the different combinations of return periods for H_{LN} and *Pp*, and the temporal distribution of the precipitation, as well as each climate change sub-scenario analyzed. For A2 and B1 scenarios, increases in instantaneous peak flow of +32 and +27% are observed between the 25th and 75th percentiles, respectively.

Discussion

When performing any flood study, it is very important to consider different return periods for H_{LN} and *Pp* since, as shown in Table 10, precipitation with T = 100 years combined with a contributing catchment area with T = 10 years will produce a more severe flood than that produced by a millennium storm, but with low temperatures (H_{LN} = 1.02 years).

The analysis of the uncertainty associated with floods can incorporate greater ranges of variability in the flows obtained, for example, in the case of conditions related to soil infiltration capacity, more sophisticated temporal precipitation distributions such as the study by Dolling and Varas (2006) using neuron networks, or different spatial distributions. Nevertheless, according to the results in Figure 8, for basins with mixed hydrological regimes H_{LN} seems to have greater effects on the determination of more severe floods and, therefore, probabilistically analyzing this variable provides highly relevant information for the hydrological design of hydraulic works. The importance of this is reflected in that flows with T = 10 000 years were obtained that were only 26% less than the likely maximum capacity of the tributary determined by the Puclaro dam design study (MOP, 1994).

In this study, the calculation of H_{LN} is one of the greatest sources of uncertainty because of the lack of sufficient stations to measure snow in the Chilean Andes. Therefore, simple, indirect calculations such as those by Garreaud (1993) appear to be viable tools given the topography of the zone, in spite of the large spread shown by the validation. In addition, it was shown that when comparing H_{LN} calculations based on temperature records with H_{LN} obtained from MOD10A satellite images, a large spread in the results is obtained (Figure 3), which is partly attributed to these images often not containing information. Therefore, the precision given by Hall and Riggs (2007) is highly dependent on the quality of the image and primarily on cloudiness, which during the winter tends to be high.

Nonetheless, this methodology is applicable to the study zone, considering the range of variation in H_{LN} and zero isotherm indicated in the section "Thermal Gradient and Calculation and Validation of H_{LN}" which on average exceeded 3 000 masl (MOP, 2008; Zavala y Trigo, 2008; MOP, 1995; MOP, 1991; Carrasco *et al*., 2005), providing values similar to the H_{LNG} methodology for observations obtained during BL.

The calculation of H_{LN} during the storm assumed a constant thermal gradient for future scenarios, although this gradient was shown to vary with respect to the BL period. This simplification makes it possible to more simply study the problem investigated herein, although it is important to recognize that lower gradients will lead to greater flows than those presented here due to higher zero isotherm elevations.

In terms of climate change, an increasing trend in the rate of daily precipitation can be observed, similar to projections by Kharin *et al*. (2007) and Rousteenoja *et al*. (2003). Likewise, temperature trends reported by Maurer *et al*. (2007) are consistent with projections by Rösenbluth *et al*. (1997). The increase in daily precipitation tends to be

greater for scenario B1 than A2, and higher still for a *Pp* event of 10 000 years, which can increase as much as +80%, versus the +39% for A2 projections. Nevertheless, the range in the projections for the 10 MCG selected is very high.

The NCEP/NCAR re-analysis (Kalnay *et al*., 1996) can be applied as a tool to discriminate among MCG, since it takes into account observations of data from different parts of the world, such that its behavior can be considered to be a good approximation of actual climate measurements, just as the comparison of Δ*Pp vs.* Δ*Temp* graphs.

The scaling process used is especially designed to decrease the spread for events with a low probability of exceedance for the BL scenario, also based on the process proposed by Wood *et al*. (2004). Nevertheless, the assumption that the relationships found in the statistical temporal *downscaling* will continue to be valid in the future represents a large source of uncertainty. Although this fact provides more credibility for dynamic scaling processes since the physical phenomenon involved are considered, given the current state of regional Chilean models they cannot be adequately used.

The climate change projections shown for maximum daily precipitation and winter temperature present increases in peak flow and direct runoff volume, both separately and together. Temperature represents the dominant variable in these increases due to the hypsometry of the basin and its elasticity at medium altitudes, where small changes in H_{LN} can determine large increases in the catchment area. This result can be generalized to other basins with mixed regimes and topography (Andean basins) for the historical BL scenario as well as for future climate change projections.

The greatest increases in flow and volume given climate changes are produced in the scenario that takes into account the joint increase in precipitation and temperature for scenarios A2 and B1. The greatest increases in peak flow with respect to BL were +73% and 70% for floods with 1 000 and 10 000-year return periods, respectively, for sub-scenarios A2-5. In terms of volumetric changes, the peaks for these same floods were +84% and +81% for the same sub-scenario.

The use of a unit hydrograph model to calculate floods does not completely reproduce the physical basis of the problem and, therefore, these results should be considered as references only. The use of a more complex model–whether it be concentrated or distributed—requires more information, especially related to meteorological forcing, which in this basin is not recorded with the spatial distribution required and, therefore, the results would also have a high degree of uncertainty.

Finally, a large spread in the resulting peak flow and direct runoff volumes can be seen for the different possible climate change sub-scenarios, given changes in precipitation and temperature and the temporal distribution of the storm, in addition to the antecedent moisture conditions and the spatial distribution of the precipitation, factors not addressed by this study. Nevertheless, as can be seen in Figure 9, considering the projections for scenarios A2 and B1, future projections always result in greater flows than historical calculations.

The above results are highly important since, under climate change conditions, floods with T = 10 000 years will be 7% larger than those for the LMC determined by the design of the Puclaro dam. Therefore, the inclusion of climate change impact studies of hydraulic works with a long useful life will benefit the hydrological safety of the works, especially for those in which their failure presents risk of death, as in the case of a dam.

Conclusions

Studies of floods in basins with mixed regimes must take into account changes in the snow line elevation along with the analysis of precipitation, in order to analyze the most unfavorable situations for a flood associated with the same probability of exceedance.

Climate change projections show an increase in winter temperatures and maximum annual daily precipitation. Precipitation increases of 80% for T = 10 000 years are seen for scenario B1 and 39% for A2. Nevertheless, the increased temperature for the latter scenario, 0.5 °C higher on average, is most significant to the generation of more severe floods, with peak flow and runoff volume as high as 73 and 84%, respectively.

Increases in temperature will mostly determine vulnerability to climate change in terms of the magnitude of floods under climate change conditions in the Puclaro Basin and in Andean basins with mixed regimes, since small changes in elevations in the snow line could result in large increase in the contributing catchment area in this type of basin.

Finally, climate change studies are recommended for the design of hydraulic works such as dams, given the consequences that would occur from their failure and their long-term projected use.

Acknowledgments

The authors would like to thank the Dirección General de Aguas, Chile, and their transparency law, for the meteorological information used in this study. We also thank Dr. James McPhee and the two anonymous reviewers for their valuable comments, which undoubtedly contributed to improving the quality and understanding of this article.

Received: 06/08/2012
Accepted: 19/06/2013

References

CARRASCO, J., OSORIO, R., and CASASSA, G. Secular trend of the equilibrium-line altitude on the western side of the southern Andes, derived from radiosonde and surface observations. *Journal of Glaciology*. Vol. 54, 2008, 186 pp.

CARRASCO, J., CASSASA, G., and QUINTANA, J. Changes of the 0° isotherm and the equilibrium line altitude in Central Chile during the last quarter of the 20th century. *Journal of Hydrological Sciences*. Vol. 50, No. 6, 2005, pp. 933-948.

CASSASA, G. Glacier inventory in Chile: current status and recent glacier variations. *Ann. Glaciol*. Vol. 21, 1995, pp. 317-322.

DGF. *Estudio de Variabilidad Climática en Chile para el Siglo XXI. Informe realizado para la CONAMA*. Santiago: Departamento de Geofísica, Universidad de Chile, 2006.

DMC. *Climatología regional* [en línea]. Dirección Meteorológica de Chile, Departamento de Climatología y Meteorología, 2001. Disponible para *World Wide Web*: http://164.77.222.61/climatologia/.

DOLLING, O. and VARAS, E. Design storms using artificial neural networks. *Hydraulic Engineering in Mexico*. Vol. XXI, No. 4, 2006, pp. 103-113.

FALVEY, M. and GARREAUD, R. Wintertime precipitation episodes in Central Chile: Associated Meteorológical Conditions and Orographic influences. *Journal of Hydrometeorology*. Vol. 8, 2007, pp. 171-193.

GARREAUD, R. *Impacto de la variabilidad de la línea de nieves en crecidas invernales en cuencas pluvio-nivales de Chile Central*. XI Congreso Chileno de Ingeniería Hidráulica, Concepción, Chile, 1993.

HALL, D. and RIGGS, G. Accuracy Assessment of the MODIS Snow Products. *Hydrological Processes*. Vol. 21, No. 12, 2007, pp. 1534-1547.

HALL, D., RIGGS, G., and SALOMONSON, V. *Updated weekly MODIS/Terra Snow Cover 8-Day L3 Global 500 m Grid V004, April 2000 to August 2010*. Boudler, USA: National Snow and Ice Data Center, digital media, 2000.

HUFF, F.A. Time distribution of rainfall in heavy storms. *Water Resources Research*. Vol. 3, No. 4, 1967, pp. 1007-1019.

IPCC. *The Physical Science Basis. Contribution of Working Group I to the Fourth Assessment Report of the Intergovernmental Panel on Climate Change*. Solomon, S., Qin, D., Manning, M., Chen, Z., Marquis, M., Averyt, K.B., Tignor, M., and Miller, H.L. (editors). Cambridge/New York: Intergovernmental Panel on Climate Change, Cambridge University Press, 2007, 996 pp.

KALNAY, M., KANAMITSU, R., KISTLER, W., COLLINS, D., DEAVEN, L., GANDIN, M., IREDELL, S., SAHA, G., WHITE, J., WOOLLEN, Y., ZHU, M., CHELLIAH,

W., EBISUZAKI, W., HIGGINS, J., JANOWIAK, K.C., MO, C., ROPELEWSKI, J., WANG, A., LEETMAA, R., REYNOLDS, R., JENNE, Y., and JOSEPH, D. The NCEP/NCAR 40-Year Reanalysis Project. *Bull. Amer. Meteor.* Soc. Vol. 77, No. 3, 1996, pp. 437-470.

KHARIN, V.V., ZWIERS, F., ZHANG, X., and HEGERL, G. Changes in temperature and precipitation extremes in the IPCC. *J. Climate*. Vol. 20, 2007, pp. 1419-1444.

KRAUSE, P., BOYLE, D., and BÄSE, F. Comparison of different efficiency criteria for hydrological model assessment. *Advances in Geociences*. Vol. 5, 2005, pp. 89-97.

LEIVA, J. Recent fluctuations of Argentinian glaciers. *Global and Planetary Change*. Vol. 22, No. 1, 1999, pp. 69-77.

LI, H., SHEFFIELD, J., and WOOD, E. Bias correction of monthly precipitation and temperature fields from Intergovernmental Panel on Climate Change AR4 models using equidistant quantile matching. *J. Geophys. Res*. Vol. 115, 2010, D10101.

MAURER, E., BREKKE, L., PRIUTT, T., and DUFFY, P.B. Fine-resolution climate projections enhance regional climate change impact studies. *Eos Trans. Agu*. Vol. 88, No. 47, 2007, 504 pp.

MOP. *Análisis de las rutas de nieve del país*. Santiago: Ministerio de Obras Públicas, República de Chile, DGA, Departamento de Hidrología, Subdepartamento de Hidrología Aplicada, 1991.

MOP. *Dinámica de la cobertura nival entre las cuencas de los ríos Copiapó y Petrohe utilizando imágenes satelitales*. Santiago: Ministerio de Obras Públicas, República de Chile, Geografía UC-Proyectos, Instituto de Geografía PUC, 2008.

MOP. *Manual de cálculo de crecidas y caudales mínimos en cuencas sin información fluviométrica*. Santiago: Ministerio de Obras Públicas, República de Chile, Dirección General de Aguas, Ayala, Cabrera y Asociados Ingenieros Consultores Ltda., 1995.

MOP. *Proyecto Embalse Puclaro*. Santiago: Ministerio de Obras Públicas, República de Chile, Consorcio de Ingeniería INGENDESA-EDIC Ltda., Vol. VII, 1994.

PERKINS, S. *A simple bias correction method for climate extremes estimated by the generalized extreme value distribution*. Melbourne, Australia: Oral presentation at IUGG, General Assembly, 2011.

RÖSENBLUTH, B., FUENZALIDA, H., and ACEITUNO, P. Recent temperature variations in southern South America. *International Journal of Climatology*. Vol. 17, 1997, pp. 67-85.

ROUSTEENOJA, K., CARTER, T., JYLHÄ, K., and TUOMENVIRTA, H. Future climate in world regions: an intercomparison of model-based projections for the new IPCC emissions scenarios. *The Finnish Environment 644*. Helsinki: Dinnish Environment Institute, 2003, 83 pp.

SEGUEL, R. y STOWHAS, L. *Estimación de crecidas de diseño en cuencas mixtas pluvionivales*. VII Congreso Chileno de Ingeniería Hidráulica, Concepción, Chile, 1985.

SUGIYAMA, M., SHIOGAMA, S., and EMORI, S. Precipitation extreme changes exceeding moisture content increases in MIROC and IPCC climate models. *PNAS*. Vol. 107, No. 2, 2010, pp. 571-575.

TEEGAVARAPU, R., TUFFAIL, M., and ORMSBEE, L. Optimal function forms for spatial interpolation of precipitation data. *Environmental Informatics Archives*. Vol. 4, 2006, pp. 343-353.

TERNIK, W., HURJMANS, R., TORFS, P., and UIJLENHOET, R. Bias correction of temperature and precipitation data for regional climate model application to the Rhine basin. *Hydrol. Earth Syst. Sci. Discuss*. Vol. 6, 2009, pp. 5377-5413.

US ARMY CORP OF ENGINEERS. *Snow Hydrology. Summary report of the snow investigations*. Portland, USA: N. Pac. Div., US Army Corps of Eng., 1956.

VARAS, E. *Hietogramas de tormentas de diseño*. VII Congreso Nacional de Ingeniería Hidráulica, SOCHID, Concepción, Chile. 1985.

VARGAS, X., BROWN, E. y ANDREANI, C. *Uso de información regional para la estimación de crecidas*. CRH 88-53-I. Concepción: Departamento de Ingeniería Civil, Universidad de Chile, 1988.

VIALE, M., NAUMANN, G., and NORTE, F. Extreme orographic precipitation events over the central Andes of Argentina and Chile. *Proceedings of 13th Conference on Mountain Meteorology*. Whistler, Canada, 2008, p. AMS P1.22.

WOOD, A., LEUNG, L., SRIDHAR, V., and LETTENMAIER, D. Hydrologic implications of Dynamical and Statistical Approaches to Downscaling Climate Model Outputs. *J. Climatic Change*. Springer Netherlands, 2004, pp. 189-216.

WMO. *Guide to hydrological practices*. No. 168. 5th edition. Geneva: World Meteorological Organization, 1994.

ZAVALA, H. y TRIGO, H. *Los sistemas naturales de la cuenca del río Elqui (Región de Coquimbo, Chile): vulnerabilidad y cambio del clima*. Cepeda, P.J. (editor). La Serena, Chile: Ediciones Universidad de La Serena, 2008, pp. 66-167.

Institutional Address of the Authors

Mtro. Miguel Ángel Lagos Zúñiga

Departamento de Ingeniería Civil
Advanced Mining Technology Center
Universidad de Chile
Avenida Tupper 2007, oficina 304
Santiago, Chile
Teléfono: +56 (2) 2977 1009
mlagos@ing.uchile.cl

Prof. Ximena Vargas Mesa

Departamento de Ingeniería Civil
División de Recursos Hídricos y Medio Ambiente
Universidad de Chile
Avenida Blanco Encalada 2002
Santiago, CHILE
Teléfono: +56 (2) 2978 4400
xvargas@ing.uchile.cl

Click here to write the autor

Location of Water Quality Monitoring Points in Distribution Systems

• Juan G. Saldarriaga* • María Ximena Hernández • Cesar Prieto •
• Mauricio Jurado • Sara Gacharná • Diego Páez •
Universidad de los Andes, Colombia
*Corresponding Author

Abstract

SALDARRIAGA, J.G., HERNÁNDEZ, M.X., PRIETO, C., JURADO, M., GACHARNÁ, S. & PÁEZ, D. Location of Water Quality Monitoring Points in Distribution Systems. *Water Technology and Sciences* (in Spanish). Vol. V, No. 2, March-April, 2014, pp. 39-52.

Companies providing drinking water services in developing countries have been using empirical procedures for years to locate points in distribution networks at which periodic sampling should be taken in order to ensure compliance with minimum water quality standards. Although these companies have excellent information tools to model the water dynamics and evolution of water quality in networks, not enough data exists to scientifically choose these points. Additionally, the coefficients for bulk and wall chlorine decay are not known. Despite this limitation, several methodologies have been developed and implemented to design sensor networks that ensure continuous monitoring of water quality in distribution systems, but that also involve a high degree of uncertainty. The study herein was to develop a methodology to choose water quality monitoring points in an environment with little data. This would simultaneously address two typical problems of distribution networks– ensure water quality by measuring residual chlorine using a software developed for this study, and detect water coloring problems (in which the water reaching a set of users is not transparent, affecting the users' perception of its quality) due to the detachment of biofilms using the TEVA-SPOT program (Berry et al., 2008). The latter approach can be developed by optimizing multi-objective functions according to the type of protection against coloration events desired. The new methodology was successfully applied in the 37 hydraulic sectors into which the drinking water network in the city of Bogota, Colombia is divided (approximately 8 million inhabitants). Lastly, although the study was performed in 37 sectors, one of these sectors was used as a prototype of the network for the purpose of this study. The results show that both methodologies are reliable and the design of sensor networks depends on the objective to be optimized.

Keywords: Early warning sensors, monitoring, drinking water distribution networks, water quality.

Resumen

SALDARRIAGA, J.G., HERNÁNDEZ, M.X., PRIETO, C., JURADO, M., GACHARNÁ, S. & PÁEZ, D. Localización de puntos de monitoreo de calidad de agua en sistemas de distribución. Tecnología y Ciencias del Agua. *Vol. V, núm. 2, marzo-abril de 2014, pp. 39-52.*

Durante años, particularmente en los países en desarrollo, las empresas prestadoras del servicio (EPS) de agua potable han utilizado procedimientos empíricos para localizar, en sus redes de distribución, los puntos en los cuales deben hacerse muestreos periódicos, a fin de garantizar que cumplen con los estándares mínimos de calidad de agua. A pesar de que hoy en día estas empresas cuentan con excelentes herramientas informáticas para modelar la dinámica del agua en las redes, así como la evolución de la calidad de agua, no se tienen suficientes datos que permitan escoger en forma científica dichos puntos. En particular, no se cuenta con los coeficientes de decaimiento del cloro tanto de cuerpo como de pared. A pesar de esta limitación, se han desarrollado e implementado metodologías con el objetivo de diseñar redes de sensores que garanticen un constante monitoreo de la calidad del agua en los sistemas de distribución, pero que implican una alta incertidumbre. En la investigación objeto de este artículo se desarrolló una metodología que permitiera en ese ambiente de pocos datos escoger los puntos de monitoreo de calidad (PMC) de agua que respondieran simultáneamente a dos problemas típicos de las redes de distribución: por un lado, se buscaba garantizar la calidad del agua, medida por un residual de cloro, haciendo uso de un software desarrollado para este estudio; por otro lado, detectar problemas de coloración del agua (fenómeno por el cual el agua que llega a un conjunto de usuarios tiene un color diferente al transparente, afectando la percepción de calidad por parte de dichos usuarios) debido al desprendimiento de biopelículas, haciendo uso del programa TEVA-SPOT (Berry et al., 2008). Este último enfoque puede desarrollarse bajo la optimización de múltiples funciones objetivo, según el tipo de protección que se desee garantizar, contra los eventos de coloración. La nueva metodología fue aplicada exitosamente en los 37 sectores hidráulicos en los que se encuentra dividida la red de agua potable de la ciudad de Bogotá, Colombia (aproximadamente ocho millones de habitantes). Finalmente, aunque el estudio se realizó para los 37 sectores, se tomó, a manera de ejemplo para este documento, uno de estos sectores como red tipo. Los resultados evidencian que ambas metodologías son confiables y que el diseño de la red de sensores depende del objetivo que se busque optimizar.

Palabras clave: *calidad de agua, redes de distribución de agua potable, monitoreo, sensores de alerta temprana.*

Introduction

Background

In a drinking water distribution network (DWDN), taking periodic samples is the traditional method used to control the quality of water delivered to users. Historically, this has been done using standardized trials with samples taken at different points in the network, such as hydrants, drainages, household discharges and special structures designed exclusively for this purpose. The purpose of locating these points varies from meeting local quality norms and monitoring accidental contamination events to detecting contamination events that may be generated intentionally. To ensure the delivery of water with a residual chlorine content above the minimum permitted by norms to users at all consumption points, methodologies have been used to determine body (K_b) and wall decay (K_w) coefficients in a particular network. These studies have found that K_b has a greater effect on chlorine decay than K_w (Chang *et al*., 2009; Hallam *et al*., 2003), while others have concluded that both K_b and K_w are necessary to determine the kinetics of chlorine in a drinking water distribution network (DWDN) (Vasconcelos *et al*., 1996).

On the other hand, in order to monitor accidental or intentional contamination events, different models for locating quality monitoring points (QMP) have been proposed according to the desired objective. These objectives are described in *The Battle of Water Sensor Networks* (BWSN; Ostfeld *et al*., 2008), and are summarized by Preis and Ostfeld (2008) as: optimization of coverage to cover the majority of the demand in the network (Lee and Deininger, 1992; Woo *et al*., 2001); minimization of both the travel time of the contaminant before detection and the at-risk population before contamination (Berry *et al*., 2005; Krause and Guestrin, 2009); minimization of the consumption of contaminated water before detection; and lastly, once the sensor network is designed, optimization of the probability of detection, directly monitoring detection time which cannot exceed the difference between the end of the simulation period and the beginning of the contamination event (Ostfeld *et al*., 2008). Therefore, this problem can be seen as an inconvenient multi-objective, which is itself an NP-hard problem (Xu *et al*., 2009).

Different authors have proposed approaches to address this problem, including graph theory (Freeman, 1997; Freeman *et al*., 1991; Newman, 2005; Xu *et al*., 2008), deterministic optimization models (Lee and Deininger, 1992; Kessler *et al*., 1998; Krause *et al*., 2006), stochastic optimization models and robust optimization models (Xu *et al*., 2008 and 2009). In addition, other methodologies have been used that combine these concepts, such as by Aral *et al*. (2010), and Shen and McBean (2011), who investigate the location of QMP as a multi-objective optimization problem with two competing objectives: (1) minimize detection time and (2) maximize redundancy of detection by the sensor. Thus, the Pareto Principal is used to evaluate the impacts of an increase in the number of QMP using NSGA-II with *TEVA-SPOT* (Berry *et al*., 2008). In addition, in order to decrease false alarms related to contamination events, a study conducted by Koch and McKenna (2011) showed that by combining data from different stations using statistical methods, statistically significant detection clusters can considerably reduce these false alarms.

In spite of the efforts over many years by a large number of researchers, an optimal methodology to locate quality sensors in DWDN has not yet been defined. Therefore, the objective of this study is to propose appropriate methodologies to locate QMP in DWDN with conditions in which hydraulic models are completely calibrated but where water quality models (ie. K_b and K_w parameters) have a high degree of uncertainty because of the lack of QMP.

Proposed Focus

This study proposes two methodologies to locate QMP based on two points of view, each of which present inherent objective functions. The first approach to the problem is related to minimum quality, understood as the monitoring of minimum residual chlorine contents at each point in the network. The second approach considers the possibility of an accidental or malicious (terrorist) contamination event in the system, so that the possible intrusion of contaminants in the DWDN can be detected to ensure the protection of consumers against the risks of exposure. The solutions should take into account normal decay of water quality as well as uncertainty in terms of where and when an external contamination event may occur and its duration (Xu *et al.*, 2009).

Since the results of this methodology are highly dependent on the hydraulic conditions of the DWDN (i.e. demand patterns, location of tanks, valves, pumps, etc.), it is crucial to take into account the most common network operations, for which a completely calibrated hydraulic model is needed. Thus, the results reported herein correspond to known operations in the network and certain previously-determined demand conditions for the hydraulic calibration process.

Theoretical Framework

Water Quality Theory

The water quality simulation model assumes a complete mixture of the solute. The model must be coupled with a hydraulic model of the network adopted by the majority of current computing programs. This type of model was developed by Clark and Coyle (1990) and Rossman *et al*. (1994), and studied by Rossman (2000) and other researchers during the 1990s. The model takes into account convective transport in the tubes, described by the following equation:

$$\frac{\partial C_i}{\partial t} = -u_i \frac{\partial C_i}{\partial x} + R\left(c_i\right) \quad (1)$$

where C_i is the concentration (ML^{-3}) in the tube i, which is a function of the distance x and time t; u_i is the flow velocity (LT^{-1}) in the tube I and R is the reaction velocity ($ML^{-3}T^{-1}$) as a function of concentration. The traditional model also considers the mixture at the junction nodes as complete and instantaneous:

$$C_{\text{outlet}} = \frac{\sum_{j=1}^{j=n} Q_j C_j}{\sum_{j=1}^{j=n} Q_j} \quad (2)$$

where C_{outlet} is the outflow concentration in the junction node ($ML^{-3}TK$); n is the amount of tubes or inlet flows; Q_j is the flow in the inlet of the tube j (L^3T^{-1}) and C_j is the inlet concentration in the tube j (ML^{-3}).

Although the present project refers to the concentration of chlorine, its kinetic reaction must be considered, which depends on the decay coefficient of the water mass (K_b) and the reaction coefficient of the tube wall (K_w). The variation in the concentration with respect to time is modeled using an n-order exponential kinetic:

$$\frac{\partial C}{\partial t} = -KC^n \quad (3)$$

where C is the concentration of chlorine in the tube inlet (ML^{-3}), n is the reaction order, which for chlorine is $n = 1$ (Clark and Coyle, 1990); and K is the reaction coefficient (T^{-1}), which contains the coefficients (K_b) and (K_w) as follows:

$$K = K_b + \frac{K_w + K_f}{r_n\left(K_w * K_f\right)} \quad (4)$$

where K_f is the mass transference coefficient from inside the fluid toward the walls (LT^{-1}) and r_h is the hydraulic radius of the tube (L). The typical reference values for the body and wall coefficients are:

- In free residual chlorine: -0.1/day < K_b < -1.5/day.
- In combined residual chlorine: -0.014/day < K_b < -0.019/day.
- For free residual chlorine: -0.001 m/day < K_w < -1.52 m/ day.
- For combined residual chlorine: $K_w \cong$ –0.006 m/día.

The mass transference coefficient (K_f) from inside the fluid toward the tube walls, introduced by equation (4), is proportional to the Sherwood non-dimensional number and the diffusion of chlorine, since the speed of decay of the disinfectant (chlorine) in the tube depends on how quickly it reaches the walls:

$$K_f + \frac{Sh * d}{D} \qquad (5)$$

where Sh is the Sherwood number; D is the tube diameter (L) and d is the molecular diffusion of the reactive (L^2T^{-1}). In the case of chlorine, the molecular diffusion is between.

$$1.2 * 10^{-9}\,\mathrm{m^2/seg} < d_{\text{cloro}} < 1.4 * 10^{-9}\,\mathrm{m^2/seg}$$

Similarly, the Sherwood number (Sh) is used in mass transference processes to represent the ratio of convection mass transference versus diffusion mass transference.

$$Sh = \begin{cases} 2 & Re < 1.0 \\ 3.65 + \dfrac{0.0668\left(\dfrac{D}{L}\right)Re\left(\dfrac{v}{d}\right)}{1+0.04\left[\left(\dfrac{D}{L}\right)Re\left(\dfrac{v}{d}\right)^{2/3}\right]} & 1 < Re < 2\,300 \\ 0.023 * Re^{0.83} * \left(\dfrac{v}{d}\right)^{0.333} & 2\,300 < Re \end{cases} \qquad (6)$$

Where L is the length of the tube (L); Re is the Reynolds number and v is the kinematic viscosity of the water [1.41 * 10^{-6} m^2/s at 20 °C].

Location of QMP to Ensure Minimum Chlorine Concentration

Since the concentration of chlorine in a DWDN decays after the water leaves the treatment plant, there may not be any residual chlorine at sites far from the plant, which would allow an increase in bacteria levels. Companies providing drinking water services normally determine the disinfectant dosage using trial and error by applying a certain dosage and measuring the concentration at various points in the network. Since it is economically and technically impossible to monitor the disinfectant at all points in a DWDN, it is not known whether all parts of the network are protected and the corresponding risk to the health of the population is therefore not certain (Tzatchkov and Yamanaka, 2004). The study by Tzatchkov (1996) presents a dynamic simulation model which can predict chlorine concentration at any point in a network for each of the simulation intervals, given certain concentrations in the supply sources. This model is composed of two parts: modeling flow in the network (hydraulic model) and modeling the physiochemical transformation of chlorine (water quality model).

Location of WMP to Detect Point Contamination

Over recent years, concern has arisen worldwide about the possibility of DWDN becoming targets of terrorist attacks, and especially of deliberate injections of chemical and biological contaminants (Ostfeld *et al.*, 2008). As a result, efforts have been undertaken to identify low-probability contamination incidents that have a high

impact, thereby providing sufficient time for companies providing drinking water services to respond appropriately in order to mitigate any adverse impact (Berry *et al.*, 2005; Krause *et al.*, 2006). These efforts are useful not only to manage deliberate injections of contaminants but also for accidental events such as the detachment of biofilms from tube walls and later coloration of water due to these "contaminants."

In the study presented by Berry *et al.* (2005), the authors consider an integer programming model based on a series of simplifications:

1. A point contamination event occurs only at one point in the network.
2. The total exposed population does not relate to a specific health impact.
3. Sensors protect the population downstream.
4. Changes in demand patterns are ignored such that each period is treated independently.

Since it is not known *a priori* where a contamination event will occur, the proposal is to locate QMP for a wide set of intrusion scenarios.

Given the complexity of DWDN, different computing tools have been developed to facilitate this type of analysis. For example, the US Environmental Protection Agency (EPA), Sandia National Laboratories, Argonne National Laboratory and the University of Cincinnati (US EPA, 2008) developed free software called *TEVA-SPOT*(Berry *et al.*, 2008) to define the number of QMP needed in a DWDN in order to reduce the risk of contamination incidents based on the norm for an objective function (Murray *et al.*, 2008).

Case Study, Prototype Network

In order to identify a methodology to optimize the location of sensors in a DWDN, 37 networks were analyzed, corresponding to each of the hydraulic sectors into which the distribution system for the city of Bogota, Colombia is divided. The project, developed along with the Bogota Aqueduct and Sewer Company (Empresa de Acueducto y Alcantarillado de Bogotá, EAAB, Spanish acronym) consisted of a first phase for the hydraulic calibration of the models, during which over 90 points were used to measure flow and/or pressure, and consumption by users was measured over four months. As a result, a hydraulic model was obtained with correlation coefficients over 0.85 for pressure and over 0.90 for flow at the calibration points. In addition, four primary hydraulic operating configurations were identified in the network at different locations in the three water storage plants (reservoirs) in the city and the 15 primary tanks in the network.

After calibrating the hydraulic models, the second phase was conducted. This consisted of identifying the optimal locations of the QMP to ensure minimum water quality (minimum levels of chlorine) as well as detect accidental or intentional contamination. In the case of the EAAB, this would enable addressing the problem of contamination from the detachment of biofilms. The latter required a method with early alerts to warn of turbidity events.

Given the size of the project and the network in the city of Bogota, the results of the second phase of the project are shown (below) from only one of the 37 sectors (sector 13).

Description of the Prototype Network

Sector 13 in Bogota (Figure 1) has 7 616 tubes, 6 692 junction nodes and 3 feed sources. This network needed to be divided for some of the analyses. Three hydraulic subsectors were created —upper, middle and lower. The

Figure 1. Layout of the Aqueduct Network (EAAB) in Bogota.

upper subsector has 1 021 tubes, 900 junction nodes, 1 valve and 1 reservoir; the middle subsector has 5 125 tubes, 4 488 junction nodes, 6 valves and 1 reservoir; and the lower subsector 1 441 tubes, 1 287 junction nodes, 1 valve and 1 reservoir (Figure 2).

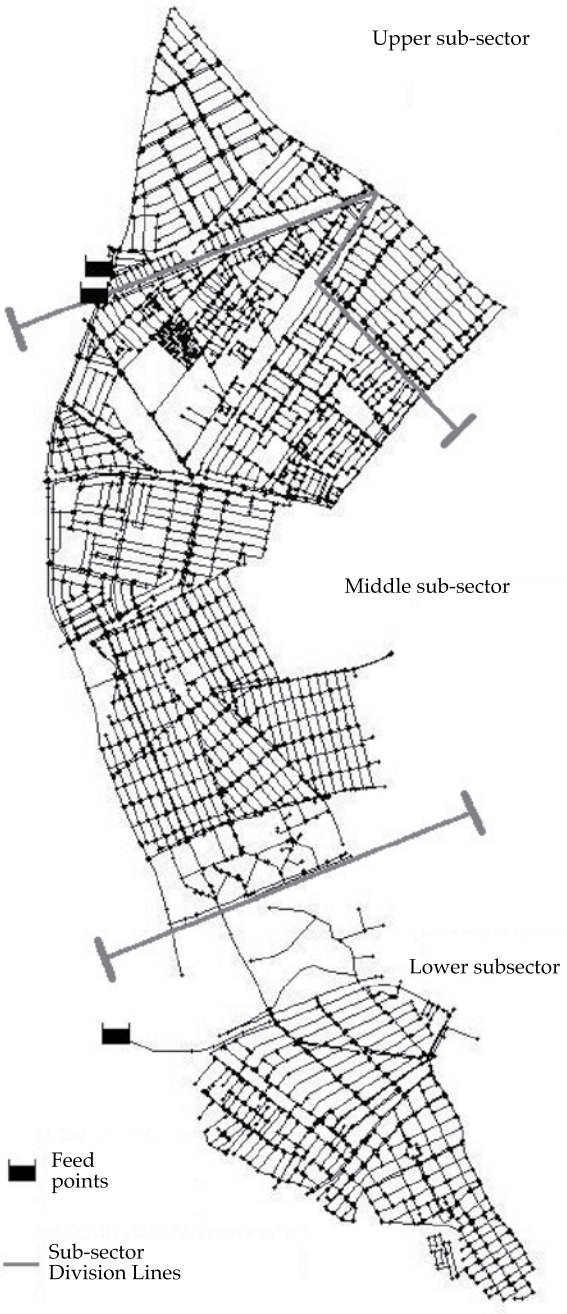

Figure 2. Sector Layout, Bogota.

Minimum Quality Methodology

To determine the ideal location of the QMP to ensure a minimum chlorine concentration, a program was developed called *Minimum Quality*, whose function is to simulate different scenarios for the quality of the water in the network (including the corresponding previous hydraulic execution), and for each scenario, to identify the junction nodes with concentrations lower than the 0.01 percentile (1.0%) of all junction nodes in the model. Nevertheless, the restriction was introduced that this set of "critical" junction nodes in each scenario must have no more than 100 junction nodes or less than 10; in those cases, the percentile value was adjusted to comply with this restriction.

Since the DWDN in the city of Bogota does not have values for K_b and K_w coefficients, and Sector 13 only has one QMP (Venecia QMP), 15 sets of values were determined based on a review of the typical values reported in the literature, thereby appropriately representing the behavior of chlorine decay in the DWDN for each sector in Bogote. Since extreme scenarios were excluded, several sensitivity analyses were performed (Table 1).

Table 1. Scenarios Corresponding to K_b and K_w Tested during the Development of the *Minimum Quality* Methodology.

Scenario	K_b (d^{-1})	K_w ($m*d^{-1}$)
1	0	-0.01
2	0	-0.1
3	0	-1
4	0	-3
5	0	-5
6	-0.1	0
7	-1	0
8	-3	0
9	-5	0
10	-10	0
11	-5	-0.5
12	-1	-0.5
13	-3	-0.5
14	-3	-0.2
15	-3	-1

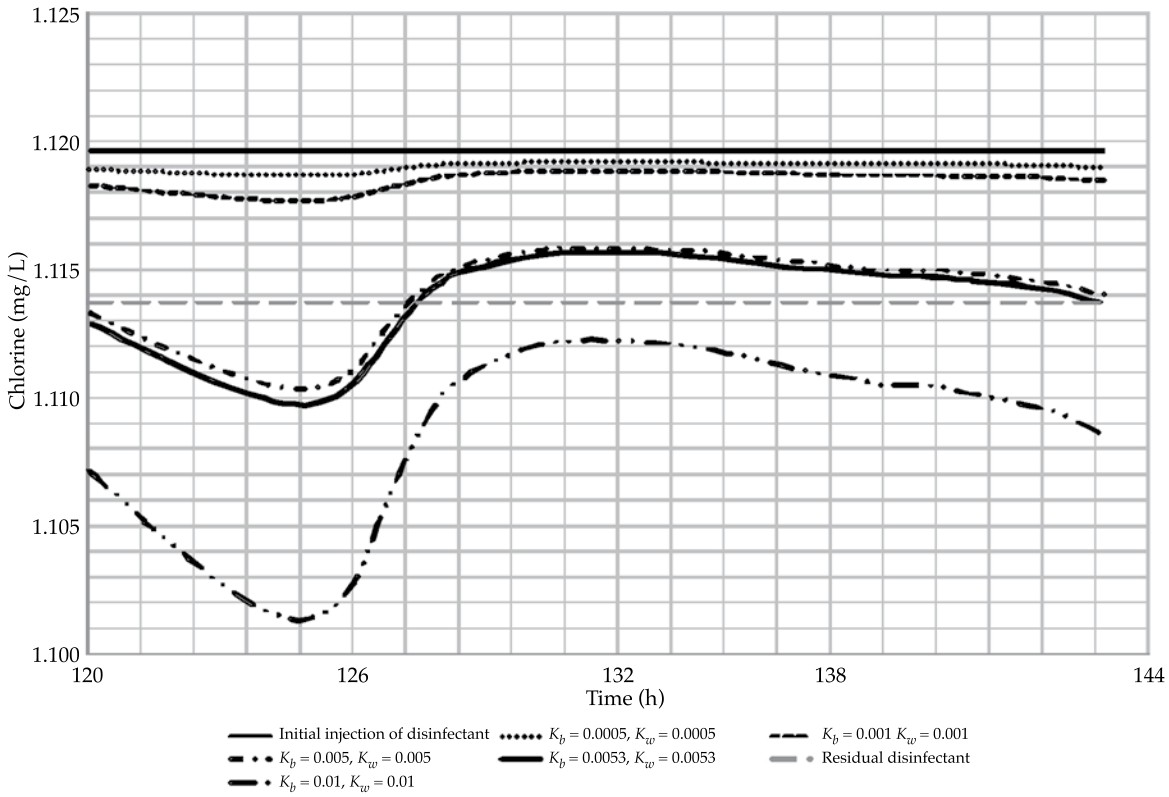

Figure 3. Sensitivity in Sector 13, Time Series Comparison.

To determine the 15 scenarios, different configurations were tested, in which the values of K_b and K_w were equaled until finding the result for chlorine decay that best fit the value registered at the Venecia QMP (Figure 3). Thus, the values 0.0053/day for K_b and 0.0053 M/day for K_w were obtained, which are very low compared to other studies (Vasconcelos *et al.*, 1996; Chang *et al.*, 2009; Hallam *et al.*, 2003). In addition, another two analyses were performed to determine scenarios for K_b and K_w by obtaining the ratios of the coefficients to identify similar scenarios resulting in roughly the same chlorine decay values. Lastly, the scenarios were selected by maintaining the K_b and K_w ratio such that in certain scenarios K_b would be the dominant coefficient and in others K_w, while resulting in similar concentrations in order to obtain a wider range of possibilities.

In addition to the number of scenarios under consideration, the start time (hours) and delta time for the quality calculations need to be defined. To determine the value of the start time, the behavior of several hydraulic models was analyzed and 120 hours was established as the start time for the quality calculation —the moment at which chlorine is stabilized at all junction nodes in the system. The second input parameter, the delta time (Δt) of the calculation, determines residual chlorine at the junction nodes. For the case study, Δt of 1 minute, 30 seconds or 1 second was used, with differences found of up to 42% in chlorine concentration values at some junction nodes but with no significant

differences in the identification of junction nodes with concentrations under the 0.01 percentile.

After inputting these data into the program, the program established a concentration of 1 mg/L of chlorine for the reservoirs and 0 mg/L for the rest of the junction nodes. The program then began to construct the data structures for the tubes, junction nodes and minimum chlorine. At this point the parameters were defined for the chlorine analysis cycle, in which the number of scenarios (m) and the coefficients K_b and K_w corresponding to each scenario were established. Although at first all the scenarios underwent the same calculation process, it is important to mention that for the first scenario ($m = 1$), the process included a filter, and after having assigned K_b and K_w and calculated the hydraulics (pressure and velocities) in EPANET, the filter adopted the valid junction nodes and discarded the rest, the former being those in which $v \geq 0.005$ m/s in the feed tube. Thus, junction nodes with velocities under this value were discarded based on the assumption that there was no demand.

Based on the 15 scenarios run with different values corresponding to the network's quality parameters (Table 1), a count (frequency analysis) was performed of the scenarios in which the junction node was within the set of junction nodes with concentrations under the 0.01 percentile, thereby identifying recurring junction nodes with low chlorine concentration.

Location of QMP in the Network's Sector 13

The frequency analysis of critical junction nodes enables identifying the repetitiveness of junction nodes with minimum chlorine. The frequency analysis is presented in the Figure 4. It is divided into five frequency intervals. Minimum chlorine frequencies

Figure 4. Frequency Analysis for Minimum Chlorine, *Minimum Quality*.

were observed between 1 and 3, 4 and 6, 7 and 9, 10 and 12, and 13 and 15. A general trend was identified in which the critical points were located near the junction nodes furthest from the supply sources, understanding these as junction nodes in which the flow must be highest, even if the topological distance is relatively short. In addition, it is worth highlighting that even with a velocity filter, special care should be taken with tubes that are closed or those

not receiving flow for some reason. For the specific case of Sector 13, most of the junction nodes with minimum chlorine values (frequency between 13 and 15) were found at the lowest point in the sector. While the program identifies the minimum chlorine points representative of the system, this does not mean that the QMP should be located at all those points, but rather, it provides an idea of the specific zone in which a QMP should be located, since this zone would be representative of the junction nodes around it. Therefore, it would be prudent to locate only one QMP in that area.

Methodology to Detect Contamination Events, TEVA-SPOT

As mentioned previously, the evaluation of the seriousness of a certain attack or detachment of biofilms in a DWDN is related to the effect of the attack on a particular aspect of the system. While this can be determined using a large number of indicators, they can be summarized as those that measure detection time, the area of the contamination and the number of persons affected. *TEVA-SPOT* (Berry *et al.*, 2008) software enables performing calculations and analyses based on results from the following parameters: 1. Detection time in minutes from the beginning until detection by the first sensor; 2. Area of the contamination in the network, measured by the total length of the tubes contaminated during the response time; 3. Consumed mass at junction nodes with demand; 4. Volume of consumed water contaminated; 5. Number of incidents not detected by any sensor before the simulation ends; 6. Number of individuals exposed to the contaminant; 7. Number of individuals who receive a contaminant dosage above a certain threshold; and 8. Number of deaths (Berry *et al.*, 2008).

As a first step in designing the QMP network, the possible scenarios against which protection is desired need to be determined. Therefore, to design of the protection system, *TEVA-SPOT* requires a calibrated hydraulic model and a file that defines the possible contamination scenarios. The second step is to calculate the impact of each of these on consumed mass, detection time, area of the contamination plume, volume of water contaminated and incidents not detected by the different scenarios proposed. After calculating the different types of impacts, the next step is to determine a certain number of QMP so as to minimize the effect of the events. In addition, the program needs the number of QMP and the type of optimization algorithm desired.

Finally, after obtaining the partial solutions for the points, the fourth step is to perform an iterative process to study the performance of those solutions in terms of the other restrictions to be met, thereby obtaining the one that best satisfies all the expectations. It is important to mention that when there are very large restrictions, the result can often be delayed a long time. In addition, *TEVA-SPOT* makes it possible to evaluate the effect produced by turbidity events (*e.g.* detachment of biofilms), for which the best indicators are those that enable determining a maximum threshold (*e.g.* consumed mass at the junction nodes).

Location of Sensors in Sector 13

Sector 13 has three feed points that divide the sector into three hydraulic subsectors. The analysis of this network found that, for each of the indicators, the location of the three sensors did not include the upper hydraulic subsector (Figure 2), which is fed by an independent source. Thus, an independent analysis of each subsector was considered useful (Figure 5). The first analysis consisted of determining the sensitivity of the points located by varying the amount of the mass

Figure 5. Location of Sensors, *TEVA-SPOT*, Sector 13.

injected at the junction nodes with demand. This analysis showed that a variation in the mass injected at the juntions results in significant changes in the consumed mass indicator. Thus, for example, by injecting 50 mg/L, the average impact is approximately 50% less than injecting 100 mg/L. In addition, when injecting 200 mg/L, the average consumed mass at the junction nodes is twice that of 100 mg/L. In contrast, the other indicators are not affected by a variation in the injected mass. The Figure 6 shows the results obtained from locating a sensor at each of the divisions in the network. The sensors to minimize detection time, consumed mass at the junction nodes and undetected incidents had the same locations, while the sensors to minimize the area of the contamination of the tubes were located at different points.

When comparing the average impact of the location of the QMP between the complete network versus each subsector

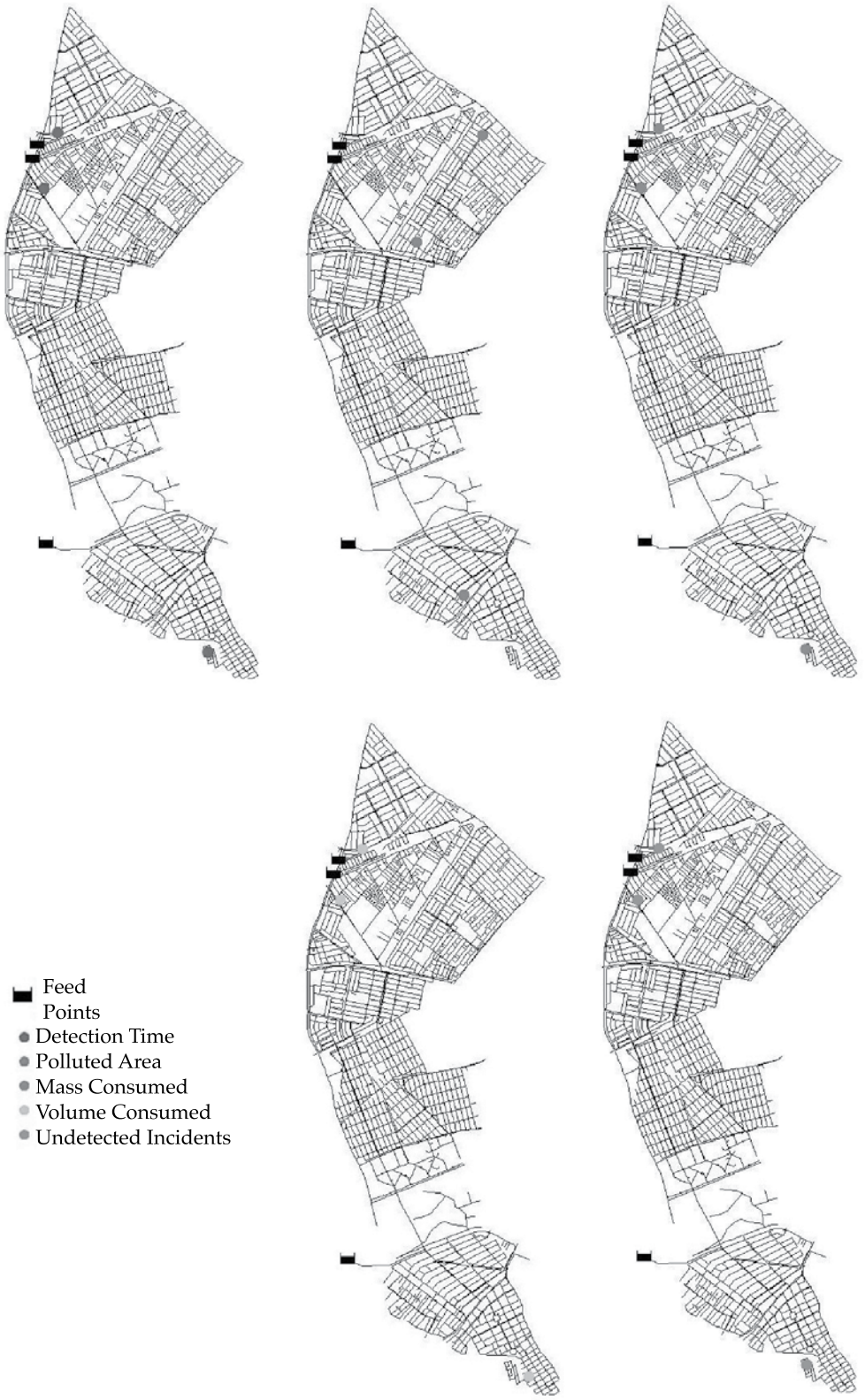

Figure 6. Location of Sensor with Five Different Location Criteria in each Subsector in the Network, *TEVA-SPOT*.

independently, the average impact of the latter was reduced across all the indicators. It is worth mentioning that although the average impact decreased notably in the upper and lower subsectors, it increased considerably in the middle subsector. This is because the latter contained more junction nodes and tubes than the other two subsectors and, therefore, when considering the complete network, *TEVA-SPOT*'s prioritized the location of sensors in the middle subsector. Therefore, in cases where the number of sensors is limited, an analysis of the location of sensors by subsector is recommended, if permitted by the DWDN for which the QMP network is being designed. In another analysis, the simulation time was varied from 144 hours (six days) to 96 hours (four days), with no change in the location of the QMP for any of the cases. In addition, it was possible to observe that the indicators for contamination area, consumed mass and undetected incidents did not significantly change according to simulation time. Meanwhile, indicators of detection time and consumed volume at the junction nodes directly increased with the duration of the simulation. The significant increase shown in these latter two indicators is because *TEVA-SPOT* assigns the duration time of the simulation to the detection time of an undetected incident. Therefore, a high percentage of undetected incidents is assigned when the simulation time is longer (144 hours), which in turn will generate a larger volume of consumed water since it is related to the incidents not detected from when the simulation begins until it ends.

Conclusions

Taking into account all of the analyses performed, the most important conclusion is that the values of K_b and K_w do not significantly influence the location of QMP in a DWDN.

It was determined that the number of QMP required does not increase linearly with population density. Thus, hydraulic modeling can use skeleton methods. Nevertheless, the different types of hydraulic operations do affect the methodology.

The two methodologies implemented require a calibrated hydraulic model of the network. Therefore, companies providing drinking water services should include this step before more precisely choosing the QMP locations.

Based on a calibrated hydraulic model, the *Minimum Quality* program makes it possible to obtain critical points that present the highest chlorine decay for different decay coefficient scenarios. Overall, the program enables locating junction nodes at which residual chlorine is minimal. It is important to highlight that the results obtained do not indicate the exact location or number of sensors to measure quality in a drinking water distribution network, but rather they provide a series of options that, along with criteria and experience, companies providing drinking water services should use to select definitive QMP.

In terms of the design of early warning QMP networks, *TEVA-SPOT* (Berry *et al.*, 2008) is a reliable tool that quickly and easily determines the location of QMP. Since the program locates them based on the information supplied, it is important for the user to apply their criteria and experience to indicate the restrictions required and to evaluate the results reported.

The analyses conducted with *TEVA-SPOT* (Berry *et al.*, 2008) demonstrate that the optimal locations of QMP to minimize detection time, consumed mass and number of undetected incidents contained several location points in common. On the other hand, when evaluating the different indicators to minimize the area of the contaminated tubes, a significant increase can be observed

in the average impact of each indicator. The analysis of simulation time and/or injected mass did not result in changes in the location of the quality monitoring points when increasing or decreasing these variables.

Finally, the different QMP network configurations obtained by this study depend on the system's specific operating mode, which is determined by hydraulic models. A change in the operating mode will imply a change in the hydraulics of the system and, therefore, the configuration of the QMP network will change according to new flow conditions. It is important to understand that the design of QMP networks is dynamic and depends on the hydraulic conditions at a particular moment. The sensor network should be designed as many times as the system has operating modes. Of course this is costly, therefore it is recommended to try to maintain similar hydraulic conditions over time and avoid significant operational changes in the networks.

Received: 18/10/2011
Accepted: 24/06/2013

References

ARAL, M., GUAN, J., and MASLIA, M. Optimal Design of Sensor Placement in Water Distribution Networks. *Journal of Water Resources Planning and Management*. Vol. 136, No. 1, 2010, pp. 5-18.

BERRY, J.W., FLEISCHER, L. HART, W., and PHILLIPS, C. Sensor placement in municipal water networks. *Journal of Water Resources Planning and Management*. Vol. 131, No. 3, 2005, pp. 237-243.

BERRY, J., BOMAN, E. RIESEN, L.A., HART, W., PHILLIPS, C., and WATSON, J.P. *User's Manual, TEVA-SPOT Toolkit 2.2*. Albuquerque, USA: Sandia National Laboratories, 2008.

CHANG, K., GAO, L. WU, W.Y., and YUAN, Y.X. Water quality comprehensive evaluation method for large water distribution network based on clustering analysis. *Proceedings of Computer and Control in the Water Industry*. Boxall, J. and Maksimovic, C. (editors). Sheffield: Taylor & Francis, 2009.

CLARK, R.M. and COYLE, J.A. Measuring and modeling variations in distribution system water quality. *Journal of the American Water Works Association*. Vol. 2, 1990, pp. 46-53.

FREEMAN, L.C., BORGATTI, S.P. and WHITE, D.R. Centrality in valued graphs: A measure of betweenness based on network flow. *Social Networks*. Vol. 13, 1991, pp. 141-154.

FREEMAN, L. A set of measures of centrality based on betweenness. *Sociometry*. Vol. 40, No. 1, 1997, pp. 35-41.

HALLAM, N.B., HUA, F., WEST. J.R., FOSTER, C.F., and SIMMS, J. Bulk decay of chlorine in water distribution systems. *Journal of Water Resources Planning and Management-ASCE*. Vol. 129, No. 1, 2003, pp. 78-81.

KESSLER, A., OSTFELD, A., and SINAI, G. Detecting accidental contaminations in municipal water networks. *Journal of Water Resources Planning and Management*. Vol. 124, 1998, pp. 192-198.

KOCH, M.W. and McKENNA, S.A. Distributed sensor fusion in water quality event detection. *Journal of Water Resources Planning and Management*. Vol. 137, No. 1, 2011, pp. 10-19.

KRAUSE, A., LESKOVEC, J., ISOVITSCH, S., XU, J., GUESTRIN, C., VANBRIESEN, J., SMALL, M., and FISCHBECK, P. *Optimizing Sensor Placements in Water Distribution Systems Using Submodular Function Maximization*. Cincinnati: WDSA Symposium 2006, March 2008, pp. 1-17.

KRAUSE, A. and GUESTRIN, C. Robust Sensor Placement for Detecting Adversarial Contaminations in Water Distribution Systems. *World Environmental and Water Resources Congress 2009*, Kansas, May 2009, pp. 1-10.

LEE, B.H. and DEININGER, R.A. Optimal locations of monitoring stations in water distribution systems. *Journal of Environmental Engineering*. Vol. 118, No. 1, 1992, pp. 4-16.

MURRAY, R., BARANOWSKI, T., Hart, W., and JANKE, R. *Risk reduction and sensor network design*. WDSA Symposium, Kruger National Park, South Africa, 2008.

NEWMAN, M.E.J. A measure of betweenness centrality based on random walks. *Social Networks*. Vol. 27, 2005, pp. 39-54.

OSTFELD, A., UBER, J. *et al*. The Battle of the Water Sensor Networks (BWSN): A Design Challenge for Engineers and Algorithms. *Journal of Water Resources Planning and Management*. Vol. 134, No. 6, 2008, pp. 556-568.

PREIS, A. and OSTFELD, A. Multiobjective Contaminant Sensor Network Design for Water Distribution Systems. *Journal of Water Resources Planning and Management*. Vol. 134, No. 4, 2008, pp. 366-377.

ROSSMAN, L.A., CLARK, R.M., and GRAYMAN, W.M. Modeling Chlorine Residuals in Drinking Water Distribution Systems. *Journal of Environmental Engineering, ASCE*. Vol. 1210, No. 4, 1994, p. 803.

ROSSMAN, L.A. *Epanet 2 User´s Manual*. Cincinnati: EPA United States Environmental Protection Agency, 2000.

SHEN, H. and McBEAN, E. Pareto optimality for sensor placements in a water distribution system. *Journal of*

Water Resources Planning and Management. Vol. 137, No. 3, 2011, pp. 243-248.

TZATCHKOV, V.G. Numerical Model of Chlorine Decay in Drinking Water Networks with Unsteady Flow. *Hydraulic Engineering in México*. Vol. XI, No. 3, 1996, pp. 53-60.

TZATCHKOV, V.G., ALCOCER-YAMANAKA, V.H., and ARREGUÍN-CORTÉS, F.I. Chlorine decay due to bulk water reaction in distribution networks. *Hydraulic Engineering in México*. Vol. XIX, No. 1, 2004, pp. 41-51.

US EPA. *User´s Manual: TEVA-SPOT Toolkit*. Cincinnati: USA Environmental Protection Agency, 2008.

VASCONCELOS, J.J. *Characteristics and modeling of chlorine decay in distribution systems*. Denver: AWWA Research Foundation, 1996.

WOO, H.-M., YOON, J.-H., and CHOI, D. *Optimal Monitoring Sites Based on Water Quality and Quantity in Water Distribution Systems*. World Water Congress 2001, Berlin, Germany, 2001.

XU, J., FISCHBECK, P., SMALL, M., VANBRIESEN, J., and CASMAN, E. Identifying Sets of Key Nodes for Placing Sensors in Dynamic Water Distribution Networks. *Journal of Water Resources Planning and Management*. Vol. 134, No. 4, 2008, pp. 378-385.

XU, J., VANBRIESEN, J., SMALL, M., and FISCHBECK, P. *Decision making under information constraints*. World Environmental and Water Resources Congress, ASCE, Kansas City, Missouri, USA, 2009.

Institutional Address of the Authors

M.C. Juan G. Saldarriaga

Profesor Titular
Departamento de Ingeniería Civil y Ambiental
Universidad de los Andes
Carrera 1 Este # 19A-40
Bogotá, Colombia
Teléfono: +57 (1) 3394 949, extensión 2805
jsaldarr@uniandes.edu.co

M.C. María Ximena Hernández
M.C. Cesar Prieto
M.C. Mauricio Jurado
M.C. Sara Gacharná

Investigadores
Centro de Investigaciones en Acueductos y Alcantarillados (CIACUA)
Universidad de los Andes
Carrera 1 Este # 19A-40
Bogotá, Colombia
Teléfono: +57 (1) 3394 949, ext. 3521
mx.hernandez41@uniandes.edu.co
ce-priet@uniandes.edu.co
c-jurado@uniandes.edu.co
sc.gacharna41@uniandes.edu.co

M.C. Diego Páez

Profesor Instructor
Departamento de Ingeniería Civil y Ambiental
Universidad de los Andes
Carrera 1 Este # 19A-40
Bogotá, Colombia
Teléfono: +57 (1) 3394 949, extensión 3717
da.paez27@uniandes.edu.co

Click here to write the autor

El Salto de San Antón, Cuernavaca, Morelos, Mexico.

Photo: Víctor Manuel Pineda Blancarte.

Methodology for the Technical-Economic Analysis of Wastewater Regeneration and Reutilization Systems

• Luis Seguí-Amórtegui* • Oscar Alfranca-Burriel •
Universidad Politécnica de Cataluña, España
*Corresponding Author

• Gabriela Moeller-Chávez •
Universidad Politécnica del Estado de Morelos, México

Abstract

SEGUÍ-AMÓRTEGUI, L., ALFRANCA-BURRIEL, O. & MOE-LLER-CHÁVEZ, G. Methodology for the Technical-Economic Analysis of Wastewater Regeneration and Reutilization Systems. *Water Technology and Sciences* (in Spanish). Vol. V, No. 2, March-April, 2014, pp. 55-70.

Establishing the cost and price of reclaimed water is important to the design and exploitation of a Wastewater Reclamation and Reuse System (WRRS). While it is possible to obtain a detailed rough estimate of the cost of a WRRS, the price of reclaimed water is a different matter. This is mainly because no reclaimed water market exists to enable determining the price and, therefore, the only reference value is the price of the water from conventional sources. Nevertheless, this price does not reflect all the impacts involved in the reclamation and reuse of wastewater. The economic-financial analysis of WRRS has traditionally focused on the system's private costs and income. The methodology presented herein, in addition to considering these private impacts, incorporates factors external to the project through the analysis of both positive and negative external impacts. The methodology is suitable to the particularities of the WRRS, serving as a "customized" tool for decision-makers to determine whether or not the implementation of this type of system is useful. This methodology evaluates the WRRS from a multi- and interdisciplinary perspective. The main objective is to optimize the benefits of the project. The methodology herein has been compared and applied to diverse case studies by the authors as well as other researchers.

Keywords: Project analysis, water reuse, water economics.

Resumen

SEGUÍ-AMÓRTEGUI, L., ALFRANCA-BURRIEL, O. & MOELLER-CHÁVEZ, G. Metodología para el análisis técnico-económico de los sistemas de regeneración y reutilización de las aguas residuales. Tecnología y Ciencias del Agua. *Vol. V, núm. 2, marzo-abril de 2014, pp. 55-70.*

Establecer el costo y el precio del agua regenerada es importante en el diseño y la explotación de un Sistema de Regeneración y Reutilización de Aguas Residuales (SRRAR). Si bien es cierto que se puede tener una aproximación detallada del costo de un SRRAR, no sucede lo mismo con el precio del agua regenerada. Esto se debe básicamente a que no existe un mercado de agua regenerada que permita determinarlo y, por tanto, el único valor de referencia es el precio del agua de las fuentes convencionales. Sin embargo, este precio no refleja todos los impactos que conllevan la regeneración y reutilización de las aguas residuales. De forma tradicional, el análisis económico-financiero de los SRRAR centraba su atención en los costos e ingresos privados del sistema; la metodología que se presenta, además de considerar estos impactos privados, incorpora las externalidades del proyecto a través del análisis de los impactos externos tanto positivos como negativos que afectan al mismo. La metodología está adecuada a las particularidades de los SRRAR, de tal forma que se convierte en una herramienta "a la medida", que le permite al tomador de decisiones emitir un juicio sobre la conveniencia o no de implementar este tipo de sistemas. Esta metodología evalúa los SRRAR desde una perspectiva multi e interdisciplinaria. El objetivo principal es determinar la maximización de los beneficios del proyecto. La metodología que aquí se expone ha sido contrastada y aplicada en diversos casos de estudio tanto por los autores como por otros investigadores.

Palabras clave: *análisis de proyectos, reúso de agua, economía del agua.*

Introduction

El avance tecnológico en el ámbito de la rege-Important advances have been made in technology used for the reclamation of wastewater over recent decades. These changes have been accompanied by changes in regulations (such as the Water Framework Directive), signifying significant changes in the analysis of wastewater reclamation and regeneration projects. As a consequence, the current feasibility of wastewater reuse projects is dependent not only on technological factors but also on a multidisciplinary analysis involving not only economic and technological factors but also environmental, cultural and social factors. Thus, a detailed analysis of costs and benefits (private and social) is key when evaluating the potential of projects to reuse reclaimed water (García *et al*., 2001; Chu *et al*., 2003; Asano, 2007).

Nevertheless, the economic aspect may be that which is least often addressed by researchers of wastewater reclamation and reuse. This is because, generally, only private costs are considered while external effects (positive and negative) are relegated to a series of statements about the advantages of reclamation and reuse. This can be observed in works such as those by Shabman and Stephenson, 2000; Hutton and Haller, 2004; AQUAREC, 2006; Bixio et al., 2006; Färe et al., 2006; Hochstrat et al., 2007; Godfrey et al., 2009; Hernández et al., 2010.

The overall methodologies used to plan a WRRS project only indicate the need to perform an economic analysis and consider the private costs of a WRRS.

In addition, the specialized literature mentions and describes both positive and negative impacts from implementing a WRRS, which in many cases are evaluated independently, as can be seen in the works by Godfrey et al., 2009; North and Griffin, 1993; Hanley and Spash, 1993; Field, 1997; Curry and Weiss, 1993; Hutton and Haller, 2004; Chen and Wang, 2009, and Veronesi et al. (2013), among others.

Nevertheless, it is not easy to find a protocol that, from a multidisciplinary perspective, collects and groups the identification and description of the most relevant impacts that should be considered in the technical-economic analysis of a WRRS project.

Thus, in the field of wastewater reclamation and reuse, no methodology exists to associate the biophysical impacts of a WRRS with their economic repercussions. This statement is supported, for example, by recommendations from a multidisciplinary group named "Reclaimed Water Task Force," whose objective is to identify limitations, obstacles and opportunities to increase the use of reclaimed water in the state of California, United States (Katz, 2003).

The objective of the article herein is to present a multidisciplinary methodology for the technical-economic analysis of a WRRS. This methodology includes and quantifies private as well as social (external) impacts related to the functioning of the water treatment system.

The primary interest of this article is to establish a simple methodology for the technical-economic analysis of WRRS to support decision-makers in resolving problems and in the implementation and operations of a WRRS. Over recent years, the literature related to WRRS has not presented a methodological procedure, applicable from a professional perspective, to relate technical and economic aspects. While the methodologies used for WRRS recognize that economic variables significantly influence the planning model, they do not consider the influence of the model on these variables. Therefore, an exogenous problem currently exists with respect to decision-making.

Economic analyses are based on cost analyses and, in the best of cases, on a comparison with water from conventional sources (surface and groundwater). Nonetheless, this type of analysis does not provide indications of whether a WRRS is cost efficient, since it does not include a cost-benefit analysis of the system. The methodology presented herein provides an intuitive and simple protocol that compares expenses and income in order to simply obtain a criterion for the cost-efficiency of the system.

A key part of this proposed methodology is the impacts generated by a WRRS. The practice of reclamation and reuse of wastewater includes a series of private and external impacts whose values are not determined, for example: negative external impacts such as the effect on third parties from the reuse of reclaimed water, or positive external impacts such as the reduction in the pollution of water bodies, the recovery of materials and energy and/or the increase in the availability of water. Together, these impacts can result in wastewater reclamation and reuse being an economically cost-efficient activity.

One of the main advantages of this methodology is its identification and discussion of these impacts. Currently, documentation of the most relevant impacts of a WRRS has been isolated, generally involving timely solutions for specific case studies. Supported by current literature, consultation with experts and professional experience, this study seeks to collect and describe the main impacts in order to include them in an economic evaluation of the construction and use of a WRRS (Seguí, 2007; Seguí *et al.*, 2009).

Description of the Methodology

The methodology presented herein seeks to provide methodological advances that decrease the uncertainty and investment risks related to WRRS.

In addition to considering private impacts, the methodological proposal herein also incorporates the externalities of a WRRS in the analysis of a project to install a wastewater reclamation plant, quantifying the external costs and benefits involved. That is, it presents a cost-benefit analysis (CBA) technique for this type of project from a social perspective.

This methodology includes the private costs and benefits (energy, staff, reagents and investments, among others) related to the operations of the system as well as factors external to the system (environment, education and health).

For the evaluation of a WRRS, the social CBA should be applied since the implementation of a project of this type involves effects that go beyond the walls of a private plant.

The CBA, which includes the externalities related to the wastewater treatment system, was adapted to the characteristics and particularities of the WRRS in order to provide decision-makers with a "custom" tool to determine the usefulness of implementing this type of project.

The methodology presented in this work has been applied to several analyses of reuse and desalination technologies, for example, Hernández *et al.*, 2006; Urkiaga *et al.*, 2006; Hlavinek *et al.*, 2008; Guerrero-García-Rojas *et al.*, 2008; Alfranca *et al.*, 2011; Uggetti *et al.*, 2011.

Figure 1 provides a schematic description of the different stages to be performed in the application of this methodology, which are described in detail in the present article.

Definition of Objectives

The objective of the economic-technological analysis is to evaluate the WRRS by

maximizing the difference between income and costs associated with the production of reclaimed water.

This optimization takes into account both the private as well as external impacts, as seen in equation (1).

This economic optimization criteria was selected because of its intuitive interpretation as well as it applicability to the type of problems to be evaluated.

The objective function to optimize is:

$$MAX\ B_T = \sum_{n=0}^{n}\left[\begin{array}{l}(ARV_n * SP_n) - (IC_n + OMC_n \\ + FC_n + TAX_n) + (PE_n - NE_n) - OC_n\end{array}\right] \quad (1)$$

Where:

B_T = Total benefit.
ARV = annual reclaimed water volume.
SP = sale price of reclaimed water.
IC = Investment costs.
OMC = operations and maintenance costs.
FC = Financial costs.
TAX = taxes.
PE = positive externalities from impact ep_j.
NE = negative externalities from impact en_j.
OC = opportunity cost.
n = year.

Definition of the Study Area

The hydrological basin should be the initial and most general area of analysis

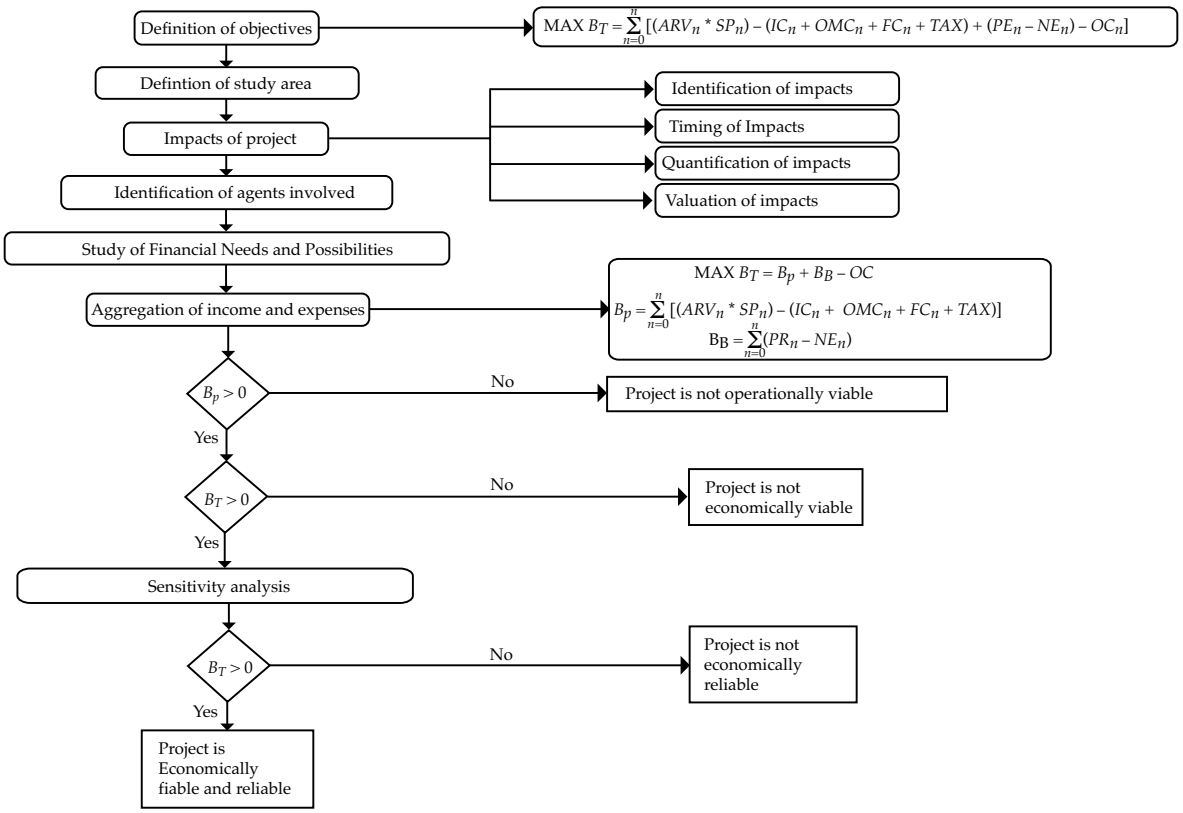

Figure 1. Stages in the Economic Analysis of Wastewater Reclamation and Reuse Projects (Seguí, 2007; Seguí *et al.*, 2009).

(Dourojeanni, 1999; Directiva CE, 2000). Based on this, and depending on the level of the project, the area can be reduced to smaller management units, such as a sub-basin, micro-basin or aquifer.

Defining the study area is key to determine the influence of the project and thereby determine the impacts produced in the area.

Impacts of the Project

An impact will be defined as any consequence resulting from the implementation of a WRRS —desired or not, intentional or accidental— that is possible to measure in a specific area of a water management unit. Internal and external impacts will be described first.

Internal, or private, impacts are those directly related to the reclaimed water production process and its later reuse. They primarily correspond to income (positive private impacts) from the sale of reclaimed water or some byproduct, or costs related to investments and operations and maintenance of the WRRS (negative private impacts).

Although external impacts (for example, effects on third parties, pollution control, increase in the availability of the water or guaranteeing supply) can be more difficult to calculate, they are not less important since an impact with these characteristics can be risky for the economic viability of a project or for the project itself.

Identification of Impacts

The identification of the impacts of a WRRS is the most complicated and difficult part of an evaluation. Detecting impacts depends on the WRRS involved and the objectives sought. The participation of a multidisciplinary team of specialists able to identify these impacts is often needed.

The greatest contribution of the methodology herein is a compilation and inventory of the impacts related to the WRRS. This compilation is primarily empirical.

The objective of this section is to provide an overall perspective of the most relevant impacts for those responsible for applying the methodology, so as to have all the elements that need to be considered when applying the methodology to a specific study case. Therefore, the impacts identified herein are only intended to provide the key elements in order to understand them conceptually.

This study seeks to describe the largest number of identifiable impacts (see Seguí, 2007; Seguí *et al.*, 2009; Seguí, 2004) in order to generalize this methodology for its application in any region. Thus, it presents the key elements of impacts that are well documented, such as a decrease in pollution of water bodies, as well as novel impacts such as the recovery of energy from wastewater in order to melt ice on streets.

Based on the sources of information cited and in order to identify and analyze the impacts related to WRRS, six broad groups have been defined (Table 1): 1) Infrastructure, 2) conditioning and reuse of pollutants, 3) use of the resource, 4) public health, 5) environment and 6) education.

Timing of Impacts

Each of the agents in the project is subject to certain impacts that are important to identify throughout the useful life of the WRRS. Since the agent seeks to obtain an income as soon as possible and delay the moment of payment, it is important to consider the date the impact occurs.

Quantification of the Impacts

Some of these impacts can be quantified directly in monetary units. Nevertheless,

Table 1. Summary of the Impacts of Wastewater Reclamation and Reuse (Seguí, 2007; Seguí *et al.*, 2009; Seguí, 2004).

Impact Group	Description of Impact
Infrastructure	Water catchment and supply
	Treatment of water supply
	Conduction and transport of drinking water
	Rehabilitation and expansion of sewage networks
	Treatment and/or discharge of wastewater
	Wastewater reclamation and reuse
Conditioning and reuse of pollutants	Nitrogen
	Phosphorus
	Sludge
	Energy
Use of the resource	Amount of water
	Supply guarantees
	Water quality
Public Health	Biological risks
	Physical-chemical risks
Environment	Surface water
	Groundwater
	Pollution of water bodies
	Hábitat de humedales y ríos
Education	Technical
	Water culture

it will often be necessary to translate biophysical and social factors into monetary values —albeit tentatively— in order to work in homogenous units that enable aggregating the total costs and income related to the WRRS.

Therefore, units for the biophysical and social aspects need to be defined for each of the impacts studied. These units will later serve as a basis for an economic evaluation. Table 2 presents the different impacts that have been identified, as well as the units suggested for their quantification.

All of these quantification units should refer to an established time during the period of the impacts. In order to homogenize the results, a period of one year is proposed for all. The quantification of each impact can be divided by the annual flow rate of the reclaimed water, and therefore the result will be expressed in cubic meters of reclaimed water.

Valuation of the Impacts

In addition to the quantities and timing of each impact, a relative value is needed.

On the one hand, there is the direct valuation in economic terms based on private costs and income. This information reflects the monetary value of the goods and services in current markets.

Table 2. Units for the Biophysical or Social Quantification of the Impacts Identified (Seguí, 2007; Seguí *et al.*, 2009; Seguí, 2004)..

Impact Group	Impacts Involved	Biophysical or Social Quantification Units
Hydraulic Infrastructure	Water catchment and supply	m^3 of water
	Treatment of water supply	
	Conduction and transport of drinking water	
	Rehabilitation and expansion of sewage networks	
	Treatment and/or discharge of wastewater	
	Wastewater reclamation and reuse	
Conditioning and Reuse of Pollutants	Nitrogen	kg of usable N
	Phosphorus	kg of usable P
	Sludge	kg of usable sludge [(a)]
	Energy	Watts produced
Use of resource	Amount of water	m^3 of water
	Supply guarantees	% confidence
	Water quality	kg of contaminant [(b)]
Public Health	Biological risks	Persons exposed
	Physical-chemical risks	
	Risks in the WRRS	
Environment	Surface water	m^3 of water
	Groundwater	m of water table [(c)]
	Pollution of water masses	kg of contaminant eliminated [(b)]
	Wetland and river habitats	Existing individuals [(d)]
Education	Technical	% efficiency [(e)]
	Water culture	Persons [(f)]

(a) The amount of usable sludge can refer to one of its constituents, for example, nitrogen, phosphorus, organic matter, etc.
(b) Whenever the analytical unit to be determined is massic; otherwise, the unit in which the determination is performed (colony forming units, CFU). For example, bacteria present in water are measured in CFU.
(c) Reference unit to evaluate the increase or decrease in water resources in the aquifer.
(d) In the case of wetlands and rivers, the value of the environmental asset can be determined based on the number of persons that use it.
(e) Ability of staff to maintain the quality levels established for the production of reclaimed water.
(f) People who are aware of the practice of reclaiming and reusing wastewater.

There is also a series of external impacts for which there is no explicit market, and in the case in which a market does exist, it is distorted. Therefore, the impacts are not appropriately valued. Different techniques exist to obtain a value for such external impacts, the most suitable one should be chosen according to each specific problem.

These economic valuation methods are usually well founded on hypothetical data or scenarios or behavior observed in related markets. Table 3 summarizes these valuation techniques. It is worth mentioning that analyzing these techniques is not the objective of this work.

While environmental valuation methods are not the objective of this article, it is considered useful to present a simplified overview of the empirical application of methods that are most frequently used for environmental problems that are directly or indirectly related to the water sector.

Table 3. Economic Valuation Techniques (Seguí, 2007; Seguí *et al.*, 2009; Seguí, 2004)..

Methodological group	Valuation Technique	Abbreviation
Conventional market approach	Change in the production function approach	CP
	Opportunity cost approach	CO
	Dosage-response approach	DR
	Defense or prevention costs	GD
	Replacement or Restoration Costs	CR
	Shadow Project	PS
	Substitute Cost	CS
	Efficiency Cost	CE
Implicit markets	Hedonics prices	PH
	Differential salary	SD
	Travel Cost	CV
Constructed markets	Artificial market	MA
	Contingent valuation	VC
Not economic	Multi-criteria analysis	AM
	Delphi	D
	Evaluation of environmental impacts	EIA
	Linear programming	PL

Identification of the Agents Involved

After identifying the impacts of the system, the agents involved can be determined. Generally, two main types of agents exist in a WRRS: 1) water institutions or government entities and 2) water users.

In addition to identifying the agents, it is important to define which specific agent corresponds to the evaluation to be performed, since the information and impacts to be included will depend on this.

Study of Financial Needs and Possibilities

The most profitable WRRS that can be imagined will be of little use if it cannot be financed. Therefore, the financial costs involved in developing and implementing the project need to be considered. Otherwise the best WRRS in technical terms will be economically unviable without financing. Determining the sources and conditions of financing is an important point that must be taken into account before aggregating the costs. In addition, the financing conditions must be included as variables in the sensitivity analysis.

Aggregation of Costs and Income

During this stage, the aggregation of the costs and income will lead to a decision about whether or not to invest in the WRRS. It is important to be clear at all times that the costs and income vary throughout the useful life of the project, and therefore must be homogenized in order to be compared. In the methodology described herein, it is proposed that the costs and income be expressed so that the results obtained are in Monetary Unit per Unit Volume (MU/m^3), with the understanding that income is any utility profit (wellbeing) and the cost is any loss in the usefulness of the project.

Total Benefit

The central objective of the economic analysis of the WRRS is to optimize the

total benefit, expressed in equation (2). This optimization is obtained from the private benefits, the benefits from externalities, and the opportunity costs, such that the objective function to optimize is:

$$MAX\ B_T = B_p + B_E - OC \qquad (2)$$

where:

B_T = total benefit (total income-total costs).
B_p = private benefit (private income-private costs).
B_E = benefit from externalities (income from externalities-costs from externalities).
OC = opportunity cost.

Private Benefit

The private benefit is obtained by subtracting private costs (*PC*) from private income (*PI*). This income results from the product of the sale price and the volume of reclaimed water. The private cost consists of 1) the sum of investment costs (*IC*), which is the set of allocations required for the physical infrastructure of the WRRS, 2) the costs of operations and maintenance (OMC), which are costs resulting from the functioning of the WRRS (most of which relate to manual labor, energy, chemical reagents and fungible materials and 3) financing costs (*CFin*) and taxes (*T*). These costs include production costs as well as those generated by bringing the product (reclaimed water) to the point of usage (reuse).

The problem we most often face is that no market exists for reclaimed water and, therefore, a price is not available, or in the best of cases, when a price of water is known it is distorted and the costs are usually not recuperated.

After characterizing the wastewater and establishing the desired quality level for the reclaimed water (quality objective), a range of technological possibilities is considered to transform the wastewater into reclaimed water.

The problem for decision-makers is the selection of the most suitable technology. Therefore, when a water quality objective can be obtained with two or more technological options, the rational decision for selection will be the financially less expensive option.

The use of a cost-efficiency analysis (Hartwick and Olewiler, 1998; OCDE, 2002) is proposed as a first step in selecting the most suitable technology, to significantly reduce the universe of alternatives to be evaluated. This method determines a monetary value of the private costs of the WRRS and compares them, as long as they have the same level of efficiency, leaving it up to the decision-maker to choose a particular efficiency level. The selection criteria will be given by the WRRS that has the lowest cost for a predetermined quality required of the water to be reused.

Once the quality criterion for the water to be reused is determined, the technology that cost the least per cubic meter (cost/m^3) will be selected according to expression (3):

$$\text{Cost}_i/\text{m}^3 = \underset{t=1\ldots T}{Min}\left\{\text{Cost}_1/\text{m}^3, \text{Cost}_2/\text{m}^3, \ldots, \text{Cost}_T/\text{m}^3\right\} \qquad (3)$$

where {cost$_1$/m^3, cost$_2$/m^3,..., cost$_T$/m^3} is the set "t" of technologies with the same level of efficiency. This cost per cubic meter is determined by taking it to be equal to the minimum sale price (MSP) needed to recuperate the costs.

The MSP is defined as the minimum price at which the agent must sell the reclaimed water to guarantee the recuperation of costs and the expected benefit, such that the investment is profitable given the current net value (CNV). In an optimization process and when there is perfect market competition,

this cost per cubic meter can be considered an approximation of the marginal cost (CMg).

The current net value (CNV) was the technique chosen to obtain the MSP. The efficiency of the project is attained when marginal income equals the marginal cost, which is the same as saying that the net benefit equals zero, as explained by Tietenberg (1992) and Griffin (2006). Based on this criteria, the MSP that satisfies the condition CNV=0 is determined. Figure 2 presents the algorithm used to determine the MSP.

It is important to clarify that the cost-benefit technique was chosen because the objective can be quantified using an efficiency indicator expressed in water quality units. The cost per unit volume is obtained based on the cost-benefit analysis. Nevertheless, this economic technique does not address the question as to whether this result justifies the cost. It only addresses the total benefit (B_T), such that the private benefit is given by equation (4):

$$B_P = \sum_{n=0}^{n} \left[\left(ARV_n * SP_n \right) - \left(IC_n + OMC_n + FC_n + TAX_n \right) \right] \quad (4)$$

Where:

B_P = private benefit.
ARV = annual reclaimed water volume.
SP = sale price of reclaimed water.
IC = Investment costs.

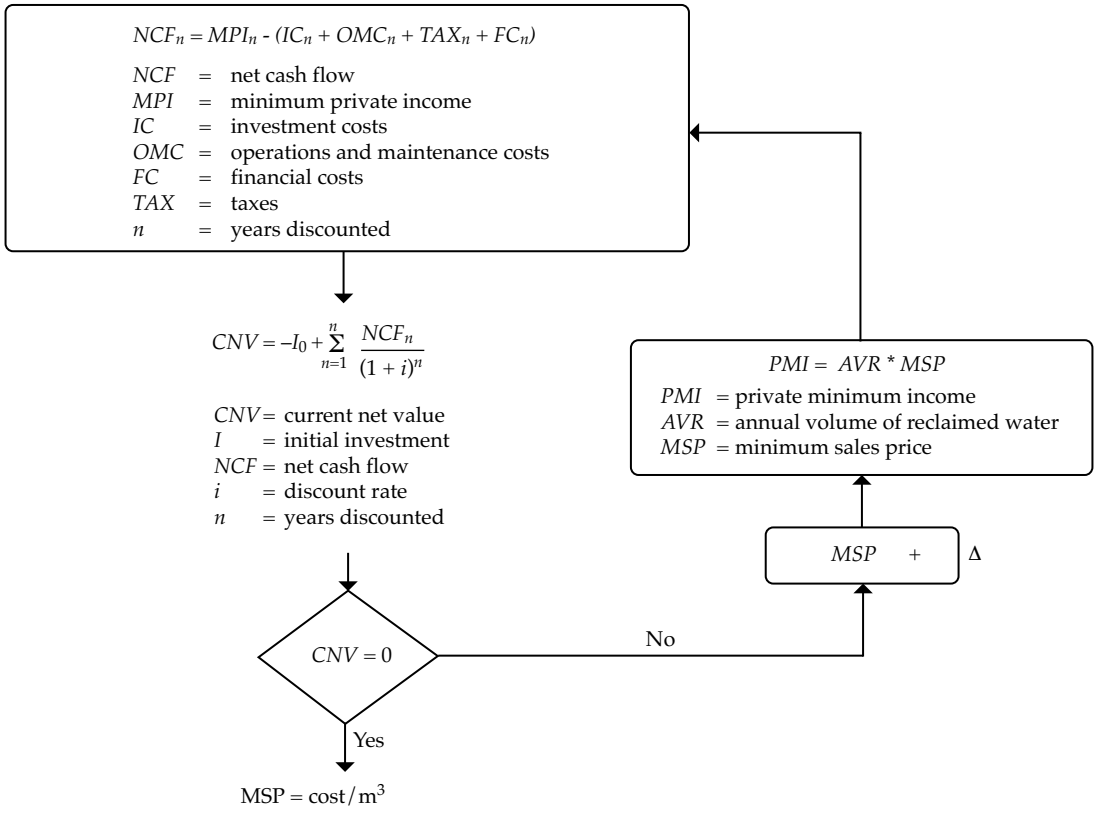

Figure 2. Algorithm to Determine the Cost per Cubic Meter (Seguí, 2007; Seguí *et al.*, 2009; Seguí, 2004).

OMC = operations and maintenance costs.
FC = Financial costs.
TAX = taxes.
n = year.

The taxes considered here refer to the payment of taxes corresponding to the tax rate of a private company that provides wastewater reclamation and/or distribution services.

To calculate the taxes, the amortization and depreciation of the capital invested need to be taken into account. It is important to keep in mind that these amortizations are only useful to determine financial benefits and to avoid the corresponding tax payments, and consequently to identify the private profit that a particular individual agent will obtain (Pasqual, 1999; Griffin, 2006).

When a private benefit (B_p) greater than zero is obtained the WRRS will be economically and financially operational from the private point of view.

Benefit of Externalities

In addition to the private benefit, this methodology includes both positive as well as negative externalities, in accordance with the new trends in the economic analysis of the water sector (Renzetti, 2003; Louis and Siriwadana, 2001; Directiva CE, 2000).

These externalities are obtained based on the positive and/or negative impacts generated by the construction and operations of the WRRS. These impacts were described in detail in the section "Impacts of the Project" and should be considered throughout the useful life of the project, and quantified and valued in monetary units.

Thus, the benefit of the externalities (B_E) would be given by equation (5):

$$B_E = \sum_{n=0}^{n} \left(PE_n - NE_n \right) \qquad (5)$$

Such that $PE = \sum_{j=1}^{J} \left(pe_j \right)$; $NE = \sum_{j=1}^{J} \left(ne_j \right)$ for $j = 1.... J$ impacts

Where:

B_E = benefit of the externalities.
PE = positive externalities of the impact pe_j.
NE = negative externalities of the impact ne_j.
n = year.

The positive externalities (PE) are given by the sum of all benefits. These external positive impacts should be identified, quantified and valued economically in monetary terms.

The negative externalities (NE) are the negative impacts of the project expressed in monetary units. The value of the NE will be greater or equal to the environmental cost (EC) of the selected technology and expressed by equation (6):

$$NE \geq EC_i \qquad (6)$$

The environmental cost of the selected technology (EC_i) is the negative impacts resulting from the creation of the WRRS. In general terms, the EC for the WRRS are given by:

1. Inadequate treatment, no treatment or disposal of sludge.
2. The environmental effect on the zone from the construction and operations of a WRRS, such as odors or noise pollution. This environmental effect can decrease the value of properties near the reclamation facilities.
3. Public health risks from contact with reclaimed water or its byproduct.
4. Health risks of workers in the WRRS due to contact with reclaimed water or a byproduct.
5. The effect on third parties due to decreased flow downstream from the discharge due to the elimination or rechanneling of the discharge.

6. The use of technologies with high energy consumption.

As in the case of private benefits (B_p), the benefits from externalities (B_E) can vary throughout the useful life of the project and therefore must be continually annualized throughout the duration of the project. The benefit of externalities is expressed in MU/m^3 of reused water in order to compare it to the private benefit.

Opportunity Cost

The most basic economical concept related to opportunity cost is the value of a good when its alternative use has been foregone (Pearce, 1983). The opportunity cost can only be present in a world in which the available resources are limited, such that not all of the needs can be satisfied. If the resources were unlimited, everyone would be able to satisfy their needs and the opportunity cost would be zero. Although the terminology varies, it is useful to talk about "private" opportunity costs when private benefits from an action are foregone and "social" opportunity costs when one of the possible alternative social goods is forgone.

Therefore, the concept of opportunity cost when applied to WRRS can be explained based on two main conditions:

1. When several alternatives exist for the reuse of reclaimed water, the opportunity cost will be given by the use that provides the best economic return, as long as the return is higher than that of a financing instrument.
2. When there are no equivalent uses for the reuse of the water produced, the opportunity cost is given by the return provided by a financing instrument by investing the investment, operations and maintenance costs.

In particular, it is important to emphasize the need to analyze the opportunity cost of the land to be used for a WRRS. Traditionally, the cost of the land selected to build the reclamation station is considered to be zero since it is generally land granted by the municipal government. Nevertheless, these areas can sometimes have alternative uses that provide greater profits.

After determining the private benefits, the benefits from the externalities and the opportunity costs, these are taken together in order to determine the total benefit of the project, resulting in whether the project is economically or environmentally viable.

Substituting equations (3), (5) and the OC in equation (2), the final objective function to be optimized is obtained, as expressed in equation (1).

$$MAX\ B_T = \sum_{n=0}^{n}\left[\left(ARV_n * SP_n\right) - \left(IC_n + OMC_n + FC_n + TAX_n\right) + \left(PE_n - NE_n\right) - OC_n\right] \quad (1)$$

It is important to mention that the precision of the result is questionable in reality, since some of the variables may be approximate values. The evaluation of the impacts related to reclamation and reuse of wastewater is improved not only in terms of methodological advances but also in terms of the quantity and quality of the data used. This improvement in the information is what provides the foundation for decision-making. To strengthen the validity of the investigation, this methodology includes a sensitivity analysis to decrease the risk of the decision.

In summary, Table 4 presents all the information needed to determine the costs and income related to a WRRS. This table systematically and concisely shows the existing information, such that the value in monetary units of all the impacts related with

Table 4. Summary of the Economic-Technological Analysis of the Impacts of the WRRS (Seguí, 2007; Seguí *et al.*, 2009; Seguí, 2004).

Impact group	Impact involved	Identification (a)	Regularity (b)	Quantification units (c)	Monetary valuation technique (UM/m³) (d) (e)	
					Negative (costs)	Positive (income)
Hydraulic infrastructure	Water catchment and storage	Section 4.2.3.1.1	Initial inversion during the useful life of the project	m^3 of water	MP, EC, OC	
	Treatment of supply water					
	Rehabilitation and expansion of sewage networks					
	Rehabilitation and expansion of sewage networks					
	Treatment and/or discharge of wastewater					
	Reclamation and reuse of wastewater					
Conditioning and reuse of pollutants	Nitrogen	Section 4.2.3.1.2	During the useful life of the project	kg of useable N		SC
	Phosphorus			kg of usable P		
	Sludge			kg of usable sludge		
	Energy			Watt produced		
Use of the resource	Amount of water	Section 4.2.3.1.3	During the useful life of the project	m^3 of water	OC	CP, HP, TC
	Supply guarantees			% reliability		TC
	Water quality			kg of pollutant		CV, TC, DPC, SP
Public health	Biological risks	Section 4.2.3.1.4	During the useful life of the project	Persons exposed		DR
	Physical-chemical risks					DR
	Risks in the WRRS					DR
Environment	Surface water	Section 4.2.3.1.5	During the useful life of the project	m^3 of water		CV, TC, HP
	Groundwater			m water table		SC
	Pollution of water masses			kg of contaminant eliminated		RC, CV, TC, HP
	Wetland and river habitats			Existing individuals		TC
Education	Technical	Section 4.2.3.1.6	During the useful life of the project	% of efficiency		DR, CP
	Water culture			Persons		
				Total	**Σ costs**	**Σ ingresos**

(a) "Identification of impacts" section.
(b) "Regularity of impacts" section.
(c) "Quantification of impacts" section.
(d) "Valuation of impacts" section.
(e) MP: market price; CP: change in productivity; OC: opportunity cost; DR: dosage-response; DPC: defense and prevention costs; RC: replacement cost; SP: shadow project; SC: substitute cost; EC: efficiency cost; HP: hedonic prices; TC: trip cost; CV: contingent valuation.

the WRRS can be obtained. It is important to clarify that this table is only for didactic purposes, since each WRRS to be analyzed will have its only particularities with their corresponding nuances in the application of this methodology.

Sensitivity Analysis

Lastly, it is necessary to evaluate the robustness of the project in light of possible changes in the most significant economic variables. The purpose of the sensitivity analysis is to observe how the result changes when the value of each one of the parameters included in the calculation varies, marginally and separately. The possible variables to conduct a sensitivity analysis include: 1) the discount rate, 2) financing conditions, 3) opportunity cost, 4) costs of energy and reagents and 5) price of reclaimed water, among others.

After the variables are modified and when the total benefit (B_T) remains positive, it can be concluded that the construction and operations of the project evaluated can proceed with confidence since all seems to indicate that the project would be profitable regardless of pessimistic scenarios.

Conclusions

This methodology has been used by several authors for various case studies, including Hernández *et al*. (2006); Urkiaga *et al*. (2006); Hlavinek *et al*. (2008); Guerrero-García-Rojas *et al*. (2008); Alfranca *et al*. (2011); Uggetti *et al*. (2011); AQUAREC (2006), and Hernández *et al*. (2010), and therefore the protocol presented herein has been replicated various times with success.

The application of the methodology consists of seven steps: 1) definition of objectives, 2) definition of the study area, 3) impacts of the project, 4) identification of the agents involved, 5) study of financing requirements and possibilities, 6) adding costs and income and 7) sensitivity analysis.

Traditionally, the economic-financial analysis of a WRRS focuses on the private costs and benefits from the system. The methodology developed herein, in addition to considering these private impacts, incorporates the externalities of the project through the analysis of both positive and negative external impacts that affect it.

The study has sought to describe a methodology that is suitable to the particularities of a WRRS so that it can be considered a "custom" tool to enable decision makers to determine whether or not it is beneficial to implement this type of system. This methodology evaluated the WRRS from a multidisciplinary and interdisciplinary perspective. The main objective was the optimization of the benefits from the project.

One of the most significant contributions made by this methodology was the identification of the impacts of the project, since it provided a detailed description of both positive and negative impacts related to the WRRS. The six impact groups described were: 1) hydraulic infrastructure, 2) conditioning and reuse of pollutants, 3) use of the resource, 4) public health, 5) environment and 6) education. This information was supported by a literature review, consultation with experts and professional experience.

Another important contribution was the adding the costs and income, establishing that the optimization of benefits is given by the sum of private benefits and benefits from externalities. This enables describing two separate situations: 1) the functioning of the WRRS is economically and financially viable, which is defined by the determination of the private benefit (normally of interest to technicians and political leaders) and 2) the WRRS is economically, financially and

environmentally viable (which is of interest to economics and the society).

Received: 14/03/2012
Accepted: 26/06/2013

References

ALFRANCA, O., GARCIA, J., and VARELA, H. Economic Valuation of a Created Wetland Fed with Treated Wastewater Located in a Peri-Urban Park in Catalonia, Spain. *Water Science and Technology*. Gener 2011. Vol. 63, No. 5, pp. 892-899.

AQUAREC. *Water Reuse System Management Natural*. Bixio, D. and Wiintgens T. (editors). Project Report, 2006. World Wide Web: http://www.aquarec.org/.

ASANO, T. *Water Reuse: Issues, Technologies and Applications*. New York: Metcalf & Eddy/AECOM, 2007.

BIXIO, D., THOEYE, C., DE KONING, J., JOKSIMOVIC, D., SAVIC, D., WINTGENS, T., and MELIN, T. Wastewater reuse in Europe. *Desalination*. Vol. 187, 2006, pp. 89-101.

CHEN, R. and WANG, C. Cost-benefit Evaluation of a Decentralized Water System for Wastewater Reuse and Environmental Protection. *Water Science and Technology*. Vol. 59, No. 8, 2009, pp. 1515-1522.

CHU, W., WANG, J., and KAO, C. 2003. A Simplified Risk-Based Approach for Process Screening in Municipal Wastewater Reclamation and Reuse. *Water Science and Technology*. Vol. 47, No. 1, pp. 257-262.

DIRECTIVA CE. *Directiva 2000/60/CE*. OCDE, Bruselas, 2000.

DOUROJEANNI, A. *Gestión de cuencas y ríos vinculados con centros urbanos*. Santiago, Chile: CEPAL, 1999.

FÄRE, R., GROSSKOPF, S., and WEBER, W. Shadow Prices and Pollution Costs in U.S. Agriculture. *Ecological economics*. Vol. 56, 2006, pp. 89-103.

GARCIA, J., MUJERIEGO, R., OBIS, J.M., and BOU, J. Wastewater Treatment for Small Communities in Catalonia (Mediterranean Region). *Water Policy*. Vol. 3, No. 4, 2001, pp. 341-350.

GODFREY, S., LABHASETWAR, P., and WATE, S. Greywater Reuse in Residential Schools in Madhya Pradesh, India- A Case Study of Cost-Benefit Analysis. *Resources, Conservation and Recycling*. Vol. 53, 2009, pp. 287-293.

GRIFFIN, R.C. *Water Resource Economics*. Cambridge: The MIT Press, 2006.

GUERRERO-GARCÍA-ROJAS, H., YÚNEZ-NAUDE, A. y MEDELLÍN-AZUARA, J. *El agua en México. Consecuencias de las políticas de intervención en el sector*. México, D.F.: Fondo de Cultura Económica (FCE), 2008.

HARTWICK, J. and OLEWILER, N.A. *The Economics of Natural Resource Use*. 2th edition. New York: Addison-Wesley, 1998.

HERNÁNDEZ, F., MOLINOS, M., and GARRIDO, S. Economic Valuation of Environmental Benefits from Wastewater Treatment Processes: An Empirical Approach for Spain. *Science of the Total Environment*. Vol. 408, No. 4, 2010, pp. 953-957.

HERNÁNDEZ, F., URKIAGA, A., DE LAS FUENTES, L., BIS, B., CHIRU, B., BALAZS, B., and WINTGENS, T. Feasibility studies for water reuse projects: an economical approach. *Desalination*. Vol. 187, No. 1-3, 2006, pp. 253-261.

HLAVINEK, P., BONACCI, O., MARSALEK, J., and MAHRIKOVA, I. *Dangerous Pollutants (Xenobiotics) in Urban Water Cycle*. Chapter: Cost Modelling In Waste Water Treatment Processes: An Empirical Analysis For Spain. New York: Springer Netherlands, 2008.

HOCHSTRAT, R., JOKSIMOVIC, D., WINTGENS, T., MELIN, T., and SAVIC, D. Economic Considerations and Decision Support Tool for Wastewater Reuse Scheme Planning. *Water Science and Technology*. Vol. 56, No. 5, 2007, pp. 175-182.

HUTTON, G. and HALLER, L. *Evaluation of the Costs and Benefits of Water and Sanitation Improvements at The Global Level*. Genova: World Health Organization, 2004.

KATZ, R. Water Recycling 2030. *Recycled Water Task Force*. California Department of Water Resources. 2003. World Wide Web: http://www.owue.water.ca.gov/recycle/docs/FinalReport.pdf.

LOUIS, G. and SIRIWADANA, M. *A Procedure for Calculating the Full Cost of Drinking Water*. Comunicación presentada en la conferencia CEWorld-a virtual, organizado por la American Society of Civil Engineers, 2001. World Wide Web: http://www.ceworld.org/.

PASQUAL, J. *La evaluación de políticas y proyectos, criterios de valoración económicos y sociales*. Barcelona: Icaria Editorial S.A., 1999.

PEARCE, D.W. *The Dictionary of Modern Economics*. General Editor. Cambridge: The MIT Press, 1983.

RENZETTI, S. *Full Cost Accounting for Water Supply and Sewage Treatment: A Case Study of the Niagara Region, Canada*. Comunicación presentada en el World Bank's Water Resources Management Group on Economic Instruments, 2003. World Wide Web: http://worldbank.org/.

SEGUÍ, L. *Sistemas de regeneración y reutilización de aguas residuales. Metodología para el análisis técnico-económico y casos*. Tesis doctoral. Barcelona: Departamento de Ingeniería Agroalimentaria y Biotecnología, Universidad Politécnica de Cataluña, 2004. World Wide Web: http://tdx.cesca.es.

SEGUÍ, L. Economic Analysis of the Reuse of Water Reclamation in the Irrigation of Vineyards. *International Journal of Agricultural Resources, Governance and Ecology (IJARGE)*. Vol. 6, No. Issue 1, 2007, pp. 124-139.

SEGUI, L., ALFRANCA, O., and GARCÍA, J. Techno-Economical Evaluation of Water Reuse for Wetland

Restoration: A Case Study in a Natural Park of Northeastearn Spain. *Desalination*. Vol. 246, No. 1, 2009, pp. 179-189.

SHABMAN, L. and STEPHENSON, K. Environmental Valuations and its Economic Critics. *Journal of Water Resources Planning and Management*. Vol. 126, No. 6, 2000, pp. 382-388.

TIETENBERG, T. *Environmental and Natural Resource Economics*. 3rd. ed. Boston: Harper Collins Publishers, 1992.

UGGETTI, E., FERRER-MARTÍ, I., MOLIST, J., and GARCÍA-SERRANO, J. Technical, Economic and Environmental Assessment of Sludge Treatment Wetlands. *Water Research*. Gener 2011. Vol. 45, No. 2, pp. 573-582.

URKIAGA, A., DE LAS FUENTES, L., BIS, B., CHIRU, B., BODO, B., HERNÁNDEZ, F., and WINTGENS, T. Methodologies for feasibility studies related to wastewater reclamation and reuse projects. *Desalination*. Vol. 187, No. 1-3, 2006, pp 263-269.

VERONESI, M., CHAWLA, F., MAURER, M., and LIENERT, J. *Climate Change and the Willingness to Pay to Reduce Ecological and Health Risks from Wastewater Flooding in Urban Centers and the Environment*. Working Paper No. 1. Verona: University of Verona, Department of Economics, 2013.

Institutional Address of the Authors

Dr. Luis Seguí Amórtegui

Departamento de Organización de Empresas (DOE)
Universitat Politècnica de Catalunya, Campus Sud
Edif. H - Planta 7
Av. Diagonal, 647
08028 Barcelona, España
Teléfono: +34 (935) 521 227
luis.segui@upc.edu

Dr. Oscar Alfranca Burriel

Departamento de Biotecnología Agroalimentaria y Sostenibilidad
Universidad Politécnica de Cataluña
Comtes d'Urgell 189, E-08036
Barcelona, España
Teléfono: + 34 (935) 521 227
oscar.alfranca@upc.es

Dra. Gabriela Moeller Chávez

Universidad Politécnica del Estado de Morelos
Boulevard Cuauhnáhuac # 566, Col. Lomas del Texcal
62550 Jiutepec, Morelos, México
Teléfono: + 52 (777) 2293 533
gabriela.moeller@gmail.com

Click here to write the autor

Redistribution of Precipitaiton in Three Native Brush Species and a Eucalyptus Plantings in Northeastern Mexico

• María Inés Yáñez-Díaz* • Israel Cantú-Silva •
• Humberto González-Rodríguez • José I. Uvalle-Sauceda •
Universidad Autónoma de Nuevo León, México
*Corresponding Author

Abstract

YÁÑEZ-DÍAZ, M.I., CANTÚ-SILVA, I., GONZÁLEZ-RODRÍGUEZ, H. & UVALLE-SAUCEDA, J.I. Redistribution of Precipitaiton in Three Native Brush Species and a Eucalyptus Plantings in Northeastern Mexico. *Water Technology and Sciences* (in Spanish). Vol. V, No. 2, March-April, 2014, pp. 71-84.

The redistribution of precipitation was studied in three scrubland species and a Eucalyptus camaldulensis plantation in Linares, Nuevo Leon, Mexico. Measurements were taken of incident precipitation, throughfall and stemflow from April 18, 2009 to June 7, 2010. The following were determined and compared for the four species studied: net precipitation, interception loss, canopy storage capacity, pH and electrical conductivity. The analysis of 48 individual rainfall events resulted in a total of 978.77 mm of incident precipitation, finding throughfall for Prosopis laevigata, Eucalyptus camaldulensis, Ebenopsis ebano and Helietta parvifolia of 74, 85, 65 and 67%, respectively. Canopy interception loss was estimated at 25, 15, 34 and 33% for P. *laevigata, E. camaldulensis, E. ebano* and *H. parvifolia*, respectively, for which most of the interception by *E. ebano* and *H. parvifolia* can be explained by the canopies of these species being more dense and the geometric arrangement of their branches, which contributed to more interception than that by *E. camaldulensis* and *P. laevigata*. Stemflow values ranged from 0.23% for P. laevigata to 3.66% for E. camaldulensis, and the canopy storage capacity ranged from 0.03 for *H. parvifolia* to 0.27 mm for *E. camaldulensis*. Rain leaching generally presented slightly acidic pH values and the electrical conductivity increased as it passed over the canopies, indicating base leaching.

Keywords: Throughflow, stemflow, interception loss, storage capacity, *Eucalyptus camaldulensis, Ebenopsis ebano, Helietta parvifolia, Prosopis laevigata*.

Resumen

YÁÑEZ-DÍAZ, M.I., CANTÚ-SILVA, I., GONZÁLEZ-RODRÍGUEZ, H. & UVALLE-SAUCEDA, J.I. Redistribución de la precipitación en tres especies arbustivas nativas y una plantación de eucalipto del noreste de México. Tecnología y Ciencias del Agua. *Vol. V, núm. 2, marzo-abril de 2014, pp. 71-84.*

Se estudió la redistribución de las precipitaciones en tres especies del matorral submontano y una plantación de Eucalyptus camaldulensis, en Linares, Nuevo León, México. Mediciones de precipitación incidente, precipitación directa y escurrimiento fustal fueron llevadas a cabo del 18 de abril de 2009 al 7 de junio de 2010. Se determinaron y compararon la precipitación neta, pérdidas por intercepción, capacidad de almacenamiento del dosel, y valores de pH y conductividad eléctrica para las cuatro especies estudiadas. El análisis de 49 eventos de lluvia individuales sumaron un total de 978.77 mm de precipitación incidente, encontrándose que la precipitación directa para Prosopis laevigata, Eucalyptus camaldulensis, Ebenopsis ebano y Helietta parvifolia representó 74, 85, 65 y 67%, respectivamente. Las pérdidas por intercepción del dosel fueron estimadas en 25, 15, 34 y 33% para P. laevigata, E. camaldulensis, E. ebano y H. parvifolia, respectivamente, donde la mayor intercepción en E. ebano y H. parvifolia puede deberse a que el dosel de estas especies es más denso y a la disposición geométrica de sus ramas, lo que contribuyó a mayor intercepción que E. camaldulensis y P. laevigata. El escurrimiento fustal presentó valores de 0.23% para P. laevigata hasta 3.66% en E. camaldulensis, y la capacidad de almacenamiento del dosel varió de 0.03 para H. parvifolia a 0.27 mm para E. camaldulensis. El pluviolavado presentó en general valores de pH ligeramente ácido y la conductividad eléctrica se incrementó conforme atravesaba el dosel de las especies, indicando un lavado de bases.

***Palabras clave**: pérdidas por intercepción, precipitación directa, escurrimiento fustal, capacidad de almacenamiento, Prosopis laevigata, Eucalyptus camaldulensis, Ebenopsis ebano, Helietta parvifolia.*

Introduction

The hydrological cycle is the overall movement of water, ascending due to evaporation and descending as a result of rainfall first and then through surface and groundwater runoff. The water balance is an equilibrium between the inputs and outputs of water in an ecosystem. Forest plantations affect these conditions depending on the amount of rainfall retained by the canopy, which is collected, stored and later evaporates. The measurement and prediction of rainfall interception loss is required for the prognosis of the effects of vegetation cover on the amount of water available for use by the soil (Aston, 1979; Cantú and González, 2002). Several studies have contributed to understanding the importance of forest covers as filters that significantly modify the spatial distribution of incident precipitation as well as spatial variations in moisture and physical and chemical soil properties (Belmonte and Romero, 1999). Precipitaiton and aquifer recharge patterns are crucial to understanding how a forest plantation affects water resources and management. Interception and vegetation cover are related —denser cover results in more rainfall intercepted and less runoff (Rutter *et al*., 1971, cited by Prado *et al*., 2007).

Precipitation, commonly represented by rainfall and snow, is the primary factor controlling the hydrological cycle (Stravs *et al*., 2008). It also plays a role in ecological and geomorphological processes in a region (De Jong and Jetten, 2007). The precipitation that reaches the tree canopy is divided into three parts: interception, stemflow and throughfall (Figure 1). The precipitation retained by the vegetation is called incident precipitation. Usually, the interception of rainfall is calculated indirectly by the difference between incident precipitation (above the canopy) and throughfall (below the canopy), which is expressed as:

$$I = Pi - (TF + S) \quad (1)$$

where I represents interception loss, Pi is incident precipitation, TF is throughfall and S is stemflow.

Interception is studied not only by hydrology but also by a variety of disciplines that are involved. It is part of the hydrological cycle of the water-atmosphere subsystem, along with precipitation, evaporation and transpiration, and it affects other components of the hydrological cycle, such as infiltration, runoff and evaporation of the soil, among other phases (Belmonte and Romero, 1999). Intercepted rainfall is primarily influenced by the characteristics of precipitation and vegetation and the weather conditions during a rainfall event (Huber, 2003).

Woodland interventions, or the replacement of vegetation, changes the components involved in the redistribution of precipitation, bringing about changes in the soil water reserve and the amount of water involved in evaporation and percolation (Echeverría *et al*., 2007). A wide range of interception loss values is found in the literature about studies that have been performed based on the type of cover or other factors involved in the process. Xiao *et al*. (2000) report interception values from 10 to 59% depending on the tree species. In the Linares region in Nuevo Leon, studies have been conducted of interception losses for some Tamaulipeco thorny submontane shrub species, because of the importance and increasing interest over recent years in using these species for plantings of native species as part of reforestation programs.

Throughfall refers to rainfall below the canopy; that is, the amount of water that flows through the canopy through openings or by dripping from leaves and branches (Crockford and Richardson, 2000; Xiao *et al*., 2000; Huber, 2003; Cantú y González, 2005). Throughfall is considered a primary source

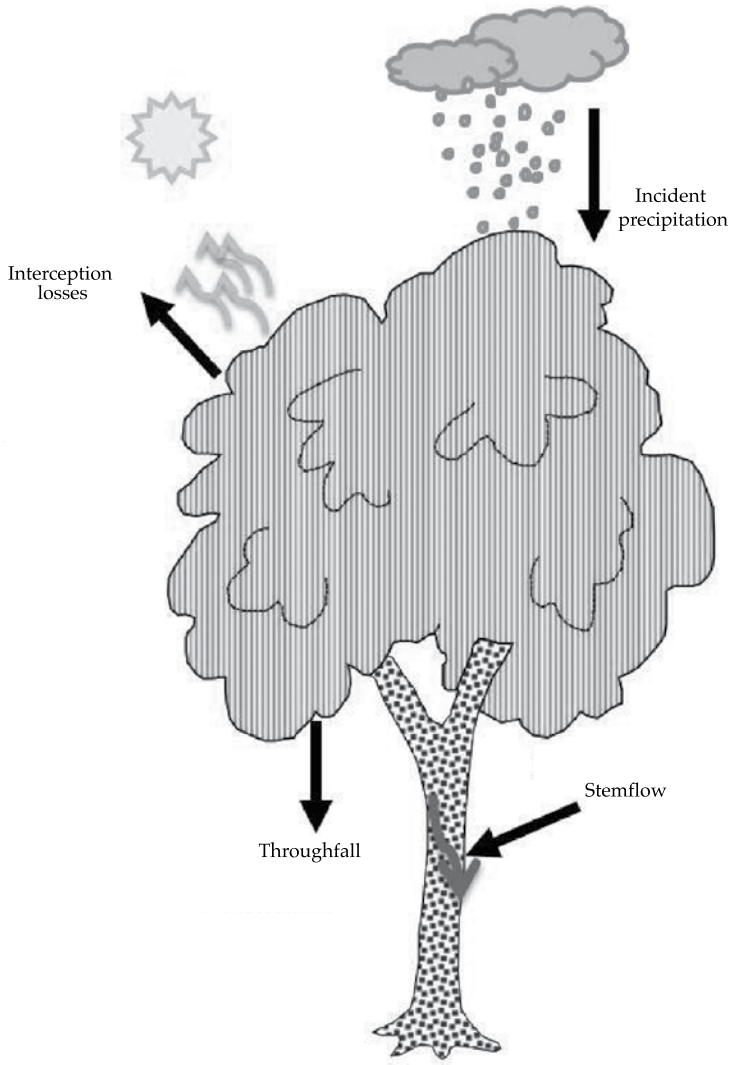

Figure 1. Diagram of the Precipitation Redistribution Process.

of water supply for the soil, and generally provides between 74 and 80% of incident precipitation (Oyarzún *et al.*, 1985). The characteristics that influence the amount of throughfall include the height of the canopy from the soil, the canopy openings and wind conditions (Crockford and Richardson, 2000).

Stemflow is the portion of precipitation that makes contact with the cover, flows downward along the trunks or stems and reaches the soil around the base. The amount of stemflow is directly related to a tree's architecture (Murakami, 2009), its basal area (Crockford and Richardson, 2000) and its age (Johnson, 1990). Since the largest and highest trees have a larger area where rainwater collects (Oyarzún *et al.*, 1985), the intensity and duration of precipitation considerably increase stemflow (Oyarzún *et al.*, 1985). The relative value of stemflow is related to

the self-supply of water to the base of the tree, since water gathers in the soil around the trunks (Huber, 2003). This supply may be especially important during periods with little precipitation (Oyarzún *et al*., 1985).

Canopy interception plays an important role in the land-atmosphere interaction (Wang and Wang, 2007). In terms of water balance, an important factor in interception is the amount of rain that a community of plants collects, stores and later loses to evaporation. The amount of water retained by the canopy without overflowing its surface is known as the storage capacity or canopy saturation capacity (Cantú and González, 2002, 2005). The canopy's water storage capacity is defined by a coefficient that expresses the amount of water required to moisten the entire canopy before it begins to run down to the soil surface (Jaramillo, 2003).

Precipitaiton contributes to the leaching of nutrients through translocation and stemflow, enabling nutrients from the aerial vegetation biomass to return to the soil. The dynamic of nutrients in ecosystems is related to the water cycle through nutrient leaching (Jiménez *et al*., 2006). Several studies have shown that throughfall and stemflow significantly affect the nutrient content of soil. Though throughfall is volumetrically greater than stemflow, the latter is chemically richer (Watters and Price, 1987). Generally, a relationship is found between pH values and electrical conductivity with nutrient contents. These physiochemical properties of rain water are altered by processes such as evaporation, ion exchange and chemical solubility, indirectly indicating the nutrient contents and making it possible to determine the nutrient value supplied to the soil by the species studied.

The present work compares the redistribution of precipitation with measurements of throughfall and stemflow for three native submontane shrub species and a Eucalyptus plantation in northeastern Mexico, where water resources are limited.

Material and Methods

Study Area

The study area is located on the experimental campus of the School of Forestry Sciences at the Autonomous University of Nuevo Leon, 8 km south of the municipality of Linares, in the state of Nuevo Leon, Mexico. This is located at N 24° 47´; W 99° 32´ at an elevation of 350 masl. It is in hydrological region RH25, known as San Fernando-Soto La Marina, or the coastal plains of the northern Gulf (Planicie Costera del Golfo Norte), in the Bravo and Panuco river basins and the Arroyo-Camacho sub-basin, next to the Eastern Sierra Madre. The climate is subtropical and semi-arid, with hot summers, rains between April and November, and an intrasummer dry period with temperatures up to 45° C during the summer and average monthly temperatures of 14.7 °C in January and 22.3 °C in August. The average annual precipitation is 805 mm, with a bimodal distribution. The region is associated with vertisol soil from Alluvial-Colluvial origins, deep and gray-black in color, with a mesic pelic suborder, a fine clay-loam texture, high montmorillonite and low organic matter contents, and a slightly alkaline pH (Uvalle, 2008).

The vegetation is submontane xerophytic shrubs in a first primary succession stage. The submontane shrub covers an approximate area of 5 000 km^2, nearly 8% of the territory of the state of Nuevo Leon. Its maximum distribution is located at an altitude between 600 and 800 m (Estrada *et al*., 2005). This plant community consists of shrubs rich in life forms. The strength, size and distribution of the dominant and co-dominant species are

dependent on the availability of water and the depth and fertility of the soil, characterized by the dominance of deciduous and thorny species most of the year, or leafless species. The factors having a direct effect on the distribution of this community include the thickness of the soil and exposure to and the influence of human activities (Alanís and González, 2003).

The study area contains a parcel for each species studied: *Helietta parvifolia* (A. Gray) Benth. (Barreta), *Prosopis laevigata* (Humb. & Bonpl. Ex Willd) (Mezquite), *Ebenopsis ebano* (Berl.) Barneby & Grimes. (*Ébano*) y *Eucalyptus camaldulensis* (Dehnh.) (Eucalipto), as well as an area without trees to establish witnesses (incident precipitation). The *Helietta parvifolia* (baretta) and *Ebenopsis ebano* (ebony) species are native, nevertheless plantings of these species were established at the experimental campus of the School of Forestry Sciences. One of the species introduced was *Eucalyptus camaldulensis* (Eucalyptus),in order to develop a variety of research studies. These plantations were created in 1985, and for 25 years they have contributed to diverse research studies, such as the one herein. *Prosopis laevigata* (mezquite) is found in a submontane shrub section bordering the established plantations, and is considered low-density in relation to submontane shrub (Figure 2). The dosimetric characteristics of the species studied are presented in Table 1.

Measurement of the Components of Precipitation

A 100 m^2 parcel (10 x 10 m) was created under the canopy of each species, where collectors were placed for throughfall and stemflow.

Figure 2. Location of Experimental Parcels, School of Forestry Sciences, Autonomous University of Nuevo Leon.

Table 1. Dosimetric Parameters of the Species Used (n = 4 per species).

Species	Diameter at chest level (cm)	Height (m)	Canopy area (m^2)
H. parvifolia	6.73	5.43	5.92
E. ebano	10.68	5.75	9.95
E. camaldulensis	19.71	21.25	15.11
P. laevigata	21.05	7.45	39.15

Collectors for incident precipitation were placed next to the parcels. After each "rainfall event," measurements were take of collected volume and a sample was taken for the analysis of pH and electrical conductivity. The "rainfall event" was considered the period of precipitation consisting of continuous rain, drizzle or downpour, separated before and after by a minimum dry period of 8 hours (Figure 3).

Precipitación incidente

Incident precipitation (above the canopy) was collected using 0.1 m^2 (10 cm wide x 100 cm long) PVC U-channel connected by hoses to 20 L containers in which the rainwater was collected. The channels were covered with a mesh to prevent clogging by leaves and insects. Four were installed 1 m from the soil in an open area without trees next to the experimental parcels.

Throughfall

The same type of channels described above was used to collect precipitation flowing through the canopy. Four per species were randomly placed below the tree canopy and remained in the same location during the experimental period.

Stemflow

Two types of collectors were used for stemflow. For the *Prosopis laevigata* and *Eucalyptus camaldulensis* species, with trunk diameters over 15 cm, plastic hoses measuring 3 cm in diameter were used, with 1.5 x 2.5 cm perforations every 4 cm. These were attached to the trunks in the form of a spiral at a height of 1 m. Data for *Ebenopsis ebano* and *Helietta parvifolia,* with trunk diameters under 15 cm, were gathered using plastic containers that covered the trunks in the shape of a collar, placed at 1 m height from the soil and connected to a hose that transported the water to the collection container. Both collection systems were placed at four randomly selected trees for each species studied, located in the experimental parcel.

Canopy Storage Capacity

The amount of water stored in the canopy from one rainfall that was enough to exceed the capacity of the vegetation to retain water on its surface was determined using the method by Leyton *et al.* (1967), related to incident precipitation versus throughfall for rain events with a maximum value of 2.5 mm, knowing the axis intercept value of the ordinate after performing a linear regression of the data.

Rain Leaching

The pH and electrical conductivity (µS cm^{-1}) values were determined, representing the physiochemical properties of the water samples collected for each component

Figure 3. Collectors Randomly Distributed for Throughfall in a *Ebenopsis ebano* Plantation.

—throughfall, incident precipitation and stemflow. Direct measurements were taken with a Corning model 542 potentiometer-conductivity meter electrode.

Data Analysis

The measurements were taken between April 18, 2009 and June 7, 2010 for 49 rainfall events. With the data obtained for incident precipitation (Pi), throughfall (TF) and stemflow (Sf), descriptive statistics and linear regression models were applied to describe the behavior of the components of the precipitation above and below the canopy for the individual rain events. A variance analysis was applied to the pH values and electrical conductivity (μS cm^{-1}) for each precipitation component using the Statistical Package for the Social Sciences (SPSS), standard version 13.0 for Windows (SPSS Inc., Chicago, IL).

Results and Discussion

Redistribution of Precipitation

The analysis of 29 rain events resulted in a total of 978.77 mm registered during 18 months of field study. The behavior of the monthly accumulated precipitation showed that the largest number of precipitation events and amount of rainfall in millimeters occurred from September 2009 to April 2010, as reported during the rainy season at the study site. The range of individual rainfalls varied from 0.47 to 115.34 mm, for which precipitation for 31% of the events registered was less than 5 mm. Precipitation for the majority of events (43%) was 5 to 25 mm, it was 25 to 50 mm for 18% of events, 50 to 75 mm for 2% of events and 75 to 100 mm for another 2%, and over 100 mm for 4% of the events (Figure 4).

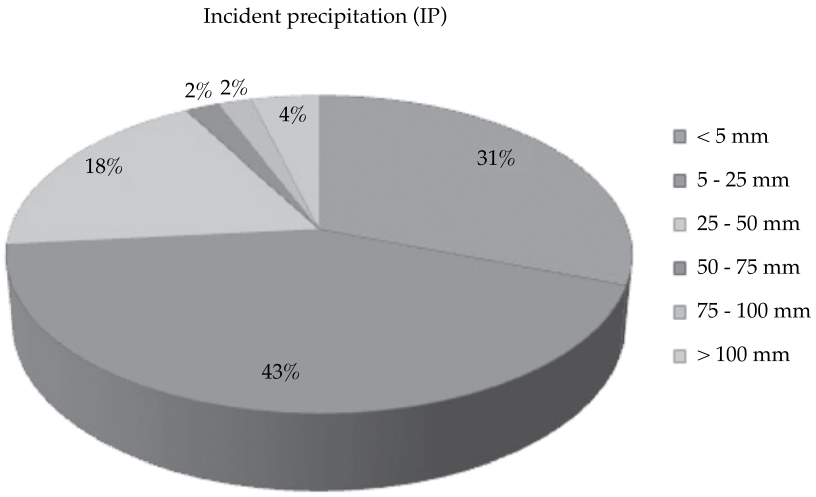

Figure 4. Percentage of rainfall events according to the amounts registered during the experimental period.

In terms of the behavior of the redistribution of precipitation, average throughfall (TF) for *Prosopis laevigata*, *Eucalyptus camaldulensis*, *Ebenopsis ebano* and *Helietta parvifolia*, represented 72.6% of incident precipitation, with 74.16, 84.68, 64.69 and 66.87% respectively. The order of the canopy permeability was *Eucalyptus camaldulensis* > *Prosopis laevigata* > *Helietta parvifolia* > *Ebenopsis ebano*. The determination coefficient (r^2) for the linear regression analysis between incident precipitation and throughfall was relatively high, from 0.91 (*Helietta parvifolia*) to 0.95 (*Eucalyptus camaldulensis*).

Average stemflow represented 2.39% of total precipitation. *Ebenopsis ebano* and *Eucalyptus camaldulensis* were the species with the greatest percentage of stemflow, between 3.29 and 3.66%, respectively, while *Prosopis laevigata* corresponded to only 0.23% and it was not possible to obtain stemflow for *Helietta parvifolia* because of technical measuring difficulties. Generally, the values observed agreed with those found by other authors, such as Oyarzún *et al*. (1985), who reported the supply by this component as not greater than 5%. In general, the determination coefficient values obtained from the regression equations for stemflow ranged between r^2 = 0.78 (*P. laevigata*) and 0.84 (*E. ebano, E. camaldulensis*). This range is larger than that of throughfall due to the characteristics of the rain and differences among the species that affect the amount of water reaching the soil at the base of the trunks, which is insignificant when there is light rainfall. It also contributes little to net precipitation. The low stemflow percentage for *P. laevigata* in comparison to the other species may be due to its rougher and more cracked bark, resulting in less self-supply towards the soil than *Eucalyptus camaldulensis* which has a smooth bark and is taller, resulting in more collection of rainwater and a larger flow of water.

The sum of throughfall (TF) and stemflow (Sf) provides the net precipitation (Pn), resulting in 72.9% of incident precipitation for the four species (74.38, 65.49 and 84.84% for *P. laevigata*, *E.* ébano and *E. camaldulensis* respectively). The value remained the same

(67%) for *H. parvifolia*, since it was not considered a component of stemflow. The linear regressions for net precipitation for the four species showed a significant correlation with incident precipitation ($r^2 = 0.92$ to 0.95).

Canopy interception loss (*I*) is presented in Table 2, where the difference between incident precipitation and net precipitation corresponded to 27.1% of the interception loss, on average, for the four species studied. The order was *Ebenopsis ebano* > *Helietta parvifolia* > *Prosopis laevigata* > *Eucalyptus camaldulensis*, where *E. ebano* had the highest interception, with 34% (337 mm), followed by *H. parvifolia* with 33% (336 mm), *P. laevigata* with 25% (215 mm); *E. camaldulensis* had the lowest interception loss with 15% (200 mm). These results indicate that the *E. ebano* and *H. parvifolia* canopies can intercept as much as 1.5 times more rainfall than other species (*E. camaldulensis* and *P. laevigata*), reflecting very different hydrological functions in the basins in which different species are found.

Calculations of canopy storage capacity, determined by the method proposed by Leytón *et al*. (1967) and obtained based on 10 rainfall events having values under 2.5 mm, were: 0.1558 mm *for Prosopis laevigata*, 0.1201 mm for *Ebenopsis ebano*, 0.2782 mm for *Eucalyptus camaldulensis* (the highest) and 0.0303 mm for *Helietta parvifolia* (Table 3). These values are generally low compared to other studies, since no species presented storage values over 1 mm. Jaramillo (2003) reported foliage water storage capacity from 0.4 mm for a coffee plantation with pine shadow to 2.2 mm for a multi-strata tropical forest. In the present study, although *H. parvifolia* had less storage capacity, interception loss values were nearly the same as *E. ebano*. This may be due to the geometric shape of the branches, which contributes to the results obtained. As mentioned by Donoso (1983), cited by Valenzuela (2003), interception loss is highest for intermediate ages when the canopy is closed.

The results from interception loss are similar to those reported by Cantú and González (2005) in an investigation of the same ecosystem while studying the species *Acacia berlandieri*, *A. rigidula* and *Diospyros texana*, which had values of 18, 15 and 22%

Table 2. Relationship between interception loss and incident precipitation (978.7 mm) during the experimental period.

Species	*n*	Interception Range (mm) (%)		Total Interception (mm) (%)	
E. ebano	49	0.4 - 52.3	2.8 - 93.2	337	34.5
E. camaldulensis	48	0.0 - 28.2	0.4 - 68.3	200	15.2
H. parvifolia	49	0.1 - 53.2	3.6 - 76.6	336	33.1
P. laevigata	48	0.3 - 38.9	1.5 - 86.5	215	25.6

Table 3. Canopy Saturation Values for the Four Study Species.

Species	Storage Capacity	
	Saturation values (mm)	r^2
H. parvifolia	0.0303	0.8911
E. ebano	0.1201	0.6842
E. camaldulensis	0.2782	0.9275
P. laevigata	0.1558	0.7092

Table 4. Summary of the Regression Analysis to Describe Interception Loss for the Canopies of the Species Studied.

Species	*n*	*Y*-value of the intercept (β_o)			Slope (β_1)			R^2 adjusted
		(β_o)	(EEE)	(*P* value)	(β_1)	(EEE)	(*P* value)	
E. ebano	49	0.345	0.023	< 0.001	0.014	0.748	0.985	0.821
E. camaldulensis	48	0.152	0.027	< 0.001	1.103	0.876	0.215	0.395
H. parvifolia	49	0.331	0.029	< 0.001	0.241	0.948	0.800	0.723
P. laevigata	48	0.256	0.032	< 0.001	0.130	0.897	0.886	0.571

and storage capacities of 0.24, 0.14 and 0.14 mm, respectively. González *et al*. (2009), cited by Guevara *et al.* (2010) reported 21 and 27% for rainfall interception by *P. laevigata* canopies in two study sites values. Huber and Trecaman (2004) mention that the canopy characteristics are more important to the percentage of interception as precipitation decreases.

The results of the regression analysis of interception are shown in Table 4, where the ranges obtained for the determination coefficient between incident precipitation and interception ranged from $r^2 = 0.40$ for *E. camaldulensis* to 0.82 for *E. ebano*, which had a higher percentage of interception loss. These values indicate that other factors are involved in interception loss, such as rainfall intensity, wind speed, daily or nightly events and evapotranspiration, among other variables required to perform a multiple regression analysis. In addition, *E. camaldulensis* is the tallest species and has a medium canopy, which presented the lowest interception values. The individual analysis of the precipitations that occurred showed that the rain reaching the soil was not a constant fraction of total rainfall, but rather, interception tends to be greater for incipient precipitation (Figure 5).

Rain Leaching

The physiochemical properties of rain water, such as pH and electrical conductivity (EC), indicate how the nutrients deposited on the species modify the chemical composition of the rainwater. Leaching or absorption of these nutrients is indirectly inferred by the pH value and the electrical conductivity during rainfall events, comparing contents above and below the canopy as well as the stemflow values of the four species studied. Table 5 shows the values obtained, in which the average pH for incident precipitation was 6.61. For throughfall, the lowest value was 6.56 for the four species (*Prosopis laevigata*, *Eucalyptus camaldulensis*, *Ebenopsis ebano* and *Helietta parvifolia*) and the pH in the stemflow was under 6.30. The pH values generally decreased as the amount of rain decreased.

On the other hand, electrical conductivity was inversely proportional to pH, which increased as water flowed through the canopy. Incident precipitation was 100.57 μS cm^{-1} and throughfall was 189.93 μS cm^{-1}; stemflow values were similar to incident precipitation. Nevertheless, a considerable increase, to 1 219 μS cm^{-1}, was observed for *Prosopis laevigata*, probably due to the phenology of this species, which may have richer nutrient leaching through its cracked trunk, and there is a very notable difference compared to the water that flows through the canopy.

The Kruskal-Wallis analysis of variance was used to detect significant differences in pH and EC for incident precipitation and throughfall for the four species during 42 rainfall events, finding significant differences

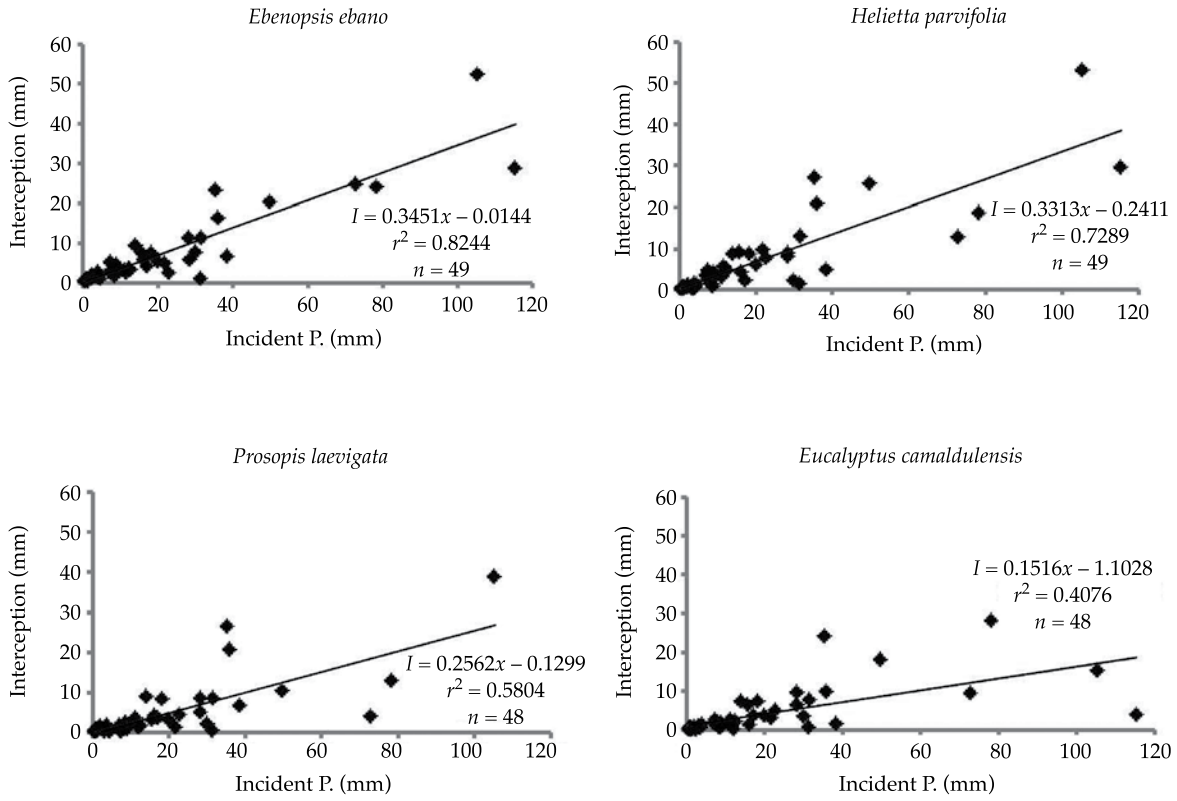

Figure 5. Relationship between Interception Loss and Incident Precipitation for the Canopies of Four Species.

Table 5. Average pH and Electrical Conductivity Values for Incident Precipitation, Throughfall and Stemflow for the Four Species Studied.

Species	Throughfall			Stemflow		
	n	pH	EC (μS cm-1)	*n*	pH	EC (μS cm-1)
E. ebano	41	6.69	281	18	6.87	104
E. camaldulensis	42	6.44	134	33	5.74	100
H. parvifolia	42	6.73	185	17	6.63	80
P. laevigata	41	6.39	158	30	5.96	1 219
Promedio		6.56	189.5		6.30	376
Incident Precipitation	**42**	**6.61**	**100**			

($P < 0.05$) for the two variables and the majority of the events. Therefore, a normality and homogeneity of variances test was performed using the Komolgorov-Smirnov statistical test and the Levene test, in which 23 events did not meet the assumption of normality for pH and EC, according to the Komolgorov-Smirnov test, and 28 events did not meet the assumption of homogeneity of variance based on the Levene test. For

the non-parametric test, the Mann Whitney U mean comparison was used to identify significant differences ($P < 0.005$) among the species studied for individual rainfall events. No significant differences were found when comparing incident precipitation and throughfall for the four species studied. The results of the statistical analysis indicate that the differences among the events are due to the particularity of each rainfall event, which is influenced by the type of storm and wind direction, carrying nutrient concentrations, depending on the area, and depositing them at the trunks of the trees. Jiménez *et al*. (2006) report an increase in pH and conductivity as water passes through the leaves and branches of the trees of a secondary forest and some forest plantations, attributing this to increases at the bases.

Conclusions

The redistribution of rain for the species studied consisted of 72.9% net precipitation and 27.1% interception loss, with a total of 978.77 mm of precipitation registered during 49 events, in which the largest number of events (43%) were between 5 and 25 mm. Of the four species studied, the *Ebenopsis ebano* and *Helietta parvifolia* canopies had the highest rainfall interception loss, with 34 and 33%, respectively, followed by *Prosopis laevigata* with 25% and *Eucalyptus camaldulensis* with 15%. While stemflow supplied the least amount of net precipitation, its ecological importance to these types of ecosystems is recognized. The canopy storage capacity was greatest for *P. laevigata* and *E. camaldulensis* due to differences in the dosimetrics of the species. The pH and electrical conductivity of rain leaching varied with the redistribution of the precipitation. The pH values obtained were slightly acidic to neutral and had a similar behavior among rainfall events. Electrical conductivity tended to increase as the rain flowed through the canopy, becoming even richer in the stemflow, where *P. laevigata* had the highest values. This type of investigation provides tools to make decisions about the reforestation and restoration of ecosystems, in terms of the selection of species to plant and their effect on the water balance of an ecosystem. This is especially important for northeastern Mexico where the prognosis for interception loss is crucial because of environmental problems in the region related to limited or reduced water resources. Thus, the management of vegetation is highly important to the amount of water available for use by the soil.

Received: 15/06/2012
Accepted: 18/06/2013

References

ALANÍS, G.J. y GONZÁLEZ, D. *Flora nativa ornamental para el área metropolitana de Monterrey, Nuevo León, México. Descripción y requerimiento de las especies para el paisaje urbano*. Monterrey, México: Universidad Autónoma de Nuevo León, R. Ayuntamiento de Monterrey, 2000-2003, 2003, 128 pp.

ASTON, A.R. Rainfall interception by eight small trees. *Journal of Hydrology*. Vol. 42, 1979, pp. 383-386.

BELMONTE, S.F. y ROMERO, D.A. *Interceptación en algunas especies del matorral mediterráneo*. Cuadernos de Ecología y Medioambiente, 7. Murcia: Universidad de Murcia, 1999, 202 pp.

CANTÚ, S.I. y GONZÁLEZ, R.H. Propiedades hidrológicas del dosel de los bosques de pino-encino en el noreste de México. *Ciencia UANL*. Vol. V, núm. 1, 2002, pp. 72-77.

CANTÚ, S.I. y GONZÁLEZ, R.H. Pérdidas por intercepción de la lluvia en tres especies de matorral submontano. *Ciencia UANL*. Vol. VIII, núm. 1, 2005, pp. 80-85.

CROCKFORD, R. and RICHARDSON, D. Partitioning of rainfall into throughfall, stemflow and interception effect of forest type, ground cover and climate. *Hydrological Processes*. Vol. 14, 2000, pp. 2903-2920.

DE JONG, S.M. and JETTEN, V.G. Estimating spatial patterns of rainfall interception from remotely sensed vegetation indices and spectral mixture analysis. International Journal of Geographical Information Science. Vol. 21, No. 5, 2007, pp. 529-545.

ECHEVERRÍA, C., HUBER, A. y TABERLET, F. Estudio comparativo de los componentes del balance hídrico en bosque nativo y una pradera en el sur de Chile. *Bosque*. Vol. 28, núm. 3, 2007, pp. 271-280.

ESTRADA, C.E., VILLARREAL, Q.J.A. y JURADO, E. Leguminosas del norte del estado de Nuevo León, México. *Acta botánica mexicana.* Vol. 73, 2005, pp. 1-18.

GUEVARA, E.A., CERVANTES, J.M., SUZÁN, A.H., GONZÁLEZ, S.E., HERNÁNDEZ, S.L., MALDA, B.G. y MARTÍNEZ, D.M. Fog interception by Ball moss (*Tillandsia recurvata*). *Hydrology and Earth System Sciences Discussions.* Vol. 7, 2010, pp. 1655-1676.

HUBER, A. Cambios en el balance hídrico provocado por la forestación con *Pinus radiata* D. Don en el secano interior del centro de Chile. *Gestión Ambiental*. Vol. 9, 2003, pp. 57-66.

HUBER, A. y TRECAMAN, R. Respuesta del balance hídrico al raleo de una plantación joven de *Pinus radiata* (D. Don) en el secano Interior de Chile. *Terra Latinoamericana.* Vol. 22, 2004, pp. 417-424.

JARAMILLO, R.A. La lluvia y el transporte de nutrimentos dentro de ecosistemas de bosques y cafetales. *Cenicafé.* Vol. 54, núm. 2, 2003, pp. 134-144.

JIMÉNEZ, R.C., CALVO, A.J.C. y ARIAS, A.D. Lavado de nutrientes en plantaciones forestales de *Vochysia ferruginea* Mart. y *Vochysia guatemalensis* Donn. Sm. Sarapiqui, Costa Rica. *Kuru. Revista Forestal*. Vol. 3, núm. 8, 2006, pp. 16-26.

JOHNSON, R.C. The interception, throughfall and stemflow in a forest in highland Scotland and the comparison with other upland forests in the U.K. *Journal of Hydrology*. Vol. 118, 1990, pp. 281-287.

LEYTON, L., REYNOLDS, E.R.C., and THOMPSON F.B. *Rainfall interception in forest and moorland*. In Int. Symp. on Forest Hydrology. Sopper, W.E. and Lull, H.W. (editors). Oxford: Pergamon, 1967, pp. 163-178.

MURAKAMI, S. Abrupt changes in annual stemflow with growth in a young stand of Japanese cypress. *Hydrological Research Letters.* Vol. 3, 2009, pp. 32-35.

OYARZÚN, C.E., HUBER, A.W. y VÁSQUES, S.G. Balance hídrico en tres plantaciones de *Pinus radiata* I. Redistribución de las precipitaciones. *Bosque*. Vol. 6, núm. 1, 1985, pp. 3-14.

PRADO, F.A., HERNÁNDEZ, S.L. y VENTURA, R.E. Intercepción de lluvia por *Lysiloma microphylla* en el Municipio de Querétaro. Querétaro, México: Universidad Autónoma de Querétaro, 2007, p. 5.

STRAVS, L., BRILLY, M., and SRAJ, M. Chapter 25: Precipitation interception modeling using machine learning methods-The Dragonja river basin case study, R.J. Abrahart et al. (editors). *Practical Hydroinformatics, Water Science and Technology*. Library 68. Springer, 2008, pp. 347-358.

UVALLE, J.I. *Características fisiológicas y nutrimentales en especies arbustivas forrajeras nativas de la flora del noreste de México*. Tesis de doctorado en Ciencias con Especialidad en Alimentos. San Nicolás de los Garza, México: Facultad de Ciencias Biológicas, Universidad Autónoma de Nuevo León, julio, 2008, pp. 171.

VALENZUELA, C.P.A. *Pérdidas de agua por intercepción en plantaciones de Pinus radiata D. Don en la zona del secano interior de la VII Región de Chile*. Tesis de Ingeniero Forestal. Valdivia: Facultad de Ciencias Forestales, Universidad Austral de Chile, 2003, 92 pp.

WATTERS, R.J. and PRICE, A.G. The influence of stemflow from standing dead trees on the fluxes of some ions in a mixed deciduous forest. *Canadian Journal of Forest Research*. Vol. 18, 1987, pp. 1490-1493.

WANG, D. and WANG, G. Toward a robust canopy hydrology scheme with precipitation subgrid variablility. *Journal of Hydrometeorology.* Vol. 8, 2007, pp. 439-446.

XIAO, Q., MCPHERSON, E.G., USTIN, S.L., and GRISMER, M.E. A new approach to modeling tree rainfall interception. *Journal of Geophysical Research*. Vol. 105, No. 23, 2000, pp. 29173-29188.

Institutional Address of the Authors

Ing. María Inés Yáñez Díaz

Área de especialidad: Edafología e Hidrología Forestal
Facultad de Ciencias Forestales
Universidad Autónoma de Nuevo León
Carretera Nacional km 145
Apartado Postal 41
67700 Linares, Nuevo León, México
Teléfonos: +52 (821) 2124 895, 2124 3010
mainnes61@hotmail.com

Dr. Israel Cantú Silva

Área de especialidad: Hidrología Forestal
Facultad de Ciencias Forestales
Universidad Autónoma de Nuevo León
Carretera Nacional km 145
Apartado Postal 41
67700 Linares, Nuevo León, México
Teléfonos: +52 (821) 2124 895, 2124 3010
icantu59@gmail.com

Dr. Humberto González Rodríguez

Área de especialidad: Fisiología vegetal
Facultad de Ciencias Forestales
Universidad Autónoma de Nuevo León
Carretera Nacional km 145
Apartado Postal 41
67700 Linares, Nuevo León, México
Teléfonos: +52 (821) 2124 895, 2124 3010
gonhumberto@gmail.com

Dr. José I. Uvalle Sauceda

Área de especialidad: Manejo de Pastizales y Fauna Silvestre
Facultad de Ciencias Forestales
Universidad Autónoma de Nuevo León
Carretera Nacional km 145
Apartado Postal 41
67700 Linares, Nuevo León, México
Teléfonos: +52 (821) 2124 895, 2124 3010
joseuvalle@yahoo.com

Click here to write the autor

Flood Forecasting Using the Discrete Kalman Filter

• Mirce Ivón Morales-Velázquez* • Javier Aparicio •
Universidad Nacional Autónoma de México
*Corresponding Author

• Juan B. Valdés •
Universidad de Arizona

Abstract

MORALES-VELÁZQUEZ, M.I., APARICIO, J. & VALDÉS, J.B. Flood Forecasting Using the Discrete Kalman Filter. *Water Technology and Sciences* (in Spanish). Vol. V, No. 2, March-April, 2014, pp. 85-110.

This study evaluates the usefulness and applicability of the discrete Kalman filter algorithm for predicting short-term floods. The algorithm is applied to the basin of the Ángel Albino Corzo (Peñitas) dam, which is part of the Grijalva Hydroelectric System, as well as to the Sayula Hydrometric Station. It is used to determine the response function for the basin and thus forecast flows into the reservoir. To that end, both flow data and precipitation recorded at weather stations located in the study area are used, as well as calculated inflows to the basin. This analysis evaluates multiple time increments and different response functions, as well as their associated parameters, using the Nash-Sutcliffe coefficient. Highly acceptable values were obtained, such that the filter is found to be useful for short-term flow forecasting, highlighting its usefulness as a tool to support policy development and the operational control of reservoirs.

Keywords: Kalman Filter, Peñitas, predicting short-term flows, recursive.

Resumen

MORALES-VELÁZQUEZ, M.I., APARICIO, J. & VALDÉS, J.B. Pronóstico de avenidas utilizando el filtro de Kalman discreto. Tecnología y Ciencias del Agua. *Vol. V, núm. 2, marzo-abril de 2014, pp. 85-110.*

Se evalúa la utilidad y aplicabilidad del algoritmo del filtro de Kalman discreto en la predicción de caudales a corto plazo. El algoritmo se aplica a la cuenca propia de la presa Ángel Albino Corzo (Peñitas), parte del Sistema Hidroeléctrico Grijalva, y a la estación hidrométrica Sayula. El algoritmo se utiliza para determinar la función de respuesta en la cuenca y con ello pronosticar los caudales de entrada al embalse. Para esto se usan tanto los registros de caudal y de precipitación provenientes de las estaciones climatológicas ubicadas en la cuenca como los caudales calculados con el tránsito inverso en el vaso. En el análisis se evalúan varios intervalos de tiempo de pronóstico, así como diferentes tipos de función de respuesta y parámetros asociados. Los resultados son evaluados por medio del coeficiente de Nash-Sutcliffe, obteniéndose valores muy aceptables, de manera que el filtro se considera aplicable al pronóstico de avenidas a corto plazo, destacando su utilidad como una herramienta de apoyo en el desarrollo de políticas de operación y control de los embalses.

Palabras clave: *pronóstico de avenidas a corto plazo, filtro de Kalman, Peñitas, recursivo.*

Introduction

Large floods have occurred throughout history and particularly in recent years in Mexico and other places around the world. For example, most notably in southeastern Mexico in Chiapas in 1998 and Quintana Roo, Chiapas, as well as in Veracruz in 2005, as a result of hurricanes Emily, Stand and Wilma. Also notable are the floods in Tabasco in 2003, 2010 and 2007 (Salas and Jiménez, 2004). The latter, in particular, increased water levels in the river systems in the Grijalva Basin, resulting in very large floods in most of the state of Tabasco and in Chiapas (Aparicio *et al*., 2009; Rivera-Trejo *et al*., 2009).

In order to address these flooding episodes using warning systems and operating criteria for control infrastructure, it is important to have a reliable and accurate flood forecasting

system. The purpose of this work is to evaluate the usefulness of the discreet Kalman filter algorithm to forecast short-term floods using the Ángel Albino Corzo (Peñitas) basin as a case study (Figure 1).

Methodology

The Kalman filter (Kalman, 1960) was used to identify the basin's response function and the resulting flows into the C.H. Peñitas reservoir. This was found through the convolution of the response function with precipitations or with flows and precipitations registered during a period prior to the time analyzed.

The Kalman filter (Kalman, 1960) describes a recursive solution to the linear filtering of discreet data. The filter attempts to calculate the state (n-dimensional space of real numbers) over time (hereafter k) of a process controlled during a discreet time, as described by the matrix-valued stochastic linear differential equation (Welch and Bishop, 2001):

$$x_k = Ax_{k-1} + Bu_k + w_{k-1} \quad (1)$$

where the measurement $z \in \Re^m$ is represented by:

$$z_k = Hx_k + v_k \quad (2)$$

The matrix $A_{n\times n}$ in equation (1) associates the state during the prior time k–1 with the state occurring at the moment k. Although this matrix can change over time, it is usually considered constant (Welch and Bishop, 2001). The matrix $B_{n\times l}$ associates the optional control of inputs $u \in \Re^l$ with state x. Matrix $H_{m\times n}$ in equation (2) associates the state with the measurement z_k. In practice, in hydrology $B_{n\times l}$ is generally also considered to be constant (*Ibid*).

The random variables w_k and v_k in equations (1) and (2) represent process noise and measurement noise, respectively. It is accepted that these variables are independent of each other, that they are white noise (that is, their signal values at two different times do not statistically correlate), and have a normal probability distribution function (Drécourt, 2003; Kottegoda, 1980; Kim *et al.*, 2004).

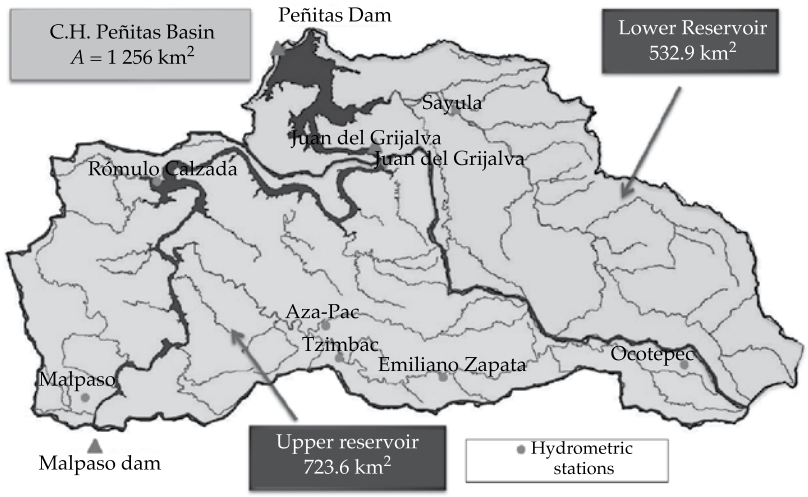

Figure 1. C.H. Peñitas Basin (Aguilar *et al.*, 2009).

$$p(w) \sim N(0,S) \quad (3)$$

$$p(v) \sim N(0,R) \quad (4)$$

S represents the covariance perturbation matrix for the process and R the covariance perturbation matrix for the measurement. Although both matrices can change over time, for simplicity, constants are commonly used in practice and can be represented as (Simon, 2001):

$$S = E\left[w_k w_k^T\right] \quad (5)$$

$$R = E\left[v_k v_k^T\right] \quad (6)$$

where $E[\bullet]$ is the mathematical expectation. These matrices represent the variation in the errors or perturbation calculation of the process or system analyzed, and the process measurements with respect to the process mean.

The Kalman filter uses a feedback control, since it estimates the process at a moment in time and then receives feedback from the measurements of the observed data (Welch and Bishop, 2001).

From this perspective, the equations used to generate the Kalman filter are divided into two groups (*Ibid.*):

- *Time updating or forecasting equations.*
- *Updating equations with observed data.*

The first group projects the current state to a future time using the state in the prior moment $k - 1$ as a reference, and updates the error covariance estimates to obtain the *a priori* estimate of the state for the next time step. The second group of equations provides feedback, that is, it provides new information for the previous estimate, with which an improved estimate of the *a posteriori* state is obtained. Thus, the Kalman filter includes a *projection-correction* algorithm by forecasting the new state and its uncertainty and correcting the projection with the new measurement.

The application of the Kalman filter can be summarized by the following steps (Welch and Bishop, 2001), shown in Figure 2. The circumflex accent indicates an estimate and the superscript indicates that the estimate is *a priori*:

1. Generate a forecast of the state for a future time using information available up until that moment, based on the initial state and the error covariance matrix $P\bar{k}$.
2. Correct the forecast of the state (process of updating based on measurements). The first task in this stage is to calculate the *Kalman gain*, K_k. This weighting or gain factor is selected in order to minimize the error covariance of the new estimate of the state, considering both the probable error of the measurements as well as the uncertainty related to the representation of the state of the system.
3. Measure the process to obtain z_k and then generate a new estimate of the state, incorporating the new measurement.
4. Obtain a new estimate of the error covariance matrix to again determine the value of the state.

After each pair of updates of both the state and measurements, the process is repeated based on the new estimates of the state and the error covariance. This recursive nature is one of the most important characteristics of the Kalman filter.

Application of the Discreet Kalman Filter (DKF) to the C.H. Peñitas Basin

To predict flow, hyetographs of effective precipitation are needed. To this end, curves that associate the antecedent precipitation index (*IPA*) with the mean infiltration index

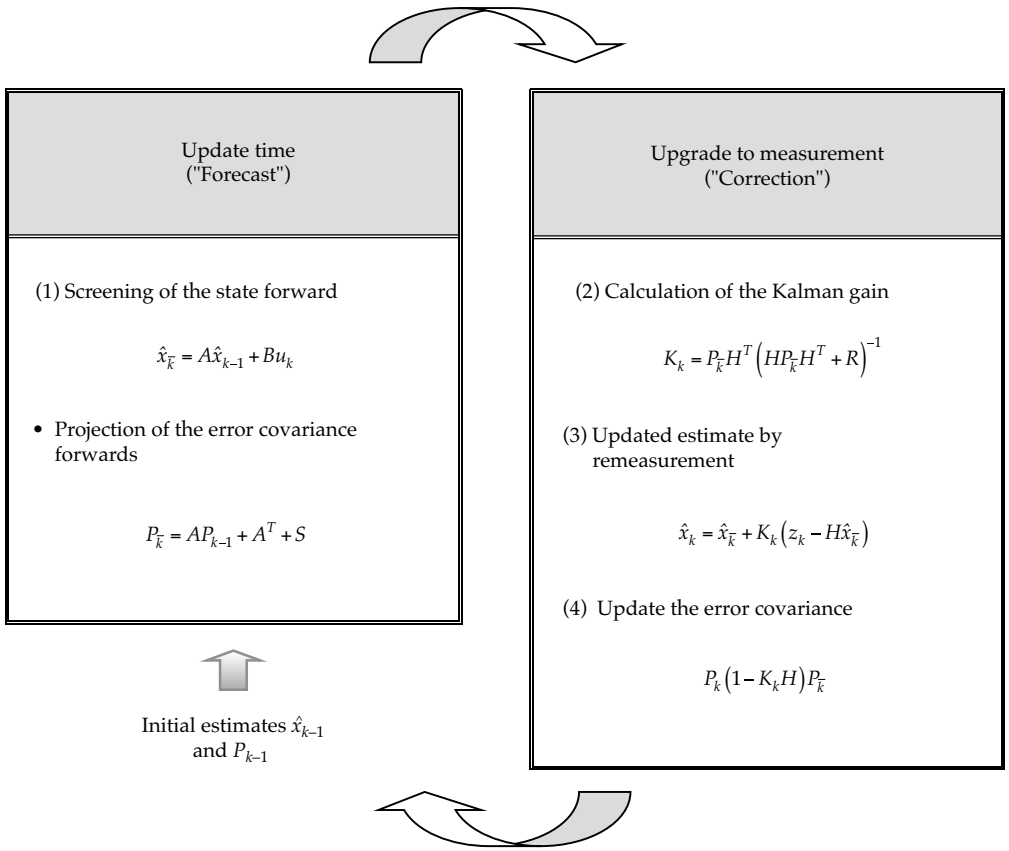

Figure 2. Complete Diagram of the Kalman Filter Operation (Welch and Bishop, 2001, p. 24).

(φ) are obtained (Aparicio, 2011). This enables deducing, based on the actual rain depth, the effective rain which will act as a stimulus in the basin, producing inflow runoff.

In this work, the analysis includes precipitation and runoff records from stations located in the lower basin (Table 1). The period analyzed is from October 31, 2005 at 24:00 hours to February 13, 2012 at 24:00 hours.

To construct the relationship *IPA vs* φ, precipitation is based on the mean $\overline{hp}$ obtained with Thiessen polygons and flows are based on records from the Sayula hydrometric stations. The resulting *IPA vs* φ curve is (see Figure 3):

$$\varphi = -4.213\ln\left(IPA\right) + 24.877 \qquad (7)$$

With equation (7), effective precipitation $hp_{\text{effective}}$ was calculated as follows:

$$\text{If } \varphi > \overline{hp} \rightarrow hp_{\text{effective}} = 0 \qquad (8)$$

$$\text{If } \varphi < \overline{hp} \rightarrow hp_{\text{effective}} = \overline{hp} - \varphi \qquad (9)$$

There are not enough hydrometric stations in the C.H. Peñitas basin to determine the actual inflow to the reservoir. As will be seen later, the filter was evaluated using the flows measured at hydrometric station Sayula, and the modified reverse transit for reservoirs, or reverse transit, was used to forecast flows in the C.H. Peñitas. Based on this, with knowledge of the total outflows in the basin and the evolution of the reservoir levels, total volume or inflow for the reservoir is

Table 1. Weather and Hydrometric Stations Used.

	Weather Stations							Hydrometric Stations	
Upper basin	Zapata	Tzimbac	Rómulo Calzada	Ocotepec	Malpaso	Juan del Grijalva Superior	Aza-Pac	Tzimbac	Aza-Pac
Lower basin	Peñitas	Ocotepec	Zapata	Sayula	Juan del Grijalva Superior			Sayula	

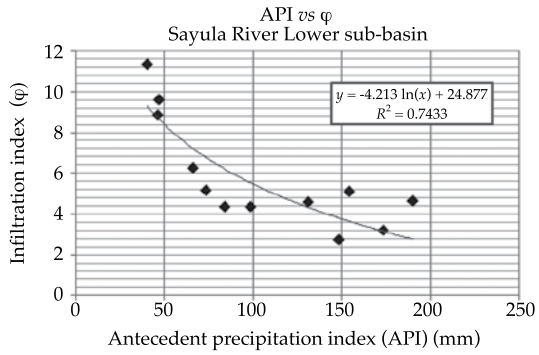

Figure 3. *IPA vs* φ curve.

calculated (Aldama and Aguilar, 1996). For the purpose of this work, reverse transit calculations for the lower basin using the DKF are used to measure inflows into the C.H. Peñitas since they implicitly contain the behavior of the entire basin (Figure 4).

The reverse transit calculation results in significant variations in inflow, which is common for this type of analysis (Aldama and Aguilar, 1996). To obtain a signal with less noise, moving averages of the last 5 measured values were applied (Aguilar *et al*., 2009).

DKF Algorithm for the Instantaneous Unit Hydrograph as a Response Function

Flows were calculated using the instantaneous unit hydrograph (IUH) as a response function. As an example of the calculation process, consider the hyetograph of effective precipitation shown in Figure 5a, which produced the one shown in Figure 5c using the IUH presented in Figure 5b.

During the forecasting of floods, the hyetograph bars are not completely known, but the response function is known —that is, the IUH, whose ordinates can be represented as an increase in flow from one instant to the next (as in the case of in Figure 5b). The hydrograph of direct runoff will be represented as:

$$Q_1 = \boldsymbol{hp_1 q_1}$$

$$Q_2 = Q_1 + hp_1 \delta q_{12} + \boldsymbol{hp_2 q_1}$$

$$\vdots$$

$$Q_6 = Q_5 + hp_1 \delta q_{65} + hp_2 \delta q_{54} + hp_3 \delta q_{43} + hp_4 \delta q_{32} + hp_5 \delta q_{21} + \boldsymbol{hp_6 \delta q_1}$$

For the prediction of each one of the flows based on the records in $k - 1$, the values shown in bold in the above system represent a prediction error since the precipitation corresponding to time k has not yet been recorded.

Therefore, and in a generalized form, the flows can be represented as:

$$Q_t = Hx_t + Q_{t-1} + \varepsilon \qquad (10)$$

$$H = \left[hp_{t-1}, hp_{t-2}, \ldots hp_{t-n}\right]; \; x_t = \begin{bmatrix} \delta q_{n-i-1,n-i} \\ \vdots \\ \delta q_{n-2,n-1} \\ \delta q_{n-1,n} \\ \delta q_{n,n+1} \end{bmatrix}$$

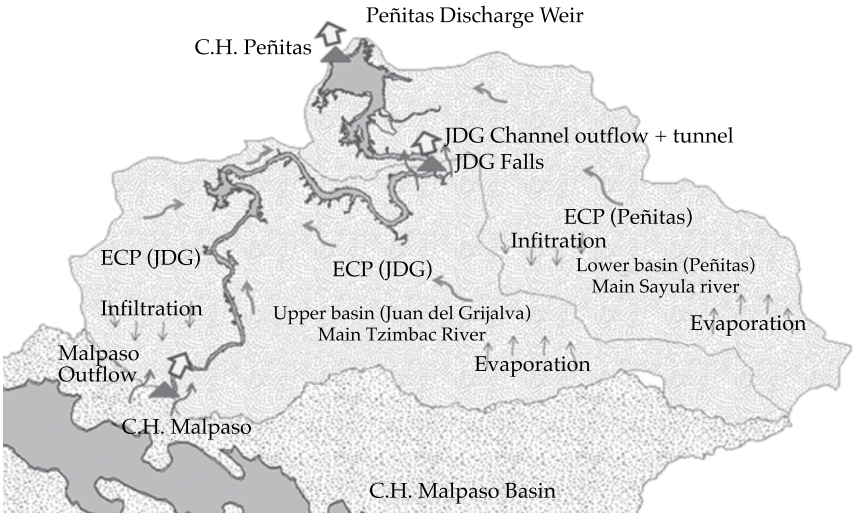

Figure 4. Functioning of the C.H. Peñitas Reservoir.

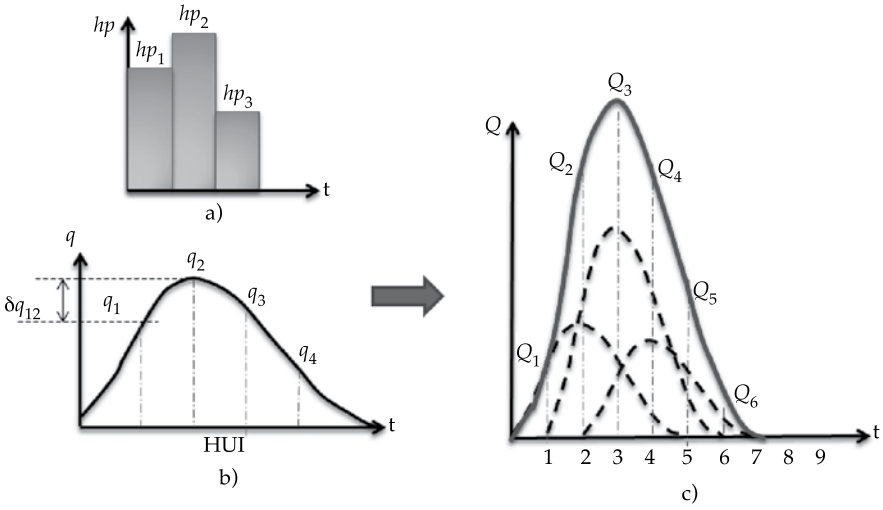

Figure 5. Instantaneous Unit Hydrogram. Example.

where:

Q_t = flow measured at moment t.

x_t = vector containing increases between successive ordinates in the IUH.

H = vector with precipitations prior to the time analyzed, available in the effective precipitation hyetograph.

n = number of bars in the effective precipitation hyetograph.

ε = error in predicting flow, absorbed by the portion of the convolution with the precipitations that have not yet been recorded.

Based on that which has been developed, the variable to be calculated using the DKF algorithm is the increase in the ordinates corresponding to the basin's response function, which in this case is represented by the IUH. These increases are indicated in the filter nomenclature by the term *state*, denoted by $\hat{x}_k$.

Since the exact value of the initial state is not known, its expected value is arbitrarily taken to be a null vector $[0]_{n\times 1}$ of dimension n, where n represents the number of bars in the effective precipitation hyetograph before the time analyzed, included in the convolution with the increase in ordinates in the response function, to obtain the inflows:

$$\hat{x}_{k-1} = [0]_{n\times 1} \tag{11}$$

while the error covariance matrix of the initial state is:

$$P_{k-1} = \eta I \tag{12}$$

where η is a large enough scale to reflect the uncertainty of the proposed values of the initial state, according to Valdés *et al*. (1980), and I is the identity matrix with dimensions $n \times n$.

State forecasting equations

Projection of the state into the future (forecasting):

$$\hat{x}_{\bar{k}} = A\hat{x}_{k-1} + Bu_k \ldots \tag{13}$$

$A_{n\times n}$ is an identity matrix that associates the state at moment $k - 1$ with that which occurs at k; $\hat{x}_{k-1}$ is the state estimated *a priori*; $B_{n\times n}$ is defined as an identity matrix with the same dimensions as matrix A; while u_k, which presents the optional control of inflows, will be taken as a vector of zeros with dimensions $n \times 1$ since the system does not contain variables that can be controlled and that influence its response.

Projection of the error covariance matrix ($P_{\bar{k}}$):

$$P_{\bar{k}} = AP_{k-1}A^T + S \ldots \tag{14}$$

S is the covariance perturbation matrix for the process, with dimensions $n \times n$. In this section, it is handled in three different ways (as a matrix of zeros, a matrix whose main diagonal depends on the errors between forecasted and updated states, and as a very small value near zero), as will be seen below.

With the previous equations, the first forecasting of the state can be obtained, as well as the error covariance matrix. After the response function is obtained, the forecasting of the inflows into the C.H. Peñitas reservoir is calculated as follows:

$$Q_{est1} = H \cdot \hat{x}_{\bar{k}} + Q_{k-1} \tag{15}$$

where $\hat{x}_{\bar{k}}$ contains the increases between the ordinates (q) of the IUH, obtained with the DKF; Q_{est1} is the forecasted flow in the C.H. Peñitas basin; Q_{k-1} is the flow registered at time $k - 1$; and $H_{1\times n} = [Hp_{t-1}, Hp_{t-2}, \ldots, Hp_{t-n-1}]$ is a vector containing the values to be convoluted with the response function, composed of the effective precipitation measurements prior to the moment k analyzed.

Forecast Updating or Correction

Calculating Kalman gain

For the present work, the covariance perturbation matrix for the measurement R (step 2, Figure 2) is $R = \alpha \cdot Q_{k-1}$, where α is a proportionality constant representing a constant error equal to a fraction of the flow measured at the prior time $k - 1$ (Valdés *et al*., 1980). For the updating of the forecast based

on current measurements (step 3 in Figure 2) with equation (10), z_k will be the actual flow measured in k less the flow measured at $k-1$, taken directly from the reverse transit calculation or from the hydrometric station records, depending on the case.

Once the forecasting of the basin's response function has been updated, the forecasting of the inflows into the C.H. Peñitas reservoir is updated as follows:

$$Q_{est2} = H \cdot \hat{x}_k + Q_{k-1} \tag{16}$$

where $\hat{x}_k$ are the corrected or updated increases in the ordinates of the response function.

The following statistics were obtained using the DKF routine, which makes it possible to quantitatively measure the accuracy of the forecast:

- Nash-Sutcliffe coefficient (Nash and Sutcliffe, 1970).
- Mean and standard deviation of the original flow series as well as the forecasted and updated flows.
- Correlation coefficients between the original series of inflows into the C.H. Peñitas, calculated with the reverse transit, and the series of forecasts and updates obtained using the DKF.

Flow Forecasting in the Entire C.H. Peñitas Basin using the IUH as a Response Function

For experimental purposes, three different ways of calculating the covariance perturbation matrix, or noise, in the process S were evaluated. For each one, different values of n, α and N were tested, but due to space limitations only the results obtained with the best combination are presented, using a forecasting interval of 1 h for evaluation purposes.

Application of the DKF using $S = [0]_{n \times n}$

For this case, matrix S was obtained, considered to be composed of a null matrix with dimensions $n \times n$. The best results were obtained with a 3 h forecasting of effective precipitation with matrix H. Figure 6a shows the calculated mean effective precipitation and Figure 6b presents the observed flows (calculated with reverse transit) and forecasts (DKF). The horizontal line between 1.026×10^4 and 1.796×10^4 h indicates the lack of flows records. Figure 7 presents forecasted flows versus observed flows. The 45° diagonal line represents perfect agreement. The relationship between observed versus actual flows (not presented in this work) is similar. Figures 8, 9 and 10 present some specific flows during the time analyzed for a detailed comparison. Only one previous flow value was used for the forecast, with a notable agreement observed among the hydrographs mentioned, in particular with respect to peak flows.

Table 2 summarizes the statistics used to quantitatively evaluate the accuracy of the forecasts, given $\alpha = 0.3$, $N = 1\,000$, $n = 3$.

The mean and standard deviation of the observed flows were 759.26 and 428.79 m^3/s, respectively, and 760.04 and 429.58 m^3/s for the forecasted flows. These data remained reasonably the same.

Application of the DKF with $S \approx 0$

In order to perform the sensitivity analysis, values were tested other than 0 but small for the components of the main diagonal of matrix S, maintaining equation (3). The response was evaluated using the same α, N and n values as in the previous analysis. The results are shown in Table 3. A marginal improvement is seen between the results, and therefore the use of this option is not recommended.

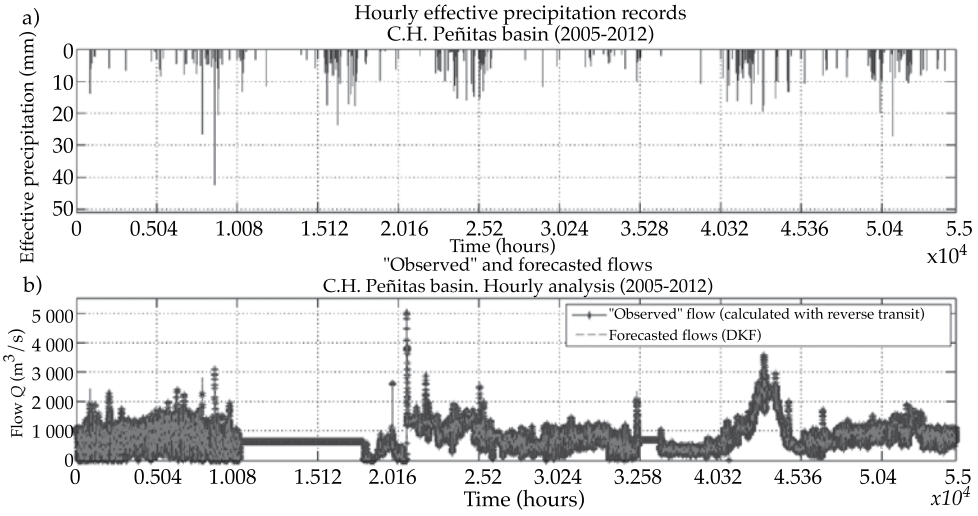

Figure 6. Precipitation and Flow Records used in the Analysis of the C.H. Peñitas basin and 1-h Flow Forecast.

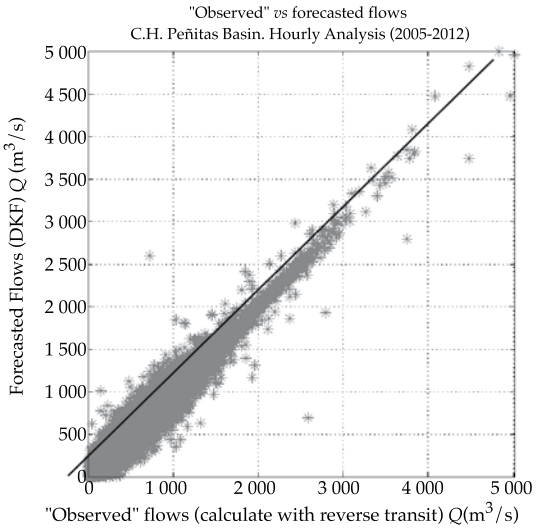

Figure 7. Observed vs Forecasted Flows in the C.H. Peñitas basin with the IUH as a response function and S = [0].

Application of the DKF with $\mathbf{S = X_f - X_u}$

An additional alternative used was to obtain the value of S from the difference between the ordinates of the forecasted X_f and updated X_u response functions, as described by Kim *et al.*, 2004. The main diagonal in matrix S will consist of the deviation in the differences between the increases in the ordinates of the forecasting and updating response functions, accumulated during the prior time step, Δt. The best results were obtained for a 3-h

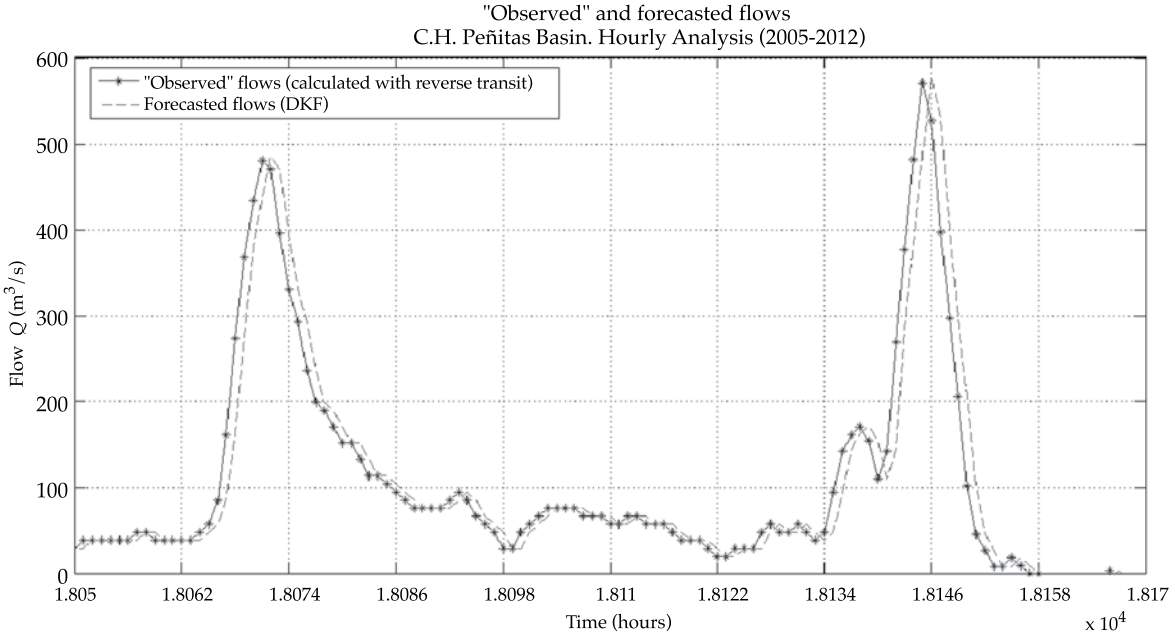

Figure 8. Observed and Forecasted Flows with the DKF (period A from 23/11/2007 01:00 h through 28/11/2007 01:00 h) for the C.H. Peñitas basin with the IUH as a response function and $S = [0]$.

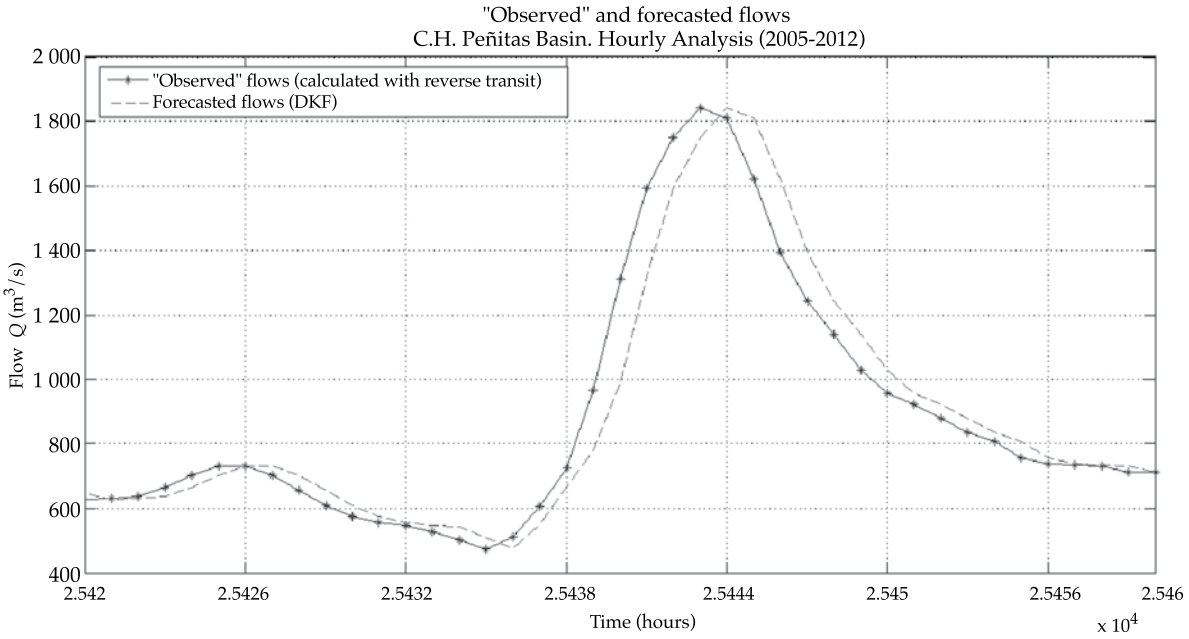

Figure 9. Observed and Forecasted Flows using the DKF (period B from 25/09/2008 03:00 h through 26/09/2008 19:00 h) for the C.H. Peñitas basin with the IUH as a response function and $S = [0]$.

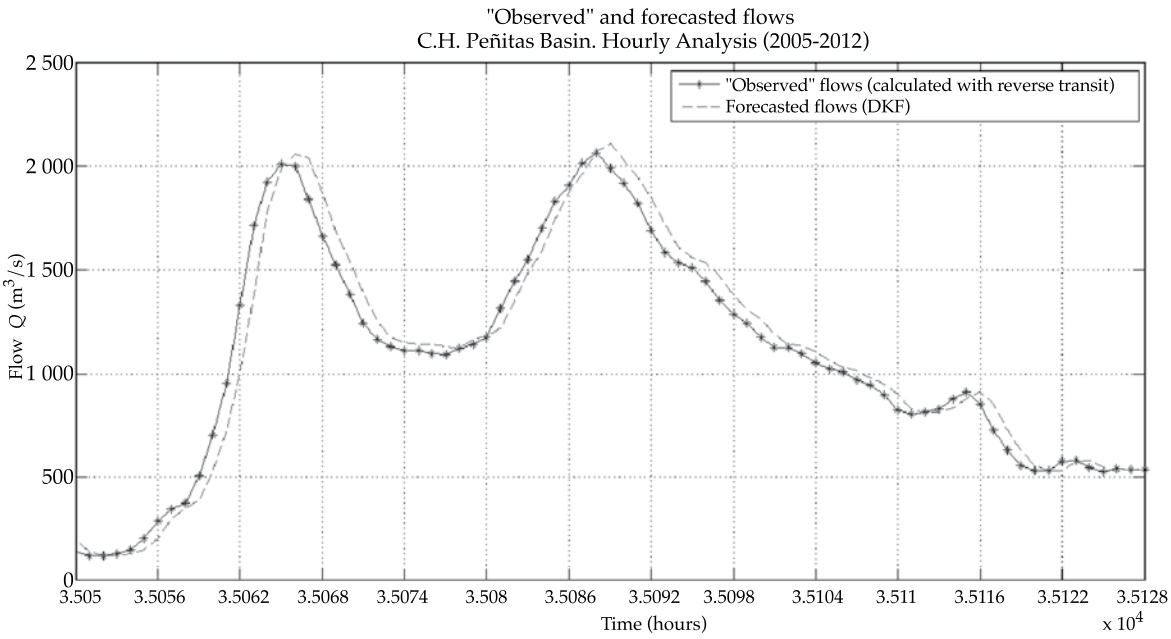

Figure 10. Observed and Forecasted Flows using DKF (period *C* from 31/10/2009 9:00 h through 03/11/2009 15:00 h) for the C.H. Peñitas basin with the IUH as a response function and $S = [0]$.

Table 2. Summary of the Statistics for the Application of the DKF, using IUH as a response function and $S = [0]$.

Concept	Value
Nash-Sutcliffe ("Observed" Q - Forecasted Q)	0.977353
Nash-Sutcliffe ("Observed" Q - Updated Q)	0.977534
Correlation ("Observed" Q - Forecasted Q)	0.99727
Correlation ("Observed" Q - Updated Q)	0.99729

Table 3. Summary of the Statistics for the Application of the DKF, using IUH as a response function and $S \approx 0$.

Errors of roughly	Nash-Sutcliffe ("Observed" Q – Forecasted Q)	Nash-Sutcliffe ("Observed" Q - Updated Q)
0.1	0.977031	0.978011
0.001	0.977389	0.977709
0.0001	0.977412	0.977633
0.00001	0.977389	0.977581
0.0000001	0.977354	0.977535

forecast for effective precipitation with the H matrix and accumulated errors in the response function during 16 prior forecasts. Figure 11 shows observed versus forecasted flows. Some significant differences are seen here as well as in Figure 12, where there is a larger spread than the previous cases. These differences are also seen in the isolated

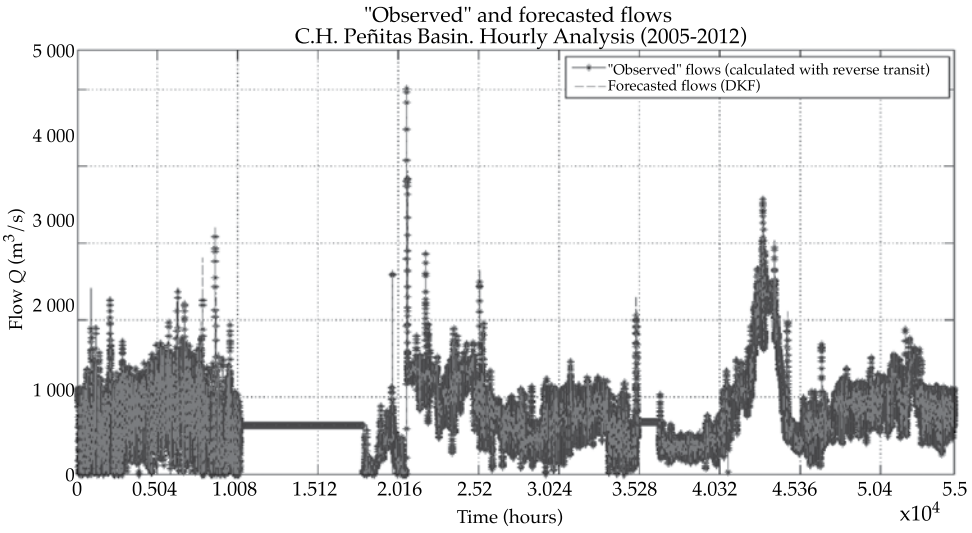

Figure 11. Observed and Forecasted Flows for the C.H. Peñitas Basin Using the IUH as a Response Function and $S = X_f - X_u$.

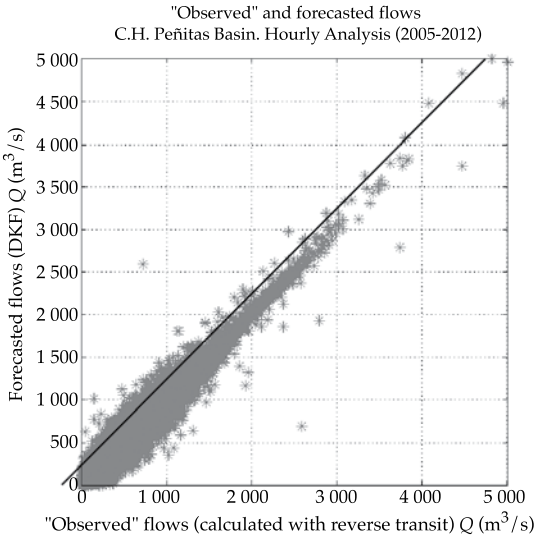

Figure 12. Observed ***versus*** Forecasted Flows for the C.H. Peñitas Basin Using the IUH as a Response Function and $S = X_f - X_u$.

flows in Figures 13, 14 and 15. Therefore, the Nash-Sutcliffe coefficient values and the correlation coefficients are lower, as shown in Table 4.

The mean and standard deviation were 759.26 and 428.79 m^3/s for the observed flows and 760.35 and 432.24 m^3/s for the forecasted flows, respectively.

Discussion and Results

After evaluating the three different alternatives for calculating matrix, it was observed that when the matrix is null, the values of the Nash-Sutcliffe coefficient are highly acceptable (NS = 0.97735), which means that the forecast

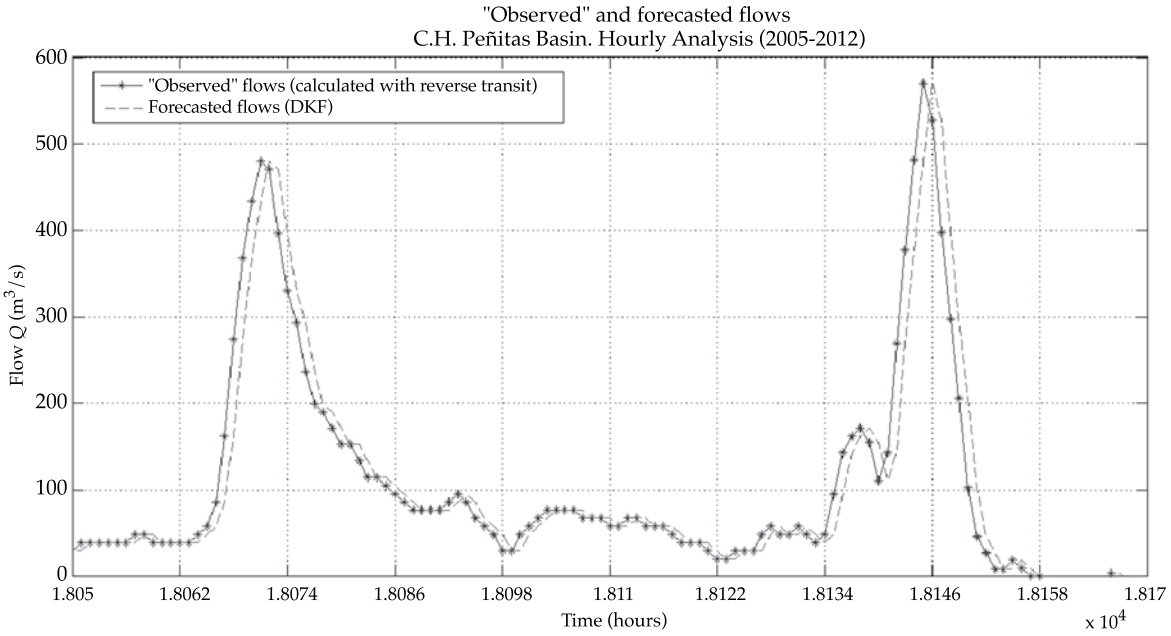

Figure 13. Observed ***versus*** Forecasted Flows with DKF (period A from 21/11/2007 1:00 h to 28/11/2007 01:00 h) for the C.H. Peñitas basin Using the IUH as a Response Function and $S = X_f - X_u$.

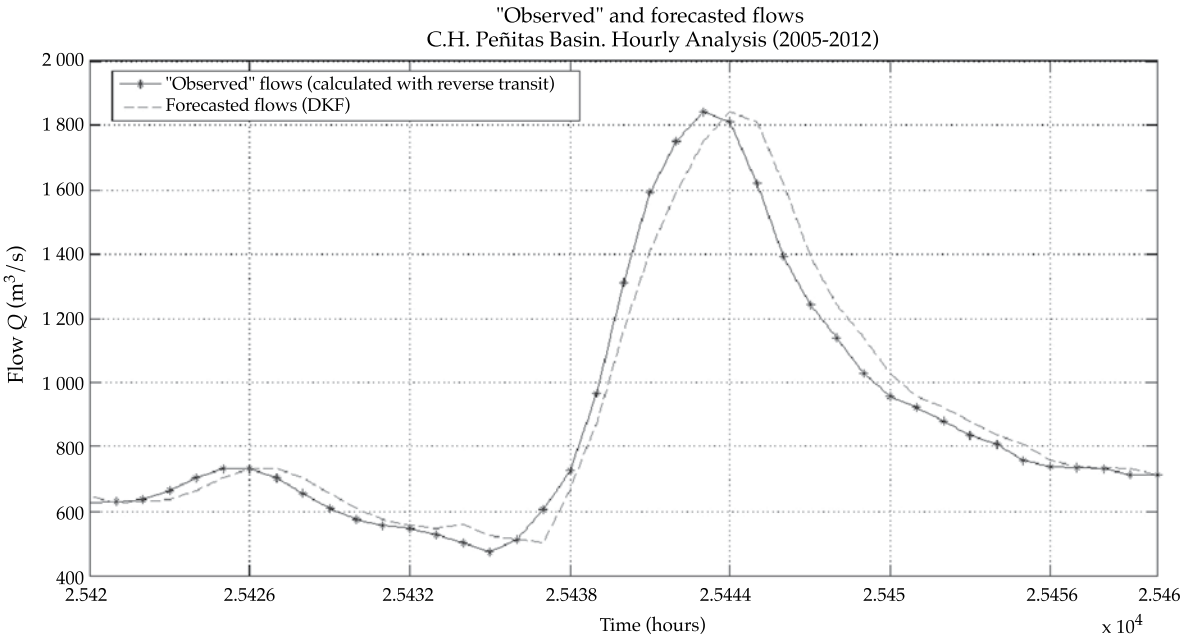

Figure 14. Observed and Forecasted Flows with DKF (period B from 25/09/2008 03:00 h to 26/09/2008 19:00 h) for the C.H. Peñitas basin Using the IUH as a Response Function and $S = X_f - X_u$.

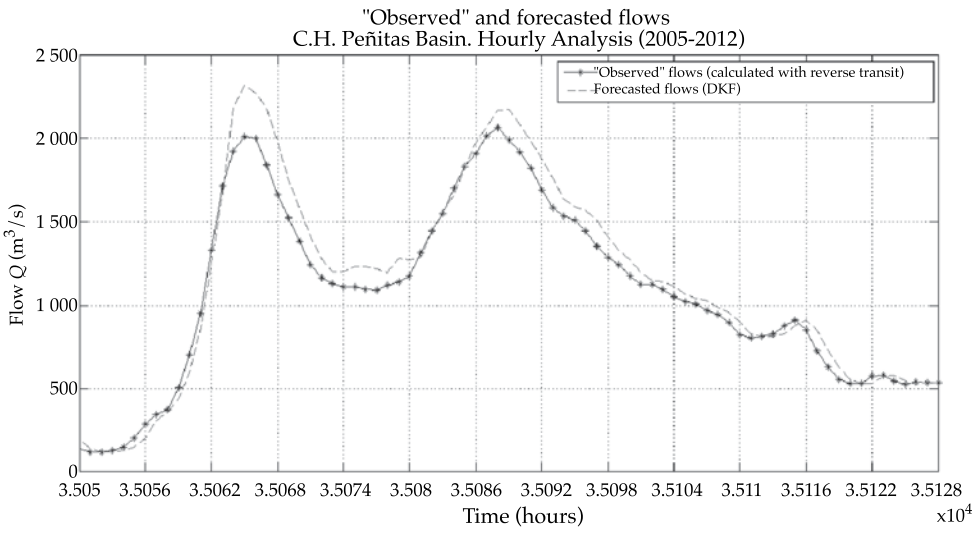

Figure 15. Observed ***and*** Forecasted Flows with DKF (period *C* from 31/10/2009 09:00 h al 03/11/2009 15:00 h) for the C.H. Peñitas basin Using the IUH as a Response Function and $S = X_f - X_u$.

Table 4. Summary of the Statistics from Applying the DKF to the C.H. Peñitas Basin Using the IUH as a Response Function and $S = X_f - X_u$, accumulating 16 prior forecasts.

Concept	Value
Nash-Sutcliffe ("Observed" *Q* - Forecasted *Q*)	0.977298
Nash-Sutcliffe ("Observed" *Q* - Updated *Q*)	0.977709
Correlation ("Observed" *Q* - Forecasted *Q*)	0.99726
Correlation ("Observed" *Q* - Updated *Q*)	0.99731

is a good approximation. When using matrix *S* with numbers near zero, the value of the Nash-Sutcliffe coefficient (NS = 0.97741) improves only marginally. If this matrix consists of errors between the forecasted and updated response functions, the results are less satisfactory. Therefore, the better calculation alternative is when $S = [0]$, which will therefore be used below.

DKF Algorithm using a Modified Response Function

Up to this point, the DKF has been applied with the forecasted response function represented by the instantaneous unitary hydrograph and using only effective precipitation in the convolution with the response function. The following will evaluate a second alternative, which in addition to effective precipitation includes flows measured during a period prior to the time analyzed in matrix *H*. The period of analysis is the same as the previous forecast, that is, October 31, 2005 at 24:00 h to February 13, 2012 at 24:00 h.

The variables included in the application of the DKF algorithm mostly represent what was described in the previous section, except that in this case the dimensions of matrices *A*, *H*, *S* etc. are $n + nQ$ instead of *n*, where *n* is the number of effective precipitation episodes and *n* y *nQ* is the number of flows

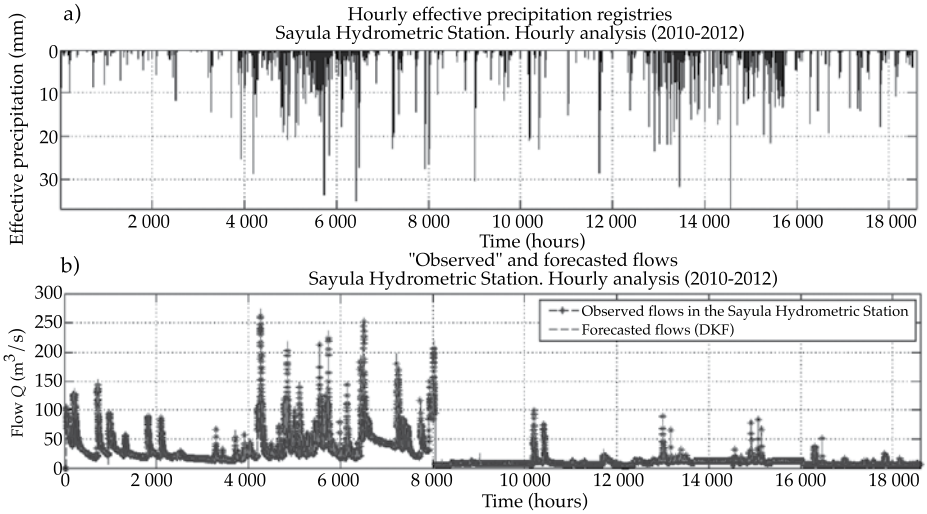

Figure 16. Precipitation and Flow Registries used to Analyze the Sayula Hydrometric Stations, Including Flow Forecasts, Using the Modified Response Function.

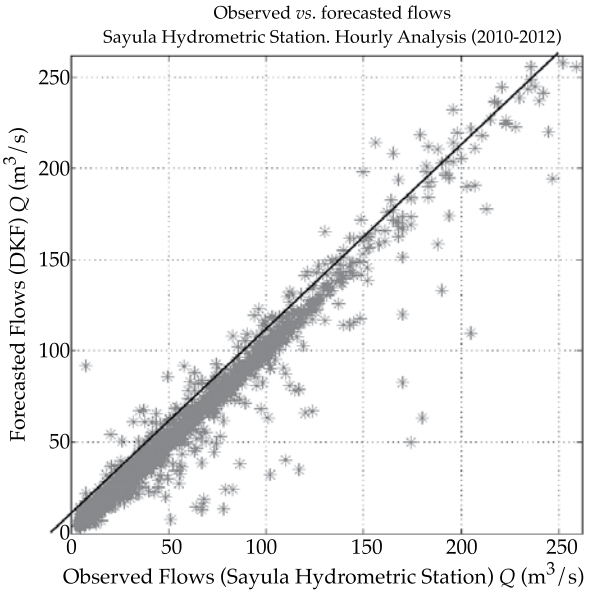

Figure 17. Observed versus Forecasted Flows for the Sayula Hydrometric Station, Using the Modified Response Function.

considered in the convolution performed with the response function. After obtaining the response function with the DKF, the inflows into the C.H. Peñitas reservoir are forecasted using the equation.

$$Q_{est1} = H \cdot \hat{x}_{\bar{k}} \tag{17}$$

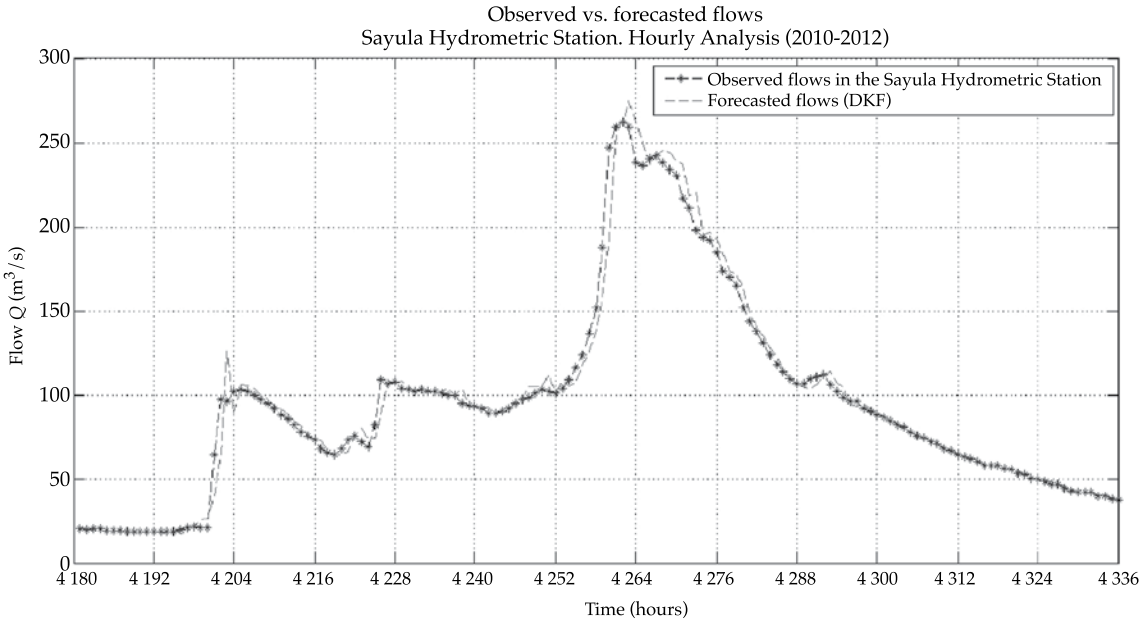

Figure 18. Observed and Forecasted Flow with DKF (flow *A* from 24/06/2010 to 30/06/2010) for the Sayula Hydrometric Station, Using the Modified Response Function.

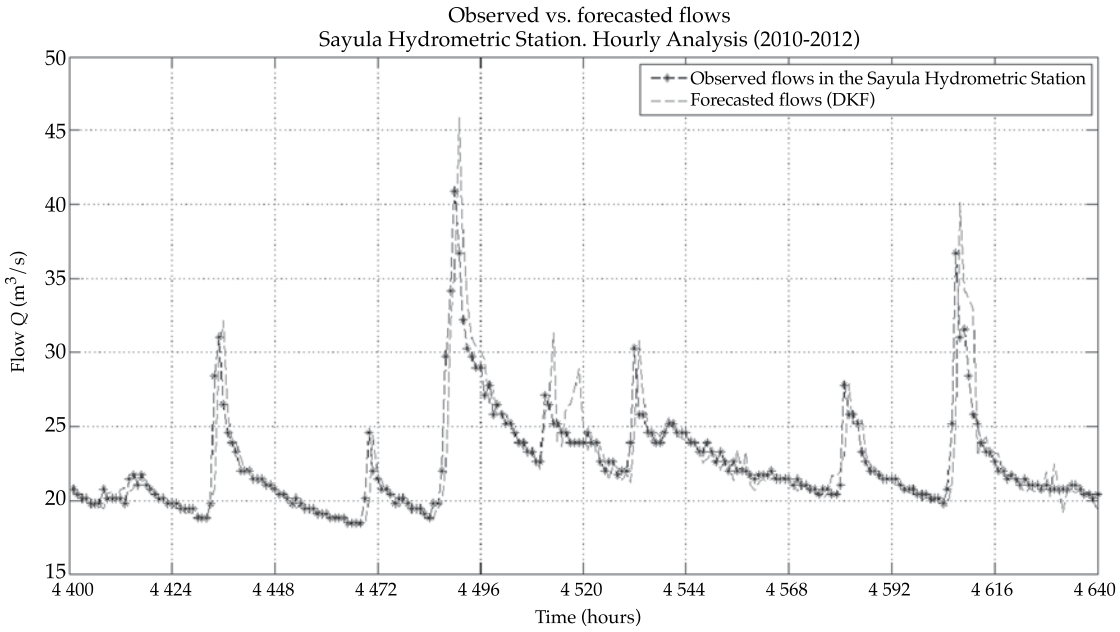

Figure 19. Observed and Forecasted Flow with DKF (flow *B* from 3/07/2010 to 13/07/2010, coinciding with Hurricane Alex) for the Sayula Hydrometric Station, Using the Modified Response Function.

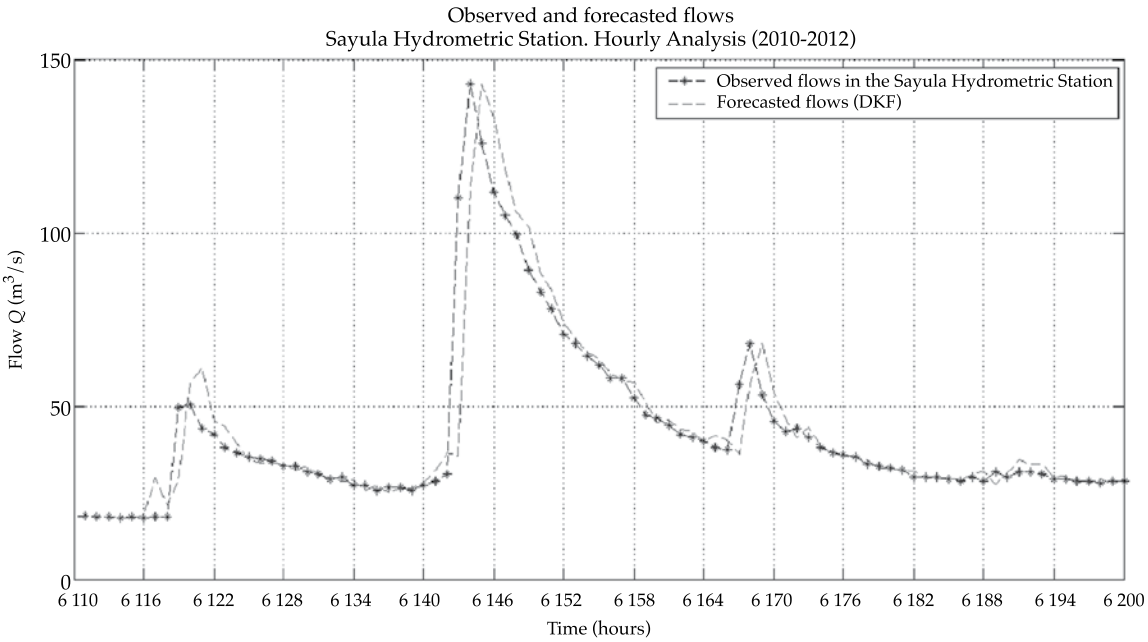

Figure 20. Observed and Forecasted Flow with DKF (flow *C* from 16/09/2010 to 12/09/2010, coinciding with Hurricane *Karl*) for the Sayula Hydrometric Station, Using the Modified Response Function.

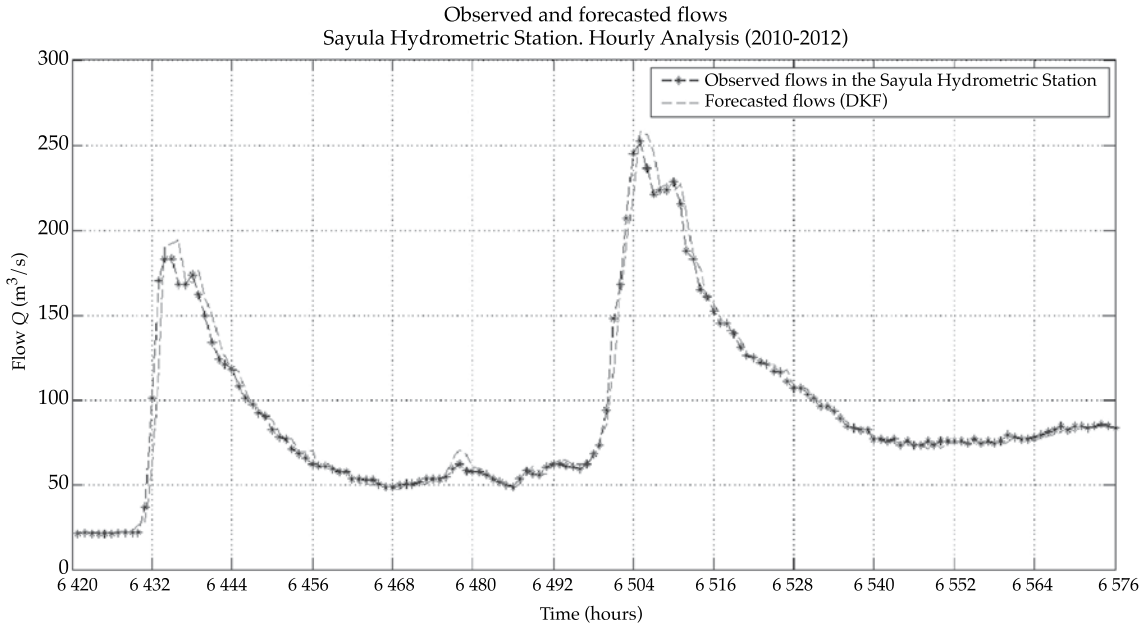

Figure 21. Observed and Forecasted Flow with DKF (flow *D* from 25/09/2010 to 02/10/2010) for the Sayula Hydrometric Station, Using the Modified Response Function.

Table 5. Summary of Statistics applying the DKF to the Sayula Hydrometric Station Using the Modified Response Function.

Concept	Value
Nash-Sutcliffe (Observed Q - Forecasted Q)	0.9775
Nash-Sutcliffe (Observed Q - Updated Q)	0.9808
Correlation (Observed Q - Forecasted Q)	0.9988
Correlation (Observed Q - Updated Q)	0.9986

where $\hat{x}_{\bar{k}}$ are the ordinates of the forecasted response function and $H_{n+nQ,1} = [Q_{t-1}, Q_{t-2}, ..., Q_{t-nQ}, Hp_{t-1}, Hp_{t-2}, ..., Hp_{t-n}]$ represent a vector that contains the flow values nQ and effective precipitation n used in the convolution with the forecasted response function, to obtain the inflows for the reservoir.

After updating the forecast as described above, the forecast of the inflows into the C.H. Peñitas reservoir is updated as follows:

$$Q_{est2} = H \cdot \hat{x}_k \tag{18}$$

where $\hat{x}_k$ is the correct or updated response function.

Flow Forecast for the Sayula hydrometric station using the modified response function

Flow records from the Sayula hydrometric station were used to evaluate the applicability of the DKF to the modified response function, with a analysis period from 01/01/2010 to 14/02/2012.

The best results were obtained with prior 48-h forecasting measurements for effective precipitation and prior 1-h forecasting for flow, with a forecast interval of 1 h. Figure 16a shows the mean effective precipitation registered in the Sayula hydrometric station and Figure 16v shows the observed and forecasted flows from the application of the DKF. Figure 17 presents forecasted flows versus "observed" flows. The 45° line represents perfect agreement, and as can be seen, the forecasted flow is underestimated in some cases and overestimated in others, but generally the results are highly satisfactory. The relationship between observed and updated flows are also satisfactory (not presented). Figures 18, 19, 20 and 21 present some isolated flows during the study period for a better analysis.

Table 5 presents the statistics used to quantitatively evaluate the accuracy of this application of the DKF. The values $\alpha = 0.3$ and $N = 1\ 000$ are the same as those used in the previous analysis and the value of the matrix $S = 0$ reflects the best results obtained from the different calculations of S.

The mean and standard deviation were 21.51 and 24.37 m^3/s for the observed flows and 21.53 and 24.61 m^3/s for the forecasted flows, respectively. Again, these statistics remained basically the same.

Discussion of Results

The results obtained by applying the DKF algorithm to the Sayula hydrometric station are highly acceptable. A 48-h forecasting interval for precipitation best represented the forecasting of flows.

Flow Forecasts for the C.H. Peñitas using the Modified Response Function

The results presented here are based on the application of the filter to the modified response function using flows calculated with reverse transit for forecasting intervals of 1 and 24 h. The period was October 31, 2005 to February 13, 2012.

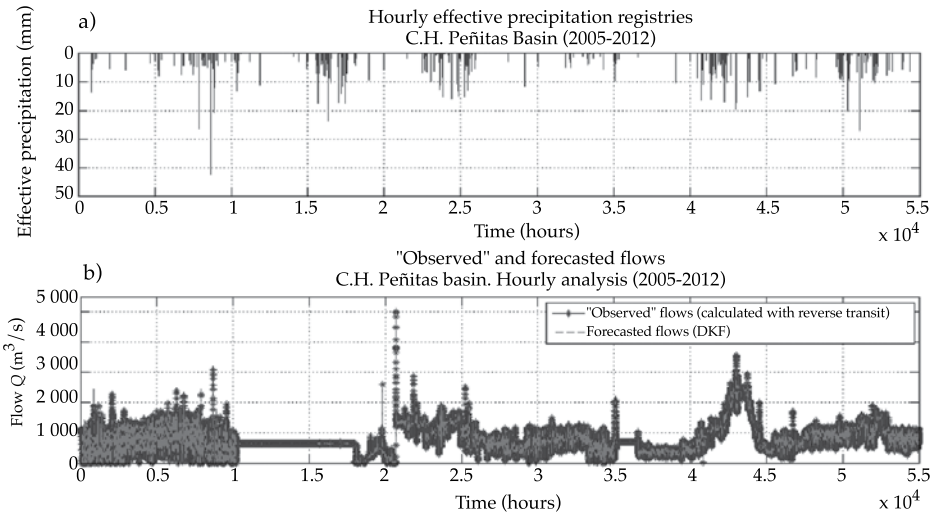

Figure 22. Precipitation and Flow Records used to Analyze the C.H. Peñitas Basin, Including 1 h Flow forecasting, Using the Modified Response Function.

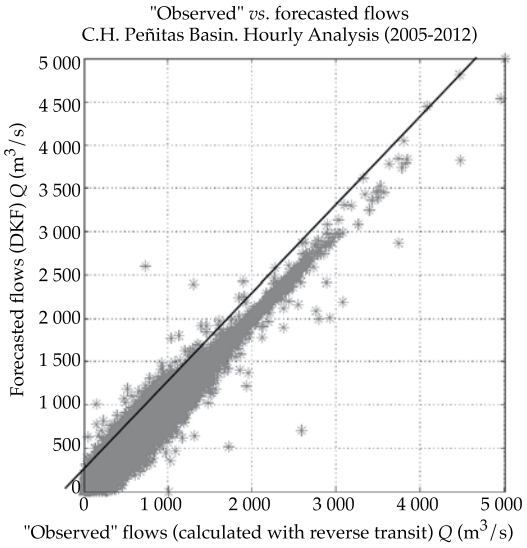

Figure 23. Observed versus Forecasted Flows for the C.H. Peñitas Basin Using the Modified Response Function.

Analysis of Hours

The best results were obtained with matrix H with 12 h forecasting for precipitation and 2 h forecasting for flow, calculating the reverse transit with respect to time k. The values α and N remained the same as those used in the previous analysis (Figure 22 through 26 and Table 6).

The means and standard deviations were 759.22 and 428.82 m^3/s for the observed flows and 758.97 and 429.61 m^3/s for the forecasted flows, respectively. Again, these statistics remained basically the same.

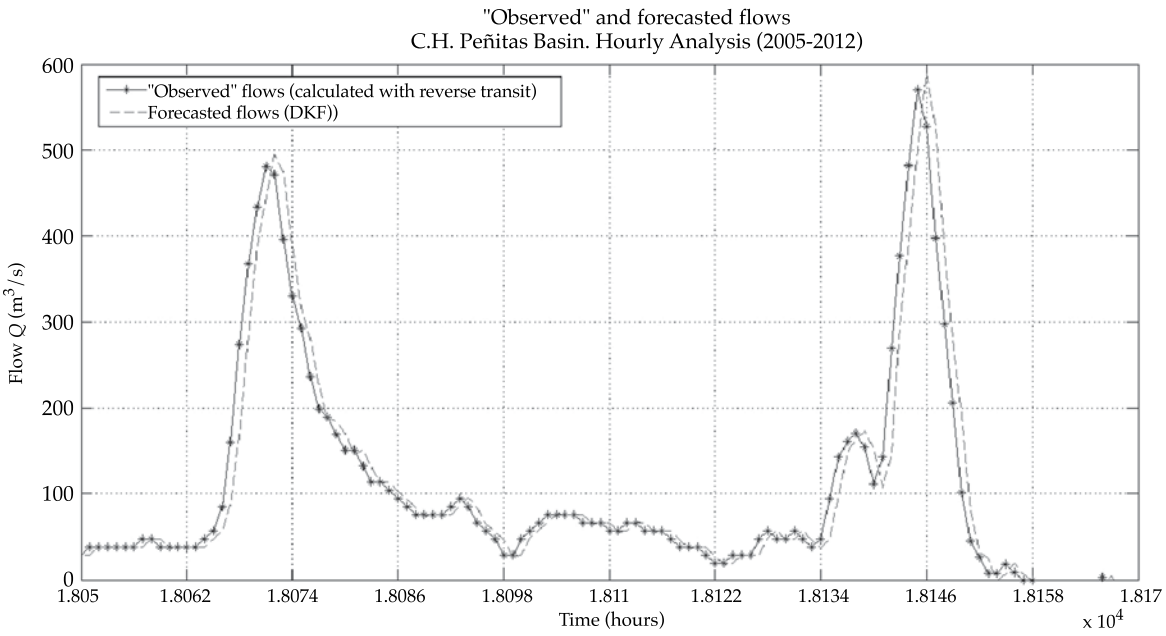

Figure 24. Observed and Forecasted Flow with DKF (period *A* from 23/11/2007 01:00 h to 28/11/2007 01:00 h) for the C.H. Peñitas Basin Using the Modified Response Function.

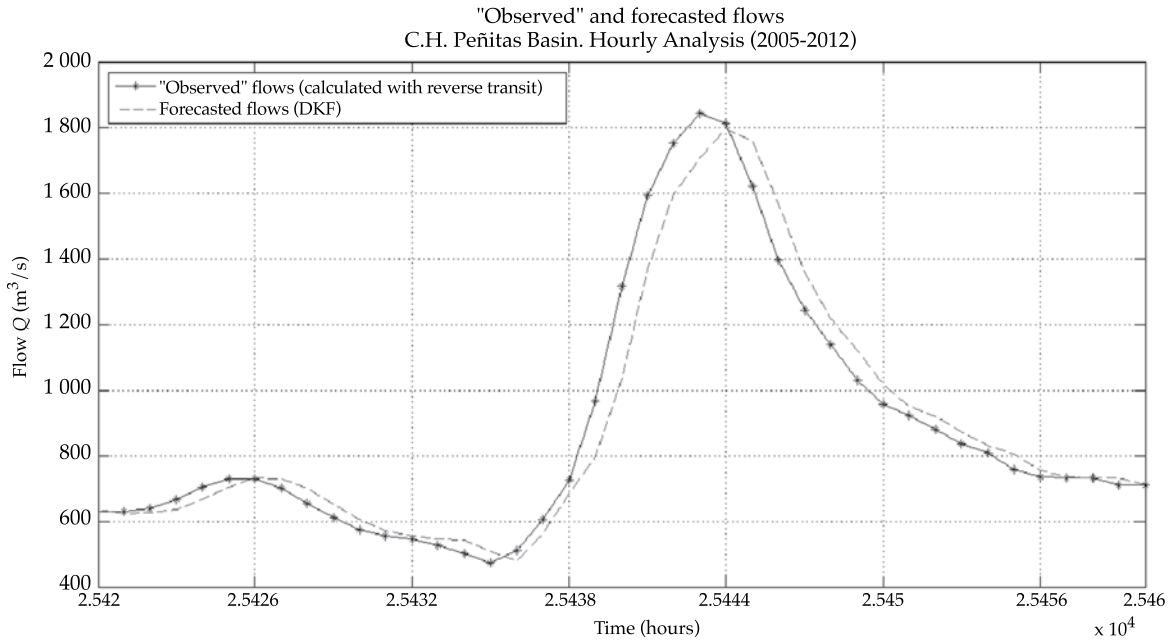

Figure 25. Observed and Forecasted Flow with DKF (period *B* from 25/09/2008 03:00 h to 26/09/2008 19:00 h) for the C.H. Peñitas Basin Using the Modified Response Function.

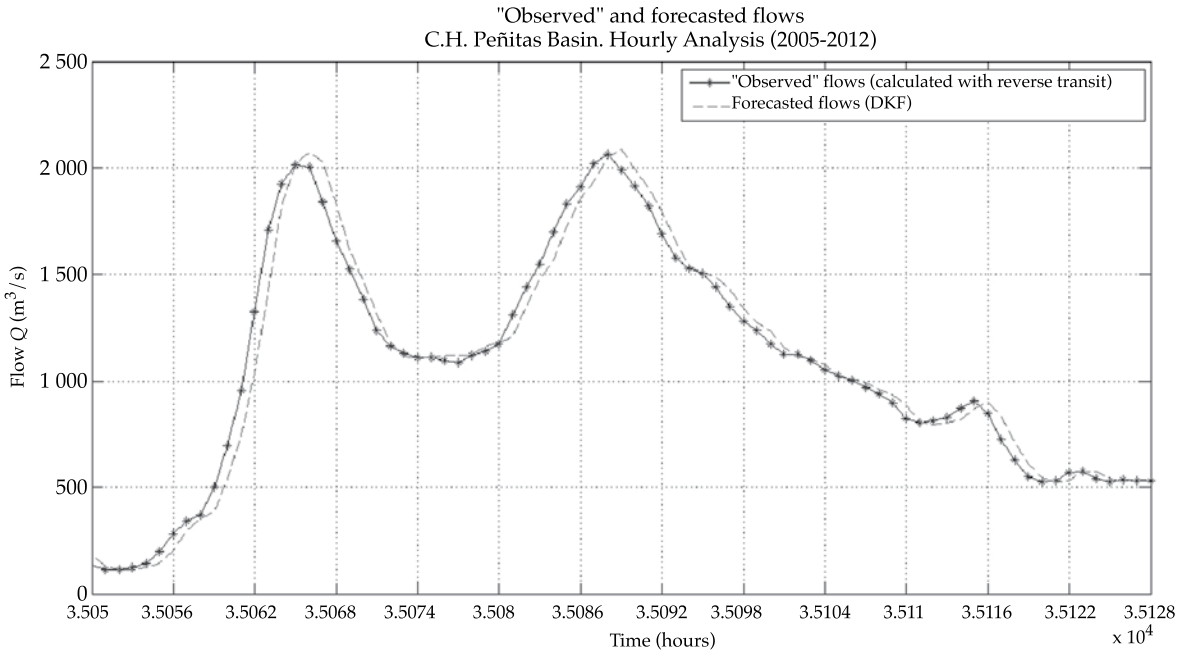

Figure 26. Observed and Forecasted Flow with DKF (period C from 31/10/2009 09:00 h to 03/11/2009 15:00 h) for the C.H. Peñitas Basin Using the Modified Response Function.

Table 6. Summary of Statistics Applying the DKF to the C.H. Peñitas Basin Using the Modified Response Function with a 1-h forecast.

Concept	Value
Nash-Sutcliffe ("Observed" *Q* - Forecasted *Q*)	0.97805
Nash-Sutcliffe ("Observed" *Q* - Updated *Q*)	0.97887
Correlación ("Observed" *Q* - Forecasted *Q*)	0.99964396
Correlación ("Observed" *Q* - Updated *Q*)	0.99970262

Daily Analysis

The best results for this analysis were obtained with a 2-day forecast of effective precipitation and 1 day for flow in matrix *H* (Figure 27 through 31 and Table 7).

The mean and standard deviation were 972.13 and 10 246.86 m^3/s for the observed flows and 16 920.24 and 10 304.58 m^3/s for the forecasted flows, respectively. Again, these statistics remained basically the same as the previous analyses.

Discussion of Results

The Nash-Sutcliffe coefficient for daily forecasting is slightly lower than that for the hourly forecast. Nevertheless, the daily forecasting interval is generally more useful than the hourly, and therefore the lower coefficient is more acceptable (although still very high) than a larger forecasting interval.

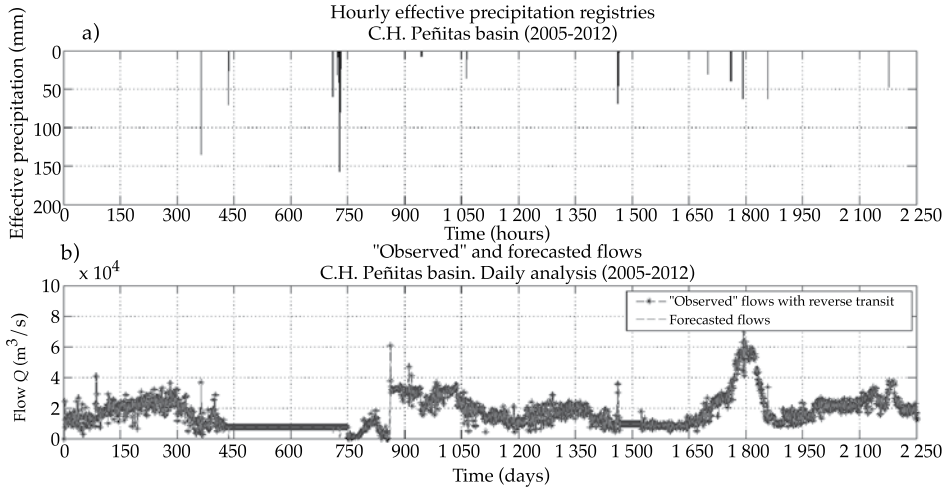

Figure 27. Precipitation and Flow Records used to Analyze the C.H. Peñitas Basin, Including 24-h Flow Forecasts Using the Modified Response Function.

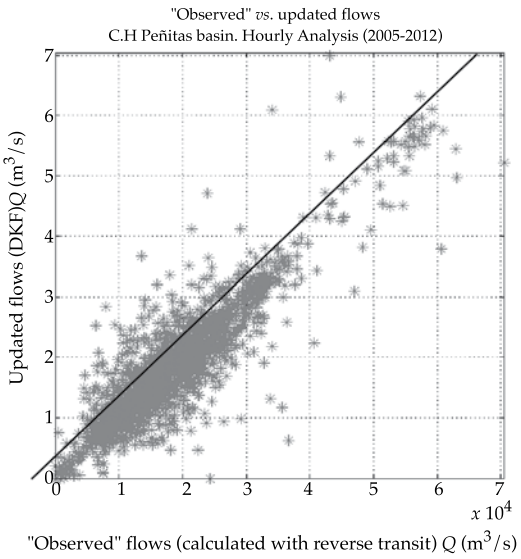

Figure 28. Observed versus Forecasted Flows for the C.H. Peñitas Basin, 24-h Forecast Using the Modified Response Function.

Variation in the Nash-Sutcliffe Coefficient in terms of the Forecasting Interval

Figure 32 presents the Nash-Sutcliffe coefficient obtained by applying the algorithm using different Δt in the flow forecast for the C. H. Peñitas basin.

It is important to mention that the large differences between observed and forecasted values for most of the points in Figures 23

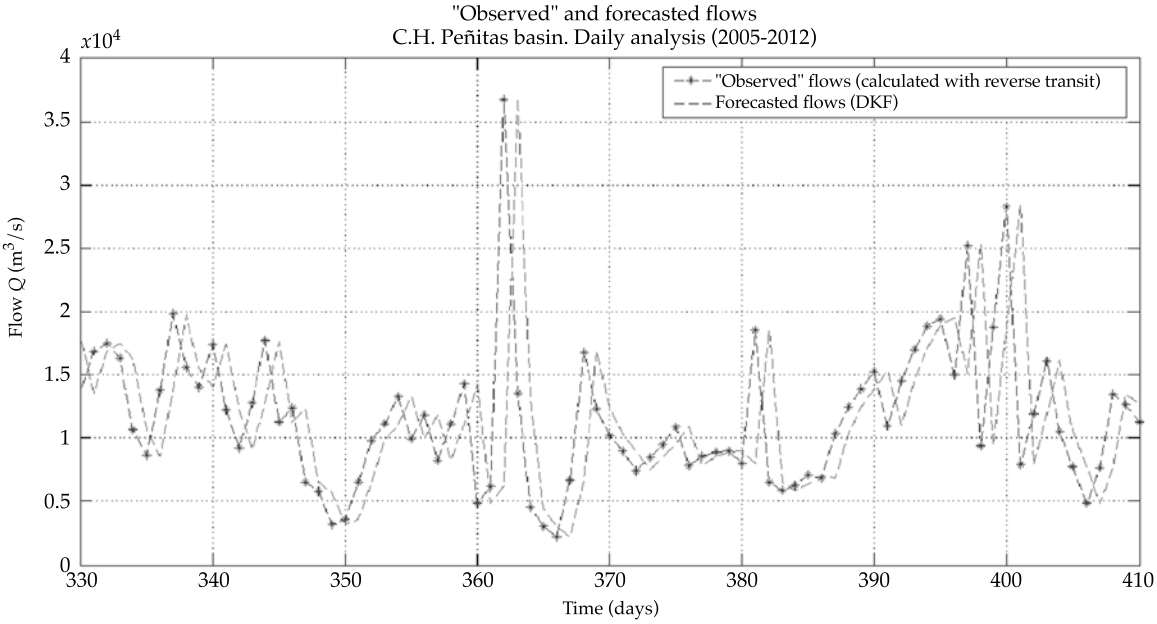

Figure 29. Observed and Forecasted Flow with DKF (period A from 26/9/2006 to 15/12/2006) for the C.H. Peñitas Basin, 24-h Forecast Using the Modified Response Function.

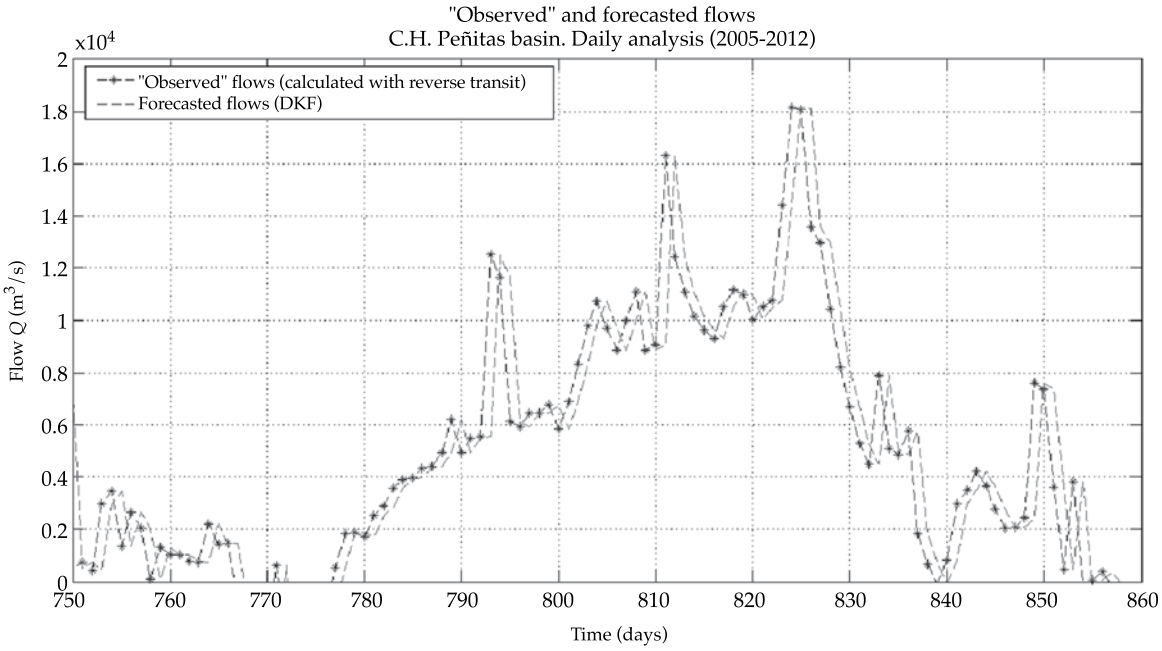

Figure 30. Observed and Forecasted Flow with DKF (period B from 20/11/2007 to 09/03/2008) for the C.H. Peñitas Basin, Daily Analysis Using the Modified Response Function.

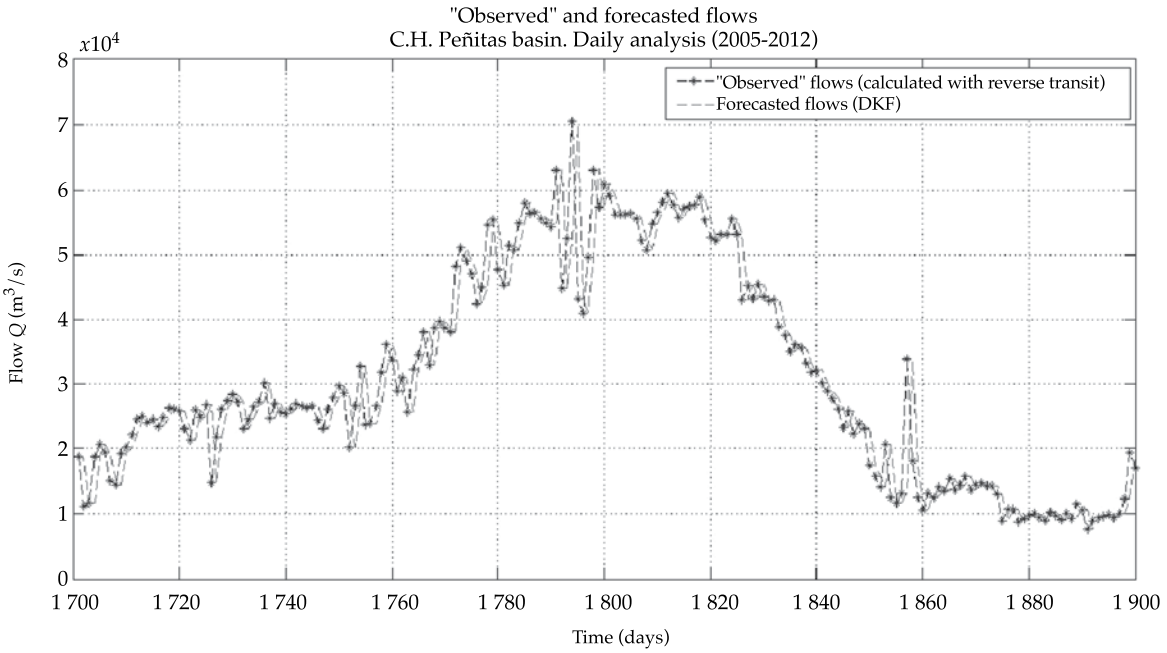

Figure 31. Observed and Forecasted Flow with DKF (period C from 27/06/2010 to 13/01/2011) for the C.H. Peñitas Basin, 24-h Forecast Using the Modified Response Function.

Table 7. Summary of Statistics Applying the DKF to the C.H. Peñitas Basin Using the Modified Response Function with 24-h forecast.

Concept	Value
Nash - Sutcliffe (Observed Q - Forescasted Q)	0.83352
Nash - Sutcliffe (Observed Q - Updated Q)	0.84129
Correlation (Observed Q - Forescasted Q)	0.9996
Correlation (Real Q - Updated Q)	0.99904

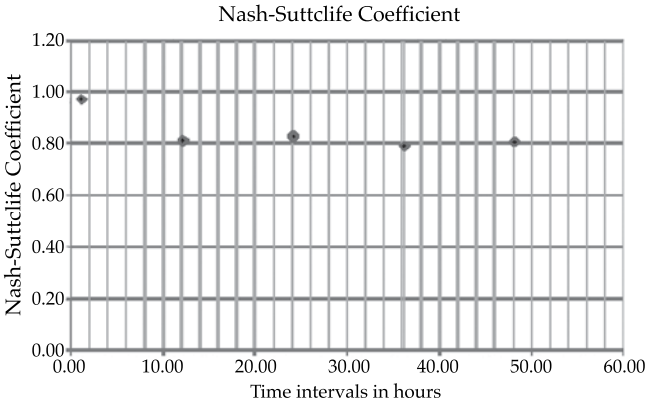

Δt (h)	n	nQ	Nash-Sutcliffe
1	12	2	0.97805
12	4	2	0.81707
24	2	1	0.83352
36	2	2	0.79546
48	1	1	0.81188

Figure 32. Variation in Δt in the Forecast.

and 28 are due to abrupt changes in the signal or, in some cases, the absence of data.

Conclusions

1. The Kalman filter is not a rainfall-runoff model but rather a mathematical algorithm that enables forecasting the state of a linear system with stochastic inputs.
2. The present work demonstrates that the filter can be applied successfully in hydrology, particularly to short-term flood forecasting.
3. The application of the Kalman filter to flow forecasting provides highly acceptable results that make it possible to obtain a forecast with small errors, since it is corrected with each new measurement and therefore can be considered a good option for managing and operating large reservoirs.
4. Reverse computation time is minimum.
5. Forecasting would improve greatly with more instruments in the basin. Indirect methods to calculate the state of the system could thereby be avoided, such as reverse transit of flows.
6. The arbitrary assignment of input variables for the algorithm, such as the initial state and the covariance matrix for the initial error, produce minimal forecasting variations since the filter is self-corrected over time, decreasing the initial errors.
7. At most of the points at which the filter shows the largest errors between forecasted and observed flows, there is an abrupt jump in the signal or the input information is not complete (such as when a station is not registering).
8. The results obtained using the instantaneous unit hydrograph as a response function for the basin are acceptable. Nevertheless, the proposed modification, which includes both flow registries as well as precipitation in matrix *H*, considerably improves the forecasts.
9. Among the different alternatives used to define the value of matrix *S*, the best result is obtained when this is null.
10. It is important to consider the possible usefulness of the DKF to other areas (hydraulics, groundwater, etc.).

Published by Invitation

References

AGUILAR, G.E., MENDOZA, U.I., LOBATO, S.R., APARICIO, J., and RIVAS A.I. *Modelo de pronóstico de avenidas para la C. H. Peñitas considerando la incorporación del vaso "Juan del Grijalva" con precipitación registrada a tiempo real y con pronóstico de precipitación del modelo MM5*. Informe final. Jiutepec, México: Instituto Mexicano de Tecnología del Agua, 2009.

ALDAMA, A. y AGUILAR, E. *Antitránsito de avenidas en vasos*. XVII Congreso Latinoamericano de hidráulica, Guayaquil, Ecuador, 1996.

APARICIO, J., MARTÍNEZ-AUSTRIA, P., GÜITRÓN, A., and RAMÍREZ, A.I. Floods in Tabasco, Mexico: a Diagnosis and Proposal for Courses of Action. *J. of Flood Risk Management*. Vol. 2, No. 2, June, 2009, pp. 132-138.

APARICIO, J. The Juan del Grijalva Landslide. Birkle, P. and Torres-Alvarado, I.S. (editors) *Proceedings*. 13th International Conference on Water Rock Interaction, Guanajuato, del 16 al 20 de agosto, 2010, CRC Press, Londres, pp. 3-7.

APARICIO, J. *Fundamentos de Hidrología de Superficie*. México, D.F.: Limusa, 2011.

CONAGUA. *Estadísticas del Agua en México*. México, D.F.: Comisión Nacional del Agua, Secretaría de Medio Ambiente y Recursos Naturales, 2011.

DRÉCOURT, J. *Kalman filtering in hydrological modeling*. DAIHM Technical Report 2003-1, DHI Water & Environment, 2003.

HINO, M. On-line prediction of hydrology systems. *Proc. Fifteenth Conf. IAHR*, Istambul, 1973.

KALMAN, R.E. A New Approach to Linear Filtering and Prediction Problems. Trans. ASME. Series D. *Journal of Basic Engineering*. Vol. 82, 1960, pp. 35-45.

KIM, S., TACHIKAWA, Y., and TAKARA, K. Embedding Kalman filter into a Distributed *Hydrological Model*. WSUD2004, 2004, pp. 278-290.

KOTTEGODA, N.T. *Stochastic Water Resources Technology*. London: The Macmillan Press, LTD, 1980.

KRAUSE, P., BOYLE, D.P., BÄSE, F. *Comparison of different efficiency criteria for hydrological model assessment. Advances in Geosciences*. European Geosciences Union. Vol. 5, 2005, pp. 89-97.

RIVERA-TREJO, F., SOTO-CORTÉS, G., and BARAJAS-FERNÁNDEZ, J. The 2007 flooding in Tabasco, Mexico: Evolution of water levels. *Hydraulic Engineering in Mexico*. Vol. XXIV, No. 4, October-December, 2009, pp. 159-166.

SIMON, D. Kalman Filtering. *Embedded Systems Programming*. Vol. 14, No. 6, 2001, pp. 72-79.

VALDÉS, J.B., VELÁZQUEZ, J.M. y RODRÍGUEZ-ITURBE, I. *Filtros de Kalman en hidrología: Predicciones de descargas fluviales para la operación óptima de embalses*. Universidad Simón Bolívar, Decanato Estudios de Postgrado, Postgrado en Planeación e Ingeniería de Recursos Hídricos, 1980.

WELCH, G. and BISHOP, G. *An Introduction to the Kalman Filter*. Department of Computer Science University of North Carolina at Chapel Hill. Course 8, 2001.

Institutional Address of the Authors

M.I. Mirce Ivón Morales Velázquez

Universidad Nacional Autónoma de México
Torre de Rectoría, Circuito interior
Ciudad Universitaria, Delegación Coyoacán
México, D.F., México
Teléfono: +52 (777) 4178 735
mirce_morales_v@live.com.mx

Dr. Javier Aparicio

División de Estudios de Postgrado de la Facultad de Ingeniería
Universidad Nacional Autónoma de México
Paseo Cuauhnáhuac 8532, colonia Progreso
62550 Jiutepec, Morelos, México
Teléfono: +52 (777) 3293 600
javieraparicio@prodigy.net.mx

Dr. Juan B. Valdés

Universidad de Arizona
1133 E James E. Rogers Way Rm 122
Tucson, AZ 85721, United States of America
Phone: +520 6218 787
jvaldes@email.arizona.edu

Click here to write the autor

Generation of Curvilinear Composite Grids for Computing Two-Dimensional Flows

• Alejandro Mendoza-Reséndiz* • Moisés Berezowsky-Verduzco •
Universidad Nacional Autónoma de México
*Coorresponding Author

Abstract

MENDOZA-RESÉNDIZ, A. & BEREZOWSKY-VERDUZCO, M. Generation of Curvilinear Composite Grids for Computing Two-Dimensional Flows. *Water Technology and Sciences* (in Spanish). Vol. V, No. 2, March-April, 2014, pp. 111-122.

A method to generate composite grids based on boundary-fitted curvilinear coordinate systems is presented. Curvilinear grids have the advantage of accurately describing the shape of the edge of the domain. The main idea is to transform a geometry given in the Cartesian space into a curvilinear coordinate system in which the grid is rectangular. In its traditional form, curvilinear grids require the definition of four axes that delimit the domain, which restricts its use for geometries that cannot be bounded by four edges. The composite grids that are formed by multiple-connected blocks of curvilinear meshes solves this limitation. While the literature shows that some authors use this type of grid for flow modeling, no practical details are provided about the generation of the mesh. This paper outlines a method to generate this kind of grid. The implications for its use in solving two-dimensional flows are also discussed.

Keywords: Grid generation, curvilinear coordinates, composite grids, two-dimensional flow.

Resumen

MENDOZA-RESÉNDIZ, A. & BEREZOWSKY-VERDUZCO, M. Generación de mallas curvilíneas compuestas para el cálculo de flujos bidimensionales. Tecnología y Ciencias del Agua. *Vol. V, núm. 2, marzo-abril de 2014, pp. 111-122.*

Se presenta un método para generar mallas compuestas con base en sistemas coordenados curvilíneos ajustados a las fronteras. Las mallas curvilíneas tienen la ventaja de describir con exactitud la forma de las orillas del dominio. La idea principal consiste en la transformación de una geometría dada en el espacio cartesiano hacia un sistema coordenado curvilíneo en el que la malla es rectangular. En su forma tradicional, una malla curvilínea requiere la definición de cuatro ejes que delimiten el dominio, lo cual restringe su uso para geometrías con formas que no pueden ser delimitadas por cuatro ejes. Con las mallas compuestas, que son conformadas por múltiples bloques en sistemas curvilíneos, conectados entre ellos, se supera dicha limitación. En la literatura se encuentra que este tipo de mallas es utilizado por algunos autores para la modelación de flujos, sin embargo, no se proporcionan detalles prácticos para su generación. En este trabajo se plantea un método para generar este tipo de mallas. Se discuten también brevemente las implicaciones de su uso en la solución de flujos bidimensionales.

Palabras clave: *generación de mallas, coordenadas curvilíneas, mallas compuestas, flujos bidimensionales.*

Introduction

Fluid equations have been solved using three methodologies: finite differences, finite volumes and finite elements (Thompson *et al*., 1998). Finite differences methods have traditionally been used for rectangular grids, although these have also been developed with boundary-fitted curvilinear grids. Examples of this include Hauser *et al*. (1986) and Mejía and Berezowsky (1996) for solving shallow water equations and Shi *et al*. (2001) for solving Boussinesq equations.

When the domain geometry is complicated and it is desired that the grid adequately represents the boundaries, two options are generally available: unstructured grids primarily associated with finite elements methods or boundary-fitted curvilinear systems. The advantage of unstructured grids

is that they can adapt to any geometry, no matter how complex. Their disadvantage is that the numerical schemes are more complicated, which affects the time it takes to solve the problem (Mejía and Berezowsky, 1996). They also require more information to describe the grid with a list of the connections of all the components, which increases the level of difficulty involved in programming the numerical solution schemes.

On the other hand, the advantage that curvilinear grids have over rectangular grids is that they adapt to the shape of the edges and therefore can be used in geometries with boundaries that are irregularly shaped, and can adequately represent them. In addition, since they are structured grids they also have those corresponding advantages, and therefore can be used with numerical schemes developed for this type of grid, which are more efficient than those developed for unstructured ones (Ahusborde and Glockner, 2010).

The following sections describe traditional curvilinear grids, their limitations, and how composite grids overcome those limitations. They also present the procedure proposed to generate this type of grid and considerations for its use.

Curvilinear Coordinate Systems

The coordinate axes of general curvilinear coordinate systems generally adapt to a given geometry. These systems are referred to as general because the coordinate axes are not necessarily perpendicular (Warsi, 1998). The curvilinear coordinate system adapts in such a way that the axes coincide with the domain boundaries or contours where the flow equations in the study are to be solved.

Figure 1 presents an example of a region represented in the Cartesian and curvilinear plane. It is bounded by four axes with irregular shapes, with which the coordinate

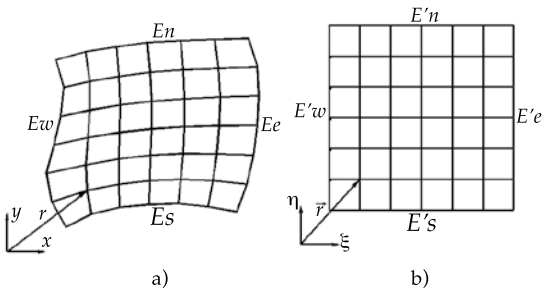

Figure 1. Representation of the Curvilinear Space: a) physical space; b) computational space.

axes coincide. Any point in the Cartesian plane is represented in what is called the computational space, where the curvilinear axes are straight lines, as indicated in Figure 1b. Without losing generality, one unit spacing in a computational grid is commonly accepted, which simplifies the solutions.

The governing equations are solved in the computational space (Figure 1b), with the advantages of a uniform rectangular grid. This means that the governing equations must be transformed from the Cartesian coordinate system with axes x, y, to the curvilinear system with axes ξ, η.

As can be seen in Figure 1b, the grid in the computational space is a rectangle bounded by four axes, and since each point has a unique representation when passing from the Cartesian to the computational plane, the four axes — *E's*, *E'w*, *E'n* and *E'e*— must be defined in the Cartesian plane; that is, a mapping exists between the *E's* and the *Es* (as well as between the other three axes). This is a limitation of the use of curvilinear coordinate systems consisting of a unique block, since the four axes that bound a physical space in which flow is to be solved cannot be defined for all geometries. An example of this is when there are internal obstacles, such as islands, and consequently internal boundaries. Such conditions make

it complicated to use four axes to define internal and external boundaries. Another case occurs in regions in which four axes that bound an area can be defined but due to their shape a deformed grid is produced, as seen in the example shown in Figure 2a. It has been demonstrated (Sankaranarayanan and Spaulding, 2003) that the truncating error in finite differences schemes increases when the angle between the curvilinear coordinates (orthogonal grids) is further away from 90%. Another factor influencing this error is related to the appearance of grid elements —elongated cells along with non-orthogonal angles contribute to increasing the truncating error.

For this same example (Figure 2a), if it were somehow possible to increase the number of boundaries to more than four, a grid with a better distribution would be obtained. This is the case of the grid shown in Figure 2b, where the angles are close to 90° and the aspect ratio of the cells is very close to 1.

The literature describes methodologies proposed to solve the limitation of curvilinear grids consisting of a unique block bounded by four axes. One involves cutting the block into branches (Thompson *et al.*, 1985) as shown by the example in Figure 2b in which the bottom of the block is cut and divided into two branches, producing a less deformed grid. Another technique is to divide the region in which the grid is going to be generated into various blocks. This is the method used by the work herein and which will be described further below. First, the concepts behind general curvilinear coordinate systems are briefly described, since some elements are used in the equations to generate the grid. They are also required in the process to transform the system from a Cartesian coordinate to a curvilinear system.

Elements in the Curvilinear System

A set of metric elements exists that is used in the curvilinear coordinate system and the transformation of equations. As indicated previously, an $\vec{r}$ point has one unique representation in curvilinear and Cartesian systems which makes it possible to define the following relation:

$$\vec{r} = x(\xi,\eta)\hat{i} + y(\xi,\eta)\hat{j} \qquad (1)$$

While on the curvilinear plane, the axes ξ, η are represented as straight, perpendicular lines, these same axes on the Cartesian plane are represented as curves. This can be seen in Figure 1b, where axis *E's* is a straight line with ξ = *cte* on the curvilinear plane, while it

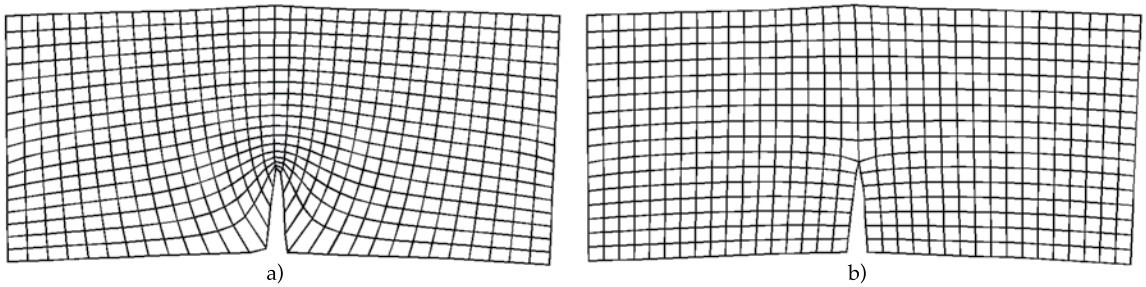

Figure 2. a) Grid defined with four axes and b) with two branches.

is represented on the Cartesian plane by the curve defined by axis *Es*, as shown in Figure 1a.

The vectors tangential to the curvilinear coordinate axes define the covariant base, whose representation in the Cartesian plane is:

$$\vec{a}_1 = \vec{r}_\xi, \quad \vec{a}_2 = \vec{r}_\eta \tag{2}$$

The sub-indices $()_{\xi,\eta}$ define the derivative of the curvilinear axes. Likewise, the vectors normal to the curvilinear axes define the contravariant base. Its representation on the Cartesian plane is:

$$\vec{a}^1 = \nabla_\xi, \quad \vec{a}^2 = \nabla_\eta \tag{3}$$

In addition to the implications of their definition, the bases defined by equations (2) and (3) are important because they are used in the process to transform flow equations to be solved in the curvilinear system. The metric elements are defined by the scalar product of the base vectors, and the Jacobian transformation is defined with the modulus of the vector product of the covariant base:

$$a_{ij} = \vec{a}_i \cdot \vec{a}_j \quad \text{con } i,j = 1,2 \tag{4}$$

$$a^{ij} = \vec{a}^i \cdot \vec{a}^j \quad \text{con } i,j = 1,2 \tag{5}$$

$$J = \left|\vec{a}_1 \times \vec{a}_2\right| = \det\left(\begin{bmatrix} x_\xi & x_\eta \\ y_\xi & y_\eta \end{bmatrix}\right) \tag{6}$$

The physical interpretation of a_{11} is obtained by taking it to be equal to the squared modulus of $\vec{r}_\xi$. This means that a differential increase in $\vec{r}$ in the physical space resulting from a differential increase in ξ in the curvilinear plane is given by $d\vec{r} = \sqrt{a_{11}}d\xi$. Likewise for a_{22} and the coordinate axis η. The elements a_{12} and a_{21} are identical because the properties of the scalar product are null when the axes ξ and η are orthogonal, as is easily observed. The Jacobian of the transformation given by equation (6) is defined using the vector product, which represents the area defined by the parallelogram that consists of the vectors of the covariant base.

Transformation of the Governing Equations

As was mentioned, rectangular grids provide advantages when working with equations in the computational plane. The transformation of the equations are performed with the independent variables, that is, the coordinate axes x and y. Or some of the dependent variables can also be transformed. This process of transforming the equations produces a larger number of terms (Baghlani *et al*., 2008).

There are three ways of transforming hyperbolic flow equations (Shi *et al*., 2001). The first is to transform only the coordinate axes without transforming the velocity components. Other types of transformations involve using the covariant or contravariant velocity components, which are tangential and normal to the curvilinear coordinate axes, respectively. The flow equations are solved with these transformed variables.

Hauser *et al*. (1986) and Soto and Berezowsky (2003) are among those who have used the approach that only transforms the coordinate axes and uses the physical velocity components. The approach using the contravariant velocity components has also been used, for example, by Baghlani *et al*. (2008) and Shi *et al*. (2001). And the use of the covariant components has been reported by Ferziger and Peric (2002) and Romanenkov *et al*. (2001).

With respect to the criteria for which of the three sets of components is more suitable to use, Romanenkov *et al*. (2001) analyze the advantages and disadvantages of each

type of transformation. These authors perform numerical tests and conclude that transformation with contravariant components has the advantage of more simply representing the continuity equation and facilitating the formulation of the boundary conditions for wall boundaries, which is complicated when using transformation with Cartesian or covariant components. On the other hand, when covariant and contravariant components are used, the representation of the advection term is more complicated, which increases the difficulty of the solution, whereas with the Cartesian velocity components the numerical stability is greater and larger time steps can be used.

Composite Meshes

If the region in which the grid is going to be generated has an irregular shape, multiple interconnected blocks can be used. Blocks are defined as curvilinear grids bounded by four axes, as in the case in Figure 1. This is better understood when using a sponge as an analogy (Thompson *et al*., 1998). A sponge that originally has a rectangular shape can be deformed by being stretched or compressed while maintaining the four axes that bound it. This is analogous to what happens in curvilinear systems. While the grid is rectangular in the computational space, it has been deformed in the physical space to adapt to the shape of its boundaries. Certain types of geometries exist in which the grid can be generated using several interconnecting grids, as if using different sponges to create the shape of the physical domain. This approach makes it possible to use curvilinear coordinate systems with eliminating the need for four axes to bound the region.

The use of this type of methodology has been widely described in the literature. There are two categories for this type of grid: one in which the blocks that make up the grid overlap, as indicated by Chesshire and Henshaw (1990) and Hu *et al*. (2006), and the other in which the blocks are connected only at their borders, as indicated by Hauser *et al*. (1986) and Thompson *et al*. (1998).

The approach using overlapping blocks has the advantage of providing more flexibility when generating the grids because the blocks do not have to meet at the axis. But in addition to transferring information between blocks, information among vertices or grid cells has to be interpolated, since they generally do not coincide. Iterative solutions between the blocks are also needed.

On the other hand, approaches without overlapping do not require the interpolation of a set of vertices from one block to another since there are no regions in common, given that only the points at the axes of the boundaries between blocks coincide. Another advantage is that, since there are no redundant regions in the grid, the storage of information is simplified and, therefore, the calculation speed is quicker.

The structure in the system of equations that is produced by the discretization of differential equations (either those governing flow or those used to generate the grid) has a peculiar shape if considering the numbering of the vertices. This is done sequentially, from one block to another, and the vertices at the boundaries of the blocks are numbered last. An example of this process is described further below.

Differential equations used to generate the grid (described below) are expressed as difference equations with a calculation template, as indicated in Figure 3, with which a system of equations is obtained. Following the scheme proposed herein to number the vertices, a grid consisting of n blocks is considered. The resulting system takes the form:

$$\begin{bmatrix} A_1 & & & & A_{1,\Gamma} \\ & A_2 & & & A_{2,\Gamma} \\ & & \ddots & & \vdots \\ & & & A_n & A_{n,\Gamma} \\ A_{\Gamma,1} & A_{\Gamma,2} & \cdots & A_{\Gamma,n} & A_\Gamma \end{bmatrix} \begin{bmatrix} [u]_1 \\ [u]_2 \\ \vdots \\ [u]_n \\ [u]_\Gamma \end{bmatrix} = \begin{bmatrix} [b]_1 \\ [b]_2 \\ \vdots \\ [b]_n \\ [b]_\Gamma \end{bmatrix} \quad (7)$$

In system (7), the matrices A_i with i = 1, 2,…, n correspond to the discretization of each of the blocks in the grid. Matrix A_Γ results from the vertices at the boundaries between blocks; the subscript Γ refers to the boundaries between blocks. The vectors $[u]$ represent the solution in blocks i and $[b]$ are the vectors of the independent terms in each of the blocks.

Expression (7) is a system of equations expressed in blocks. The block Gauss method (Ortega, 1988) is used to transform it into a system with an upper triangular matrix:

$$\begin{bmatrix} A_1 & & & & A_{1,\Gamma} \\ & A_2 & & & A_{2,\Gamma} \\ & & \ddots & & \vdots \\ & & & A_n & A_{n,\Gamma} \\ & & & & S \end{bmatrix} \begin{bmatrix} [u]_1 \\ [u]_2 \\ \vdots \\ [u]_n \\ [u]_\Gamma \end{bmatrix} = \begin{bmatrix} [b]_1 \\ [b]_2 \\ \vdots \\ [b]_n \\ [g] \end{bmatrix} \quad (8)$$

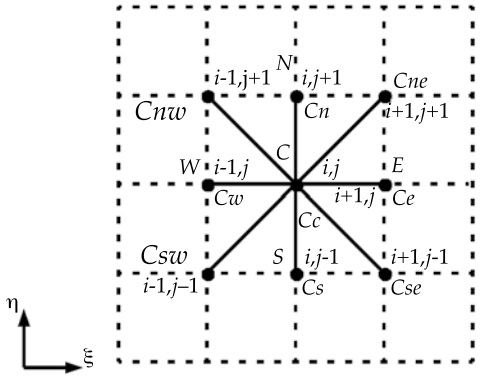

Figure 3. Calculation Template with Nine Vertices.

As can easily be verified, the matrices in the bottom row are:

$$S = A_\Gamma - \sum_{i=1}^{n} A_{\Gamma,i} A_i^{-1} A_{i,\Gamma} \quad (9)$$

$$[g] = [b]_\Gamma - \sum_{i=1}^{n} A_{\Gamma,i} A_i^{-1} [b]_i \quad (10)$$

The solution for the boundary between the blocks is obtained by solving the system of equations corresponding to the last row in the system of blocks given by equation (8), whose matrix and vector of independent terms compose equations (9) and (10), respectively.

Although the solution in the blocks in the grid is obtained by regressive substitution, given the block structure of the matrix the solution in each block can be obtained independently by solving the system of equations associated with each one, as below:

$$A_i [u]_i = [b]_i - A_{i,\Gamma} [u]_\Gamma \quad (11)$$

To provide an example of the methodology to number the vertices in the grid, an L-shaped row is presented in Figure 4a, which has been divided into three blocks.

The numbering of the vertices is shown in Figure 4b. The interior vertices are numbered sequentially from the first to the last block, and the vertices at the boundaries of the blocks are numbered last, which are denoted by Γ in Figure 4a. Table 1 indicates the overall numbering of the vertices, the internal numbering of each block or boundary and the vertices located in the vicinity. The latter is very useful to determine the vertices to be used in the template shown in Figure 3, which in the end results in the generation of a system of equations with a structure such as that indicated by expression (7).

It can be said that Table 12 is similar to the incidence tables in the unstructured grids; nevertheless, the data contained in

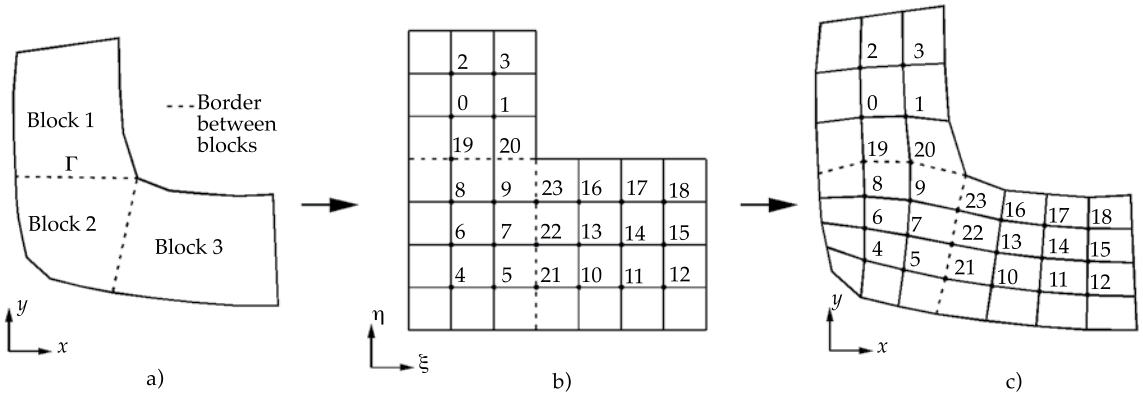

Figure 4. Scheme for Numbering a Composite Grid.

Table 1 is generated automatically. If the indices *i*, *j* indicate the row and column of a vertex within a block, the local identifier of the vertices is determined by id local = *j* * *nc* + *i*, where *nc* is the number of nodes in the horizontal direction. Thus, the identifier of each of the nine neighboring vertices surrounding point C indicated in Figure 3 can be determined by adding or subtracting 1 from the indices *i*, *j* shown in the same figure.

Table 1. Relationship of the Vertices of the Composite Grid shown in Figure 4.

Global id	Block	Local id	South id	West id	East id	North id	South-east id	South-west id	North-west id	North-east id
0	1	0	19	-	1	2	20	-	-	3
1	1	1	20	0	-	3	-	19	2	-
2	1	2	0	-	3	-	1	-	-	-
3	1	3	1	2	-	-	-	0	-	-
4	2	0	-	-	5	6	-	-	-	7
5	2	1	-	4	21	7	-	-	6	22
6	2	2	4	-	7	8	5	-	-	9
7	2	3	5	6	22	9	21	4	8	23
8	2	4	6	-	9	19	7	-	-	20
9	2	5	7	8	23	20	22	6	19	-
10	3	0	-	21	11	13	-	-	22	14
11	3	1	-	10	12	14	-	-	13	15
12	3	2	-	11	-	15	-	-	14	-2
13	3	3	10	22	14	16	11	21	23	17
14	3	4	11	13	15	17	12	10	16	18
15	3	5	12	14	-	18	-	11	17	-
16	3	6	13	23	17	-	14	22	-	-
17	3	7	14	16	18	-	15	13	-	-
18	3	8	15	17	-	-	-	14	-	-
19	Γ	0	8	-	20	0	9	-	-	1
20	Γ	1	9	19	-	1	23	8	0	-
21	Γ	2	-	5	10	22	-	-	7	13
22	Γ	3	21	7	13	23	10	5	9	16
23	Γ	4	22	9	16	-	13	7	20	-

Numerical Generation of the Grid

There are basically three methodologies to generate the grid: algebraic methods, differential equations or variational methods. This work uses elliptical differential equations. Elliptical generators have the advantage of creating a grid with a uniform distribution of interior vertices even when the shape of the boundaries is very irregular (Knupp and Steinberg, 1993). This problem is related to the boundary value (Mejía and Berezowsky, 1996), since the positions of the boundaries are known and what is sought is the position of the vertices inside the grid.

The differential equation to be solved to generate the grid is (Thompson *et al*., 1998):

$$a_{22}\vec{r}_{\xi\xi} - a_{12}\vec{r}_{\xi\eta} + a_{11}\vec{r}_{\eta\eta} + \left(a_{22}P_{11}^{1} - a_{12}P_{12}^{1} + a_{12}P_{22}^{1}\right)\vec{r}_{\xi} + \left(a_{22}P_{11}^{2} - a_{12}P_{12}^{2} + a_{12}P_{22}^{2}\right)\vec{r}_{\eta} = 0 \qquad (12)$$

The subscripts $()_{\xi,\eta}$ denote the derivative with respect to the curvilinear coordinate axes; the metric elements $a_{i,}$ are defined by expression (4). The coefficients P_{ij}^{k} are control functions. If these are zero, then (12) is a Laplaciano equation. The control functions are specified according to the grid conditions desired; that is, orthogonal boundaries or interior vertices or a given cell size in certain regions. The values of the control functions for these cases can be found, by example, in Thompson *et al*. (1998).

Discretization with finite differences in (12) leads to a system of linear equations with nine diagonals, which produces a calculation template for the difference equations, as indicated in Figure 3. Given that the metric elements $a_{i,j}$ depend on the location of the interior vertices $\vec{r}(\xi,\eta))$, the solution process is iterative, beginning with generating an initial grid, for example, using transfinite interpolation. Nevertheless, the authors have used a Laplaciano system to generate the initial grid, which consists of solving:

$$\vec{r}_{\xi\xi} + \vec{r}_{\eta\eta} = 0 \qquad (13)$$

To solve equation (13), only the boundaries need to be known. Satisfactory results have been obtained with this procedure. This is the most suitable technique to generate the initial grid for composite grid systems. The system of equations resulting from expressions (12) and (13), with a scheme for numbering the vertices as explained above, can be reduced to a system such as that indicated in (8) and solved with the proposed scheme.

To apply this method, in addition to knowing the location of the boundaries, the region needs to be adequately divided into blocks and the system of equations needs to be assembled and solved as described in the above paragraphs.

Examples

In order to show the advantages this type of grid provides when applied to complex geometries, three application cases are shown, in which the grids were obtained with a numerical generator using the methodology proposed here. The first example corresponds to the joining of two channels in an acute angle. For this case, the region is divided into four blocks, as shown in Figure 5a. The grid generated is shown in Figure 5b. For this example, an alternative to define the blocks is possible. For example, blocks 2, 3 and 4 can be considered to be one, thereby defining only two blocks —one for the main channel and the other for the channel that meets with the acute angle (block 1). Nevertheless, the authors found that it is simpler to structure the information if there is a complete connection between the axes of the blocks. This can be seen in Figure 5a, for example, where the north axis of block

1 is connected to the south axis of block 3; or the east axis of block 2 is connected to the west axis of block 3.

In this case, if a rectangular Cartesian grid is used, the boundaries corresponding to the channel of block 1 would be represented by steps. Although this problem is reduced when using a finer grid, the calculation time would increase. On the other hand, if a curvilinear grid made up of one block is used for this same example, the cells of the grid would be very distorted.

The second case analyzed corresponds to an estuary. The geometry of the domain boundary is taken from Shi *et al*. (2001). The region analyzed consists of the confluence of three rivers that discharge into the sea (blocks 8 through 13). The inlets of these rivers correspond to blocks 1, 2 and 5, as indicated in Figure 6a, which join and lead to the channel represented by block 7. The domain geometry and the division into blocks to generate the grid are shown in the same figure. The grid was divided into 13 blocks. Figure 6b shows the grid generated using the proposed methodology. As can be seen, it adequately represents the shape of the boundaries. It is made up of 1 827 internal vertices and 377 boundary vertices. To adequately represent the boundaries using a rectangular grid, the degree of refinement required would considerably increase the number of vertices.

The last case to be analyzed corresponds to the branching of the Mezcalapa River into the Samaria and Carrizal rivers, in the state of Tabasco, Mexico. The make-up of the terrain was taken from Jiménez *et al*. (2007) to determine the position of the banks of the rivers. Figure 7 shows that in addition to branching there are two islands. The grid was generated using 18 blocks, indicated in the same figure. The grid obtained with the generator is shown in Figure 7b.

In the three examples, the boundaries between the blocks (indicated as dashed lines in Figure 5a, 6a and 7a) do not correspond to the real boundaries between the blocks, but rather, this location is solved by the same scheme, in accordance with equation (12).

Conclusions

Curvilinear grids are useful when boundaries have irregular shapes, whereas when rectangular grids are used, greater refinement is required to adequately represent the boundaries, affecting calculation time. When the domain shape is complex, the traditional approach of using a single block produces a

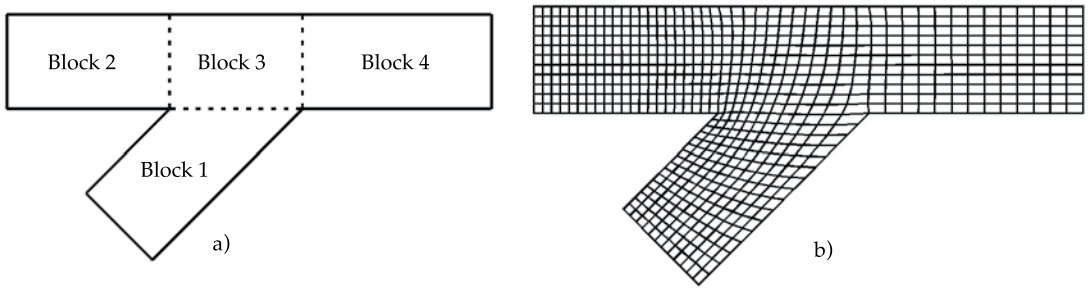

Figure 6. Generation of a Grid at the Union of Two Channels: a) Definition of the Blocks; b) Grid Generated with the Proposed Methodology.

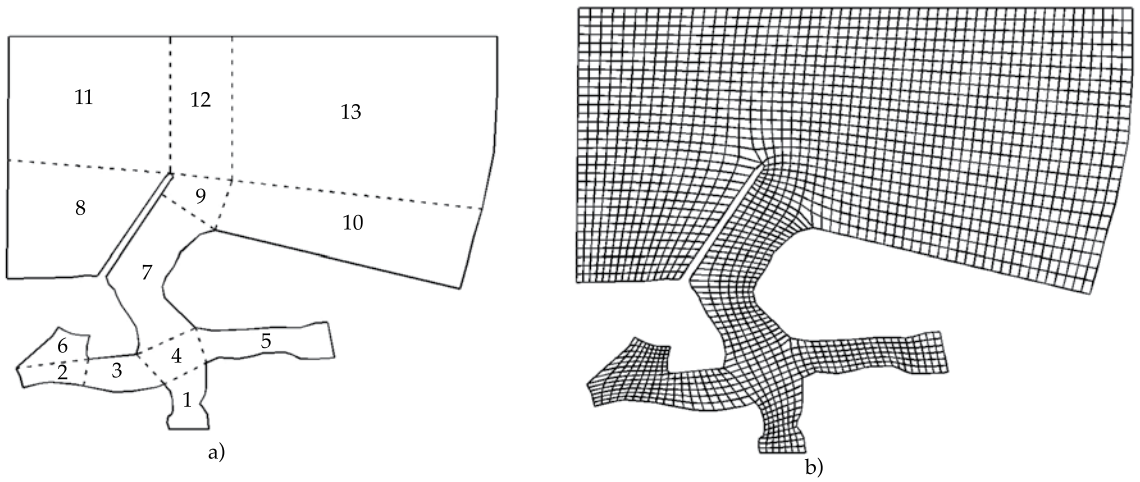

Figure 6. a) Geometry of the Estuary and Definition of Blocks; b) Grid Generated.

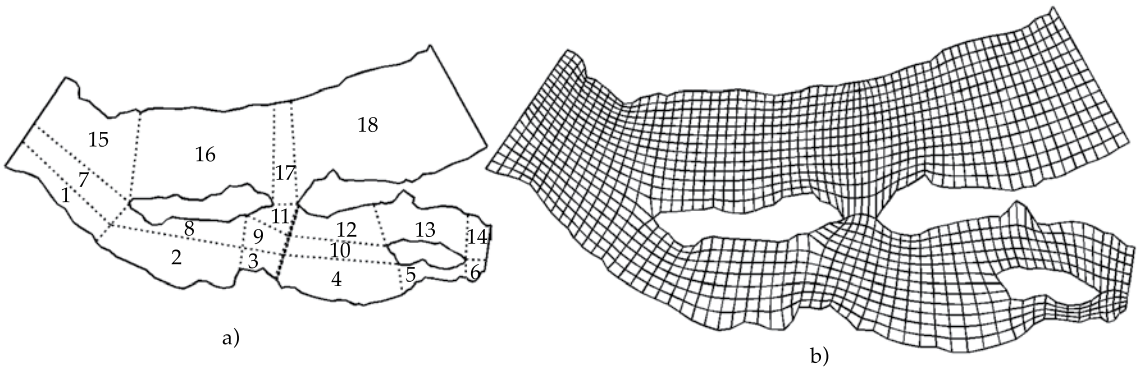

Figure 7. Grid for the Branching of a River with Islands.

grid with distorted cells or it may not even be possible to generate the grid. The shape of a grid composed of blocks provides cells with more uniform shapes. The method proposed herein makes it possible to generate this type of grid. The resulting system of equations to obtain the grid is structured by block, making it possible to independently solve for each block after obtaining the solution of the interfaces between them. In addition, since the location of boundaries between blocks is also unknown, a smooth transition between them is obtained. The quality of the grids obtained is satisfactory, as can be seen in the three cases analyzed, which were calculated with a grid generator that used the methodology proposed in this work.

The use of curvilinear grids involves the transformation of flow equations, which increases the number of terms in the equations. The complexity of transformed equations varies according to the velocity

components used in the transformation. These components are covariants, contravariants and physical. Each one presents advantages and disadvantages in terms of managing boundary conditions, the number of terms in the equations and numerical stability. The criteria for the use of one of these depends on the problem to be solved.

It is worth mentioning that although the scheme proposed herein was based on the generation of grids to solve two-dimensional flows, the method can be applied to solve other types of problems. The process is the same, the governing equations for the phenomenon studied need to be transformed to the curvilinear coordinate system.

Acknowledgements

The authors would like to thank the insightful observations by the anonymous reviewer, which helped to improve the manuscript. And CONACYT for the financial support to carry out this research.

Received: 12/04/2011
Accepted: 03/07/2013

References

AHUSBORDE, E. and GLOCKNER, S. A 2D Block-Structured Mesh Partitioner for Accurate Flow Simulations in Non-Rectangular Geometries. *Computers & Fluids*. Vol. 43, 2011, pp. 2-13.

BAGHLANI, A., TALEBBEYDOKHTI, N., and ABEDINI, M.J. A Shock Capturing Model Based on Flux-Vector Splitting Method in Boundary-Fitted Curvilinear Coordinates. *Applied Mathematical Modeling*. Vol. 32, 2008, pp. 249-266.

CHESSHIRE, G. and HENSHAW, W.D. Composite Overlapping Meshes for the Solution of Partial Differential Equations. *Journal of Computational Physics*. Vol. 90, No. 1, 1990, pp. 1-64.

FERZIGER, J.H. and PERIC, M. *Computational Methods for Fluid Dynamics*. Tercera edición. Berlín: Springer, 2002, 422 pp.

JIMÉNEZ, A.A., GRACIA, J., BEREZOWSKY, M. y MARTÍNEZ, J. *Estudio de la bifurcación de un río con modelación numérica*. México, D.F.: Instituto de Ingeniería, CI-29, 2007, 45 pp.

HAUSER, J., PAAP, H.G., EPPEL, D., and SENGUPTA, S. Boundary Conformed Co-ordinate Systems for Selected Two-Dimensional Fluid Flow Problems. Part I: Generation of BFGs. *International Journal for Numerical Methods in Fluids*. Vol. 6, 1986, pp. 507-527.

HU, K., MINGHAM, G., and CAUSTON, D.M. A Mesh Patching Method for Finite Volume Modeling of Shallow Water Flow. *International Journal for Numerical Methods in Fluids*. Vol. 50, 2006, pp. 1381-1404.

KNUPP, P. and STEINBERG, S. Fundamentals of Grid Generation. Boca Ratón, USA: CRC Press, 1993, 286 pp.

MEJÍA, M.A. y BEREZOWSKY, M. Numerical Generation of Grids with Curvilinear Coordinates for Free Surface Flow Calculations. *Hydraulic Engineering in Mexico*. Vol. IX, No. 3, September-December, 1996, pp. 13-24.

ORTEGA, J.M. *Introduction to Parallel and Vector Solution of Linear Systems*. New York: Plenum Press, 1988, 305 pp.

ROMANENKOV, D.A., ANDROSOV, A.A., and VOLTZINGER, N.E. Comparison of Forms of the Viscous Shallow-Water Equations in the Boundary-Fitted Coordinates. *Ocean Modelling*. Vol. 3, 2001, pp. 193-216.

SANKARANARAYANAN, S. and SPAULDING, M.L. A Study of the Effects of Grid Non-Orthogonality on the Solution of Shallow Water Equations in Boundary-Fitted Coordinate Systems. *Journal of Computational Physics*. Vol. 184, 2003, pp. 299-320.

SHI, F., DALRYMPLE, R.A., KIRBY, J.T. CHEN, Q., and KENNEDY, A. A Fully Nonlinear Boussinesq Model in Generalized Curvilinear Coordinates. *Coastal Engineering*. Vol. 42, 2001, pp. 337-358.

SOTO, C.G. y BEREZOWSKY, V.M. Numerical Simulation of Wetting and Drying in Shallow Waters Using a Curvilinear Adaptive Scheme. *Hydraulic Engineering in Mexico*. Vol. XVIII, No. 3, July-September, 2003, pp. 29-44.

THOMPSON, J.F., WARSI, Z.U.A., and WAYNE, C. *Numerical Grid Generation, Foundations and Applications*. Mississippi: North-Holland, 1985, 483 pp.

THOMPSON, J.F., SONI, B.K., and WEATHERILL, N.P. *Handbook of Grid Generation*. Boca Ratón, USA: CRC Press, 1998, 1096 pp.

WARSI, Z.U.A. *Fluid Dynamics, Theoretical and Computational Approaches*. Boca Ratón, USA: CRC Press, 1998, 683 pp.

Institutional Address of the Authors

M.I. Alejandro Mendoza-Reséndiz
Dr. Moisés Berezowsky-Verduzco

Instituto de Ingeniería
Coordinación de Hidráulica, edificio 5
Universidad Nacional Autónoma de México
Ciudad Universitaria
Delegación Coyoacán
04510 México, D.F., México
Teléfono: +52 (55) 5623 3600, extensiones 8644 y 8629
Fax: +52 (55) 5665 1344
amendozar@iingen.unam.mx
mbv@pumas.iingen.unam.mx

Click here to write the autor

Effect of Tillage and Soil Amendments on Moisture Retention and Root Growth

• Genaro Demuner-Molina* • Martín Cadena-Zapata •
• Santos Gabriel Campos-Magaña • Alejandro Zermeño-González •
• Félix de Jesús Sánchez-Pérez •
Universidad Autónoma Agraria Antonio Narro, México
*Corresponding Author

Abstract

DEMUNER-MOLINA, G., CADENA-ZAPATA, M., CAMPOS-MAGAÑA, S.G., ZERMEÑO-GONZÁLEZ, A. & SÁNCHEZ-PÉREZ, F.J. Effect of Tillage and Soil Amendments on Moisture Retention and Root Growth. *Water Technology and Sciences* (in Spanish). Vol. V, No. 2, March-April, 2014, pp. 123-130.

The effect of three tillage systems (conventional (**CT**), vertical (**VT**) and no-tillage (**NT**)) and three organic soil amendments (algaenzims, compost and mycorrhizae) was evaluated in clay loam soil to study moisture retention, root growth and oat yield. The experiment was carried out with an experimental random block array using a factorial fit of A-B with three repetitions. The soil moisture was determined using a TDR FIELDSCOUT 300 probe in strati of 7.6 and 12 centimeters. At the end of the crop cycle, the root growth and yield were measured with amendment and a tillage system based on dry matter. According to tillage levels, a significant difference in moisture retention was found, with a value of 21.23 % in the ANOVA, and **NT** retained moisture better. For root growth, **CT** showed a significant difference, with a value of 0.04 m3, and resulted in a higher yield of 5.16 tons per hectare. **VT** and **NT** showed no significant differences in terms of root growth and grain yield. Soils amendments do not influence moisture retention or root growth, although they have positive effects on yield. Tillage systems affect moisture retention and favor root growth.

Keywords: Tillage systems, soil amendments, moisture retention, root growth, yield, dry matter, gravimetric method, TDR probe.

Resumen

DEMUNER-MOLINA, G., CADENA-ZAPATA, M., CAMPOS-MAGAÑA, S.G., ZERMEÑO-GONZÁLEZ, A. & SÁNCHEZ-PÉREZ, F.J. Efecto de labranza y mejoradores de suelo en humedad y desarrollo radicular. Tecnología y Ciencias del Agua. *Vol. V, núm. 2, marzo-abril de 2014, pp. 123-130.*

*Se evaluó el efecto de tres sistemas de labranza: convencional (**LC**), vertical (**LV**) y cero (**NL**); y mejoradores orgánicos (algaenzimas, composta y micorrizas) en un suelo franco arcilloso para determinar retención de humedad, desarrollo radicular y rendimiento de avena forrajera (avena sativa). El experimento se estableció bajo un arreglo experimental, bloques al azar con arreglo factorial A-B y tres repeticiones. La humedad del suelo se determinó utilizando una sonda TDR FIELDSCOUT 300 en estratos de 7.6 y 12 centímetros. Durante la extensión del tallo y el espigamiento se midió el desarrollo radicular y rendimiento por mejorador y sistema de labranza basado en materia seca. Con los niveles de labranza se obtuvo diferencia significativa en la retención de humedad, con un valor de 21.32% en el ANOVA, donde **NL** es la que retiene mayor humedad. En el desarrollo radicular, **LC** muestra significancia, con un valor de 0.04 m^3, y obtiene el mayor rendimiento de 5.16 t ha^{-1}; **LV** y **NL** no muestran diferencia para exploración de raíces y rendimiento. Los mejoradores no inciden en la retención de humedad y desarrollo de raíces, tienen efecto positivo para rendimiento; los sistemas de labranza impactan en la retención de humedad y permiten el desarrollo radicular.*

Palabras clave: *sistemas de labranza, mejoradores de suelo, retención de humedad, desarrollo radicular, rendimiento, materia seca, método gravimétrico, sonda TDR.*

Introduction

Conservation tillage such as zero and reduced tillage are feasible options in agriculture in terms of productivity (Van den Putte *et al*., 2010). Agricultural activities consume a large amount of water and, therefore, practical and innovative water collection and management solutions are needed in regions where the resource is scarce (Santos-Pereira *et al*., 2009). In this context, the separation of seasonal and

irrigation agriculture should be reconsidered based on a new investment and management perspective that takes into account all water supply options, among them tillage practices required by agricultural systems (Rockström *et al*., 2010).

In order to maintain food security, agricultural systems should increase their productive capacity in a sustainable manner. To this end, suitable practices and technologies are sought, such as conservation tillage, to increase the resilience of production systems to climate-related risks (Branca *et al*., 2011).

Zero and vertical tillage are the most used and disseminated conservation techniques, and therefore their advantages need to be tested in terms of moisture retention, which increases the yield-to-water used relation during the cultivation cycle (Hook and Gascho, 1998).

A fundamental part of mechanical soil tillage is its effect on hydraulic conductivity and porosity, since the movement of water in a soil profile at a certain saturation point is related to porosity, which is more significant to the infiltration speed in strata at depths over 8 centimeter (López-Santos *et al*., 2012).

Mechanical tillage does not always function as expected, regardless of the type used (Conant *et al*., 2007). Its excessive application can cause deformation in the structure, compacting of the subsurface layers and changes in the availability of moisture in radicle areas of crops (González *et al*., 2004).

In Mexico, there is very little record of the use of conservation tillage since conventional tillage continues to be the method used to prepare soil in the majority of agricultural regions. This involves removing the soil with a disc plough, raking and planting, which leads to degradation of the soil and even low crop yields (Mora-Gutiérrez *et al*., 2001).

Investigations of different levels of tillage performed in the country have been limited to evaluating and comparing technological results related to the use of different implements, such as ploughs, rakes, chisels, coulter discs, use of organic soil amendments and/or the combination of these, measuring certain parameters such as the size of the final structure, fuel demand, power demand, etc. (Cadena-Zapata *et al*., 2004).

Low yield in agricultural production with traditional systems in arid and semi-arid zones and the high costs of tillage are associated with a lack of knowledge about the quality of the soil structure needed for plants to grow well, and minimizing the loss of moisture due to the size and volume of aggregates, as well as the percentage of cover (Silva *et al*., 2000).

With respect to the interaction between tillage and soil amendments, López-Martínez *et al*. (2000) report that the physical properties of soil are affected by different organic fertilizer coverage and reduced tillage, with no effect on apparent density and moisture and resulting in higher yields than conventional tillage.

The combination of soil management practices such as conservation tillage systems and organic fertilization has increased the biological quality indicators of soil over a short period, representing a sustainable management option (Miganjos *et al*., 2006).

Given the importance of tillage and soil amendment to sustainable management, this work is aimed at determining the effect of the interaction between these two factors on the moisture contents in a soil profile as well as on root growth and oat yields.

Materials and Methods

Ecological-Geographic Characteristics of the Study Area

Location

La presente investigación se realizó dentro del campo experimental ubicado en las instala-

ciones de la Universidad Autónoma Agraria The investigation herein was performed in an experimental field located in the facilities of the Antonio Narro Autonomous Agrarian University (Universidad Autónoma Agraria Antonio Narro), located at geographic coordinates 25° 23′ 42″ north latitude and 100° 59′ 57″ west longitude, at an altitude of 1 743 meters above sea level (masl). According to the climate classification by Koppen, modified by García (1973), the climate of Buenavista is expressed by the formula $BS_0kx'(w)(e')$, that is, it is dry-arid, temperate with a long cool summer and scarce precipitation throughout the year, tending to rain more during the summer, with an extreme climate. The mean annual temperature is 16.9 °C, with a mean annual precipitation of 435 millimeters, mean annual evaporation of roughly 1 956 millimeters and predominantly northeasterly winds with average speed of 25.5 km h^{-1}.

Initial Characterization of Experimental Lots

The initial characteristics of the experimental site were: xerosol soil with a loam-clay texture, apparent density of 1.28 g cm^{-3}, infiltration speed of 3.98 cm h^{-1}, moisture retention of 230 mm m^{-1} at field capacity, soil over 2 meters deep, low organic matter content (2.5%) and resistance to penetration of 3 768.5 kPa.

Experimental Design

The experiment was conducted during the A-W 2011-2012 cycle with a statistically random A-B factorial arrangement of blocks using three tillage systems: conventional (disc plough and raking 30 cm deep), vertical (chisels 30 cm deep) and zero (direct planting), with the residuals from the prior harvest. Each block or experimental unit was divided into four sections to apply amendments with their respective recommended dose: mycorrhizae (1 kg h^{-1}), compost (3 t ha^{-1}) algaenzims (1 l ha^{-1}) and the witness control without application. Each amended section covered an area of 120 m^2 and the area of each experimental unit was 480 m^2. Fodder oats (avena sativa) were planted with a planting density of 120 kg ha^{-1}. The seed used was the Chihuahua variety, certified with 99% germination. An irrigation depth of 10 cm was applied during the cultivation cycle.

Instrumentation and Measuring Techniques

Soil Moisture

The moisture was monitored during the cultivation cycle using a TDR FIELDSCOUT 300 probe at depths of 7.6 and 12 centimeters to record the volumetric moisture contents in the soil. For 7.6 centimeter depths, samples were taken on four dates between December 29, 2011 and February 13, 2012. For 12 cm depths, samples were taken on five dates between February 3, 2012 and March 30, 2012. The sampling was conducted after irrigation, waiting two days to reach field capacity, after which samplings were taken daily until the moisture percentage was low and the next irrigation was to begin.

Root Volume Exploration

To determine radicle growth, random samples were taken (10 plants per section) during the peak of the crop by careful digging and extraction to obtain the complete root, for each tillage and amendment treatment. The roots were cleaned in the same spot, removing the soil by adding water and later measuring with a vernier caliper based on the three coordinates (Hidalgo and Candela, 1969). The results were averaged to obtain the volume exploration per treatment.

Crop Yield

The field fodder was sampled using a framing method, for which a wooden frame was built with sides measuring 0.25 meters and a total area of 0.0625 m^2 (Martínez *et al*., 1990). The frame was placed in the soil, the matter in the center of it was cut, weighed while green, and then dehydrated at a temperature of 70° C for 72 hours until depletion of moisture and so its weight was constant to obtain the yield of the dry fodder. This was taken as the dry matter weight of the crop to calculate yield per hectare.

Data Analysis

To process the data obtained, a random, factorial arrangement of blocks was used with the *R* program, version 2.9.0, distributed with a license from R Foundation for Statistical Computing. This is free software used by statistical and research communities. Data from ANOVA were obtained with their respective interactions and a comparison of means was performed using the Tukey method for each factor analyzed.

The Linear Model

The statistical model proposed (Montgomery, 1991) for a random block experiment with an A and B factorial arrangement is:

$$Y_{ijk} = \mu + \beta_i + \alpha_j + \tau_K + \alpha\tau_{jk} + \varepsilon_{ijk}$$

Where:

Y_{ijk}: is the ijk^{th} observation in the i^{th} block, which contains the j^{th} level for factor *A* and the k^{th} level for factor B.
μ: is the overall mean.
β_i: is the factor of the i^{th} block.
α_j: is the effect of the j^{th} level for factor A.
τ_k: is the effect of the k^{th} level for factor B.
$\alpha\tau_{jk}$: the interaction of the j^{th} level of factor A with the k^{th} level of factor B.
ε_{ijk}: is the random NID error ($0 - \sigma^2$).

Results and Discussion

Analysis of Moisture According to the Respective Interactions (Depth, Tillage, Amendment)

In the variance analysis of the moisture variable, with its respective interactions (Table 1), only tillage showed a high significance, with a value of 0.007227**. As seen in Table 2, which shows the DMS, **ZT** retained more moisture than **CT** and **VT**. Similar studies found that for soil in a semi-arid region, more water is retained in the profile with zero tillage than with conventional tillage (Fernández-Ugalde *et al*., 2009).

As can be seen in Table 3 which presents the DMS test with soil amendments, no positive effect on moisture retention was found. As described by Querejata *et al*. (2000), the beneficial effects of organic amendments

Table 1. ANOVA for Moisture.

	***F* value**	***Pr* (> *F*)**
Depth	0.6714	0.415254
Tillage	5.2835	0.007227**
Amendment	0.5723	0.635060
Prof:Lab	0.1198	0.887257
Prof:Mej	0.5135	0.674264
Lab:Mej	1.2281	0.302143
Prof:Lab:Mej	0.6177	0.715412
CV: 4.014557		

Table 2. Multiple Comparison of Tillage based on Means obtained according to Amendments.

Groups	Treatments	Means (%)
a	LV	15.53
ab	LC	16.40
b	NL	21.32

Table 3. Multiple Comparison of Moisture based on Means obtained with Amendments.

Groups	Treatments	Means (%)
a	Mycorrhizae	16.38
a	Compost	17.60
a	Witness Control	17.81
a	Algaenzims	19.21

Table 4. Moisture with respect to Depth.

Groups	Treatments	Means (%)
a	P2 (12 cm)	17.83
a	P1 (7.6 cm)	17.67

on retaining moisture are observed over 4 years after application.

Brown and Cotton (2011) indicated increased moisture retention capacity in soils with compost applications, and these increases are greater in thick than fine soils. They also reported more benefits for soil using large compost application rates as compared to lower application rates.

Table 4 shows the values of the moisture variable obtained with the DMS according to sampling depth. No significant differences exist; both depths retained the same amount of moisture. Dalrymple *et al*. (1993) reported no significant differences in the availability of water in the soil profile among zero, minimal and conventional tillage.

Analysis of the Effect of Tillage and Amendment on Volume Exploration

The variance analysis for the roots exploration was significant only for tillage,

Table 5. Multiple Comparison of Means of Volume Exploration in Relation to Tillage.

Groups	Treatments	Means (m^3)
a	LC	0.001736536
a	LV	0.001627895
a	NL	0.001087346

with a value of 0.04099, with no influence from amendments. In addition, the DMS test shown in Table 5 presents the values for the tillage systems with respect to volume exploration, with no significant differences and all treatments being equal.

The primary cause of deficient radicle growth is the compacting and hard layers resulting from the use of a mechanical device. This mechanical impediment can be corrected by using suitable tillage implements (subsoil and chisels) in a timely manner to break up the compact layers and decrease the apparent density of the soil. Martínez *et al*. (2008), studying the more long-term effects of tillage (from four to six years), found that the length and density of the roots of a wheat crop were greater with zero tillage than with conventional tillage.

Table 6 shows the DMS test for amendments in terms of the root volume exploration. As can be seen, all the amendment treatments were equal, since no differences were found among them in terms of radicle volume exploration. The apparent density of a soil tends to limit the development of the plant roots, and therefore changing the density with the use of organic amendments is desirable.

Table 6. Multiple Comparison of Means for Volume Exploration in Relation to Amendments.

Groups	Treatments	Means (m^3)
a	Mycorrhizae	0.001804756
a	Algaenzims	0.001448125
a	Compost	0.001549260
a	Witness Control	0.001133563

Table 7. Multiple Comparison of Means for Yield with respect to Tillage.

Groups	Treatments	Means (ton/ha)
a	LC	5.16
ab	NL	2.92
b	LV	2.76

Carmen *et al*. (1998) used organic residues from Crotalaria (*Crotalaria juncea*) and elephant grass (*Pennisetum purpureum*) to evaluate the effects on some of the physical properties of a corn crop. The experiment was systematically repeated over three years, at the end of which favorable effects were identified on apparent density as compared to the witness, thereby confirming the beneficial effects of using residues in the soil.

Effects of Tillage and Amendments on Fodder Oats Yield

The variance analysis of yield shows significance with respect to tillage, with a value of 0.03367*. Table 7 shows the DMS test for yield in relation to tillage, with CT having a higher yield than ZT and VT.

The benefits of conservation tillage on decreasing erosion and conserving moisture do not necessarily result in increased yield. Vetsch and Randall (2002) found that over four years of continuous corn production, yield was always greater for conventional tillage than zero tillage.

De Vita *et al*. (2007) reported higher yield during years with more moisture using conventional tillage in a long-term (10 years) experiment with seasonal wheat crops. Nevertheless, during years with scarce precipitation (around 300 millimeters of rainfall), yield was greater with zero tillage because of the lower evaporation rate, which provides more water availability.

Table 8. Multiple Comparison of Means for Yield with respect to Amendments.

Groups	Treatments	Means (ton/ha)
a	Micorrizas	3.84
a	Witness control	3.78
a	Algaenzims	3.35
a	Compost	3.49

Table 8 presents data obtained with the DMS test for the effect of amendments on yields. As can be seen, the treatments are equal and no differences exist among them.

Singer *et al*. (2003) used different types of organic composts and obtained increases in yield the first year with tillage using a plough and chisels in a corn and soybean crop in 1998. Therefore, during the next cycle with rotation, differences in the tillage-amendment interaction and significant increases in yields could be obtained.

Conclusions

Organic amendments applied during the development of a crop did not show a positive influence on moisture and radicle growth.

The effect obtained on yield at the end of the cycle using different tillage systems was shown to be favorable with conventional tillage. The amendments tended to increase the yield of the crops because they act as organic fertilizers.

To calculate the yield obtained at the end of a cultivation cycle, plant density should be sampled for each tillage treatment on the days before harvesting.

When performing vertical tillage, raking is necessary since a planted seed can be lost in the deeper strata and may not germinate and therefore not complete its cycle, which will affect yield.

The medium-term results obtained may indicate positive effects on yields, especially with regard to testing the efficiency of conservation tillage systems and their

influence on moisture retention in semi-arid regions of the country, where the primary problem is the availability of water for crops.

Received: 07/09/2012
Accepted: 24/06/2013

References

BRANCA, G., MAcCARTHY, N., LIPPER, L., and JOLEJOLE, M.C. *Climate Smart Agriculture: A Synthesis of Empirical Evidence of Food Security and Mitigation Benefits from Improved Cropland*. Mitigation of Climate Change in Agriculture Series 3. Rome: FAO, 2011.

BROWN, S. and COTTON, M. Changes in Soil Properties and Carbon Content Following Compost Application: Results of On-Farm Sampling. *Compost Science and Utilization*. Vol. 19, No. 1, 2011, pp. 88-97.

CADENA-ZAPATA, M., GAYTÁN-MUÑIZ, T. y ZERMEÑO-GONZÁLEZ, A. Desempeño de implementos de labranza en términos de consumo de energía y calidad de trabajo. *Revista Agraria Nueva Época*. Vol. 1, No. 3, 2004, pp. 12-17.

CARMEN, R., DEYANIRA, L.L. y ALFREDO, L.P. Efectos de la incorporación de residuos orgánicos sobre algunas propiedades físicas de un alfisol degradado. *Venesuelos*. Vol. 1 y 2, núm. 6, 1998, pp. 29-33.

CONANT, R., EASTER, M., PAUSTIAN, K., SWAN, A. and WILLIAMS, S. Impacts of Periodic Tillage on Soil C Stocks: A Synthesis. *Soil and Tillage Research*. Vol. 95, 2007, pp. 1-10.

DALRYMPLE, A.W., MILLER, S.D., and FORNSTROM, K.J. Soil Water Conservation and Winter Wheat Yield in Three Fallow Systems. *Journal of Soil Water Conservation*. Vol. 48, 1993, pp. 53-57.

DE VITA, P., DI PAOLO, E., FECONDO, G., DI FONZO, N., and PISANTE, M. No-Tillage and Conventional Tillage Effects on Durum Wheat Yield, Grain Quality and Soil Moisture Content in Southern Italy. *Soil and Tillage Research*. Vol. 92, No. 1-2, 2007, pp. 69-78.

FERNÁNDEZ-UGALDE, O., VITRO, I., BESCANSA, P., IMAZ, M.J., ENRIQUE, A., and KARLEN, D.L. No-Tillage Improvement of Soil Physical Quality in Calcareous, Degradation-Prone, Semiarid Soils. *Soil and Tillage Research*. Vol. 106, 2009, pp. 29-35.

GARCÍA, E. Modificaciones al sistema de clasificación climática de Koppen (para adaptarlo a las condiciones de la república mexicana). México, D.F.: Instituto de Geografía, Universidad Nacional Autónoma de México, 1973, 246 pp.

GONZÁLEZ, C.G., SÁNCHEZ-COHEN, I. y GARCÍA-ARELLANO, D. Relaciones entre el manejo del huerto de nogal y la porosidad del suelo. *Terra Latino*. Vol. 22, 2004, pp. 279-287.

HIDALGO, I. y CANDELA, M. *Morfología radicular de la vid*. Madrid: Instituto Nacional de Investigación y Tecnología Agraria y Alimentaria (INIA), 1969, p. 101.

HOOK, J.E., and GASCHO, J.G. Multiple Cropping for Efficient Use of Water and Nitrogen. In *Cropping Strategies for Efficient Use of Water and Nitrogen*. Hrgrofe, W.L. (editor). Madison, USA: ASA Special Publication. America Society of Agronomy, Inc., Vol. 51, 1998, pp. 7-20.

LÓPEZ-MARTÍNEZ, J.D., GUTIÉRREZ-PUENTE, G. y BERÚMEN-PADILLA, S. Labranza de conservación usando coberturas de abono orgánico en alfalfa. *Terra Latinoamericana*. Vol. 18, No. 2, 2000, pp. 161-171.

LÓPEZ-SANTOS, A., GONZÁLEZ-CERVANTES, G., CADENA-ZAPATA, M. y GONZÁLEZ-BARRIOS, J.L. Effect of primary Tillage on the Physical Quality of Soil, as Evaluated by Disk Permeameter. *Water Technology and Sciences*. Vol. 3, No. 4, 2012, pp. 127-141.

MARTÍNEZ, E., FUENTES, J.P., SILVA, P., VALLE, S., and ACEVEDO, E. Soil Physical Properties and Wheat Root Growth as Affected by No-Tillage And Conventional Tillage Systems in a Mediterranean Environment of Chile. *Soil and Tillage Research*. Vol. 99, 2008, pp. 232-244.

MARTÍNEZ, J., MILERA, M., REMY, V., YEPES, I. y HERNÁNDEZ, J. Método ágil para estimar la disponibilidad de pasto en una vaquería comercial. *Pastos y Forrajes*. Vol. 13, núm. 1, 1990.

MIGANJOS, I., PEREZ, R., ALBIZU, I., and GARBISU, C. Effects of Fertilization and Tillage on Soil Biological Parameters. *Enzyme and Microbial Technology*. Vol. 40, 2006, pp. 100-106.

MONTGOMERY, D.C. *Diseño y análisis de experimentos*. México, D.F.: Iberoamérica, 1991, 589 pp.

MORA-GUTIÉRREZ, M., ORDAZ, V., CASTELLANOS, J.Z., AGUILAR-SANTELISES, A., GAVI, F. y VOLKE, V. Sistemas de labranza y sus efectos en algunas propiedades físicas en un vertisol, después de cuatro años de manejo. *Terra Latinoamericana*. Vol. 19, núm. 1, 2001, pp. 67-74.

QUEREJATA, J.I., ROLDAN, A., ALBALADEJO, J., and CASTILLO, V. Soil Physical Properties and Moisture Content Affected by Site Preparation in the Afforestation of a Semiarid Rangeland. *Soil Science Society American Journal*. Vol. 64, 2000, pp. 2087-2096.

ROCKSTRÖM, J., KARLBERG, L., WANI, S.P., BARRON, J., HATIBU, N., OWEIS, T., BRUGGEMAN, A., FARAHANI, J., and QUIANG, Z. Managing Water in Rainfed Agriculture-The Need for a Paradigm Shift. *Agricultural Water Management*. Vol. 97, No. 4, 2010, pp. 543-550.

SANTOS-PEREIRA, L.A., CORDERY, I., and IACOVIDES, I. *Coping with Water Scarcity: Addressing the Challenges*. The

Netherlands: Springer Science and Business Media B.V., 2009.

SILVA, L.A., GUTIÉRREZ, N.C. y VENIALGO-CHAMORRO, C. *Efectos de cultivos forrajeros y de escarda en la porosidad de un durustol típico*. Comunicaciones Científicas y Tecnológicas. Cátedra de Conservación y Manejo de Suelos. Corrientes, Argentina: Facultad de Ciencias Agrarias, Universidad Nacional del Nordeste, 2000.

SINGER, J.W., KHOLER, K.A., LIEBMAN, M., RICHARD, T.L., CAMBARDELLA, C.A., and BUHLER, D.D. Tillage and Compost Affect Yield Corn, Soybean and Wheat and Soil Fertility. *Agronomy Journal*. Vol. 96, No. 2, 2003, pp. 531-537.

VAN DEN PUTTE, A., GOVERS, G., DANIELS, J., GILLIJNS, K., and DEMUZERE, M. Assessing the Effect of Soil on Crop Growth: A Meta-Regression Analysis on European Crop Yields Under Conservation Agriculture. *European Journal of Agronomy*. Vol. 33, 2010, pp. 231-241.

VETSCH, J.A., and RANDALL, G.W. Corn Production as Affected by Tillage System and Starter Fertilizer. *Agronomic Journal*. Vol. 94, 2002, pp. 532-540.

Institutional Address of the Authors

M.C. Genaro Demuner Molina
Dr. Martín Cadena Zapata
Dr. Santos Gabriel Campos Magaña
Dr. Alejandro Zermeño González
M.C. Félix de Jesús Sánchez Pérez

Especialidad en Ingeniería Agrícola
División de Ingeniería
Universidad Autónoma Agraria Antonio Narro
Calzada Antonio Narro núm. 1923
25315 Buenavista, Saltillo, Coahuila, México
Teléfonos: +52 (844) 4110 224 y 4110 323
gdemuner@gmail.com
martincadenaz@gmail.com
camposmsg@hotmail.com
azermenog@hotmail.com
fel1925@yahoo.com

Click here to write the autor

Advances in Geomatic to Solve Water Problems in Mexico

• Felipe Omar Tapia-Silva* •
Universidad Autónoma Metropolitana, México
*Corresponding Author

Abstract

TAPIA-SILVA, F.O. Advances in Geomatic to Solve Water Problems in Mexico. *Water Technology and Sciences* (in Spanish). Vol. V, No. 2, March-April, 2014, pp. 131-148.

As in a previous work (Tapia-Silva 2011a, 2011b, written in 2008), this paper reviews representative studies that are examples of the capabilities of Geomatics and its convergent disciplines to support the study of water cycle variables as part of a territorial analysis of water resources and related problems in Mexico. The aim of the article review is to generate public initiatives and policies to help solve these problems. Therefore, the idea of this new article is to update and supplement the information, knowledge, definitions and concepts about water problems and Geomatics provided in Tapia-Silva (2011a, 2011b). An innovative feature of this manuscript is its emphasis on the role of GIS as an integrating axis for the other disciplines involved in Geomatics. The article is structured as follows: Geomatics, Updated Summary of Water Problems in Mexico, Advances in Geomatics to Solve Water Problems and Final Remarks. The first section defines Geomatics and describes its relationship with society and its needs. The second summarizes water-related problems in Mexico, complementing the information provided in Tapia-Silva (2011a, 2011b). The third section reviews the work published on the subject of creating solutions to this problem from the viewpoint of integrated disciplines in Geomatics. The last section summarizes what is included in the previous sections and concludes with some final thoughts.

Keywords: Geographic information systems, geospatial modeling, remote sensing.

Resumen

TAPIA-SILVA, F.O. Avances en geomática para la resolución de la problemática del agua en México. Tecnología y Ciencias del Agua. *Vol. V, núm. 2, marzo-abril de 2014, pp. 131-148.*

Como en un trabajo precedente (Tapia-Silva 2011a, 2011b, escrito en 2008), este manuscrito tiene la intención de conjuntar una muestra ilustrativa de los trabajos que permiten apreciar las capacidades de la geomática y sus disciplinas convergentes para apoyar el estudio de las variables del ciclo hidrológico en un contexto de análisis territorial de la problemática del agua para la generación de iniciativas y políticas públicas que ayuden a su resolución. Este nuevo artículo actualiza y complementa información y conocimiento presentados en el artículo antes citado, y amplía definiciones y conceptos relativos a la geomática provistos en el mismo. Otro elemento innovador del presente manuscrito consiste en hacer énfasis en el papel de los SIG como eje integrador de las otras disciplinas convergentes en el ámbito de la Geomática. El artículo está estructurado en los apartados siguientes: "Geomática", "Resumen actualizado de la problemática del agua en México", "Avances desde la geomática para la resolución de la problemática hídrica en México" y "Apuntes finales". El primer apartado define a la geomática y la ubica en el contexto de su relación con la sociedad y su problemática. El segundo resume la problemática del agua en México, complementando con otros trabajos científicos lo publicado en Tapia-Silva (2011a, 2011b). El tercero aporta una revisión actualizada de los trabajos científicos publicados respecto al tema de generación de soluciones a esta problemática desde el enfoque de las disciplinas integradas en la geomática. El último apartado sintetiza lo incluido en los anteriores y concluye con una serie de reflexiones finales a manera de conclusiones.

***Palabras clave**: sistemas de información geográfica, modelaje geoespacial, percepción remota.*

Geomatics

According to authors such as Pagiatakis (2013), the term geomatics was coined by Bernard Dubuisson in Canada in the late 1970s. Other authors, such as Gomarazca (2010), indicate that it was first used in Laval University, Canada in the early 1980s, in relation to the

idea that the increased power of electronic computing revolutionized the sciences that represent and survey field data, and the use of computerized design was compatible with the handling of large quantities of information. Authors such as Pagiatakis (2013) consider geomatics to be a part of engineering. A series of highly technical definitions exist, such as that proposed by Gomarazca (2010): Geomatics is defined as a systemic, multidisciplinary, integrated approach to select the instruments and the appropriate techniques for collecting, storing, integrating, modeling, analyzing, retrieving, transforming, displaying and distributing, in a digital format, spatially georeferenced data from different sources with good definition, accuracy and continuity. Meanwhile, according to Levi (2006), the resulting discipline transcends the sum of its parts, becoming a system of thinking in which the boundaries between the parts are not important, nor is defining the precise origin of the elements that compose its conceptual framework. Rather, it is a unit aimed at providing integral solutions presented by society, which are generally addressed using spatial analysis theory and methodologies. Thus, the term can be used to define a transdisciplinary, scientific field of knowledge whose objective is to solve societal problems occurring in space and time. The discipline has emerged from the space in which other previous ones have converged, such as geographic information systems (GIS), cartography, remote sensing, geodesy and photogrammetry. In addition, geomatics studies a series of methods to acquire, process, represent, communicate, analyze and systematize data, information and knowledge having a specific location and spatial surroundings. Geomatics is a type II science stemming from the needs of society and aimed at solving them (Tapia-Silva, 2011c). According to Reyes and Monroy (2000), it emerged from an interrelated process between GIS and geography. These authors indicate that during this process a need was detected to integrate other scientific activities, such as cartography and geodesy, which had been developing in parallel and with significant points of contact. They also mention that this relationship resulted in the maps that constitute the traditional technique or tool to store, present and analyze spatial data. The map is therefore one of the foundations of GIS, serving as a source of geospatial data and a structure in which to store it, as well as an analysis and display instrument.

As can be seen in Figure 1, GIS is an important integrating axis for the other geomatic disciplines. Elements from other disciplines are integrated into GIS, to a greater or lesser degree, including: general systems theories (von Bertalanffy, 1979), cartographic modeling, spatial analysis (including geostatistics) and other emergent disciplines such as cybercartography and computational imaging, geocomputation, geodesy, quantitative and qualitative modeling and remote sensing. This means that GIS needs to integrate a vast quantity of elements from other disciplines in order to record, analyze and image phenomena associated with the territory (georeferenced). Other disciplines such as photogrammetry and digital image processing provide important elements that are also used by GIS.

Developments in the spatial analysis field, related to GIS, have played a key role in the emergence of geomatics. Rogerson and Fotheringam (1994) write that GIS were first generated as tools to store, search and display geographic information, and the spatial analysis capabilities were poor or non-existent in the early systems. Star and Estes (1990) describe the factors that enabled the creation of digital GIS in the 1970s as: refinements in cartographic techniques

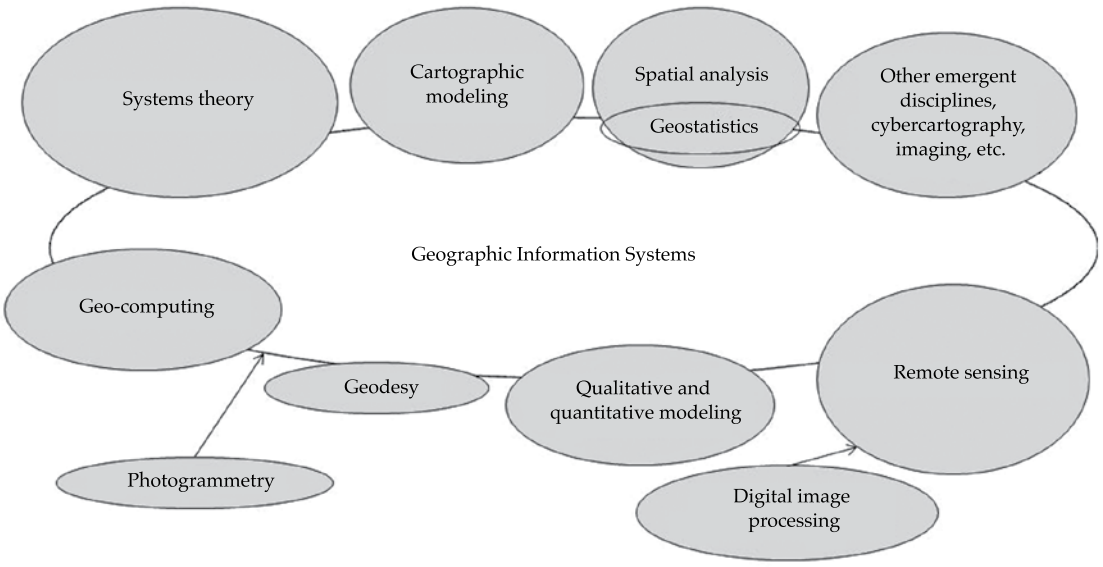

Figure 1. Integration of Geomatic Disciplines with Geographic Information Systems (GIS).

which began to be used in early Egyptian times (2500 b.c.e.); rapid development of computerized digital systems; and especially, a quantitative revolution in spatial analysis. Demers (2000) states that the heart of GIS is its analysis capability. That is, without spatial analysis there is no GIS.

As indicated earlier, geomatics sees society as the main beneficiary of its studies and developments, and includes society in its knowledge models of the functioning of the territory by identifying the actors involved in natural and constructed changes (Tapia-Silva 2011a, 2011b). In this context, Centro de Investigación en Geografía y Geomática "Ing. Jorge L. Tamayo" (Jorge L. Tamayo Center for Investigations in Geography and Geomatics; CentroGeo, Spanish acronym) has undergone a process to generate knowledge according to what is called the knowledge spiral (Figure 2). This process is based on empirical work motivated by the dynamics of connecting with the problems of diverse organizations in the public, social and private sectors. In response, prototypes (technological developments presented as geomatic artifacts, as defined below) and geomatic solutions are generated, which can later be formalized by basic and empirical research in order to have an impact on society by introducing solutions to social problems posed by the users.

To analyze territorial problems (the problem of water, for example), a geospatial abstraction process is required in which the observer possesses the spatial-temporal perspective and knowledge of the processes that occur in a territory, which are used to integrate and construct the elements needed for modeling (Freire-Cuesta, 2011). The systems approach and the generation of information based on remote sensors and geospatial models increase the capabilities of geomatics to analyze and communicate the functioning of processes that occur in a territory and to support decision-making (Tapia-Silva 2011a, 2011b).

Hydrology is defined as a geographic science because the functioning of the water cycle and water usage are phenomena which

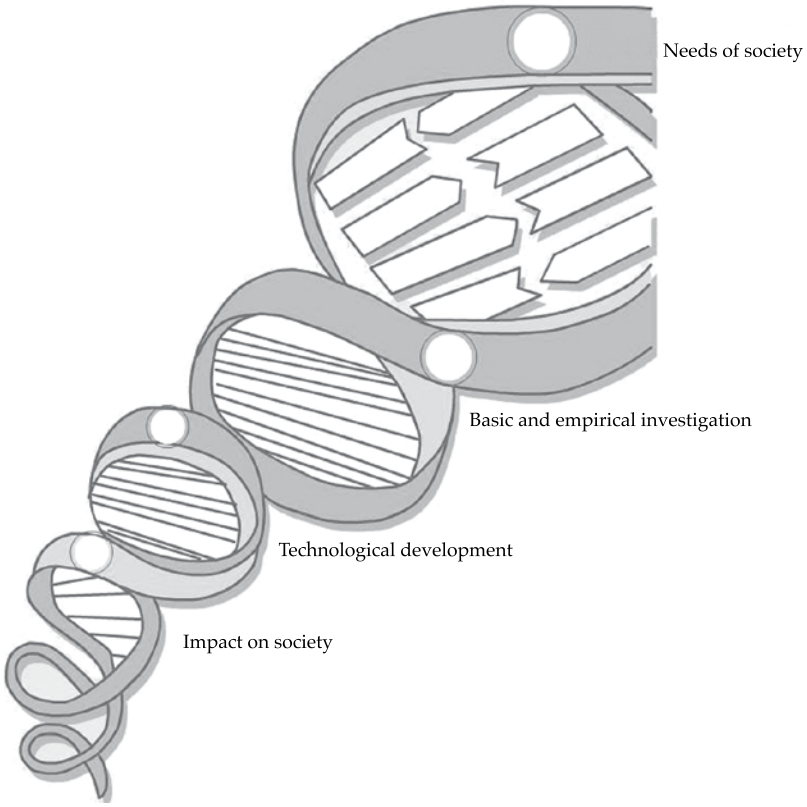

Figure 2. Knowledge Generation Spiral in Geomatics (created by CentroGeo).

are intrinsically associated with space. The components of the cycle and other factors involved in the complex water problem have a geographic reference and an observable spatial and temporal variability. From a territorial perspective, studies intended to contribute to solving the water problem must use a systems approach and require information and knowledge that reflect the spatial and temporal variability of the factors involved. With this approach, a systems view must identify the elements that make up the hydrological system in question (a basin or a specific territory delimited by other criteria such as political boundaries) and analyze the relationships and changing dynamics observed among these elements (Tapia-Silva, 2011a, 2011b).

Geomatic artifacts can be considered the most finished product provided by geomatics to solve hydrological and other types of environmental problems (Tapia-Silva, 2011a, 2011b). These artifacts include cybernetic developments, prototypes and applications which in turn contribute to geospatial knowledge and information, such as atlases, documents, systems and geomatic solutions. Its development involves a series of elements that are combined to make it possible to have two-way communications processes with users, who then access the elements that enable seeing themselves as actors within each application's specific environment. Martínez and Reyes (2005) describe this process as second-order cybernetics. During the implementation of

geomatic artifacts, a process is generated which modifies the views of the users of the artifact, who propose improvements to it, enabling them to again access another series of concepts, information and ideas so that the perspectives and solutions regarding the problem related to the artifact continue to evolve. Other important characteristics of geomatic artifacts is the holistic and systems view of the problems or phenomena they represent. One of the key ideas of the holistic view is the requirement to include socioeconomic and technical-natural aspects or characteristics when observing and representing the phenomenon in question. Thus, the problem surrounding an artifact is observed and analyzed in a comprehensive manner, thereby maximizing the ability to identify solutions that may be socioeconomic, technical, biophysical, or a combination thereof. Knowledge models provide important elements to represent the complexity of the hydrological problem. As mentioned earlier, cases involving the application of geomatic artifacts to solve the water problem will not be reviewed since they were described in detail in the previous article (Tapia-Silva, 2011a, 2011b) and no other notable developments have occurred since then.

Updated Summary of the Water Problem in Mexico

Water is typically considered to be a renewable natural resource. Unfortunately, it is possible to verify that this no longer is the case, as demonstrated by the overexploitation of aquifers, drying up of water bodies and problems associated with pollution, among other phenomena. Water consumption worldwide has doubled in two decades, and Mexico's water resources are limited (Oswald-Spring and Sánchez Cohen, 2011). The emergence of problems caused by changes in precipitation patterns (unpredictable according to Allen and Ingram, 2002) as a consequence of climate change exacerbate the problems related to the availability and excess of water. These changes are increasingly associated with extreme phenomena (droughts and intense rains) and the destabilization of precipitation regimes (Easterling *et al*., 2000). Another predominant negative effect is that reported by Douglas (1997), who identified a global increase in the sea level of 1.8 mm/year over the last 100 years. In addition, on the national level more serious complications exist due to the reduction and pollution of aquifers and surface water bodies (described in the following sections).

These situations indicate that, in a context of poorly planned human intervention in the territory, water is a resource whose conditions cannot be maintained in such a way as to continue to provide for the development of human society and the ecosystem in which it lives. The following list supplements the most important hydrological problems observed in Mexico, presented by Tapia-Silva (2011a, 2011b):

- Little water availability. Oswald-Spring and Sánchez-Cohen (2011) mention that 58% of the national territory is located in zones with little precipitation (arid, semi-arid and desert regions). In addition, authors such as Díaz-Padilla *et al*. (2011) document the seasonality of precipitation (87% from May to October), which means quite a long period during the year with low or no precipitation. According to Arreguín-Cortés *et al*. (2011), the annual per capita availability of water decreased from 17 742 m^3 in 1950 to 4 261 m^3 in 2009¾ an impressive reduction of 76%. These authors also indicate that water availability no longer exists in six basins located in northern (north and south

Sonora, closed basins in the north and the Bravo River) and central (Lerma-Chapala and Balsas Rivers) Mexico, according to the definition of water availability by the National Waters Law (difference between mean annual runoff volume in a basin and volume of water reserves).

- Inefficient water usage in agricultural and urban zones. Conagua (2007) reports usage for agriculture purposes at roughly 80% of the national total, suggesting the need to improve the efficiency of irrigation through water savings technologies. Oswald-Spring and Sánchez- Cohen (2011) indicate an efficiency of 40% for the agriculture sector, which reflects an enormous percentage (60%) of water loss.
- Drying up and pollution of aquifers (104 of a total of 653 according to Conagua, 2007) due to overexploitation and serious deficiencies in water use planning in the country, as well as the regulation of the consumption of potentially polluting products.
- Reduction and disappearance of water bodies as a result of negative balances between inputs (from precipitation and surface and groundwater flows) and outputs (caused by evaporation and intakes by anthropogenic uses). Studies about this subject have been conducted only in relation to particular water bodies, such as Chapala Lake (Lopez-Caloca *et al*., 2008).
- Incidence of torrential rains and impermeability of surfaces that cause floods and mudslides and impede the recharge of aquifers. With regard to hurricanes, Conagua (2007) observed 47 between 1980 and 2006, and category 3 or higher have been registered with greater frequency. With respect to impermeable surfaces, only isolated determinations have been obtained for certain cities (Mexico City, Campeche, Leon and Mexicali), which will be reviewed in the next session.
- Poor use and polluting of rainwater from mixing with sewage. Conagua (2097) reports that 36% of municipal water is treated and treatment levels by plants vary widely, primary treatment is usually carried out, according to information from Conagua (2007).
- Pollution of surface water by polluted wastes. According to Conagua (2007), 8 to 30% of total surface runoff is polluted, according to the results from the monitoring of three quality parameters (biochemical oxygen demand, chemical oxygen demand and total suspended solids).
- Increased flow in rivers due to deforestation or poorly planned usage upstream in the basins. This requires investigation to accurately define the current situation. Only some preliminary results are available, such as those indicated in the next section.

These points illustrate the complexity of the water problem in Mexico. The following sections review the progress in geomatics to contribute to the solutions.

Advances in Geomatics to Solve the Water Problem in Mexico

This section is divided into several parts, focusing on studies related to applications of remote sensing, GIS and other spatial analyses used to solve the water problem in Mexico. The subjects addressed include: analysis of efficiency of water usage; comprehensive studies of basins; spatial variability of aquifers in terms of vulnerability and usage capacity; sealing and impermeability of surfaces; monitoring of water bodies and the relationship with hydrological variables; zones prone to flooding; effects of land use

in relation to variables; environmental water services and; analysis of the spatial-temporal variability of water variables.

Analysis of Water Use Efficiency

The study of regions with low water use efficiency indices and the generation of proposals to increase these indices is a feasible activity for geomatics. For example, to calculate crop yields, water consumption and a water use efficiency index, Mo *et al*. (2005) used geographic land use layers, digital elevation models (DEM), soil textures and a foliage area index for crops using AVHRR (Advanced Very High Resolution Radiometer), as well as interpolated climate data. The study of water availability in aquifers, the water balance and consumption of water resources for farming is supported by studies that calculate evaporation using remote sensing (Bastiaanssen *et al*., 2005). For example, Zwart *et al*. (2006) used SEBAL (Bastiaanssen *et al*., 1998)) to calculate water productivity for wheat crops in the Yaqui Valley, Sonora, Mexico. Garatuza-Payan *et al*. (2001) used GOES (Geostationary Operational Environmental Satellites) images to obtain radiation values, based on which they calculated evapotranspiration according to the Makkink formula. Values from satellite images were approximately 9% lower than field measurements. In addition, Garatuza-Payan *et al*. (2005) calculated crop coefficients as a function of vegetation indices (NDVI and SAVI (Soil Adjusted Vegetation Index)) and thereby obtained real evapotranspiration based on reference evapotranspiration. Scott *et al*. (2003) validated the use of SEBAL to calculate soil moisture in an agricultural area in Cortázar, Guanajuato and analyzed these results in the context of resource management. In regard to desertification, Lira (2004) proposed a model based on the TSAVI (Transformed Soil-Adjusted Vegetation Index) vegetation index and applied it to a LandSat image from 1996 in the northern part of the country. Coronel *et al*. (2008) estimated real evaporation for a large part of Mexico using SEBAL (Bastiaanssen *et al*., 1998) and SSEB (Senay *et al*., 2007) methodologies, as well as data from MODIS and PAN evaporation measurements. In another study, Ojeda-Bustamante *et al*. (2007) presented the advantages of applying a GIS to water management for agricultural purposes. Included among the functions reported is the generation of maps of crop maturity and resource usage. A study by Gutiérrez-Castorena *et al*. (2008) integrated geographic information related to irrigated area, cultivated area and harvested area into a GIS to determine plans to change crop patterns in order to adjust them to the reduction in water availability resulting from the construction of a dam. The authors report this case to have been successful, in which the use of information from the processing of geospatial data prevented migration and the abandonment of lands.

Comprehensive Studies of Basins

Galván-Fernández (2011) provides an example of this type of investigation, in which hydrology, physiography, climate, soil, vegetation and productive systems were studied in a coastal basin to define land management actions. This was conducted with the management of geospatial information in GIS. A study by Carrera-Hernández and Gaskin (2008) proposed a GIS to improve the regional management of data for the Valley of Mexico basin. The GIS is composed of data related to climate, wells and runoff. The study presents examples of the spatial consultation of geographic data as well as a geostatistical analysis (*kriging* with external drift) to more accurately calculate the spatial variability of precipitation. In

another study, conducted by Mendoza *et al*. (2010), a distributed water balance model was developed to define the regional influence of land use and its temporal variation in the Cuitzeo Lake basin in Michoacan. This study applied remote sensing methods and the geographic information was integrated in a GIS. The results showed improvement in regional hydrological conditions (uncommon for hydrological systems in Mexico). Studies of the availability of the resource in hydrogeological basins are also highly valuable. For example, Ramos-Leal and Hernández-Moreno (2008) presented a series of reflections about the usefulness of a regional approach to study and manage hydrogeological basins in San Luis Potosí and the Valley of Mexico.

Spatial Variability of Aquifers in Terms of Vulnerability and Usage Capacities

The spatial variability of the vulnerability of an aquifer to becoming polluted and the location of sources of pollutants (geographic points and zones) of surface and groundwater bodies have been successfully determined using disciplines integrated in the field of geomatics. One such study was carried out by Ramos-Leal *et al*. (2010) for Mexico City and its metropolitan area. Another similar study, by Ramos- Leal *et al*. (2011), generating a geospatial database in a GIS environment, applied the geographically weighted regression (GWR) spatial analysis technique and the SINTACS method (Civita and De Maio, 1997) to define the vulnerability and water quality of the aquifer in the Central Valleys of Oaxaca. Figure 3 shows images from this investigation, presenting the layers used to generate the pollution source index (PSI) and the area for this parameter, as well as the geographic determination by the SINTACS index, adjusted correlation coefficients for the GWR and the spatial distribution in the Central Valleys of Oaxaca, Mexico. This information is useful to identify areas that are more vulnerable to becoming polluted and the association with potential polluting factors. Another study by Ramos-Leal *et al*. (2012) determined the vulnerability to pollution for the aquifer in the Chapala region (Jalisco), in which it was possible to study the vertical movement of the pollutant using SINTACS and its lateral movement using GWR.

A recent study by Marín *et al*. (2012) used spatial analysis procedures to define buffer zones for spatial variables (water bodies, human settlements and rivers, among others) in the GIS environment. This procedure made it possible to locate suitable areas for sanitary landfills in the state of Morelos, taking into account the hydrogeological characteristics of the place. Rangel-Medina *et al*. (2011) generated an integration scheme in the GIS environment using previously available hydrogeological information related to flows from wells in operation, measurements of groundwater quality and the interpretation of satellite images in order to propose strategies for the appropriate use of coastal aquifers in northeastern Mexico. In this study, three-dimensional views generated by GIS were presented, which constitute important elements to strengthen the ability to visually analyze the processed information. Subsidence and pollution of groundwater by anthropogenic activities were analyzed in a study performed by Rodríguez-Castillo and Rodríguez-Velázquez (2011). This investigation identified faults and fractures in land affected by subsidence, determined the geolocation of the faults and superimposed those faults with urban maps in GIS to identify damage and risk zones. This type of study enables locating points for reconditioning an aquifer's recharge wells or points for rainwater or surface water catchment, as performed by Saraf *et al*. (2004).

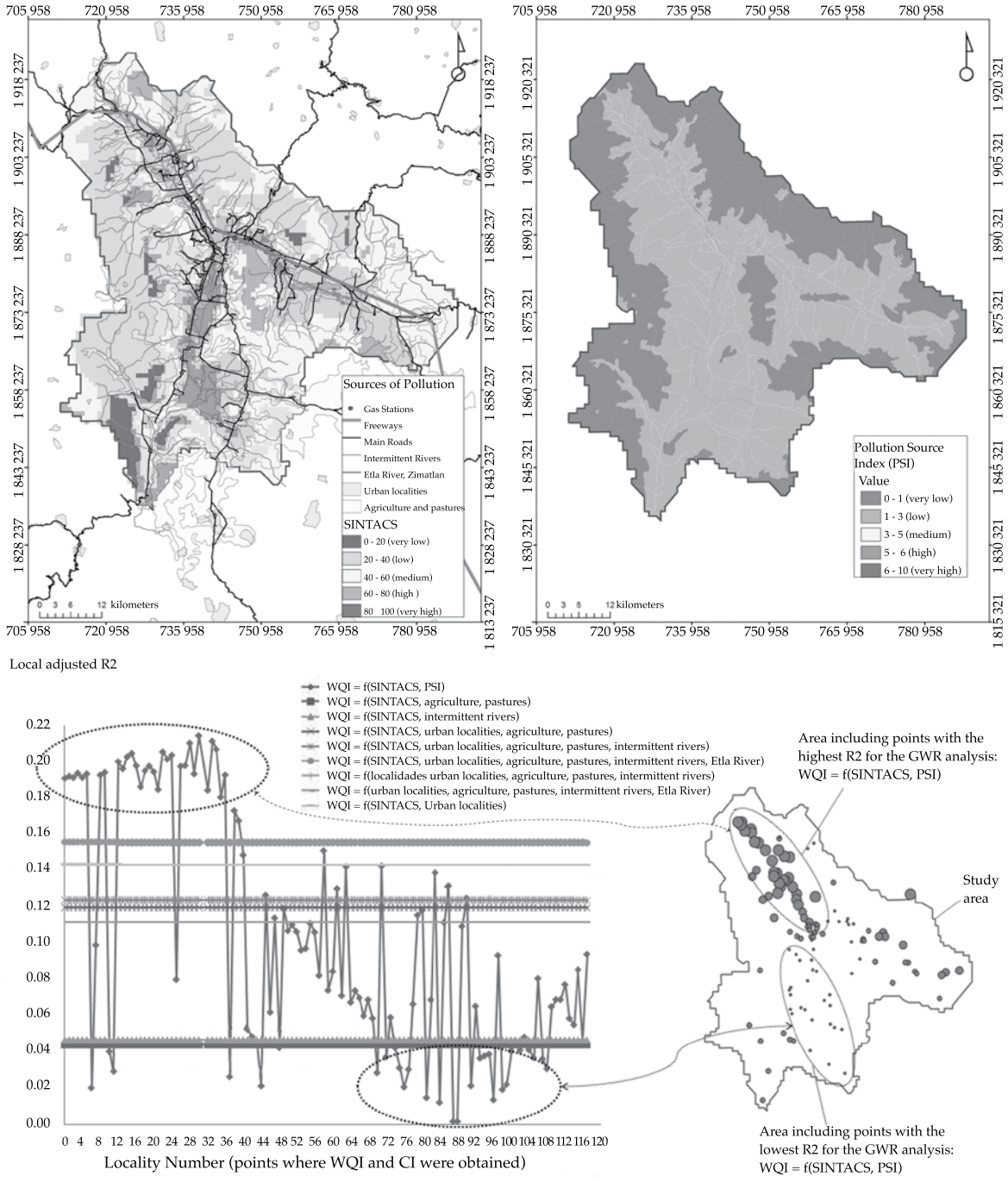

Figure 3. Layers used to generate the pollution source index (PSI) on a geographic representation of the SINTACS index (upper left). PSI spatialization (upper right). Results (adjusted local correlation coefficients) for the geographically weighted region (lower left) and their spatial distribution in the Central Valleys of Oaxaca, Mexico (lower right) (Ramos-Leal *et al.*, 2011).

Sealing and Impermeable Surfaces

In the field of remote sensing and GIS, studies can be performed related to sealing of permeable surfaces that are suitable to the aquifer recharge process (for example, Tapia-Silva and Mora 2004). With regard to the characterization of impermeable surfaces, methodologies can be created such as that conducted by CentroGeo (2007) for Mexico's Ministry of Social Development, which used SPOT-5 images to study precarious settlements. This methodology includes the application of the V-I-S model (vegetation-impermeable surface-bare soil; Ridd 1995). This is an empirical model which relates ground cover data obtained with remote sensing and biophysical aspects of the urban environments in a hierarchical decision-making scheme. Another study, by Freire-Cuesta (2011), established a consistent and reproducible methodology using a geomatic focus to calculate the percentage of sealing of types of surface cover in an urban catchment area using multispectral optical images with high spatial resolution. The author applied the results to hydrological runoff models (SIMWE, Mitasova *et al*., 2004) using as inputs the results from the calculation of surface sealing and elevation data generated with LiDAR technology. The work demonstrated the feasibility of an approach involving geomatic disciplines to determine flood risk zones according to the degree of impermeability in the areas located upstream in urban catchment areas (basins determined with a homogenous size suitable for land management and planning purposes). These investigations have addressed the need to define sealed surfaces for only some isolated regions in the country, with much left to be done to obtain key information required to create initiatives to control the negative process of sealing of permeable surfaces.

Monitoring Water Bodies and Relationship to Hydrological Variables

Another option in geomatics is to monitor changes in the size of lakes and relate those with trends in hydrological and climate variables, as well as other variables such as extraction and availability of water in surface bodies. For example, in the study of Chapala Lake performed by Lopez-Caloca *et al*. (2008) a temporal sequence was defined (images corresponding to 10 years during the period 1973 to 2007) which showed the changes in the Chapala Lake size monitored by LandSat and SPOT. In this study and that by Lira (2006), segmentation methods were applied based on the interpretation of water indices such as NDWI (Normalized Difference Water Index). Lira delimited lakes such as Patzcuaro, the Centla marshes and lakes in the Mexico City. Another option for monitoring water bodies is to use remote sensing procedures to determine the values of characteristics related to their productivity and health. Martínez-Clorio *et al*. (2011) reported on a series of investigations of diverse water bodies (Meztitlan lagoon in Hidalgo and Montebello lakes in Chiapas) to establish relationships between values measured in the field (such as chlorophyll-a and suspended solids) and remote sensing products with the idea of developing monitoring schemes that eliminate or reduce the need for field measurements. That was due to the large costs associated with this process. Figure 4 shows the results from this study, which indicate the feasibility of calculating chlorophyll-a and water transparency using the unmixed spectral method (Adams *et al*., 1986), which basically calculates the degree to which each pixel is composed of "pure" pixels (associated with one single type of material in the pixel, such as clear water, chlorophyll-a, etc.). Much needs to be done with respect to monitoring

water bodies using remote sensing methods and spatial analysis in order to positively address the challenge of extending the life of water bodies.

Zones Prone to Flooding

Another very current application of geomatic techniques is the definition of zones prone to flash flooding. Examples of this are studies conducted by Tapia- Silva *et al*. (2007b) in areas containing urban ravines in Mexico City. Maps of flood zones can be generated in real-time in order to plan immediate disaster response activities, as reported by Matgen *et al*. (2007). Another example of this are maps of floods in Tabasco published by UNOSAT (2007), which provided crucial information on November 7, 2007 to address the disaster that began one week earlier and ended in late November. In this case, MODIS and SRTM sensors were used (2003). The study by Freire-Cuesta (2011) mentioned previously showed the feasibility of including the definition of urban zones that are prone to flooding in a comprehensive methodological proposal. As previously indicated, this study included the use of satellite images with high spatial resolution, highly accurate elevation models obtained using LiDAR

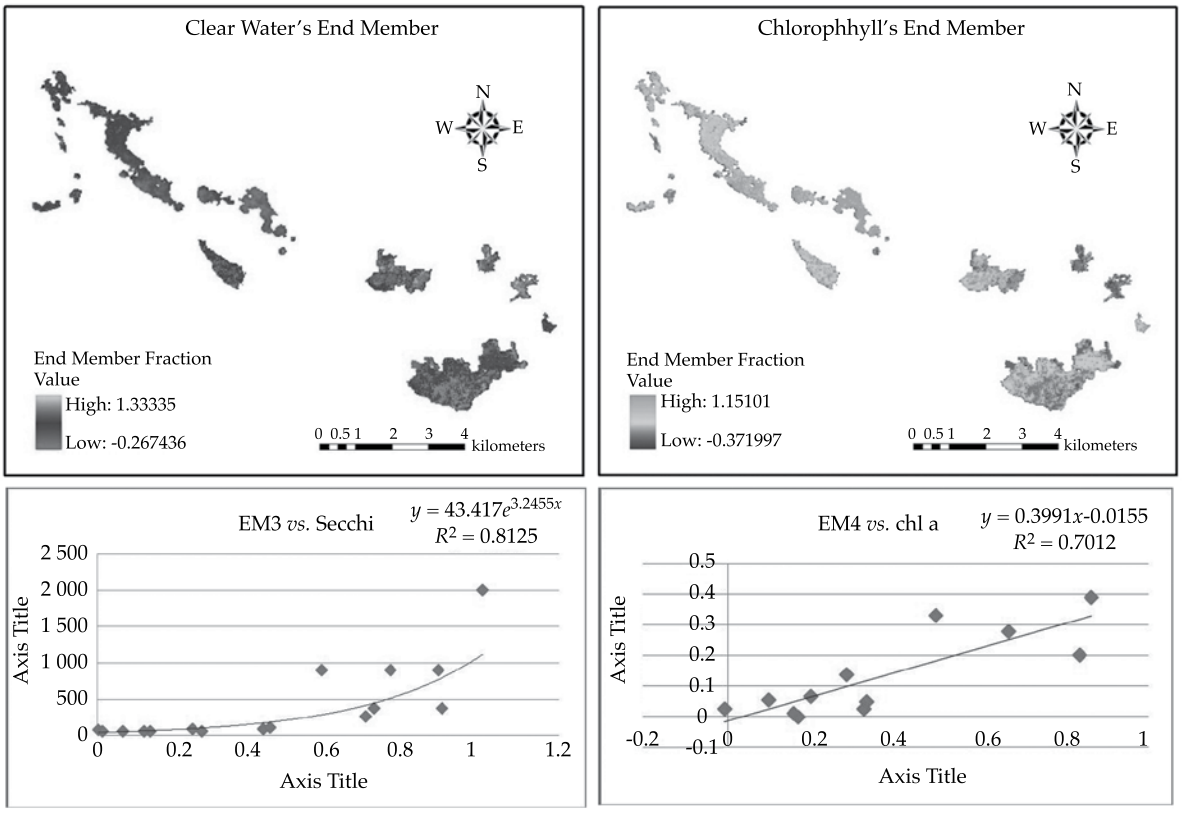

Figure 4. Fractions of pure components in images pertaining to the Motebello lakes (Chiapas) for clear water (upper left) and chlorophyll-a (upper right). Lower left: spread diagram between the Secchi depth (indicator of the transparency of a lake) and pure component 3 (EM3). Lower right: spread diagram between chlorophyll-a and pure component 4 (EM4). The lower areas of the figure show the correlation coefficients (R^2) as well as the equation obtained indicating the feasibility of calculating these parameters for each pixel using satellite images (in this case LandSat images were used) (Martínez-Clorio *et al*., 2011).

technology, the application of techniques to contextually classify satellite images and the use of a physical spatially distributed model (SIMWE, Mitasova *et al*., 2004). There is also much to do nationwide in terms of this topic in order to support the decision-making process to prevent and respond to floods.

Effects of Land Use in Relation to Hydric Variables and Environmental Services

It is also possible to determine the influence of deforestation on increased runoff, as illustrated by the study by Benítez *et al*. (2004). For the case of the Grijalva and Usumacinta basins (southeastern Mexico and Guatemala), Tapia-Silva *et al*. (2007a) processed LandSat images and performed hydrological modeling procedures to define deforestation rates between 1990 and 2000 and their relationship with increased runoff. A similar study was conducted by Preciado *et al*. (2004) for the Quelite basin on the Guatemala border.

In terms of land use planning to assure the sustainability of water resources, geomatics makes it possible to identify zones with greater aquifer recharge capacity, which should remain intact, or zones that should not be urbanized or occupied by housing because of serious hazards due to the accumulation of runoff. An example of this is the study by Tapia-Silva and Arauz (2007). In another interesting study, conducted by CentroGeo for the Mexico City Agency on the Environment and Land Planning (PAOT Spanish acronym, Procuraría Ambiental y de Ordenamiento Territorial del D.F.), a large series of determinations were made based on remote sensing and spatial analysis and the integration of geographic information in GIS to characterize high conservation value areas (HCVA). The intention is to use these areas as tools for land use planning since they were defined based on their high capacity to supply three key ecosystem services provided by conservation land in Mexico City ¾ infiltration, carbon capture and provision of habitat. This work uses the definition of the abovementioned catchment areas (CA) as basic geographic units of analysis and for the generalization of punctual estimates for reference ecosystem services. This considers the catchment area to be the fundamental area in which the hydrological cycle occurs and functions, a factor which directly influences the capacity to provide the ecosystem services mentioned. Another important aspect of this study is its ability to identify HVCA that were threatened by processes such as urbanization and deforestation. For example, in the cartographic products generated for this project, Figure 5 shows conservation areas with high infiltration values which are threatened by the expanding urban footprint.

Analysis of the Spatial-Temporal Variability of Hydric Variables

Gochis *et al*. (2007) present a series of analyses of the spatial-temporal characteristics of the intensity of precipitation in northeastern Mexico for the period 2002 to 2004. Golicher and Morales (2004) used universal *kriging* to define *El Niño*–related precipitation and temperature patterns on the southern border. In Tapia-Silva (2011a), results were presented of an interpolation procedure for multi-annual daily precipitation for September in Mexico City. *Kriging* with external drift was used the linear dependence between precipitation and elevation values was taken into account. Díaz-Padilla *et al*. (2011) tested different spatial interpolation methods (inverse distance squared (IDW), *kriging*, *cokriging*, and Thin Plate Smoothing Spline, TPSS) with national accumulated annual precipitation data, adjusted to a gamma probability distribution for May through October. The authors found a good fit to this

Figure 5. Example of cartographic products from the project conducted by CentroGeo for PAOT showing the HCVA (high conservation value areas) with high infiltration potential and threats from the existing urban footprint.

distribution for all the data processed and observed that the TPSS offered the lowest mean squared error. Brito-Castillo *et al*. (2011) integrated historical field measurements for precipitation and runoff and calculations of the temperature of the ocean surface from the AVHRR sensor (Advanced Very High Resolution Radiometer) in a statistical analysis scheme to verify an anomalous rain pattern for the month with maximum precipitation in northeastern Mexico. A study by Rosales and Tapia-Silva (2011) analyzed the feasibility of generating models to calculate the air temperature (Ta) using MODIS surface temperature products (LST) at different spatial aggregates. Considering the spatial configuration of the location of the stations in Mexico (number of stations and distance between them), the study determined that the spatial aggregation of the

stations at the national level was not the most adequate to represent the spatial variability of *Ta*. It is worth mentioning that *Ta* is a climate variable that is highly associated with hydric variables, evaporation and precipitation. This study observed that functional models can be generated by correlating the variables analyzed only for semi-arid regions with little cloudiness.

Final Remarks

The following are the water problem issues that have been most widely studied by geomatic disciplines: analysis of water use efficiency; spatial variability of aquifers in terms of vulnerability and usage capacity; effects of land use in relation to hydric variables and environmental services and; analysis of the spatial-temporal variability of hydric variables. This does not imply that these subjects have been sufficiently studied. The size of the Mexican territory, the spatial-temporal variability of the processes associated with the hydrological cycle and the use of resources reflect an enormous need for new studies that address the growing complexity of the hydrological problem. Nevertheless, these studies¾ produced by disciplines that are integrated in geomatics¾ exemplify the ability to provide information, knowledge and analytical methods to contribute to the process of improving water resources management. The review that has been presented makes it possible to verify which spatial analysis techniques and remote sensing methods used to obtain information and knowledge contribute to the study of hydrological and other related variables, for the purpose of identifying suitable solutions to the specific conditions in the geographic regions studied.

The water problem issues that have been least studied include: reduction and disappearance of water bodies due to negative water balances, incidence of torrential rainfall and impermeability, pollution of surface waters by contaminated wastes and increased flows in rivers produced by deforestation. Studies about these subjects with the support of geomatic disciplines should be encouraged. Generating information and knowledge about these subjects can represent a significant contribution by geomatics to the decision-making process. In addition, the study of these subjects by generating scenarios provides an excellent opportunity, which has been little explored, and could increase the potential of geomatics to contribute to solving the water problem. Furthermore, because of the complexity of this problem, addressing it may require the modeling of geomatic artifacts such as those found in Tapia-Silva (2011a, 2011b). As explained in this article, artifacts enable analyzing complex situations and developing solutions that take into account this complexity, thereby facilitating the decision-making process related to solving the water problem in our country.

Received: 15/06/2012
Accepted: 27/06/2013

References

ADAMS, J.B., SMITH, M.O., and JOHNSON, P.E. Spectral Mixture Modeling: A New Analysis of Rock and Soil Types at the Viking Lander 1 Site. *Journal of Geophysical Research*. Vol. 91, 1986, pp. 8098-8112.

ALLEN, M.R. and INGRAM, W.J. Constraints on Future Changes in Climate and the Hydrologic Cycle. *Nature*. Vol. 419, 2002, pp. 224-232.

ARREGUÍN-CORTÉS, F.I., LÓPEZ-PÉREZ, M. y MARENGO-MOGOLLÓN, H. *Los retos del agua en México en el siglo XXI*. Cap. 1. En Oswald-Spring, U. (coordinador). *Retos de la investigación del agua en México*. Cuernavaca, México: Centro Regional de Investigaciones Multidisciplinarias UNAM, 2011a, 754 pp.

BASTIAANSSEN, W.G.M., NOORDMAN, E.J.M., PELGRUM, H., DAVIDS, G., THORESON, B.P., and

ALLEN, G.R. SEBAL Model with Remotely Sensed Data to Improve Water-Resources Management under Actual Field Conditions. *Journal of Irrigation and Drainage Engineering*. Vol. 131, No. 1, 2005, pp. 85-93.

BASTIAANSSEN, W.G.M., MENENTI, M., FEDDES, R.A. and HOLTSLAG, A.A.M. A Remote Sensing Surface Energy Balance Algorithm for Land (SEBAL): 1. Formulation. *Journal of Hydrology*. Vol. 212-213, 1998, pp. 198-212.

BENÍTEZ, J.A., SANVICENTE, H., LAFRAGUA, J., ZAMORA, P., MORALES, L.M., MAS- CAUSSEL, J.F., GARCÍA, G., COUTURIER, S.A., ZETINA, R., CALAN-YAM, R.A., AMABILIS-SÁNCHEZ, L., ACUÑA, C.I. y MEJENES, M.C. Sistema de Información Geográfica de la cuenca del río Candelaria: reconstrucción histórica de los cambios en la cobertura forestal y su efecto sobre la hidrología y calidad del agua. En Kauffer, M.E.F. (editor). *El agua en la frontera México-Guatemala-Belice*. San Cristóbal de Las Casas, Chiapas: El Colegio de la Frontera Sur, 2004, 543 pp.

BRITO-CASTILLO, L., FILONOV, A., TERESCHENKO, I., PALACIOS-HERNÁNDEZ, E. y MONZÓN, C. Interrupción de la secuencia del mes de máxima precipitación y sus implicaciones en el entendimiento de las lluvias de verano. Cap. 11. En Oswald-Spring, U. (coordinador). *Retos de la investigación del agua en México*. Cuernavaca, México: Centro Regional de Investigaciones Multidisciplinarias, UNAM, 2011a, 754 pp.

CARRERA-HERNÁNDEZ, J.J. and GASKIN, S.J. The Basin of Mexico Hydrogeological Database (BMHDB): Implementation, Queries and Interaction with Open Source Software. *Environmental Modelling & Amp*. Software, Vol. 23, No. 10-11, 2008, pp. 1271-1279.

CENTROGEO. *Metodología para el mapeo y caracterización de asentamientos precarios* [en línea]. México D.F., 2007. Consultado el 11 de diciembre de 2008. Disponible para *World Wide Web*: http://xsei.centrogeo.org.mx/ap/campeche/MainCMP.htm.

CIVITA, M. y DE MAIO, M. SINTACS. *Un Sistema Parametrico per la Valutazione e la Cartografia della Vulnerabilita´ Degli Acquiferi All´inquinamento. Metodologia & Automatizzazione*. Bologna, Italia: Pitagora Ed., 1997, 191 pp.

CONAGUA. Estad*ísticas del Agua en México*. México D.F.: Comisión Nacional del Agua, 2007, 259 pp.

CORONEL, C., ROSALES, E., MORA, F., LOPEZ-CALOCA, A.A., TAPIA-SILVA, F.O., and HERNANDEZ, G. Monitoring Evapotranspiration at the Landscape Scale in Mexico: Applying the Energy Balance Model Using Remote Sensing Data. En *Proceedings of SPIE Europe Remote Sensing*. Volume 7104-Remote Sensing for Agriculture, Ecosystems, and Hydrology X. Wales, United Kingdom: University of Wales Institute, Cardiff Cardiff, 2008.

DÍAZ-PADILLA, G., SÁNCHEZ-COHEN, I. y GUAJARDO-PANES, R.A. Análisis de series de tiempo de clima para tomar decisiones en México. Cap. 3. En Oswald-Spring, U. (coordinador). *Retos de la investigación del agua en México*. Cuernavaca, México: Centro Regional de Investigaciones Multidisciplinarias, UNAM, 2011a, 754 pp.

DOUGLAS, B.C. Global sea rise: a redetermination. *Surveys in Geophysics*. Vol. 18, No. 2, 1997, pp. 279-292.

EASTERLING, D.R., MEEHL, G.A., PARMESAN, C., CHANGNON, S.A., KARL, T.R. and MEARNS, L.O. Climate Extremes: Observations, Modeling, and Impacts. *Science*. Vol. 289, 2000, pp. 2068-2074.

FREIRE-CUESTA, T. *Estimación del sellamiento de suelo en áreas de captación urbana y sus efectos en la escorrentía*. Tesis de Maestría en Geomática. México, D.F.: Centro de Investigación en Geografía y Geomática "Ing. Jorge L. Tamayo" A.C., 2011.

GALVÁN-FERNÁNDEZ, A. Determinación de los espacios de Intervención en una cuenca costera. En Oswald-Spring, U. (coordinador). *Retos de la investigación del agua en México*. Cuernavaca, México: Centro Regional de Investigaciones Multidisciplinarias, UNAM, 2011a, 754 pp.

GARATUZA-PAYAN, J., PINKER, R.T., SHUTTLEWORTH, W.J., and WATTS, C.J. Solar Radiation and Evapotranspiration in Northern Mexico Estimated from Remotely Sensed, Measurements of Cloudiness. *Hydrological Sciences*. Vol. 46, No. 3, 2001, pp. 465-468.

GARATUZA-PAYAN, J. and WATTS, C.J. The Use of Remote Sensing for Estimating ET of Irrigated Wheat and Cotton in Northwest Mexico. *Irrigation and Drainage Systems*. Vol. 19, 2005, pp. 301–320.

GOCHIS, D.J., WATTS, C.J., GARATUZA-PAYAN, J., and RODRIGUEZ, J.C. Spatial and Temporal Patterns of Precipitation Intensity as Observed by the NAME Event Rain Gauge Network from 2002 to 2004. *Journal of Climate*. Vol. 20, No. 9, 2007, pp. 1734-1750.

GOLICHER, J.D. and MORALES, J. Correlations between Precipitation Patterns in the State of Chiapas and the El Niño Sea Surface Temperature Index. En Kauffer, M.E.F. (editor). *El agua en la frontera México-Guatemala-Belice*. San Cristóbal de Las Casas, Chiapas: El Colegio de la Frontera Sur, 2004, 543 pp.

GOMARAZCA, M.A. Basis of Geomatics. *Applied Geomatics*. Vol. 2, 2010, pp. 137-146.

GUTIÉRREZ-CASTORENA, E.V., ORTIZ-SOLORIO, C.A., GUTIÉRREZ-CASTORENA, M.C., CAJUSTE-BONTEMPS, L., and ROCHA-AGUILAR, M. Technical, Economical and Social Actions of Farmers to Mitigate Water Deficit in Tamaulipas, Mexico. *Agriculture, Ecosystems & Amp., Environment*. Vol. 128, No. 1-2, 2008, pp. 77-85.

LEVI, S. Geografía Humana y Geomática. *Bolletim Goiano de Geografia*. Vol. 26, No. 1, 2006, pp. 11-29.

LIRA, J. *A Model of Desertification Process in a Semi-Arid Environment using Employing Multi-Espectral Images*. En Sanfeliu, A., Martínez-Trinidad, J. F. y Carrasco-Ochoa, J. A. *Progress in Pattern Recognition, Image Analysis and Applications*. 9th Iberoamerican Congress on Pattern Recognition, Puebla Mexico: CIARP, Springer, 2004, 703 pp.

LIRA, J. Segmentation and morphology of open water bodies from multispectral. *International Journal of Remote Sensing*. Vol. 27, No. 18, 2006, pp. 4015-4038.

LOPEZ-CALOCA, A.A., TAPIA-SILVA, F.O., and ESCALANTE, B. Lake Chapala Change Detection Using Time Series. *Proceedings of SPIE Europe Remote Sensing*. Vol. 7104. Remote Sensing for Agriculture, Ecosystems, and Hydrology X. Wales, United Kingdom: University of Wales Institute, Cardiff Cardiff, 2008.

MARÍN, L.E., TORRES, V., BOLONGARO, A., REYNA, J.A., POHLE, O., HERNÁNDEZ-ESPRIÚ, A., CHAVARRÍA, J., GARCÍA-BARRIOS, R., and PARRA-TABLA, H.F. Identifying Suitable Sanitary Landfill Locations in the State Of Morelos, México, Using a Geographic Information System. *Physics and Chemistry of the Earth*. Parts A/B/C. Vol. 37-39, 2012, pp. 2-9.

MARTÍNEZ-CLORIO, M.I., TAPIA-SILVA, F.O., and GARCÍA-CALDERÓN, J.L. *Use of Remote Sensig for the Limnological Characterization of Mexican Lakes and Reservoirs*. Poster 14th World Lake Conference: Lakes, Rivers, Groundwater, and Coastal Areas: Understanding Linkages October, 31-November 4, 2011, Austin, Texas.

MARTÍNEZ, E. and REYES, C. Cybercartography and Society. In Taylor, F. (editor). *Cybercartography: Theory and Practice*. Amsterdam: Elsevier Scientific, 2005, 594 pp.

MATGEN, P., SCHUMANN, G.H., HOFFMANN, J.B., and PFISTER, L. Integration of SAR-Derived River Inundation Areas, High-Precision Topographic Data and a River Flow Model toward Near Real-Time Flood Management. *International Journal of Applied Earth Observation and Geoinformation*. Vol. 9, No. 3, 2007, pp. 247-263.

MENDOZA, M.E., BOCCO, G., LÓPEZ-GRANADOS, E., and BRAVO-ESPINOZA, M. Hydrological Implications of Land Use and Land Cover Change: Spatial Analytical Approach at Regional Scale in the Closed Basin of the Cuitzeo Lake. Michoacán, Mexico. *Singapore Journal of Tropical Geography*. Vol. 31, No. 2, 2010, pp. 197-214.

MITASOVA, H., THAXTON, C., HOFIERKA, J., MCLAUGHLIN, R., MOORE, A., and MITAS, L. Path Sampling Method for Modeling Overland Water Flow, Sediment Transport and Short Term Terrain Evolution in Open Source GIS. *Proceedings XVth International Conference on Computational Methods in Water Resources, USA*. Elsevier, 2004, pp. 1479-1490.

MO, X., LIU, S., LIN, Z., XU, Y., XIANG, Y., and MCVICAR, T.R. Prediction of crop yield, water consumption and water use efficiency with a SVAT-crop growth model using remotely sensed data on the North China Plain. *Ecological Modelling*. Vol. 183, 2005. pp. 301-322.

OJEDA-BUSTAMANTE, W., GONZÁLEZ-CAMACHO, J.M., SIFUENTES-IBARRA, E., ISIDRO, E., and RENDÓN-PIMENTEL, L. Using Spatial Information Systems to Improve Water Management in Mexico. *Agricultural Water Management*. Vol. 89, No. 1-2, 2007, pp. 81-88.

OSWALD-SPRING, U. y SÁNCHEZ-COHEN, I. Introducción. En Oswald-Spring, U. (coordinador). *Retos de la investigación del agua en México*. Cuernavaca, México: Centro Regional de Investigaciones Multidisciplinarias, UNAM, 2011a, 754 pp.

PAGIATAKIS, S.D. *Encyclopedia of Environmetrics Wiley Online Library*. Publicado en línea el 15 de enero de 2013, doi: 10.1002/9780470057339.vnn121.

PRECIADO, M.E., RAMÍREZ, A.I. y OCÓN, A.R. Metodología para el uso de los sistemas de información geográfica para la estimación de la pérdida de bosque y el cálculo de los números de escurrimiento. Caso de aplicación: la cuenca del río El Quelite. En Kauffer, M.E.F. (editor). *El agua en la frontera México-Guatemala-Belice*. San Cristóbal de Las Casas, Chiapas: El Colegio de la Frontera Sur, 2004, 543 pp.

RAMOS-LEAL, J.A., TAPIA-SILVA, F.O., and ISMAEL-SANDOVAL, I. Analysis of Aquifer Vulnerability and Water Quality using SINTACS and Geographic Weighted Regression. *Environmental Earth Sciences*. Vol. 66, No. 8, 2011, pp. 2257-2271.

RAMOS-LEAL, J.A., NOYOLA, C., and TAPIA-SILVA, F.O. Aquifer Vulnerability and Groundwater Quality in Mega Cities: Case Mexico Basin. *Environmental Earth Sciences*. Vol. 61, 2010, pp. 1309-1320.

RAMOS-LEAL, J., NOYOLA-MEDRANO, C., TAPIA-SILVA, F., SILVA-GARCÍA, J., and REYES-GUTIÉRREZ, L. Assessing the Inconsistency between Groundwater Vulnerability and Groundwater Quality: The Case of Chapala Marsh, Mexico. *Hydrogeology Journal*. Vol. 20, 2012, pp. 591-603.

RAMOS-LEAL, J.A. y HERNÁNDEZ-MORENO, J.I. Las cuencas hidrogeológicas desde el punto de vista regional. *Aquaforum*. Vol. 48, 2008, pp. 14-18.

RANGEL-MEDINA, M., MONREAL-SAAVEDRA, R. y WATTS, C.J. Los acuíferos costeros de Sonora, México. Un reto de análisis hidrogeológico para mantener su equilibrio sustentable. Cap. 14. En Oswald-Spring, U. (coordinador). *Retos de la investigación del agua en México*. Cuernavaca, México: Centro Regional de Investigaciones Multidisciplinarias, UNAM, 2011a, 754 pp.

REYES, C. y MONROY, G.S. Sistemas y geomática. *Memoria 3er. Seminario Internacional de Ingeniería de Sistemas,*

Ixtapa-Zihuatanejo, Guerrero, México, noviembre de 2000. Facultad de Ingeniería, Universidad Nacional Autónoma de México (FI-UNAM) y Academia Mexicana de Ingeniería A.C. (AMIAC), pp. 2-107 a 2-112.

RIDD, M.K. Exploring a V-I-S (Vegetation-Impervious Surface-Soil) Model for Urban Ecosystem Analysis through Remote Sensing: Comparative Anatomy for Cities. *International Journal of Remote Sensing*. Vol. 16, No. 12, 1995, pp. 2165-2185.

RODRÍGUEZ-CASTILLO, R. y RODRÍGUEZ-VELÁZQUEZ, I. Subsidencia y contaminación acuífera: ni desastre ni conflicto. En Oswald-Spring, U. (coordinador). *Retos de la investigación del agua en México*. Cuernavaca, México: Centro Regional de Investigaciones Multidisciplinarias, UNAM, 2011a, 754 pp.

ROGERSON, P.A. and FOTHERINGAM, S. GIS and Spatial Analysis: Introduction and Overview. In Fotheringam, S. and Rogerson, P.A. (editors). *Spatial Analysis and GIS*. London: Taylor & Francis, 1994.

ROSALES, E. y TAPIA-SILVA, F.O. Efectos de la agregación espacial en la estimación de temperatura del aire mediante imágenes *MODIS*. En Maas, J.F. (editor). *Aplicaciones del Sensor MODIS para el monitoreo del territorio*. Morelia, México: SEMARNAT, INE, UNAM, CIGA-UNAM, 2011, 318 pp.

SARAF, A.K., CHOUDHURY, P.R., ROY, B., SARMA, B., VIJAY, S., and CHOUDHURY, S. GIS Based Surface Hydrological Modelling in Identification of Groundwater Recharge Zones. *International Journal of Remote Sensing*. Vol. 25, No. 24, 2004, pp. 5759-5770.

SCOTT, A.C., BASTIAANSSEN, W.G.M., and AHMAD, M.U.D. Mapping Root Zone Soil Moisture Using Remotely Sensed Optical Imagery. *Journal of Irrigation and Drainage Engineering*. ASCE, September/October, 2003, pp. 326-335.

SENAY, G.B., BUDDE, M., VERDIN, J.P., and MELESSE, A.M. A Coupled Remote Sensing and Simplified Surface Energy Balance Approach to Estimate Actual Evapotranspiration from Irrigated Fields. *Sensors*. Vol. 7, 2007, pp. 979-1000.

SRTM (Shuttle Radar Topography Mission). *The Shuttle Radar Topography Mission SRTM-30, Global 1 km Digital Elevation Model 2003* [en línea]. Consultado el 19 de diciembre de 2008. Disponible para *World Wide Web*: ftp://e0srp01u.ecs.nasa.gov/srtm/version1/SRTM30/SRTM30_Documentation.

STAR, J. and ESTES, J. *Geographic Information Systems, An introduction*. Englewoods Cliffs: Prentice Hall, 1990, pp. 665.

TAPIA-SILVA, F.O. Advances in Geomatics and Geospatial Technologies to Solve Water Problems in Mexico. In Oswald-Spring, U. (editor). *Water Resources in Mexico. Scarcity, Degradation, Stress, Conflicts, Management, and Policy*. Heidelberg: Springer-Verlag, 2011b, 524 pp.

TAPIA-SILVA, F.O. *A*vances en Geomática y tecnología geoespacial para la resolución de la problemática del agua en México. En Oswald-Spring, U. (coordinador). *Retos de la investigación del agua en México.* Cuernavaca, México: Centro Regional de Investigaciones Multidisciplinarias, UNAM, 2011a, 754 pp.

TAPIA-SILVA, F.O. Geomática y sociedad, ciencia emergente para generar conocimiento hacia la resolución de la problemática socioambiental. *Geopuce. Revista de la Escuela de Ciencias Geográficas Puce, Quito, Ecuador*. Vol. 2, 2011c, pp. 7-16.

TAPIA-SILVA, F.O. and ARAUZ, G. Geomatics Procedure to Allocate Infiltration Areas and to Relate them with Green Areas in the Mexico Basin. *Proceedings 32nd International Symposium on Remote Sensing of Environment*, 2007, San José, Costa Rica.

TAPIA-SILVA, F.O. y MORA, F. The Application of Spatial Analysis in the Implementation of a Qualitative Infiltration Model to Evaluate the Aquifer's Potential Recharge for Conservation Areas of Mexico City. *Proceedings of the 19th International CODATA Conference, The Information Society: New Horizons for Science*, Berlin, Germany, 2004.

TAPIA-SILVA, F.O., MORA, F., and NUÑEZ, J.M. Characterization of Tropical River Basins in Mexico and Central America by Remote Sensing and Hydrological Spatial Analysis. *Proceedings 32nd International Symposium on Remote Sensing of Environment*, San José, Costa Rica, 2007a.

TAPIA-SILVA, F.O., NUÑEZ, J.M., and LÓPEZ-LÓPEZ, D. Using SRTM DEM, LANDSAT ETM+ Images and a Distributed Rainfall-Runoff Model to Define Inundation Hazard Maps on Urban Canyons. *Proceedings 32nd International Symposium on Remote Sensing of Environment*, San José, Costa Rica, 2007b.

UNOSAT. *Mexico Maps*. 2007 [en línea]. Citado el 21 de enero de 2009. Disponible para *World Wide Web*: http://unosat.web.cern.ch/unosat/asp/prod_free.asp?id=70.

VON BERTALANFFY, L.V. *Perspectivas en la teoría general de sistemas*. Madrid: Alianza Universidad, 1979, 203 pp.

ZWART, S.J., BASTIAANSSEN, W.G.M., GARATUZA-PAYAN, J., and WATTS, C.J. SEBAL for Detecting Spatial Variation of Water Productivity for Wheat in the Yaqui Valley, Mexico. *AIP Conference Proceedings*. Vol. 852. Guadalajara, Jalisco, 2006, pp. 154-161.

Author's address institutional

Dr. Felipe Omar Tapia Silva

Universidad Autónoma Metropolitana
Departamento de Hidrobiología
División de Ciencias Biológicas y de la Salud
Avenida San Rafael Atlixco 186
Vicentina, Iztapalapa
09340 México, D.F., México
Teléfono: +52 (55) 5804 4600, extensión 3056
feomtasi@yahoo.com.mx

Click here to write the autor

Formulas for Drag Coefficient and the Navier-Stokes Fractional Equation

• José Roberto Mercado* • Pedro Guido • Jorge Sánchez-Sesma •
• Mauro Íñiguez •
Instituto Mexicano de Tecnología del Agua
*Corresponding Author

Abstract

MERCADO, J.R., GUIDO, P., SÁNCHEZ-SESMA, J. & ÍÑIGUEZ, M. Formulas for Drag Coefficient and the Navier-Stokes Fractional Equation. *Water Technology and Sciences* (in Spanish). Vol. V, No. 2, March-April, 2014, pp. 149-160.

The aim of this paper is to find the relationship between the Navier-Stokes fractional equation and formulas for the drag coefficient, such as the Kármán-Schoenherr, Prandtl-Kármán, and Nikuradse. Scale changes produce a renormalization of boundary layer equations, which contains the key hypothesis about the thinness of this layer and leads to a multifractal description. A generalization is obtained from the Blasius experimental result for friction. By adjusting the relation of the number of features of the multifractal, the formulas that are the objective of this study can be inferred and represented as a bi-multifractal. This allows for an analysis with the critical Reynolds number and indicates that the Kármán-Schoenherr is the most suitable formula for the right boundary of the viscous sub-layer. The adjustments resulted in refining the relation between Euler and Reynolds numbers, or obtaining the decays related to the drag coefficient. The results are applied to the description of the turbulent boundary layer and the interactions between flows and bottoms (for rivers, deserts and hurricanes).

Keywords: Navier-Stokes fractional equation, drag coefficient, multifractal, boundary layer.

Resumen

MERCADO, J.R., GUIDO, P., SÁNCHEZ-SESMA, J. & ÍÑIGUEZ, M. Fórmulas para el coeficiente de arrastre y la ecuación Navier-Stokes fraccional. Tecnología y Ciencias del Agua. *Vol. V, núm. 2, marzo-abril de 2014, pp. 149-160.*

Se quiere encontrar la relación entre la ecuación de Navier-Stokes fraccional y las fórmulas para el coeficiente de arrastre, como las de Kármán-Schoenherr, Prandtl-Kármán, y Nikuradse. Los cambios de escala producen una renormalización para las ecuaciones de la capa límite, que contiene la hipótesis esencial de la delgadez de dicha capa, y da lugar a una descripción multifractal. Se obtiene una generalización del resultado experimental de Blasius para el factor de fricción. Si se reajustan las relaciones del número de rasgos del multifractal, se infieren las fórmulas, objeto de este estudio, y se las representa como un bi-multifractal, lo que permite un camino analítico para el número de Reynolds crítico y señala a la de Kármán-Schoenherr como la fórmula apropiada para el límite a la derecha de la subcapa viscosa. Los reajustes se traducen en matizar las aproximaciones de la relación entre los números de Euler y Reynolds, o bien en los decaimientos relativos del coeficiente de arrastre. Se aplican los resultados a la descripción de la capa límite turbulenta y a las interacciones entre corrientes y fondos (en ríos, desiertos y huracanes).

Palabras clave: *ecuación Navier-Stokes, coeficiente de arrastre, multifractal, capa límite.*

Introduction

The main purpose of the present article is to find the relationship between the fractional Navier Stokes equation and the Karman-Schoenherr, Prandlt-Karman and the Nikurdse drag coefficient formulas and the friction factor.

In the references, Mercado *et al*. (2013 y 2012) present the fractional Navier-Stokes equation. The basic proposal is that viscous forces produce a dispersive flow of *momentum*, described using a fractional Darcy law, and the divergence of the dispersive flow coincides with the temporal change in momentum in accordance with Newton's law.

As in the classical case, the significant simplification of the fractional Navier-Stokes equation, which leads to the boundary layer equations, is due to its relative thinness. This

in turn implies that the predominant velocity is in the longitudinal direction, with a vertical velocity greater than the longitudinal, resulting in the velocity meeting the non-shifting condition at the channel bottom; and conversely, with light pressure gradients in the vertical transverse direction compared to stronger ones in the longitudinal direction (Landau and Lifshitz, 1987).

Changes in scale are obtained by identifying the horizontal and macroscopic characteristic length and velocity and finding the vertical complements that maintain their shape with the conservation of mass and *momentum*.

The velocity potential is introduced, from which we get the velocity component downstream and the vertical transverse component. Then, the *momentum* equation is expressed in terms of the velocity potential downstream.

The frictional force is found by calculating the fractional derivative of the potential function, finding the force to be of the form of a power of the inverse of the indexed Reynolds number and dependent on the spatial occupation index. This decreases with the horizontal distance to a power that is also dependent on the degree of spatial occupation. The proportionality constant contains the power of the viscosity and the value of the curvature of the sub-potential function at the origin. It can also be seen that when the spatial occupation index approaches 1, the frictional force of the flow boundary layer is expressed by the classical expression.

The Falkner-Skan approximation establishes the equilibrium based on a dynamic triangle composed of the viscous and inertial forces and the force of the longitudinal pressure gradient through the free or external velocity dependent on a power of the longitudinal coordinate. Whereas in the Blasius approximation, there is no pressure gradient due to the annulment of the power of the external velocity.

The friction force is obtained with the two approximations mentioned by integrating and expressing as a dimensionless term, introducing the drag coefficient. This coefficient also is represented as a power of the indexed Reynolds number, determined by coupling with the spatial occupation index and the power of the external velocity. The power is a product of two factors. The first is an increasing function such that the higher the spatial occupation index the greater the indexed Reynolds number exponent, which is obtained with viscous motion. Whereas the higher the turbulence the lower the indexed Reynolds number. The second factor increases with a negative exponent, indicating an adverse longitudinal gradient, and increases for an exponent greater than 1 reflecting a favorable pressure gradient.

In addition, the friction force can be described as a fractional derivative of a multifractal, where the order of the derivative depends on the spatial occupation index, and the spectrum of dimensions of the multifractal depends on both the power of the external velocity and the spatial occupation index.

The Chezy coefficient can also be an alternative magnitude and the dimensionless velocity the ratio of mean velocity to shear velocity.

The classical Navier-Stokes equation has a parameter that reflects the fractal character of the motion of the fluid. Its fractional version expresses it on the order of the derivative that provides the viscous friction force. To see what this order corresponds to, the friction force on a large flat bottom can be studied using boundary layer equations. The result is an experimental Blasius equation which is interpreted as a multifractal. If this multifractal interpretation is maintained for the other formulas, such as the Prandtl-

Karman, the fractal dimensions do not exceed the value 1, and decrease as the motion becomes more turbulent.

Therefore, the statement is as follows: The fractional Navier-Stokes equation applied to a boundary layer with a scale that reflects the thinness of this layer, and interpreted as a multifractal, produces the Blasius, Karman-Schoenherr, Prandtl-Karman and Nikuradse formulas, in forms that establish differing degrees of dependency relationships between the Euler and Reynolds numbers. Each of these can be described with a dimension similar to the Blasius, which becomes smaller as the Reynolds number increases.

In the section "Fractional Navier-Stokes Equation," the fractional Navier-Stokes equation is described, as already considered in Mercado *et al*. (2012). The simplification presented by the boundary layer are included. Force, friction force and drag coefficient are found. A generalization of the experimental result from Blasius is obtained. Its multifractal structure is analyzed. Then the Karman-Schoenherr, Prandtl-Karman and Nikuradse formulas are considered. An expression is found for the critical Reynolds number. Lastly, these are applied to interactions between fluids and surfaces such as between rivers and riverbeds, winds and sand and winds and oceans, as with hurricanes.

Methods

Fractional Navier-Stokes Equation

The motion of a fluid is described from the Eulerian perspective, considering a volume of fluid restricted by a boundary surface, with its momentum per unit of volume given by $\rho\mathbf{v}$. Because of its importance, first the interaction with internal friction is considered. The fractional gradient is expressed by $\nabla_M^\beta \rho\mathbf{v}$, where ρ is the mass density, $\mathbf{v}$ is the velocity, β is the spatial occupation index and M is the measurement of the combination of the different spatial directions. The diffusivity of momentum is kinematic α-viscosity, $\mathbf{v}_\alpha$, and the Darcy flow of the momentum is $\mathbf{q}_D$. The change ratio of momentum per unit of time is the negative divergence, or convergence of the Darcy flow. Or, M is chosen such that the flow is proportional to the negative of the fractional Laplacian (Mercado *et al*., 2013), which is shown in (1), with $\alpha = 1 + \beta$:

$$\mathbf{q}_D = -\nu_\alpha \nabla_M^\beta \rho\mathbf{v}, \quad \frac{d}{dt}\rho\mathbf{v} = -\nabla\cdot\left(-\nu_\alpha \nabla_M^\beta \rho\mathbf{v}\right)$$
$$= -\nu_\alpha \left(-\Delta\right)^{\alpha/2} \rho\mathbf{v} \qquad (1)$$

Next, the contribution of the variations in pressure with the change in the *momentum* of the fluid through the force of the pressure gradient is considered, such that the sum of the viscous friction force and the hydrostatic pressure make up the tensor $\mathbf{T} = \nu_\alpha \nabla_M^\beta \rho\mathbf{v} - p\boldsymbol{I}$ and lead to the deformation law. Next, a potential external force is incorporated, per unit volume, of the type $-\nabla\rho\phi$. Then, the hypothesis for the incompressibility of the fluid is introduced. The material derivative that composes the local variation with the advective is made explicit. The demand for objectivity requires invariance given changes in coordinates, and therefore the advective contribution must be modified and the vorticity term appears. Lastly, the contribution of vorticity to inertial force is written to the right of the equation as $\mathbf{v} \times rot\mathbf{v}$, and can be thought of as originating from an external force that dynamizes the evolution of the velocities field through the vorticity, contrary to the viscous force. The other term is interpreted as a restriction that contains the D. Bernoulli equation along the flow lines. The coefficient ν_α can be compared with the Boussinesq turbulent viscosity:

$$\frac{\partial}{\partial t}\mathbf{v} = -\nu_\alpha\left(-\Delta\right)^{\alpha/2}\mathbf{v} + \mathbf{v}\times rot\mathbf{v} - \nabla\left(\frac{1}{2}\left(\mathbf{v}\cdot\mathbf{v}\right) + \frac{p}{\rho} + \varphi\right) \quad (2)$$

As was mentioned, the boundary layer equations are obtained from the fractional Navier-Stokes equation because of the simplifications introduced based on the premise of the relative thinness. Now the two-dimensional boundary layer equation is considered in its steady or permanent form, along with the conservation of mass with zero divergence, as shown in equation (3):

$$u\partial_x u + v\partial_y u = \nu_\alpha \partial_y^\alpha u - \partial_x\left(p/\rho\right), \quad \partial_x u + \partial_y v = 0 \quad (3)$$

where the pressure gradient is given by $-\partial_x\left(p/\rho\right) = U\frac{d}{dx}U, \quad U = u\left(x,y\right)\big|_{y\to\infty}$.

The potential form is given to the principal velocity downstream, represented by the velocity potential $\psi(u,v)$ as $u = \partial_y\psi, v = -\partial_x\psi$. In the Blasius approximation, an equilibrium is established between two forces —viscous and inertial— by assuming the pressure gradient contribution to be zero. In the Falkner-Skan approximation, the longitudinal gradient of the pressure is present as the third contribution to equilibrium, so that the free or external velocity depends on the longitudinal coordinate. The sub-potential then appears, $g(\xi)$, as the solution of the differential equation of the fractional Blasius or Falkner-Skan equation (Landau y Lifshitz, 1987; White, 2006).

Force is calculated by $\tau_{xy} = \mu_\alpha \partial_y^\beta \partial_y \psi\left(u,v\right)$, where $\mu_\alpha = \rho\nu_\alpha$. With the fractional Blasius coefficient $B_\beta = \frac{\alpha}{\beta}\frac{\nu_\alpha}{\nu_2}C_{g,\beta}$ where $C_{g,\beta} = \partial_y^{-(1-\beta)}\left(g''\left(\xi\right)\right)\big|_{\xi=0}$, and the indexed Reynolds number $R_{l\beta} = ul^\beta/\nu_\alpha$, the force can be written as in (4):

$$\tau_{xy} = \left(\beta/\alpha\right)B_\beta\frac{\nu_2}{\left(\nu_\alpha\right)^{1/\alpha}}\left(\rho U^{2-\frac{\beta}{\alpha}}\right)x^{-\frac{1}{\alpha}} \quad (4)$$

The friction force is calculated per binormal, or transverse-horizontal unit length, as $F_f = 2\int_0^l \tau_{xy}\,dx$ and with the force represented as in (4), it can be written as $F_f = 2\left(\frac{\beta}{\alpha}\frac{\nu_2}{\left(\nu_\alpha\right)^{1/\alpha}}\right)B_\beta\int_0^l\left(\rho U^{2-\frac{\beta}{\alpha}}\right)x^{-\frac{1}{\alpha}}dx$ (Mercado, 2010). The Falkner-Skan approximation considers $U = Kx^m$, with $m \neq 0$. The coefficient is denoted by $C_{g,\beta,m} = 4\frac{\alpha}{\left(1+\alpha\right)m+\beta}\left(\nu_\alpha^\beta K^{1/m}\right)^{1/\alpha}C_{g,\beta}$.

After integrating we get:

$$F_f = \frac{1}{2}\rho C_{g,\beta,m}\left(U\big|_l\right)^{2-\frac{\beta}{\alpha}\left(1+1/m\beta\right)} \quad (5)$$

The friction force is made dimensionless per unit area of the tangential surface, resulting in the appearance of the drag coefficient (6):

$$C_f = C_{g,\beta,m}\left(\left(U\big|_l\right)^{-1}\right)^{\frac{\beta}{\alpha}\left(1+1/m\beta\right)} \quad (6)$$

The exponent of the drag coefficient is called the Blasius exponent (7):

$$\theta\left(\beta,m\right) = \frac{\beta}{1+\beta}\left(1+1/m\beta\right) \quad (7)$$

In addition, for the Blasius approximation $m = 0$; integrating, the Blasius exponent is obtained:

$$\theta\left(\beta,m=0\right) = \frac{\beta}{1+\beta} \quad (8)$$

The two can be joined in one single expression (9):

$$\theta\left(\beta,m\right) = \begin{cases} \frac{\beta}{1+\beta}\left(1+1/m\beta\right), & m\neq 0, \\ \frac{\beta}{1+\beta}, & m = 0, \end{cases} \quad (9)$$

The Blasius exponent in terms of the dimension must be $\theta \geq 0$, therefore $m > 0$, which implies a favorable pressure gradient,

or $m \leq -1/\beta$, which reflects and adverse pressure gradient.

In particular, the state given by $\beta \to 0$ is equal to the state $m = -1/\beta$ and can be called turbulent.

The representation $\theta = \beta(\sigma + 1/(1 + \beta))$ is also observed to be possible, because for $\sigma > 0$ there is $m > 0$, given by $m = \frac{1}{\sigma\beta(1+\beta)}$, making this representation possible, and can be considered a generalization of the Blasius experimental result. For $m = 0$ we have $\beta/(1 + \beta)$, which contains, among others, the Blasius experimental result for $\beta = 1/3$, as well as the result of the laminar flow $\theta = 1/2$ for $\beta = 1$ (Mercado *et al.*, 2013). The value $\sigma > 0$ can be seen to become quite large as $m > 0$ approaches zero.

In the Falkner-Skan approximation, in order to define the similarity variable, the disjunctive is presented, $m = 1$ or $\beta = 1$, since those are the two options under which the coefficients of the equation, for the sub-potential function, are independent of x.

In the first option, $m = 1$, we have $\theta(\beta,1) = 1$, therefore the variation in pressure with velocity is linear as in the Hagen-Poiseuille model for laminar flow.

For the second option, the Blasius exponent is $\theta(1,m) = \frac{1}{2}\frac{m+1}{m}$, and the value m is arbitrary, while the value $m = 0$ is of course excluded. And it is required that $m > 0$ or $m \leq -1/\beta$, which in this case would be reduced to $m \leq -1$. The first is part of the inviscid flows against an elevation or wedge with angle $\frac{m}{m+1}\pi \geq 0$. The second of the inviscid flows is clockwise through a depression with angle $\frac{m}{m+1}\pi \leq 0$ (White, 2006). In addition, this exponent contains the Blasius experimental result with $m = -2$. In this case, the turbulent law describes the variation in pressure with velocity, similar to the Chezy formula, which is assumed when it takes the exact value $m = -1$.

The friction factor can be represented by the expression shown in (10) and described as a transformation using fractional derivatives of the order $\gamma = \beta^2/(1 + \beta)$ for a multifractal with dimensions $\sigma\beta = \frac{1}{m(1+\beta)}$ in another analogue with dimensions θ:

$$f_\beta = 8\tilde{C}(\beta)D_x^\gamma\left(1/R_{x\beta}\right)^\sigma,$$

$$\theta = \beta\left(1/m\beta(1+\beta)+1/(1+\beta)\right) \qquad (10)$$

Blasius and a Multifractal

The multifractal term was generally used before 1980 and was coined as turbulence by Frisch (1995). The multifractal properties are notable when a distribution is shown in sets that exhibit the characteristics of being uneven and scattered. This measurement provides the probability that a points falls in a determined set, but with a singular distribution, such that no density exists to describe it, which is when the multifractal formalism becomes relevant. The multifractal properties provide the appropriate context to describe the quality of a particular scaling law.

A grid is made up of cubes $(C_k)_k$ with side $1/R_e$, and $0 < 1/R_e < 1$, $1/R_e$ is called the resolution. On the microscopic level, a measurement μ is considered, with which the probability that a particular point falls in the cube C_k can be estimated, since $\mu(C_k) \approx (1/R_e)^\beta$ under the natural condition that the grid of cubes intersects the support of the measurement. Now all the cubes in which the measurement is of the order β are considered, such that $(1/R_e)^{\beta+\varepsilon} \leq \mu(C_k) < (1/R_e)^\beta$, where $1/R_e$ is small and ε is arbitrary, positive and small. The number of cubes for which the measurement is of the order β is called the features (Falconer, 1990; Riedi and Scheuring, 1997; Meneveau and Sreenivasan, 1991):

$$N_{R_e}(\beta)=\left\{k:\mu(C_k)\geq(1/R_e)^{\beta}\right\} \qquad (11)$$

The scaling law is defined by the particularity that the features $N_{R_e}(\beta)$ are of the order $\theta(\beta)$, and therefore obey a power law when the resolution approaches zero:

$$N_{R_e}(\beta)\approx(1/R_e)^{-\theta(\beta)} \qquad (12)$$

Statement 1. The Blasius exponent represents a multifractal structure.

The properties of a multifractal can be analyzed based on the estimate resulting from the Blasius approximation $\theta(\beta,m=0)=\frac{\beta}{1+\beta}$. It is important to remember that the order of the singularity or local dimension is β, which represents the spatial occupation index or ratio of the fractal dimension to the topological dimension, and the multifractal singularity spectrum, as $\theta(\beta)$. The micro measurement is scaled as $\mu\approx R_e^{-\beta)}$, with resolution $1/R_e$ and R_e is the Reynolds number; the features are $N_{R_e}\approx R_e^{\theta(\beta)}$. It is proven that $\theta(\beta)$ is concave with respect to β, which because of its differentiability can be analyzed using the second derivative, since $\frac{d^2}{d\beta^2}\theta(\beta)\leq 0$. The structure function is the transformed Legendre of the spectrum which, due to optimization, changes the local dimension β to the order of reiteration s or the order of momentum. $\tau(s)$ is always the transformed Legendre of the spectrum, denoted here by $\theta(\beta)$, that is $\sup_{\bar{\beta}}\left(\theta(\bar{\beta})-s\bar{\beta}\right)=\tau(s)$. As long as the spectrum is differentiable and reaches its maximum value the condition of optimality produces $\frac{d}{d\beta}\theta(\beta)=s$. The expression $\theta(\beta)-s\beta=\tau(s)$ o $\frac{\beta}{1+\beta}-s\beta=\tau(s)$ is written and the optimality condition results in $\frac{1}{(1+\beta)^2}=s$, therefore inverting we get $\tau(s)=\left(\sqrt{s}-1\right)^2$. And then the optimality condition becomes $\frac{d}{ds}\tau(s)=-\beta$ which has the property of convexity $\frac{d^2}{ds^2}\tau=\frac{1}{2\left(\sqrt{s}\right)^3}>0$ with the normalization condition $\tau(1)=0$.

What physical magnitude represents the partition function? $S_{R_e}(s)\approx(1/R_e)^{-\tau(s)}$, $(R_e)^{\left(\sqrt{s}-1\right)^2}=(R_e)^{(\theta(\beta))^2}$, and then $S_{R_e}(s)\approx\left(\frac{8B_\beta}{f_\beta}\right)^2$. Therefore, the partition function represents the square of the inverse of the friction factor.

So, using the fractals as a guide, the friction factor is represented by $f_\beta=8B_\beta\left(\frac{1}{R_e}\right)^{\theta}$ or $\theta=\frac{ln\left(\frac{8B_\beta}{f_\beta}\right)}{ln(R_e)}$, where $1/R_e$ is the resolution under the condition $0<1/R_e<1$ and the quantity $\frac{8B_\beta}{f_\beta}$ the number of features. Therefore a multifractal of dimension θ is obtained, which varies with β. Similarly, the drag coefficient $\frac{2B_\beta}{C_{f\beta}}$ corresponds to the number of features of a multifractal of dimension $\theta(\beta)$. Also, the Chezy coefficient satisfies $\frac{C_{h\beta}}{g/\sqrt{B_\beta}}=\sqrt{B_\beta}\sqrt{\frac{8}{f_\beta}}=\left(\frac{1}{R_e}\right)^{-\theta/2}$, where $\frac{C_{h\beta}}{g/\sqrt{B_\beta}}$ corresponds to the number of features of a multifractal of dimension $\theta/2$, and with resolution $1/R_e$:

$$\frac{U}{U_*/\sqrt{B_\beta}}=\left(\frac{1}{R_e}\right)^{-\theta/2} \qquad (13)$$

Karman Schoenherr

The experimental results from the coefficient of drag over a flat surface corresponds to

a first phase with a 1/2 exponent for low Reynolds numbers and a thick or high resolution, followed by a transition region with slight growth in the drag coefficient, a plateau, a decrease approximated by a 1/5 exponent for the mean resolution, and lastly Karman-Schoenherr is represented (Rouse, 1946).

The Blasius Law is generalized and interpreted as a multifractal, taking the inverse of the Reynolds number as the resolution and the singularity spectrum as the Blasius exponent. This law can explain the exponent phases 1/2 and 1/5 described in the above paragraph as well as the plateau in the boundary when the exponent approaches zero $\theta \to 0$. This can be interpreted as fully developed turbulence, where the effect of viscosity can be eliminated by annulling the exponent.

The Karman-Schoenherr result can be rewritten by weakening the features from B/C_f to $Ke^{\frac{1}{A\sqrt{C_f}}}$ with two constants, A and K. As with the Blasius result, the dimension $1-\theta = \dfrac{ln\left(K\left(e^{\frac{1}{A\sqrt{C_f}}}\right)\right)}{ln R_e}$ is now considered, where $\theta = \dfrac{ln\left(B/C_f\right)}{ln R_e}$; if in addition $A = 4.131\log e$ and $KB = 1$, the Karman-Schoenherr, or KS formula is rewritten as in (14):

$$\frac{1}{\sqrt{C_f}} = 4.13 log_{10}\left(R_e C_f\right) \qquad (14)$$

Therefore, the KS formula also corresponds to an approximation that establishes a weak dependency between the Euler and Reynolds numbers, given by $\dfrac{1}{\sqrt{C_f}} \approx A\left(1-\dfrac{1}{B\left(R_e\right)^{1-\theta}}\right)$, with the particularity that the value of the exponent of the Reynolds number will be $1-\theta$ when the turbulence is more intense. This exponent depends on β as well as m, with the restriction $m \geq 1$ required so that $\theta \leq 1$.

Decay is now considered and compared with decay for the Blasius law. When the dimension θ decreases, the decay C_f relative to itself becomes smaller, since if $\theta_2 \leq \theta_1$ then $\left(\dfrac{C'_f}{C_f}\right)_{\theta_2} \leq \left(\dfrac{C'_f}{C_f}\right)_{\theta_1}$. Therefore, if the dimension θ decreases, the speed of decay also decreases. In the case of Karman-Schoenherr, $\dfrac{C'_f}{C_f} = -\left(\dfrac{1}{1+1/\left(2A\sqrt{C_f}\right)}\right)\dfrac{1}{R_e}$, so the dimension $\theta_B \mapsto \theta_{KS}\left(C_f\right) = \dfrac{1}{1+1/\left(2A\sqrt{C_f}\right)}$ is changing, which would be defined implicitly. Since $A\sqrt{C_f} > 0$, then $\theta_{KS} < 1$, which becomes smaller as C_f becomes less, which occurs when the Reynolds number is sufficiently high, and therefore the inclination or slope is smaller. An integer n_{KS} can be introduced as the largest integer larger or equal to $\dfrac{1}{2A\sqrt{C_f}}$, which results in $\theta_n = \dfrac{1}{1+n} \leq \theta_{KS}\left(C_f\right)$. Therefore, eventually, an increase in the Reynolds number will produce a lesser decrease with Karman-Schoenherr than with the Blasius law. For example, in a change interval in which the drag coefficient decreases from 0.010 to 0.001, the number n_{KS} changes from 3 to 9 and θ_{KS} also decreases from 1/4 to 1/10.

Prandtl-Karman Formula

Similar to the above, for the Prandtl-Karman formula, or PK, a multifractal with the resolution $1/R_e$ is assumed, with features proportional to $P\sqrt{f_\beta}e^{\frac{1}{A}\left(\frac{1}{\sqrt{f_\beta}}+D\right)}$ and dimension $1-\theta$. Then with $A = 2\log e$, $D = 0.8$ and $PB = 1$, the Prandtl-Karman formula is:

$$\frac{1}{\sqrt{f}} = 2log_{10}\left(\sqrt{f}R_e\right) - 0.8 \qquad (15)$$

In the Prandtl-Karman case, the relative decay of the drag coefficient is $\frac{C_f'}{C_f} = -\theta_{PK}\frac{1}{R_e}$, where the dimension is $\theta_{PK}\left(C_f\right) = \frac{1}{\frac{1}{2}\left(1+1/\left(2A\sqrt{C_f}\right)\right)}$. Since $A\sqrt{C_f} > 0$, then $\theta_{PK} < 1$, when $\frac{1}{2A\sqrt{C_f}} \geq 1$. Therefore θ_{PK} becomes smaller as C_f decreases, which occurs when the Reynolds number is sufficiently high. Therefore, a smaller inclination or slope is also obtained. An integer n_{PK} is introduced as the largest integer greater or equal to $\frac{1}{2A\sqrt{C_f}}$, which results in $\theta_n = \frac{1}{\frac{1}{2}\left(1+n\right)} \leq \theta_{PK}\left(C_f\right)$. Therefore, eventually, with an increase in the Reynolds number, a smaller decrease is produced with Prandtl-Karman than with the Blasius law. For example, in a change interval where the drag coefficient decreases from 0.010 to 0.001 the n_{PK} number changes from 6 to 8, and θ_{PK} also decreases, from 2/7 to 1/10.

Nikuradse Formula

Now, instead of the features B/C_f from the Blasius Law, these are weakened by $NC_f e^{\frac{1}{A\sqrt{C_f}}}$. The idea is that if C_f decreases, with the increase in the Reynolds number the quantity NC_f decreases, but this increases the intensity of the quantity $e^{\frac{1}{AC_f}}$. Therefore $1-\theta = \frac{ln\left(NC_f e^{\frac{1}{A\sqrt{C_f}}}\right)}{lnR_e}$ and again with the hypothesis $\theta = \frac{ln\left(B/C_f\right)}{lnR_e}$ we get:

$$Aln\left(R_e\right) = \frac{1}{\sqrt{C_f}} \qquad (16)$$

Relative decay is given by $\frac{C_f'}{C_f} = -\theta_N\frac{1}{R_e}$ with $\theta_N\left(C_f\right) = 2A\sqrt{C_f}$. In this case, θ_N can be larger than 1 when $\sqrt{C_f} \geq 1/2A$. Nevertheless, in the opposite case it will be less than one as in the three previous formulas, but the decay property θ_N remains when the Reynolds number increases. For example, in the range 0.01 to 0.001 for the drag coefficient, θ_N decreases from 0.358 to 0.113.

Therefore, the different formulas can be seen as consequences of the fractional Navier-Stokes equation, the reduction of the boundary layer, the multifractal interpretation and readjustment of the features or relative decays, which enables the dimensions to decrease as the Reynolds number increases. Therefore, at least one bi-multifractal can be distinguished such that for relatively high Reynolds numbers the features are proportional to $Ke^{\frac{1}{A\sqrt{C_f}}}$, the resolution $1/R_e$ and the dimensions $1-\theta$. For low Reynolds numbers, the features are inversely proportional to the friction factor $\frac{8B_\beta}{f_\beta}$, the resolution $1/R_e$ and the dimensions θ:

$$N_{R_e} = \begin{cases} \frac{8B_\beta}{f_\beta} & R_e \downarrow \\ Ke^{\frac{1}{A\sqrt{C_f}}} & R_e \uparrow \end{cases} \qquad (17)$$

In particular, the change in representation provides an analytical method to find the critical Reynolds number that indicates the change from a laminar to a turbulent regime, or more specifically, from the viscous sub-layer to the mixed or transition sub-layer.

If the change in regime is defined by the change in the law for the variation in

pressure with velocity, then the change in the dimension from θ = 1 changes to a lower value, θ < 1 (Sommerfeld, 1950). Therefore, relatively low Reynolds numbers correspond to the behavior given by the Blasius law whereas for relatively high numbers the Karman-Schoenherr could be applicable and the Reynolds number corresponding to the transition can be considered as the critical Reynolds. Thus, in the KS formula, θ = 1, it is inferred that $e^{1/A\sqrt{C_f}} = B$ and with $f = 4C_f$ we get $f = 4/(A \ln B)^2$; therefore with the Blasius formula $f = 4/(B/R_e)$, with θ = 1, and therefore the critical Reynolds number that indicates the transition can be calculated with $R_{ec} = B\ (A \ln B)^2$, or the coefficient B can be expressed in terms of A and R_e, using the Lambert W function, and we get $B = \frac{R_{ec}}{4A^2}\frac{1}{W^2\left(\sqrt{R_{ec}}/2A\right)}$. In particular, for $B = 64$ and $A = 4.13 \log e = 4.13/\ln 10$, we get $R_{ec} = 3\,561.1$, which has the same order of magnitude as the experimental value estimated at 2000, and recall that both the value of B as well as A are determined experimentally (Rouse, 1946).

In the case of the Nikuradse formula, $2/A\sqrt{f} = ln\,4B/f$ is combined with $f = 4B/R_e$ and we get $\sqrt{R_e}/A\sqrt{B} = ln\,R_e$, which translates into $\frac{1}{\sqrt{R_e}} ln\left(\frac{1}{\sqrt{R_e}}\right) = -\frac{1}{2A\sqrt{B}}$, whose solution is expressed by the Lambert W function as $R_{ec} = 4A^2BW^2\left(-1/2A\sqrt{B}\right)$. Its numerical evaluation with $B = 64$ and $A = 4.13/\ \ln 10$ produces $R_{ec} = 1.0749$, which is in a different order of magnitude than the value 2000. Similarly, for the KP formula also using the Lambert function an estimate of 0.86709 results. In conclusion, the KS formula is the one that is appropriate for the lower boundary of the mixed or transition sub-layer.

Results and Discussion

Three applications are considered. The first relates to the description of the structure of the turbulent boundary layer. The second corresponds to the interaction between the roughness of sand and wind speed. The third involves the interaction between wind speed and ocean roughness.

Turbulent Layer

These applications can contribute to the description of the structure of a turbulent boundary layer. Four boundary layer regions are known: the wall (composed of two sub-layers), viscous (transition or mixed), the inertial layer (with fully developed turbulence) and the wake.

For smooth or even surfaces, the viscous sub-layer can extend up to five wall units or five characteristic lengths. For the second, the mixed, up to 30 characteristic lengths. The third from 30 to 400 wall units. The rest correspond to the wake. Meanwhile, for rough surfaces, the characteristic length decreases since a downward shift must occur because the roughness increases the loss in momentum (Clifford *et al.*, 1993; Landau and Lifshitz, 1987; Levi, 1989).

The multifractal for relatively low or intermediate Reynolds number is described by $\frac{8B_\beta}{f_\beta} = \left(R_e\right)^\theta$ and the dimensionless velocity is $\frac{U}{U_*} = \sqrt{\frac{8}{f_\beta}}$, therefore $\frac{U}{U_*/\sqrt{B_\beta}} = \left(R_e\right)^{\theta/2}$ is proposed to represent the dimensionless velocity. Now, the height y is made dimensionless with the characteristic or intrinsic length $\frac{\nu_2}{U_*}$, and we get $\frac{U_* y}{\nu_2}$ as the Reynolds number associated with the shear velocity, which is taken as the resolution of the multifractal with dimension β/2. Then $\frac{U}{U_*/\sqrt{B_\beta}} = \left(\frac{U_* y}{\nu_2}\right)^{\theta/2}$, which could be written as

$U_+ = (y_+)^{\theta/2}$. It is observed that $\frac{\partial}{\partial y_+} U_+ = \frac{\theta}{2}(y_+)^{\frac{\theta}{2}-1}$, the approximation of the law for the wall is $\theta \geq 2$. The slope is $\frac{\partial}{\partial y_+} U_+ = \frac{\theta}{2}(y_+)^{\frac{\theta}{2}-1}$, and later increases since $\theta \geq 0$. For the curvature $\frac{\partial^2}{\partial y_+^2} U_+ = \frac{\theta}{2}\left(\frac{\theta}{2}-1\right)(y_+)^{\frac{\theta}{2}-2}$, then the first convex sub-phase is shown if $\theta \geq 2$, and has a parabolic behavior even when $\theta = 4$.

A second concave sub-phase for $\theta \leq 2$ can be represented as a Blasius law $U = y^{1/7}$, which is concave. Thus, the mixed layer can be described from the inflection point to the fully turbulent layer, and then the wake or intermittent sub-layer as well (Barenblatt *et al.*, 1997):

$$\frac{U}{U_*} = \frac{1}{\sqrt{B_\beta}}\left(\frac{U_* y}{\nu_2}\right)^{\frac{\theta}{2}}, \quad \frac{\theta}{2} = \frac{ln\left(\frac{8B_\beta}{f_\beta}\right)}{2ln R_e} \approx \frac{3}{2ln R_e} \qquad (18)$$

For the fully turbulent region the Nikuradse formula is used, from which we get: $\frac{U}{U_*} = \sqrt{\frac{8}{f_\beta}} = \sqrt{\frac{2}{C_f}} = \sqrt{2}A ln R_e$; and $U_+ = \sqrt{2}A ln(y_+)$, which is linear to the logarithm, $\frac{\partial}{\partial y_+} U_+ = \sqrt{2}A\frac{1}{y_+}$N, increasing and $\frac{\partial^2}{\partial y_+^2} U_+ = -\sqrt{2}A\frac{1}{(y_+)^2}$ concave.

For a rough surface, the roughness and the shear velocity are the magnitudes used to make the hydraulic slope J dimensionless, ensuring invariance according to the slope cited when taking $y_r = C_5\frac{U_*^2}{g}$, where U_* is the shear velocity and g is gravity, whose shape is similar to the Charnock roughness (1955) for the ocean surface (Mercado *et al.*, 2012).

Sand and Wind

The transport of sand by wind varies, roughness is described by $y_r = C_5\frac{U_*^2}{g}$ where U_* is shear velocity and g is gravity. The values of C_5 are in the interval [0.02, 0.05] for flow of sand in wind tunnels and up to 0.18 for field experiments (Clifford *et al.*, 1993). Although the formula is the same, the range of values for parameter C_5 is different than the Charnock roughness.

Hurricanes

Again $\frac{U_* y}{\nu_2} = (U_+)^{\frac{2}{\theta}}$. This roughness controls the vertical change in wind speed (Powell *et al.*, 2003), which is similar to the friction factor described by Nikuradse, which is sufficiently justified for the fully rough regime, such that the rippling of the sea surface produced by the wind classifies the sea surface as a rough state and makes it possible to approximate the friction factor using the Nikuradse formula.

In the model by Barenblatt *et al.* (2005), this is explained by the decrease in turbulent energy in the boundary layer of the air fluid over the ocean roughness which is based on the presence of relatively large or heavy drops of water, translating into a decrease in the drag coefficient.

Rivers and Riverbeds

The interaction between flow and the riverbed results in coherent structures in the bed. One of the quantitative characteristics of this is the roughness height, which makes it possible to take $\frac{U_* y}{\nu_2} = (U_+)^{\frac{2}{\theta}}$ as a boundary, or if $\beta \rightarrow$ we have $U_+ \approx \frac{U_* y}{\nu_2} = y_+$.

The value of the roughness height can be made to correspond to the boundary condition for the logarithmic profile of the inertial layer. According to the results from Nikuradse, for an even or smooth surface, the thickness of the viscous sub-layer is 100 times greater than the boundary condition,

while the thickness of the sub-layer of the rough surface is somewhat greater (Rouse, 1946; Landau and Lifshitz, 1987). The roughness height y_r is made dimensionless with the intrinsic length $\frac{\nu_2}{U_*}$, and we get $\frac{U_* y}{\nu_2}$ again as the Reynolds number associated with the shear velocity. Nevertheless, since the shear velocity for a rough surface is somewhat greater than for a smooth surface this Reynolds number increases. The characteristic length is $\frac{\nu_2}{U_*} = \frac{\nu_2}{\sqrt{\tau/\rho}}$, its numerical value with data cited in Clifford *et al*. (1993), A. Kirkbride, chap. 7., is $\frac{1.31\times10^{-6}}{\sqrt{5/(1\,000)}} = 1.8526\times10^{-6}$. The length of the Charnock roughness (1955) is $y_r = C_5\frac{U_*^2}{g}$ $C_5 \in [0.015, 0.035]$, but now with values from the constant in the interval [0.02, 0.05], and even with the value 0.18. The values are found in $\frac{\left(\sqrt{5/1\,000}\right)^2}{9.8}\times\begin{pmatrix}0.02\\0.05\\0.18\end{pmatrix} = \begin{pmatrix}1.0204\times10^{-5}\\2.551\times10^{-5}\\9.1836\times10^{-5}\end{pmatrix}$. The thickness of the viscous layer will be of the order $107\times\begin{pmatrix}1.0204\times10^{-5}\\2.551\times10^{-5}\\9.1836\times10^{-5}\end{pmatrix} = \begin{pmatrix}1.0918\times10^{-3}\\2.7296\times10^{-3}\\9.8265\times10^{-3}\end{pmatrix}$.

The value reported for the thickness of the viscous sub-layer is 2.1 × 10^{-7} *m*. Nevertheless, the known lower boundary for gravel is 2.1 × 10^{-3} *m*. This is value is comparable to the second cited, with a coefficient $C_5 = 0.05$. The comparison between the roughness height and the thickness of the viscous layer $\frac{y_r}{\delta'} \approx \frac{1.0204\times10^{-5}}{10^{-7}} = 102.4$ is within the expected order. Nevertheless, for $\frac{y_r}{\delta'} \approx \frac{9.1836\times10^{-5}}{10^{-3}} \approx \frac{1}{100}$ the viscous sub-layer cannot be developed because the length of the roughness exceeds (greatly) the thickness of this sub-layer.

Conclusions

- By studying the interaction of a fluid with a flat surface based on its boundary layer, it can be stated that the friction force, and therefore the drag coefficient, is characterized by a power of the inverse of the indexed Reynolds number. This power is called the Blasius exponent, which presents the dependency of the two parameters as coupled variables —viscosity and pressure gradient.
- Based on this exponent, an estimate corresponding to a multifractal structure can be established, which is reduced to the known estimate of the viscous sub-layer (1/2) when the spatial occupation index approaches 1.
- The features increase and the multifractal structure is maintained, thereby obtaining the Karman- Schoenherr, Prandtl-Karman and Nikuradse formulas for the friction factor for flat surfaces and smooth and rough tubes.
- Combining the multifractal expression with the dimensionless velocity, and introducing the height of the dimensionless roughness, the four sub-layers of the turbulent boundary layer can be described.
- The bi-multifractal provides an analytical method to find the critical Reynolds number, and only the Karman-Schoenherr formula produces a estimate in accordance with the order of magnitude of the experimental results.

Received: 31/05/2012
Accepted: 03/07/2013

References

BARENBLATT, G., CHORIN, A., and PROSTOKISHIN, V. *A Note Concerning the Lighthill "Sandwich Model" of Tropical Cyclones*. PNAS, 2005, 102 pp.

BARENBLATT, G.I., CHORIN, A.J., and PROSTOKISHIN, V.M. Scaling Laws for Fully Developed Turbulent Flow in Pipes: Discussion of Experimental Data. *Proc. Natl. Acad. Sci. USA. Applied Mathematics*. Vol. 94, 1997, pp. 773-776.

CHARNOCK, H. Wind Stress on a Water Surface. *Q.J.R. Meteorol. Soc*. Vol. 81, 1955, pp 639-640.

CLIFFORD, N.J., FRENCH, J.R., and HARDISTY, J. *Turbulence, Perspectives on Flow and Sediment Transport*. Chichester: Sand Transport Response to Fluctuating Wind Velocity, 1993, pp. 304-334.

FALCONER, K. *Fractal Geometry*. Chichester: John Wiley, 1990, 288 pp.

FRISCH, U. *Turbulence. The Legacy of A.N. Kolmogorov*. Cambridge: Cambridge University Press. ISBN 0-521-45103-5. MR 1428905, 1995, pp. 294.

LANDAU, L.D. and LIFSHITZ, E.M. *Fluid Mechanics*. Oxford: Pergamon Press, 1987, 539 pp.

LEVI, E. *El agua según la ciencia*. México, D.F.: Conacyt, Ed. Castell Mexicana, 1989, pp. XXX.

MENEVEAU, C. and SREENIVASAN, K.R. The Multifractal Nature of Turbulent Energy Dissipation. *J. Fluid Mech*. Vol. 224, 1991, pp. 429-484.

MERCADO, J.R., GUIDO P., SÁNCHEZ-SESMA, J., ÍÑIGUEZ, M., and GONZÁLEZ, A. Analysis of the Blasius' Formula and the Navier-Stokes Fractional Equation. In: Klapp, J., Medina, A., Cros, A., and Vargas, C.A. (editors). *Fluid Dynamics in Physics, Engineering, and Environmental Applications, Environmental Science and Engineering*. Berlin: Springer-Verlag, 2013, pp. 475-480.

MERCADO, J.R. *Ecuación Blasius fraccional*. Artículo publicado en las Memorias bajo la referencia 237. Congreso Latinoamericano de Hidráulica, Punta del Este, Uruguay, 2010.

MERCADO, J.R., GUIDO, P., OJEDA, W., SÁNCHEZ-SESMA, J., and OLVERA, E. Saint-Venant Fractional Equation and Hydraulic Gradient. *Journal of Math., and System Science*. Vol. 2, No. 8, 2012, pp. 494-503.

POWELL, M.D., VICKERY, P.J., and REINHOLD, T.A. Reduced Drag Coefficient for High Wind Speeds in Tropical Cyclones. *Nature*. Vol. 422, No. 20, March, 2003, pp. 279-280.

RIEDI, R.H. and SCHEURING, I. Conditional and Relative Multifractal Spectra. *Fractals*. Vol. 5, No. 1, 1997, pp. 153-168.

ROUSE, H. *Elementary Mechanics of Fluids*. New York: Dover, Publ., 1946, pp. 376.

SOMMERFELD, A. *Mechanics of Deformable Bodies*. New York: Academic Press, 1950, pp. 396.

WHITE, F.M. *Viscous Fluid Flow*. New York: McGraw-Hill, 2006, pp. 629.

Institutional Address of the Authors

Dr. José Roberto Mercado
Dr. Pedro Guido
Dr. Jorge Sánchez-Sesma
Dr. Mauro Íñiguez

Instituto Mexicano de Tecnología del Agua (IMTA)
Paseo Cuauhnáhuac 8532, Colonia Progreso
62550 Jiutepec, Morelos, México
Teléfono: +52 (777) 3293 600
rmercado@tlaloc.imta.mx
pedroguido@tlaloc.imta.mx
jsanchez@tlaloc.imta.mx
mic@tlaloc.imta.mx

Click here to write the autor

The Discharge Coefficient and the Beta Density

• José Roberto Mercado* • Mauro Íñiguez • Pedro Guido •
• Javier Ramírez-Luna • Arturo González-Casillas •
Instituto Mexicano de Tecnología del Agua
*Corresponding Author

Abstract

MERCADO, J.R., ÍÑIGUEZ, M., GUIDO, P., RAMÍREZ-LUNA, J. & GONZÁLEZ-CASILLAS, A. The Discharge Coefficient and the Beta Density. *Water Technology and Sciences* (in Spanish). Vol. V, No. 2, March-April, 2014, pp. 161-175.

Discharge coefficient and turbulence intensity distribution are studied. With Torricelli´s theorem and the approach of probability theory, flow discharge and discharge coefficient equation are derivate, following an unimodal Beta density function, renormalized, with two shape parameters. A multifractals model for the kinetic energy cascade in the turbulence was build, starting from the methods of Pearson and Kolmogorov. For turbulence intensity, with the first method, a Beta distribution was created; with the second, a power law. The multifractals model is completed, recognizing the structure function as a Kummer function. The compatibility between the two models are searched and so the identification of its parameters. It is found that the two shape parameters determine the cascade model resolution. Local dimension and dimension spectra are determine for the two states that produces Torricelli theorem. Redefining the structure function, resolution is defined by the water depth for the regime change. Analogously, different prototypes could be define, which we have call: the four experimentals, three channels, Kolmogorov, Kármán, Taylor, Verhulst (logistic), Cauchy-Manning, and Euclides (golden proportion). We conclude that the discharge coefficient is a renormalized Beta; turbulence intensities distribution is a Beta; Torricelli prototype results representative for the four experimentals and the Euclides, far away from the Gaussian distribution that is contained in von Karman model, meanwhile the Taylor´s model yield the Dirac function.

Keywords: Discharge equations, self-similarity, turbulence models, density function, Kummer function, multifractals, kinetic energy.

Resumen

MERCADO, J.R., ÍÑIGUEZ, M., GUIDO, P., RAMÍREZ-LUNA, J. & GONZÁLEZ-CASILLAS, A. El coeficiente de descarga y la densidad beta. Tecnología y Ciencias del Agua. *Vol. V, núm. 2, marzo-abril de 2014, pp. 161-175.*

Se estudia el coeficiente de descarga y la distribución de intensidades de la turbulencia. Con el teorema de Torricelli y la teoría de probabilidades se formulan el caudal y el coeficiente de descarga, siguiendo una densidad beta unimodal, renormalizada, con dos parámetros de forma. Se había construido un modelo multifractal para la cascada de la energía cinética en la turbulencia, partiendo de los métodos de Pearson y de Kolmogorov. Para la intensidad de la turbulencia, con el primero se creó una distribución beta; para el segundo, una ley en potencia. Se completa el modelo multifractal, reconociendo la función de estructura como la función Kummer. Se busca la compatibilidad entre los dos modelos y la identificación de sus parámetros. Se encuentra que los dos parámetros de forma determinan la resolución del modelo de cascada. Se determina la dimensión local y el espectro de dimensiones para los estados que producen el teorema de Torricelli. Redefiniendo la función de estructura, la resolución queda determinada por el tirante para el cambio de régimen. Análogamente, pueden identificarse diversos prototipos, a los que hemos denominado: cuatro experimentales, tres canales, Kolmogorov, Kármán, Taylor, Verhulst (logística), Cauchy-Manning y Euclides (áurea). Se concluye que el coeficiente de descarga es una beta renormalizada; la distribución de intensidades de la turbulencia es una beta; el prototipo Torricelli resulta representativo para los cuatro experimentales y el de Euclides, quedando lejos de la distribución Gaussiana, que está contenida en el de Kármán; en tanto, el de Taylor produce la delta de Dirac.

***Palabras clave**: ecuaciones de descarga, autoafinidad, modelos de turbulencia, funciones de distribución, función de Kummer, multifractales, energía cinética.*

Introduction

Many investigations exist regarding the determination of the discharge coefficient for free surface flows and several documents propose equations for free and submerged flow. There is also the classical deduction of discharge equations for broad-crested

weirs in rectangular channels (Henderson, 1966). Sotelo (1999) cites different discharge equations for weirs using empirical methods. The difficulty of moving from one regime to another can been seen with these equations, whose empirical coefficients continue to be valid when changes in regimes occur. In general, for control and extraction structures, no discharge equation exists that adequately works for all regimes imposed by the flow dynamics in irrigation channels. For different regimes it is helpful to couple a discharge equation without variance with the flow dynamic in a channel. According to con Baume (1992), invariant discharge equations have rarely been derived under different regimes.

Since discharge equations have been derived using different empirical approaches and a deterministic perspective, these equations contain empirical discharge coefficients that depend on several parameters (Henderson, 1966; Chow, 1959; Swamee *et al*., 1993; Baume, 1992).

Functioning flow regimes in a weir are typically called submerged flow, or submerged discharge, when the flow depends on hydraulic conditions downstream and upstream from the structure. And when it only depends on the hydraulic conditions upstream, it is called free-flow discharge (Ramírez, 1997). Regime changes correspond to the minimum energy state. In addition, flow is classified in two ways according to the structure¾ as free surface flow in a weir and load flow in an orifice structure.

The purpose of this work is to study the discharge coefficient with an experimental and theoretical perspective and its invariance for different weirs and different functioning regimes, which can be done using a statistical approach. Karman studied the correlation function using the Navier- Stokes equation, including up to a double correlation and excluding a triple or higher correlation (correlation among three components), based on the hypothesis that the isotropic turbulence leads to a Kummer equation whose inverse Laplace transform produces a beta distribution (De Karman and Howarth, 1938). We use the symmetries in the Navier-Stokes equation to find some of the properties of the correlation function and complete the description with a generalized Cantor process (Mercado, 2008). With the discharge coefficient described by a beta distribution and a direct Laplace transform, we test the correlation function, which according to the work by Karman reflects the Navier-Stokes equation as an approximation up to a two-fold correlation. In addition, since the symmetries of the Navier-Stokes equation are independent of viscosity, the correlation function can also be used for the fractional Navier-Stokes equation.

This work presents five sections. The first defines the concept of the discharge coefficient, and the method is outlined in the introduction, which is based on the Navier-Stokes equation. The Bernoulli equation and the Torricelli theorem are then discussed. In the second section, this theorem is applied and a covariant is developed for the dimensionless generalized flow. The beta density is identified and the change in specific energy in the section is described, in terms of depth, until obtaining its beta form. The third section studies the relationship between the discharge coefficient and the Kummer function, known as the hypergeometric confluent, and its description as a Fox function. Using the model (Mercado, 2008), the relationship between the shape parameters of the beta and the resolution are determined, to complete the construction of the Torricelli multifractal, identifying the structure function as a Kummer function. In the fourth subsection, the correlation function is studied based on the symmetries in the Navier-Stokes equation, proposing

two water depth values and the correlation function with an exponent, which contains the information pertaining to the characteristic numbers and the Reynolds and Froude numbers. The last subsection describes the prototypes and the numbers that identify them, as well as the corresponding tables containing that information. Euler numbers are studied for different weirs and the values of their parameters are identified. The main conclusions are then stated.

Methods

The discharge coefficient can be considered to be a Euler number expressed in function of the relative characteristic lengths and the Froude and Reynolds numbers. Clarifying that dependency is an essential objective. Euler and Froude numbers are defined by:

$$E^2 = \frac{\frac{1}{2}\rho v^2}{\Delta p}, \quad F_d^2 = \frac{v^2}{gl} \tag{1}$$

respectively, where ρ, v, Δp, g and l are density, velocity, pressure variation, gravity and characteristic length.

Mercado *et al*. (2012) presents a fractional view of the Navier-Stokes equation, whose classical version is considered in the present work. Its vector form is (2):

$$\frac{\partial}{\partial t}\mathbf{v} = \mathbf{v} \times rot\mathbf{v} - \nabla\cdot\left(-\nu\nabla\mathbf{v}\right) - \nabla\left(\frac{1}{2}\mathbf{v}\cdot\mathbf{v} + \frac{p}{\rho} + \phi\right) \tag{2}$$

where $\mathbf{v}$, p, ρ, ν, t and ϕ are velocity, pressure, density, kinematic viscosity, time and scalar potential of the external force, such as gravity. Integrating along a line of flow between any two of its points, and given the steady inviscid flow hypothesis, we get the D. Bernoulli (1738) equation. This is an equation of energy and expresses its constancy. The expression $\left(\frac{1}{2}\mathbf{v}\cdot\mathbf{v} + \frac{p}{\rho} + \phi\right)_{i=1,2}$ is identified as the total load and the total load is determined to be the same throughout each line of current (Rouse, 1946). The application of the D. Bernoullli equation to different states along a line of current can be expressed as variations between any two of these states.

From the historical perspective, the D. Bernoulli equation is a generalization of the Torricelli theorem. This theorem is obtained by considering that the upper free surface of a recipient of water is in the state described by atmospheric pressure, which is constant and revalued as $p = 0$, the piezometric charge by h, and the velocity $v = 0$. For the bottom surface the state is given by the atmospheric pressure $p = 0$, the load by $h = 0$ and the output velocity by v. Therefore, the variation in energy is $\Delta E = \left(0 - \frac{1}{2}v^2\right) + \left((0 + gh) - (0 + 0)\right) = 0$, and then $-\frac{1}{2}v^2 + gh = 0$, followed by $v = \sqrt{2gh}$. This equivalent form of this result corresponds to the velocity gained by a fluid particle in free fall, which starts at rest and descends height h due to the sole action of the gravitational field.

Discharge Coefficient

For the conditions of the Torricelli theorem, with the decrease in depth H-h and the differences in energy throughout the lines of current $\Delta E = \Delta K + \Delta U$, with C as the Coriolis coefficient, we have $\left(\frac{1}{2}C\frac{v^2}{g} - 0\right) + \left(h - H\right) = \Delta E$. For a zero loss in load $\Delta E = 0$, then $H = \frac{1}{2}C\frac{v^2}{g} + h$, such that for a unit width $A = h$, the flow is $Q = Av$ or $Q = h\sqrt{\frac{2g}{C}\left(H - h\right)}$, which can be formulated as:

$$Q = \sqrt{\frac{2g}{C}H^3}\left(\frac{h}{H}\right)\left(1 - \frac{h}{H}\right)^{1/2} \tag{3}$$

Since the Coriolis coefficient is greater than 1, and can approach the value 2, its effect can be interpreted as reinforcing the Froude number, seen as an intensification of inertia or a weakening of gravity. In a dimensionless form, the flow for a broad-crested weir in a rectangular channel is $Q_* = \sqrt{C}\frac{Q}{\sqrt{2gH^3}} = \left(\frac{h}{H}\right)\left(1-\frac{h}{H}\right)^{1/2}$ (Ramírez, 1997). This takes the form $Q_* = \left(\frac{h}{H}\right)^{2-1}\left(1-\frac{h}{H}\right)^{3/2-1}$. To define peak flow, according to the change in the functioning regime, the minimum energy principle is applied to the dimensionless equation and the condition of the regime change is obtained $\left(\frac{h}{H}\right)_{cr} = \frac{1}{1+1/2} = \frac{2}{3}$ (the mode), based on which the following can be defined:

$$Q_* = \frac{\left(\frac{h}{H}\right)^{2-1}\left(1-\frac{h}{H}\right)^{3/2-1}}{\frac{2}{3}\left(\frac{1}{3}\right)^{1/2}}, 0 < \frac{h}{H} \le \left(\frac{h}{H}\right)_{cr} \quad (4)$$

Therefore, the equation must be formulated in terms of dimensionless flow, adopting a form that generalizes the flow derived from the Torricelli theorem $Q_* = \left(\frac{h}{H}\right)^{a-1}\left(1-\frac{h}{H}\right)^{b-1}$. According to probability theory, the factor $(1-h/H)^{b-1}$ is proportional to flow (volume) per unit of time and unit of area and, therefore, represents the probability current density. Therefore, the factor $(h/H)^{a-1}$, as proportional to the area, represents the risk function and the product of the two determine the probability per unit of time, where h/H is the upper limit of the domain of the values that can take on a random variable in the interval $(-\infty, h/H)$. Although it is equally likely to define the first as the flow and the second as the area, since it would be sufficient to change the variable and measure h/H from right to left, and not the opposite, as is usually done. This is equal to the change $h/H \mapsto 1-(h/H)$. Regardless, one represents the flow of energy and the other represents risk.

Ramírez (1997) formulates a discharge coefficient as follows:

$$C_d = \frac{Q_*}{Q_{*\text{máx}}} = \frac{\left(\frac{h}{H}\right)^{a-1}\left(1-\frac{h}{H}\right)^{b-1}}{\left(\frac{h}{H}\right)_{cr}^{a-1}\left(1-\frac{h}{H}\right)_{cr}^{b-1}}, 0 < \frac{h}{H} \le \left(\frac{h}{H}\right)_{cr} \quad (5)$$

Where $Q_{*\text{max}}$ is the value of the free discharge flow and a and b are shape parameters which depend on the characteristic relative lengths and the Froude and Reynolds numbers. If L is the length of the weir crest, it is observed that $Q = C_d L Q_{max}$. The change of regime $(\cdot)_{cr}$ is given by $\left(\frac{h}{H}\right)_{cr} = \frac{a-1}{a+b-2}$, which corresponds to the mode of the density of the beta distribution. Therefore, the discharge coefficient is represented in general from as:

$$C_d = \frac{\left(\frac{h}{H}\right)^{a-1}\left(1-\frac{h}{H}\right)^{b-1}}{\left(\frac{h}{H}\right)_{cr}^{a-1}\left(1-\frac{h}{H}\right)_{cr}^{b-1}}, 0 < \frac{h}{H} \le \left(\frac{h}{H}\right)_{cr} \quad (6)$$

This is a renormalized beta density $\frac{\left(\bar{h}\right)^{a-1}\left(1-\bar{h}\right)^{b-1}}{\left(\bar{h}\right)_{cr}^{a-1}\left(1-\bar{h}\right)_{cr}^{b-1}}$, such that $\bar{h} = \bar{h}_{cr}$ equals 1, and therefore it is normalized by its maximum and not by the area below the curve, as is usually the case with the beta density. This is the most likely distribution function in terms of the minimum energy principle and it is determined by the renormalized beta equation (6), defined until the change in regime.

The section presenting the prototypes shows its application to broad-crested and narrow-crested weirs, gates, etc. The characteristic behavior of the specific energy of a section is known, showing a sub-range given by an increasing function of energy with depth, which is sub-critical or slow flow. The other is a super-critical or rapid flow sub-range, with a decreasing function with depth. The point that both separates and joins them is the critical depth, with minimal energy with respect to depth.

The depth can be made dimensionless with the critical depth, defining h/h_c. With the change in the variable $\bar{h}=\frac{h/h_c}{1+h/h_c}$ the variation interval is shrunk from the real positives up to the unit interval $0\le h/h_c<\infty\mapsto 0\le\bar{h}<1$ and with the change in the sign of the specific energy for the section, $H\mapsto\bar{H}=-H$. The increasing branch of the function represents the supercritical sub-range and the decreasing branch the subcritical sub-range, separated by the maximum point, representing the critical state. Thus, the change in the probability density is $\bar{h}^{a-1}\left(1-\bar{h}\right)^{b-1}\leftrightarrow\left(\frac{h/h_c}{1+h/h_c}\right)^{a-1}\left(\frac{1}{1+h/h_c}\right)^{b+1}$.

Discharge Coefficient and Kummer Function

The representation of the discharge coefficient obtained in the above section allows for another interpretation of it, which is related to the Kummer differential equation. The discharge coefficient is the inverse Laplace transform of the Kummer function, in the sense that it is a solution of the Kummer differential equation. Or vice versa, the Laplace transform of the discharge coefficient is the solution of the Kummer differential equation. A cross-section of the weir is divided into squares and for each square a representative depth value is measured, made dimensionless, and a completely monotonous function is defined, $f\left(h_k\right)=\frac{\left(a\right)_k}{\left(a+b\right)_k}h^{-(k+1)}$. With the generalized Cantor process and the discretization $h_n=\frac{n}{s}$ (understanding s to be the variable with two water depth values, which also must be dimensionless), we get ${}_1F_1(-s;\,a,a+b)$ (Mercado, 2008). Nevertheless ${}_1F_1(z;\,a,a+b)$ is a solution to the ordinary differential equation $zu''+(a+b-z)u'-au=0$, and in addition ${}_1F_1\left(-s;a,a+b\right)=L\left(\frac{h^{a-1}\left(1-h\right)^{b-1}}{B\left(a,b\right)}\right)(s)$, which is renormalized and produces (7):

$$L^{-1}\left(C_d\left(h\right)\right)(s)=\left(\frac{B\left(a,b\right)}{h_{cr}^{a-1}\left(1-h_{cr}\right)^{b-1}}\right){}_1F_1\left(-s;a,a+b\right)\quad(7)$$

Therefore, the function ${}_1F_1(-s;\,a,a+b)$, solution to the Kummer differential equation, uniquely determines the discharge coefficient once the two shape parameters have been established. Nevertheless, according to our hypothesis, a relationship exists between the two parameters, which depends on the spatial occupation index or the Levy stability index.

On the other hand, that function is also represented as a Fox function and, therefore, as the inverse Mellin transform (Metzler andKlafter, 2000):

$$\begin{aligned}&{}_1F_1\left(-s;a,a+b\right)\\&=\frac{\Gamma\left(a+b\right)}{\Gamma\left(a\right)}H_{2,2}^{1,1}\left(s\,\middle|\,\begin{matrix}\left(1-a,1\right)\\\left(0,1\right),\left(1-\left(a+b\right),1\right)\end{matrix}\right)\\&=\frac{\Gamma\left(a+b\right)}{\Gamma\left(a\right)}M^{-1}\left(\chi\left(t\right)\right)(s)\end{aligned}\qquad(8)$$

where $\chi\left(t\right)=\frac{\Gamma\left(-t\right)}{\Gamma\left(a+b+t\right)}\frac{\Gamma\left(a+t\right)}{1}$, and $\Gamma(t)$ is the Euler gamma function.

Torricelli's Multifractal

In Mercado (2008), a multifractal model for turbulent energy cascade is presented based on Pearson and Kolmogorov methods, showing the base of the resolution as q, where $q > 1$. In addition, $f(\bar{\alpha})$, which is the multifractal spectrum, $\bar{\alpha}$ is the local fractal dimension, D_B the maximum of the multifractal spectrum and measurement of the support, ε is the kinetic energy transfer rate, l_0 the length of the dimension of the initial vortices, and n represents the nth stage of the fractalization process. The intensity of the turbulence I_T is understood as the quadratic mean of the module of the variations in velocity (as a substitute for the rms value, which is undetermined for the Levy distribution, with the exception of Gaussiana). This can be described by $\langle|\Delta u|\rangle^2 = (\varepsilon l_0)^{2/3}\left(q^{-n}\right)^{\frac{2}{3}+\frac{4}{3}(D_T - f(\bar{\alpha}))}$ with $u_0 = \varepsilon l_0^{1/3}$, $\beta = \frac{f(\bar{a})}{D_T}$, and D_T is the topological dimension. Thus, (9) is obtained:

$$I_T = \langle|\Delta u|\rangle = (\varepsilon l_0)^{1/3}\left(q^{-n}\right)^{\frac{1}{3}+\frac{2}{3}D_T(1-\beta)} \qquad (9)$$

If the distribution of the intensity of the turbulence is assumed to follow a beta distribution $h^{a-1}(1-h)^{b-1}$, the substitute of the rms value will be calculated, for which the integral $\left(\int_0^\infty h^{2\sigma}B\,dh\right)^{1/2}$ needs to be evaluated. But its square is the Mellin transform $2\sigma + 1$ of the beta density, recalling that in that distribution it is defined as null outside the unitinterval $\int_0^\infty h^{2\sigma}B\,dh = M(B)(2\sigma+1)$. Interms of the Pochhammer symbols, the value of the integral is $\frac{(a)_{2\sigma}}{(a+b)_{2\sigma}} = \frac{\Gamma(a+2\sigma)}{\Gamma(a)}\frac{\Gamma(a+b)}{\Gamma(a+b+2\sigma)}$, which behaves as $\frac{(a)^{2\sigma}}{(a+b)^{2\sigma}}\sqrt{\cdot}\to\left(\frac{a}{a+b}\right)^{\sigma}$ for a very high level of the fractalization process, and therefore the intensity of the turbulence is represented by its mean value raised to the power σ so there is compatibility. The base of the resolution is defined by the two shape parameters $q^{-1} = \frac{a}{a+b} \mapsto \kappa$ and will be denoted below as κ. In addition, the first moment of the beta is the tangent of the Kummer function at zero. Therefore, if a multifractal model is constructed in which the structure function is the Kummer function, it can be said that the inverse Laplace transform of the discharge coefficient provides the structure function. To complete the description of the multifractal model, the local dimension is obtained, $\bar{\alpha} = -\frac{d}{ds}\tau(s) = -\frac{d}{ds}\left({}_1F_1(-s;a,a+b)\right)$ $= \frac{a}{a+b}\,{}_1F_1(-s;a+1,a+b+1)$, and therefore the spectrum is:

$$f(\bar{\alpha}(s)) = {}_1F_1(-s;a,a+b) + s\frac{a}{a+b}\,{}_1F_1(-s;a+1,a+b+1) \qquad (10)$$

In particular, for the Torricelli data, the inverse of the resolution is $\kappa = \frac{2}{7/2} = \frac{4}{7}$ and therefore the power must be $\sigma(\alpha) = \left.\frac{\kappa}{7\kappa-1}\right|_{\kappa=4/7} = \frac{4}{21} = 0.19048 < 1$.

So, based on the Torricelli theorem and the energy cascade, the distribution of the intensities of turbulence can be constructed and renormalized to obtain the discharge coefficient. For which, then, the Laplace transform provides the moment-generating function, which is the Kummer function. But in addition, for each of the prototypes, the corresponding multifractal can be constructed based on shape parameters a and b, and the Kummer function, similarly to what we have referred to as Torricielli. Alternatively, the structure function can be defined as a linear combination of the reiteration

variable s and the shifted Kummer function $g(s) = {}_1F_1(-s; a, a+b) - 1$, thus g(s) satisfies the three conditions $g(0) = g'(\infty) = 0$, $g(\infty) = -1$ and the two coefficients of the linear combination must be determined for each case (Liu *et al.*, 2003).

Correlation Function

The present method is the reciprocal of the above, where the correlation function of the velocity is described and the associated probability distributions can be obtained. In general, the correlation function depends on the distance between the two points and the orientation, but since the Navier-Stokes equation does not change with rotations, the correlation function only depends on the distance between the two points and time (Olver, 1993).

On the other hand, the symmetries of the Navier-Stokes equation include those related to scale, having the following generators: a: $\mathbf{G}_1 = x\partial_x + y\partial_y + z\partial_z + t\partial_t$ y $\mathbf{G}_2 = t\partial_t - u\partial_u - v\partial_v - w\partial_w - 2p\partial_p$, where x,y,z, and t are the usual Cartesian coordinates and time, and u,v,w, and p are the usual coordinates for velocity and pressure. For a channel with axis x in the direction of the dominant current, the lines of the vector field satisfy $\frac{dt}{t} = \frac{du}{-u}$ or $ln\left(\frac{t}{t_0}\right)^{-1} = ln\left(\frac{u}{u_0}\right)$, so $\left(\frac{u}{u_0}\right) = \left(\frac{t}{t_0}\right)^{-1}$.

In general, as was mentioned, the correlation function is a function of distance and time, but because of the scale transformations it will depend on characteristic lengths and Strouhal, Reynolds and Froude numbers. For the Strouhal number, the dependency on velocity is proportional, which due to the friction factor, will depend on the Reynolds and Froude numbers. According to the characteristic lengths, the two possible hydraulic states have to be taken into account —smooth and rough. When the roughness is submerged in the boundary layer and the state is completely smooth, the scale of the turbulence length is given by the intrinsic longitude $l_0 = \frac{\nu}{U_*}$. The rough state is given by the length assigned to the roughness k_s. The local Reynolds numbers are given by $\frac{r}{l_0} = \frac{rU_*}{\nu}$ for the smooth state and $\frac{k_s}{l_0} = \frac{k_s U_*}{\nu}$ for the rough state. Also for the rough state, the Strouhal number is given by $\frac{Ut}{l_1} \mapsto \frac{U\frac{k_s}{U_*}}{k_s} = \frac{U}{U_*}$ and for the smooth state by $\frac{U\frac{l_0}{U_*}}{l_0} = \frac{U}{U_*}$. Thus for the two states that invariant number is given by the proportional velocity, which due to the friction factor includes the dependency of the characteristic lengths and the Reynolds and Froude numbers, a dependency that will end up being transferred to the power of the velocity. Therefore, the correlation function is expressed using the dimensionless variables $\frac{r}{l_0}$ and $\frac{U}{U_*}$, in the inertial sublayer, therefore $f\left(\frac{r}{l_0}, \frac{U}{U_*}\right)$ (De Karman, 1938; Chen, 2006).

Based on the experimental results for the roughness state the velocity can be represented as the power distribution $\frac{u}{u_0} = \left(\frac{y}{y_0}\right)^{\sigma}$, with $0 < \sigma \leq 1$. With the changes in scale, $\frac{u}{u_0} = \left(\frac{t}{t_0}\right)^{-1}$ or raised again:

$$\frac{u}{u_0} = \left(\left(\frac{t}{t_0}\right)^{-1}\right)^{m_\sigma \kappa} \qquad (11)$$

where $m_\sigma > 1$ is the largest integer, such that $\sigma_{exp} = \frac{1}{m_\sigma}$ measured. If in (11), with $0 < \sigma \leq 1$, the

scale is modified, then $\frac{u}{u_0}=\left(\left(\frac{y}{y_0}\right)^{m_\sigma}\right)^{\sigma}=\left(\frac{y}{y_0}\right)^{\sigma m_\sigma}$ and $\frac{u}{u_0}=\frac{l/t}{l_0/t_0}=\frac{l/l_0}{t/t_0}=\left(\frac{t}{t_0}\right)^{-m_\sigma\kappa}$. In which case $\frac{l}{l_0}=\left(\frac{t}{t_0}\right)^{-(m_\sigma\kappa-1)}$, and therefore in equation

(11) $\left(\frac{t}{t_0}\right)^{-m_\sigma\kappa}=\left(\left(\frac{t}{t_0}\right)^{-(m_\sigma\kappa-1)}\right)^{\sigma m_\sigma}$ and then $\sigma=\frac{\kappa}{m_\sigma\kappa-1}<1$.

The process is based on the Taylor and Karman criteria. Let $m(\sigma)=m$, the minimum σ permitted in the sequence (or the maximum σ^{-1}). With the Karman criteria $m\kappa-1=\kappa$, then $\kappa=\frac{1}{m-1}$, for which $\kappa>\frac{1}{m}$, or $m\kappa-1>0$. But since $\kappa=\frac{a}{a+b}$, then $m=2+\frac{b}{a}$. And for Karman, $b=1$; therefore, $a=\frac{1}{m-2}$, where I$m>2$. The values proposed by Karman and also by Taylor are $m_\sigma=5$ (De Karman, 1938). Nevertheless, this normalization leaves out important results reported in Cheng-Lung (1991), though $m>5$ can be chosen so that other exponents of the roughness range are taken into account, such as the Manning. To this end, in the Kolmogorov expression $a=\frac{1}{3}+\frac{2}{3}D_T(1-\beta)$, the term $\frac{2}{3}D_T(1-\beta)$ must approach zero when the turbulence is suppressed and transformed into a mono-fractal, with $\beta(s=0)=\frac{D_B}{D_T}=\frac{D_B}{3}$. Therefore, $\frac{2}{3}D_T(1-\beta)\to\frac{2}{3}D_T\left(1-\frac{D_B}{3}\right)\to 0$, if $D_B\to 3$. Nevertheless, the term $\frac{1}{3}$ is relative, since it can be absorbed by the resolution and substituted by another. Thus, let the Kolmogorov expression be $a=\frac{1}{5}+\frac{6}{5}(1-\beta)$ and the condition $D_B\to 3$, in which case $m-2=5$, and therefore $m=7$ is the lower threshold and the maximum σ^{-1} permitted is 6 or $\sigma=\frac{1}{6}$, which corresponds to the experimental result proposed by Manning and is reported in Cheng-Lung (1991). The relationship between the Kolmogorov energy cascade and the Gaussiana distribution of the velocities is well documented (Chen, 2006). This relationship is maintained because if $\kappa(\alpha)=\frac{1}{6}$ then $\alpha=2.0$. Reciprocally, if $b=1$ to mimic the factor $(1-h)^{b-1}$, as is implicitly done in the cascade model, and with the inverse of the resolution being $\kappa=\frac{1}{6}$, then $\kappa=\frac{a}{a+b}=\frac{a}{a+1}=\frac{1}{6}$, and $a=\frac{1}{5}$ as proposed in the cascade model. On the other hand, if the maximum accepted for the inverse of the exponent of velocity is $\sigma^{-1}_{\text{máx}}=m$ and according to the Karman criterion $m\kappa-1=\kappa$, then $\kappa=\frac{1}{m-1}$, therefore $m=2+\frac{b}{a}$, and if $m=7$, Taylor and Karman criterion, then $\frac{b}{a}\le 5$, and then $0<\frac{b}{a}\le 5$. Therefore, from $\sigma=\frac{a}{m_\sigma\kappa-1}\kappa<1$, it can be inferred that $\frac{2}{\kappa}=m-\sigma^{-1}$, and since $\kappa=\frac{a}{a+b}$ then $\frac{b}{a}=m-\sigma^{-1}-1$. Therefore, given the Karman -Taylor criterion, $\frac{b}{a}=6-\sigma^{-1}$.

For example, if the exponent related to Lacey $\kappa=\frac{1}{4}$ is examined, it results in $6-4=2$; which satisfies it. On the other hand, with the Blasius exponent $\kappa=\frac{1}{7}$ we have $6-7=-1\notin(0,5)$, which does not satisfy this classification criteria. The Manning exponent $\kappa=\frac{1}{6}$ produces $6-6=0\in\overline{(0,5)}$ and satisfies it in the limit. In conclusion, from the physical perspective the fraction $\frac{1}{7}$ could be considered that which separates the exponents between the smooth and rough ranges. For the experimental interval reported by Agroskin $\frac{1}{2}\le\sigma\le\frac{4}{7}$ for the endpoint $\frac{1}{2}$, we have 6 – 2 =

$4 \in (0,5)$, and for $\frac{4}{7}$ we get $6-\frac{7}{4}=\frac{17}{4}\in(0,5)$. Therefore, the entire Agroskin interval is included and can be added to the rough range (Agroskin, 1980). Finally, the proposal for the correlation function is $f\left(\frac{r}{l_0},\frac{U}{U_*}\right)=f(s)$, where $s\approx\frac{U/U_*}{r/l_0}=\left(\left(\frac{r}{l_0}\right)^2\right)^{\sigma(\alpha)}$ and $\sigma(\alpha)=\frac{\kappa(\alpha)}{7\kappa(\alpha)-1}$, normalized as follows: if $\alpha\to 2^-$, we get $\sigma(\alpha)\to 1$, and for Taylor $\kappa\to\frac{1}{7}\Leftrightarrow\sigma(\alpha)\to\infty$, which symbolizes a Dirac delta.

Results and Discussion

This section describes the prototypes, the numbers that identify them and presents the tables related to this information. In addition, Euler numbers are studied for different weirs and the values of their parameters are identified.

Prototypes

Next, various prototypes are considered from very different sources.

For these, if the shape parameters are provided, the inverse of the resolution is obtained, given by $\kappa=\frac{a}{a+b}$. Next, the exponent of the velocity can be found, $\sigma(\alpha)=\frac{\kappa}{7\kappa-1}\le 1$. Then the Levy index is found solving for α in the equation $\kappa(\alpha)=\left(\frac{2}{3}-\frac{1}{6}\alpha\right)\frac{\Gamma\left(\frac{3}{\alpha}\right)}{\Gamma\left(\frac{1}{\alpha}\right)}$.

Finally, the spatial occupation index is obtained with $\beta(\alpha,D_T)=1-\frac{1}{\alpha D_T}$ (Ramírez *et al.*, 2009).

The authors have called the main prototype "Torricelli" because it is obtained from the Torricelli theorem. This prototype is based on the states of the Torricelli theorem and corresponds to the broad-crested weir. The exponents that define the beta density are determined by $a = 2$, $b = 3/2$, then $\kappa=\frac{a}{a+b}=\frac{4}{7}$. Next, $\sigma(\alpha)=\frac{\kappa}{7\kappa-1}=\frac{4}{21}<1$ and $\left(\frac{h}{H}\right)_{cr}=\frac{a-1}{a+b-2}=\frac{2}{3}$. From the Mercado reference (2008), reformulated as $\kappa(\alpha)=\left(\frac{2}{3}-\frac{1}{6}\alpha\right)\frac{\Gamma\left(\frac{3}{\alpha}\right)}{\Gamma\left(\frac{1}{\alpha}\right)}=\frac{4}{7}$, it is determined that $\alpha = 1.1843$, where also $\beta(\alpha,D_T)=1-\frac{1}{\alpha D_T}=0.71854$, $D_T=3$, $DT=3$.

For a broad-crested weir, and according to the Torricelli theorem, if the total load upstream is H, to later reduce it to h, the flow velocity is determined as a point particle in free fall, exclusively subject to the action of gravity. Therefore $v = (2g(H - h))^{1/2}$ and for the flow in a unit width, we have $Q=\left(2gH^3\right)^{1/2}\left(\frac{h}{H}\right)^{2-1}\left(1-\frac{h}{H}\right)^{3/2-1}$ which in dimensionless form is $Q_*=\left(\frac{h}{H}\right)^{2-1}\left(1-\frac{h}{H}\right)^{3/2-1}$. In particular, over the crest of the weir we have $\frac{Q_*}{Q_{*\text{máx}}}=\frac{\left(\frac{h}{H}\right)^{2-1}\left(1-\frac{h}{H}\right)^{3/2-1}}{\left(\frac{h}{H}\right)_{cr}^{2-1}\left(1-\frac{h}{H}\right)_{cr}^{3/2-1}}$ with $\left(\frac{h}{H}\right)_{cr}=\frac{2-1}{2+3/2-2}=\frac{2}{3}$.

Table 1. Characteristics of vertedores

Weir	Broad-crested and sharp edge	Triangular	Rounded broad-crested	Broad crested and rounded edge	Creager
(a-1)	1.9	1.3	1	0.8	0.618
(b-1)	0.5	0.5	0.5	0.5	0.5
$(h/H)_c$	0.792	0.722	0.667	0.615	0.553

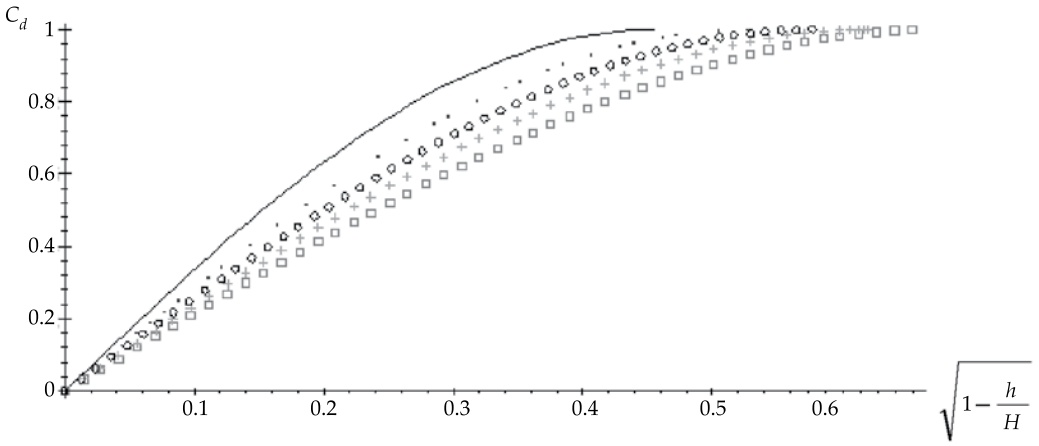

Figure 1. Discharge coefficients.

Table 2. Parameters for the four experiments.

	Parameters	Solution	Levy Index	Occupation index	Exponent
1	$a = 2.9, b = \frac{3}{2}$	$\kappa = 0.65909$	$\alpha = 1.1303$	$\beta(\alpha,3) = 0.70509$	$\sigma(\alpha) = 0.18239$
2	$a = 2.3, b = \frac{3}{2}$	$\kappa = 0.60526$	$\alpha = 1.1618$	$\beta(\alpha,3) = 0.71309$	$\sigma(\alpha) = 0.18699$
3	$a = 1.8, b = \frac{3}{2}$	$\kappa = 0.54545$	$\alpha = 1.2031$	$\beta(\alpha,3) = 0.72294$	$\sigma(\alpha) = 0.19355$
4	$a = 1.618, b = \frac{3}{2}$	$\kappa = 0.51892$	$\alpha = 1.224$	$\beta(\alpha,3) = 0.72767$	$\sigma(\alpha) = 0.19713$

The inverse of the resolution is $\kappa = \frac{4}{7}$, and therefore coincides with the same value as those of Torricelli. Therefore, the broad-crested weir is represented by the case that has been called Torricelli.

The first group includes the prototypes developed primarily from the experimental examples. Some are located inside the weirs and others are used as channels. The parameters of the weirs were determined for the four experiments —broad-crested sharp edge and rounded, rounded edge, triangular and Creager (Table 1), according to equation (6), and the values of the variables for the change in the hydraulic functioning is added. The experimental data are presented in Ramírez (1997).

Figure 1 shows the graphs of the discharge coefficient on the vertical axis and according to equation (6). $(1 - h/H)^{1/2}$ is represented on the horizontal axis, and the graphs are valid up to the regime change. They are read from left to right according to the columns in Table 1. The top solid line corresponds to the first column or broad-crested sharp edged weir and the bottom line of small squares represents the Creager weir. Table 2 shows the values of the shape parameters for the unimodal beta function, the resolution, the Levy index and spatial occupation index and

Table 3. Parameters for the three channels.

	Resolution	Levy Index	Occupation Index	Exponent
Brannif	0.17845	1.934	0.82765	0.71624
San Nicolás	0.19413	1.856	0.8204	0.54089
Coria	0.22114	1.743	0.80876	0.40355

Cuadro 4. Results in Agroskin (1980).

	Exponent	Resolution	Levy Index	Occupation Index
I	1/2	1/5	1.8293	0.81778
D	4/7	4/21	1.8733	0.82206

the velocity exponent. Column 4 is omitted for the rounded broad-crested weir.

The data for the three channels are presented in Table 3 (Ramírez *et al*., 2009).

Table 4 shows the experimental results cited in Agroskin (1980), which are located in the rough range.

The results from Lacey (1930), cited by Cheng-Lung (1991) were generated experimentally, resulting in one of the highest powers in the rough range. From the velocity power we have $\sigma = \frac{\kappa}{7\kappa - 1} = \frac{1}{4}$, which produces $\kappa = \frac{1}{3}$, then $\alpha = 1.45$, and therefore $\beta(\alpha,3) = 0.77011$.

Submerged Orifice

For the case of flow through an orifice, C_c is the coefficient of the narrowing of the stream soon after the outlet and is given by the quotient of the area of the stream divided by the area of the outlet orifice (Rouse, 1946):

$$E_u = \sqrt{\frac{\frac{1}{2}\rho v^2}{\Delta p}} = \left(\frac{C_d}{C_c}\right) = \left(1 - \left(C_c \frac{\bar{b}}{B}\right)^2\right)^{\frac{1}{2}-1} \qquad (12)$$

Therefore, with the values of the random variable related to the depth and expressed by $h = \left(C_c \frac{\bar{b}}{B}\right)^2$, we have $E_u = h^{1-1}(1-h)^{\frac{1}{2}-1}$.

Consequently, the inverse of the resolution is $\kappa(\alpha) = \frac{1}{1+\frac{1}{2}} = \frac{2}{3}$, then $\alpha = 1.1262$ with $\sigma(\alpha) = \frac{2}{11}$ and $\beta = (\alpha,3) = 0.70402$.

Horizontal submerged orifice

For discharge through a horizontal submerged orifice, the borders ratio $\frac{\bar{b}}{B} \mapsto \frac{\bar{b}}{2\bar{h}}$ must be substituted, where $2\bar{h}$ is relatively large with respect to $\bar{b}$, that is, the substitution of the width $B \mapsto 2\bar{h}$, then (Rouse, 1946):

$$E_u = \sqrt{\frac{\frac{1}{2}\rho v^2}{\Delta p}} = \left(1 - \left(C_c \frac{\bar{b}}{2\bar{h}}\right)^2\right)^{\frac{1}{2}-1} \qquad (13)$$

Therefore, with $h = \left(C_c \frac{\bar{b}}{2\bar{h}}\right)^2$ we find $E_u = h^{1-1}(1-h)^{\frac{1}{2}-1}$ and, consequently, the values of the prior case repeat.

In the above result, if $\bar{h} \mapsto \frac{b}{2}$, it becomes a narrow-crested weir, and with $2\bar{h} \mapsto h$ the flow is $q = \frac{2}{3} C_c \sqrt{2g} \left(\left(\frac{v_0^2}{2g} + h\right)^{3/2} - \left(\frac{v_0^2}{2g}\right)^{3/2}\right)$ (Rouse, 1946), shifting $q_d = q + \frac{2}{3} C_c \sqrt{2g} \left(\frac{v_0^2}{2g}\right)^{3/2}$

we get $q_d = \frac{2}{3} C_c \frac{v_0^2}{\sqrt{2g}} \left(1+\tilde{h}\right)^{3/2}$, $\tilde{h} = \frac{h/h_0}{F_{d0}^2}$, $F_{d0}^2 = \frac{v_0^2}{h_0}$, where low F_d numbers represent large gravitation deflections:

$$E_u = \frac{C_d}{C_c} = \left(1+\tilde{h}\right)^{3/2} \qquad (14)$$

Therefore, $\kappa = \frac{5/2}{5/2+1} = \frac{5}{7}$ and $\sigma = \frac{5/7}{7(5/7)-1} = \frac{5}{28}$, located in the rough range and near the Manning range. In addition, we get $\alpha = 1.1022$ and $\beta(\alpha,3) = 0.69757$.

Recalling that for this weir the piezometric pressure decreases from the point located at the base to the top edges of the weir with height w, where it becomes zero, accompanied by an increase in the velocity load. This edge represents an abrupt change, a break in the slope of the piezometric pressure. Later in the stream, another increase in the pressure depth occurs up to its maximum value inside the stream, followed by a decrease until the outer upper surface of the stream, which returns to zero along with a decrease in the velocity load, followed by an increase up to the outer surface of the top edge of the stream (Rouse, 1946).

Gate

This prototype is different than that for the horizontal submerged orifice since the pressure outside the stream of the former is atmospheric pressure, whereas the gate has a hydrostatic distribution. With the continuity and the D. Bernoulli equations we have $q = \frac{C_c}{\sqrt{1+\left(C_c \frac{\bar{b}}{B}\right)}} \sqrt{2gh}$ (Rouse, 1946) then:

$$E_u = \frac{C_d}{C_c} = \left(1+\tilde{h}\right)^{\frac{1}{2}-1}, \quad \tilde{h} = C_c \frac{\bar{b}}{B} \qquad (15)$$

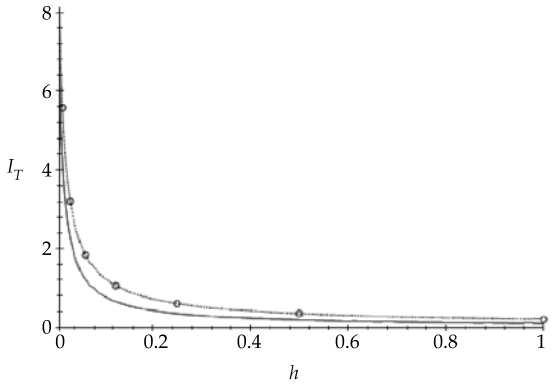

Figure 2. Cascade model.

Then $\kappa = \frac{1/2}{1/2+1} = \frac{1}{3}$ and Lacey is reproduced. The depth of pressure and the velocity behave similarly to the prior weir, with the change in height w from the opening $\bar{b}$.

The second group of prototypes correspond to theory (some based on shape parameters), others to the Levy index and others the power.

Kolmogorov

This prototype corresponds to the energy cascade I_T (equation (9)), producing a power model which corresponds to a beta density $B = h^{a-1}(1-h)^{b-1}$, with $b = 1$, and the Levy index $\alpha = 2$ assigned to the Gaussiana distribution. Therefore $\kappa(\alpha) = \frac{1}{6}$ and from $\kappa = \frac{a}{a+b} = \frac{1}{6}$ we get $a = \frac{1}{5}$. In addition, $\beta(2,3) = \frac{5}{6}$. Therefore, the exponent of the velocity is $\sigma(\alpha) = \frac{\kappa}{7\kappa-1} = 1$. The depth for the regime change is $\left(\frac{h}{H}\right)_{cr} = \frac{a-1}{a+b-2} = 1$. The cascade model is shown in Figure 2. The vertical axis represents the intensity of the turbulence I_T and on the horizontal axis $h = q^{-n}$. The

dotted curve is $\frac{1}{5}h^{\frac{1}{5}-1}$, since the coefficient of the beta function $B(a,b)=\frac{\Gamma(a)\Gamma(b)}{\Gamma(a+b)}$ is $u_0=(\varepsilon l_0)^{1/3}=\frac{\Gamma\left(\frac{1}{5}+1\right)}{\Gamma\left(\frac{1}{5}\right)\Gamma(1)}=\frac{1}{5}$. On this dotted curve, the fractalization process can be seen by the line represented by small circles, from right to left, in which the resolution series is taken to be $h\mapsto\left(\frac{1}{2}\right)^n$ according to the original Kolmogorov proposal, although $h\mapsto\left(\frac{1}{6}\right)^n$ can also be taken, for example. The solid line represents $\frac{1}{B(1/10)}h^{\frac{1}{10}-1}$ and serves as a reference for the change in the shape parameter $a=\frac{1}{5}$ up to $a=\frac{1}{10}$, as well as for the change in the resolution series from $h\mapsto\left(\frac{1}{2}\right)^n$ to $h\mapsto\left(\frac{1}{10}\right)^n$.

Karman´s prototype results from the correlation function by taking the inverse of the resolution as $\kappa=\frac{1}{6}$, therefore $b = 5a$ in the distribution. The power of the velocity $\sigma(\alpha)=1$, therefore it agrees with Kolmogorov. The quotient of the gamma functions can be expressed as a Pochhammer function $\frac{\Gamma\left(\frac{3}{\alpha}\right)}{\Gamma\left(\frac{1}{\alpha}\right)}=\left(\frac{1}{\alpha}\right)_{\left(\frac{3}{\alpha}-\frac{1}{\alpha}\right)}$ and this is reduced to the identity if $\frac{3}{\alpha}-\frac{1}{\alpha}=1$, which is equal to $\alpha = 2$, and then $\left(\frac{2}{3}-\frac{1}{6}\alpha\right)\frac{\Gamma\left(\frac{3}{\alpha}\right)}{\Gamma\left(\frac{1}{\alpha}\right)}=\left(\frac{1}{\alpha}\right)_{(1)}=\frac{1}{\alpha}$ and $\kappa=\frac{1}{3}\cdot\frac{1}{2}=\frac{1}{6}$. Inversely, near the flow regime $\alpha \to 2$, therefore $\kappa\to\frac{1}{3}\left(\frac{1}{2}\right)_{\left(\frac{3}{2}-\frac{1}{2}\right)}=\frac{1}{3}\cdot\frac{1}{2}=\frac{1}{6}$, which reflects the effect of viscosity.

Taylor

The Taylor model is based on the correlation function, where $\kappa(\alpha)=\frac{1}{7}$ is the inverse of the resolution. From that we have $\alpha = 2.1563$, which is not possible, because $\alpha \leq 2$ and $\sigma \to \infty$.

Manning

If the Levy index is $\alpha=1$, a Cauchy distribution exists. Later the inverse of the resolution is $\kappa(1)=1$, then $\frac{a}{a+b}=1$ and $b\to 0$. The power of the velocity is $\sigma=\frac{1}{6}$ and the spatial occupation index is $\beta(1,3)=\frac{2}{3}$. Similarly, according to the results from Manning, the power of the velocity is $\sigma=\frac{1}{6}$, which produces $\kappa(\alpha) = 1$, then we have $\alpha = 1$ and $\beta(1,3)=\frac{2}{3}$. This exponent is usually located in the rough range.

Euclid

This stems from state-of-the-art and can be described according to the distribution. Recalling the definition of the Euclid's golden ratio, one segment can be divided in

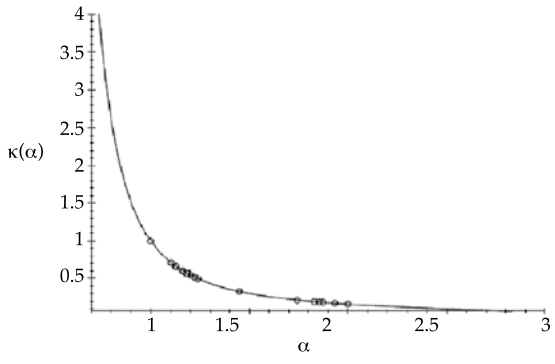

Figure 3. Inverse of the solution κ(α).

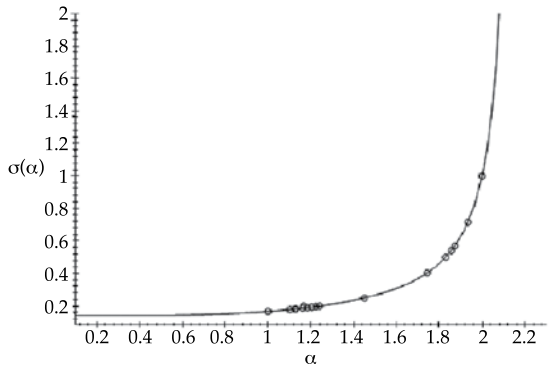

Figure 4. The exponent of the velocity σ(α).

two longitudinal sub-segments. The larger is the proportional measurement between the total and the least $\frac{a+b}{a}=\frac{a}{b}$, which results in the solution $a=\left(\frac{1}{2}-\frac{1}{2}\sqrt{5}\right)b$, or approximating, it is derived by dividing a segment into five parts and highlighting three versus the remaining two. Then, the inverse of the resolution is $\kappa=\frac{2}{1+\sqrt{5}}=0.61803\approx\frac{3}{5}$. For the Levy index, α = .1652. The power of the velocity is $\sigma(\alpha)=0.1858\approx\frac{1}{5}$. The spatial occupation index is β = 0.71393.

Logistical

This can be based on either distribution or correlation functions. When using the distribution, if $a=2=b$, then the inverse of the resolution is $\kappa=\frac{1}{2}$ and for the Levy index α = 1.2401. The power of the velocity is $\sigma(\alpha)=\frac{1}{5}$ and β(α,3) = 0.7312. Figure 3 shows the graph of the inverse of the resolution with respect to the stability index, where the relative locations can be seen and their positions in relation to the two ends noted by α = 1 and α = 2. The horizontal axis represents the values of the Levy index, α. The solid line describes the graph of $\kappa(\alpha)=\left(\frac{2}{3}-\frac{1}{6}\alpha\right)\frac{\Gamma\left(\frac{3}{\alpha}\right)}{\Gamma\left(\frac{1}{\alpha}\right)}$. The Taylor case stands out, which is located out the interval shown. The four experimentals as well as Euclid's golden ratio are grouped around the Torricelli position and therefore are similar to the broad-crested weir. All of these are located closer to 1 in Figure 3, thereby denoting its turbulent behavior.

The power of the velocity is shown in Figure 4, which indicates the endpoints represented by α = 1, the Cauchy case $\mapsto\sigma(\alpha)=\frac{2}{11}>\frac{1}{7}$ and α = 2, the Gauss case $\mapsto\sigma(\alpha)=1$. In particular, for Taylor, the power diverges at infinity, therefore it is outside the interval $0<\sigma\leq 1$, as already mentioned. The solid line represents $\sigma(\alpha)=\frac{\kappa(\alpha)}{7\kappa(\alpha)-1}$. The Levy index is represented on the horizontal axis.

Equation (6) makes it possible to generally represent the discharge equations for different weirs. The equation is assumed to be valid for other weirs, which is illustrated by finding the shape of the Euler numbers for the submerged orifice, the horizontal submerged orifice and the gate. The data for the parameters of the three channels show the validity of the relationships presented in the first paragraph of the Prototypes section. The parameters corresponding to the Torricelli theoretical model are representative of the four experimentals, which are also clearly located in the turbulent regime (Figure 3), while, conversely, the Kolmogorov theoretical model is more representative of the three channels, which are closer to the flow regime.

Conclusions

1. The discharge coefficient adopts the covariant form derived from the Torricelli theorem or the broad-crested weir.
2. The distribution of the intensity of the turbulence is beta.
3. The correlation function is the Kummer function.
4. The exponents of the velocity in the rough range extend from the Manning to the Kolmogorov or Karman.
5. Based on an approximation, discharge coefficient (6) reflects the Navier-Stokes equations.

Received: 08/12/2009
Accepted: 26/06/2013

References

AGROSKIN, I.I. *Hidráulica*. Tomo I. Torralba, V.J. (traductor). La Habana: Ministerio de Educación Superior, Instituto Superior de Ciencias Agropecuarias de La Habana, 1980, 521 pp.

BAUME, J.P. *Cemagref Mtp. Modélisation des ouvrages de type : déversoir, vanne, orifice, dans les modèles d'hydraulique à surface libre*. Rapport interne. Montpellier: Cemagref, 1992.

CHEN, W. A Speculative Study of 2/3-order Fraccional Laplacian Modeling of Turbulence: Some Thoughts and Conjectures. *Chaos*. Vol. 16, 2006, 023126.

CHENG-LUNG, C. Unified Theory on Power Laws for Flow Resistance. *J. of Hydraulic. Eng*. Vol. 137, No. 12, 1991, pp. 1696-1699.

CHOW, V.T. *Open-channels hydraulics*. New York: McGraw-Hill Book Company, 1959, pp. 33-37.

DE KÁRMÁN, T. and HOWARTH, L. On the Statitical Theory of Isotrópic Turbulence. *Proc. Roy. Soc. A*, 164, London, 1938, pp. 192-215.

HENDERSON, P.J. *Open Channel Flow*. New York: MacMillan Publishing Co., 1966.

LIU, S.D., LIU, S.K., FU, Z.T., REN, K., and GUO, Y. *The Most Intensive Fluctuation in Chaotic Time Series and Relativity Principle*. *Chaos, Solitons and Fractals*. Vol. 15, 2003, pp. 627-630.

MERCADO, J.R. La ecuación de Navier-Stokes y multifractales. *Revista de Matemática: Teoría y Aplicaciones*. Vol. 15, núm. 1, 2008, pp. 49-72.

MERCADO, J.R., GUIDO, P., OJEDA, W., SÁNCHEZ, J., and OLVERA, E. Saint-Venant Fractional Equation and Hydraulic Gradient. *Journal of Math. and System Science*. Vol. 2, No. 8, 2012, pp. 494-503.

METZLER, R., and KLAFTER, J. *The Random Walk's Guide to Anomalous Diffusion: A Fractional Dynamics Approach*. *Phys. Rep*. Vol. 339, 2000, pp. 1-77.

OLVER, P.J. *Applications Lie Groups to Differential Equations*. New York: Springer-Verlag, 1993, 513 pp.

RAMÍREZ, J. *Modélisation des ouvrages frontaux et lateraux dans les canaux d´irrigation*. These de Doctorat. Paris: L'École Nationale du Génie Rural, des Eaux et des Forêts (ENGREF), 1997.

RAMÍREZ, J., MERCADO, J.R., PEREA, H., OLVERA, E., RUIZ, V., and ÍÑIGUEZ, M. Reynolds Equations and Water Distribution in Irrigation Canals. *Hydraulic Engineering in México*. Vol. XXIV, No. 3, July-September, 2009, pp. 121-130.

ROUSE, H. *Elementary Mechanics of Fluids*. New York: Dover, Publ., 1946, pp. 376.

SOTELO, G. *Hidráulica General*. Volumen I. México, D.F.: Editorial Limusa, 1999, pp. 126.

SWAMEE, P.K., PATHAK, S.K., and ALI, M.S. Analysis of Rectangular Sluice Gate. *Journal of Irrigation and Drainage Engineering*. Volume 119, Issue 6, November, 1993, pp. 1026-1035.

Institutional Address of the Authors

Dr. José Roberto Mercado
Dr. Mauro Íñiguez
Dr. Pedro Guido
Dr. Javier Ramírez Luna
Dr. Arturo González Casillas

Instituto Mexicano de Tecnología del Agua (IMTA)
Paseo Cuauhnáhuac 8532, Colonia Progreso
62550 Jiutepec, Morelos, México
Teléfono: +52 (777) 3293 600
rmercado@tlaloc.imta.mx
mic@tlaloc.imta.mx
pedroguido@tlaloc.imta.mx
jramirez@tlaloc.imta.mx
arturo_gonzalez@tlaloc.imta.mx

Click here to write the autor

Experimental greenhouse tomato crop located at the Humboldt University of Berlin, Germany.

Photo: Raquel Salazar Moreno.

Technical Note

Water Use Efficiency in Controlled Agriculture

• Raquel Salazar-Moreno* • Abraham Rojano-Aguilar •
• Irineo Lorenzo López-Cruz •
Universidad Autónoma Chapingo, México
*Corresponding Author

Abstract

SALAZAR-MORENO, R., ROJANO-AGUILAR, A. & LÓPEZ-CRUZ, I.L. Water Use Efficiency in Controlled Agriculture. *Water Technology and Sciences* (in Spanish). Vol. V, No. 2, March-April, 2014, pp. 175-181.

Many regions in the world have reached water usage limits, resulting in surface and groundwater overexploitation and its negative environmental impacts. In countries that depend on groundwater for irrigation, such as Mexico, excess water extraction has depleted the water table to an alarming level. Also, 77% of available water in Mexico is used in agriculture, for this reason it is important to increase water use efficiency in this sector. This brief review is about modern agricultural techniques to increase water use efficiency, such as environmental control, closed hydroponic systems and semiclosed greenhouses.

Keywords: Environmental control, hydroponics, closed systems.

Resumen

SALAZAR-MORENO, R., ROJANO-AGUILAR, A. & LÓPEZ-CRUZ, I.L. La eficiencia en el uso del agua en la agricultura controlada. Tecnología y Ciencias del Agua. *Vol. V, núm. 2, marzo-abril de 2014, pp. 175-181.*

Muchas regiones del mundo han alcanzado el límite de aprovechamiento del agua, lo que las ha llevado a sobreexplotar los recursos hidráulicos superficiales y subterráneos, creando un impacto negativo en el ambiente. En los países en los que se depende del agua subterránea para el riego, como es el caso de México, el exceso de extracción está provocando que los niveles freáticos de agua dulce estén descendiendo a un ritmo muy alarmante. Aunado a lo anterior, el 77% del agua concesionada en México es utilizada en la agricultura; por tal razón, es urgente incrementar la eficiencia en el uso del agua en este sector. Este trabajo representa una breve revisión sobre las técnicas modernas de producción para incrementar la eficiencia del uso del agua, tales como el control ambiental en los invernaderos, sistemas hidropónicos de circuito semicerrado y cerrado, y los invernaderos semicerrados.

Palabras clave: *control ambiental, hidroponía, sistemas cerrados.*

Introduction

The efficient use of water in farming is one of the key factors in ensuring food production and work for Mexican families in the agricultural sector (Álvarez, 2011). "Efficiency in the use of water (EUW)" or "water productivity" (WP) refers to the existing relationship between the biomass of a crop and the unit of water it uses at a particular moment. When using water for a purely productive and economic activity, biomass is substituted by yield in kg of product per m^3 of water used (Fernández and Camacho, 2005).

$$Ef\ \text{Water} = \frac{\text{Production}\ (\text{kg})}{\text{Water used}\ (\text{m}^3)} \qquad (1)$$

Water productivity is an important indicator in areas with essential water resources and enables calculating the economic value of

irrigation water that can be maximized. Therefore, its use will be a requirement by policies related to food production.

Table 1 presents the liters of water used per kilogram of tomato (the inverse of water use efficiency) for different types of technologies¾ ranging from various types of open fields to high-technology greenhouses (Stanghellini, 2010).

To produce a unit of mass, a high-technology greenhouse can use up to 75 times less water than an open field with low technology. The challenge is how to decrease the use of water from 300 to 4 l/kg.

Next, some modern techniques developed over recent years to increase the efficient use of water by controlled agriculture are discussed and the authors' personal experiences are included.

Converting from Open Field to Greenhouse Production Systems

A greenhouse is a production system that can increase the efficient use of water by creating a microclimate that improves plant photosynthesis, reduces excessive evapotranspiration and increases yield.

The need for water for greenhouse farming is less than for open field farming. In regions with high solar radiation, a plastic greenhouse can reduce the amount of water used for farming by 30% (FAO, 1991). While in Almeria, Spain water usage has been reduced 40 to 50% due to the decrease in solar radiation and wind (Fernández and Camacho, 2005). In addition, Antón *et al.* (2003) report a reduction in evapotranspiration in greenhouses of 70% as compared to open air fields.

In general, greenhouse production increases water use efficiency for three reasons:

1. It reduces evapotranspiration (less radiation, more humidity).
2. It increases yield due to better control of infestation and disease.
3. It uses advanced irrigation techniques (droplet irrigation and reuse of water).

Fernandez and Camacho (2005) report that tomato production in Almeria, Spain requires 27 m^3/ton (37 kg/ m^3) of water compared to open field production which uses 50 to 60 m^3/ ton (16-20 kg/ m^3). These figures demonstrate a marked increase in productivity when converting from open fields to greenhouse production. For example, in countries such as the United States, irrigation regions with limited water resources have converted from large-scale farming to horticulture (Eumedia, 2007).

Different types of technology and conditions in greenhouse production result in large ranges in water use efficiency, as shown

Table 1. Liters of water used per kilogram of tomato produced.

Method of Production	Country	l/kg
Open field, generally	Various	100-300
Open field, droplet irrigation	Israel	60
Open Field	Alemria, Spain	50-60
Unheated Plastic Greenhouses	Israel, Spain	30-40
Glass greenhouses with advanced controls and heat, CO_2 enrichment	Holland	22
As above with hydroponic system	Holland	15
As above with closed hydroponic system	Holland	4

Table 2. Comparison of water use efficiency in greenhouses in the Mediterranean and Holland.

Product	Mediterranean Countries (kg/m³)	Holland (kg/m³)
Tomato	21.8	58.2
Cucumber	14	28
Bell Pepper	30.3	77

(Pardossi *et al.*, 2004).

in Table 2 which compares Mediterranean countries and Holland (Pardossi *et al.*, 2004). Holland has been able to increase water productivity by 36.4 kg/m³ just for tomatoes.

Control of Environmental Conditions

High water use efficiency can be attained by greenhouses through the optimal control of the environmental parameters inside them, as well as by cultural practices. Both factors generate high yields and less water usage. Climate control techniques affect water productivity (WP) by changing the evaporative demand and commercial production. Water use efficiency can be monitored by the transpiration of plants and the exchange of O_2 and CO_2.

In Holland, Stanghellini (2003) report WP values of 45 kg/m³ for tomatoes in a heated greenhouse with carbon enrichment (Figure 1). The more advanced the technology inside a greenhouse the higher the water use efficiency.

In Europe, water productivity increases when comparing protected crops such as strawberries (3.5 € m³) to horticulture greenhouse crops (13.5 € m³). The high productivities in the use of water in regions such as Almeria, for example, are explained by the combination of high yields and low water consumption.

Monitoring the principal climatological and physiological variables is essential to understanding behavior patterns and processes inside greenhouses, and can thus

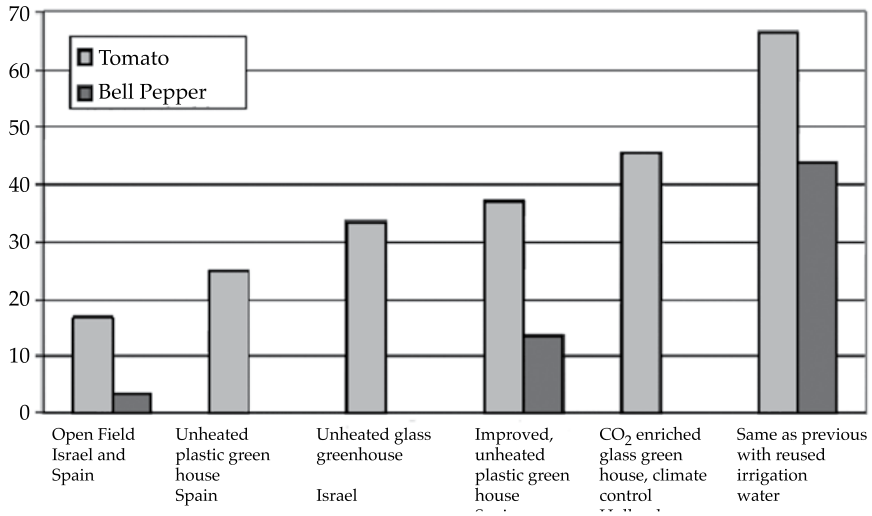

Figure 1. Kilograms of fresh product per m³ of water applied (Stanghellini, 2010).

increase water use efficiency. Over recent years, a large variety of low-cost sensors have become available on the market. It is possible to begin by monitoring the most important variables, such as temperature and relative humidity, and with that information predict the environmental conditions in the greenhouse during the different seasons of the year and make decisions about the most suitable controls.

Sophisticated measurement equipment also exists (Figure 2) that can perform continuous measurements of parameters to describe the functional state of the plants and their environmental conditions. The complexity of a system can be increased to the point of being able to monitor all the variables that affect the growth of plants.

Semi-closed and Closed Hydroponic Recycling Systems

Investigations related to water management in greenhouses have focused on identifying the best technology to meet the water requirements of the plants. The results have led to the development of techniques such as hydroponics, a production system in which the plants' roots are irrigated with a mixture of essential nutrients dissolved in water. In addition, instead of soil an inert or sterile material is used as a substrate, or even the nutritive solution itself.

Water conservation is one of the advantages of hydroponics, since the techniques recycle water containing nutrients. These techniques have been adapted to diverse situations, such as open air and greenhouse farming. The only limitations in hydroponics is the source of potable water and nutrients. In some advanced systems, such as in northern Europe and Israel, water is applied through automated computerized systems to decrease water loss.

In an open hydroponic system, the excess nutritive solution is continually drained, making the use of water and nutrients inefficient. The use of water for tomatoes in greenhouses with hydroponics can range from 1.51 (in experimental conditions) to 24 l/kg of tomato. On the other hand, in Sweden, the average loss in nutrients with open hydroponic systems is 850 kg of N, 80 kg of P and 850 kg of K per hectare (Bergstrand, 2010). Therefore, more efficient water usage techniques have been introduced that reuse the wastewater or slurry water.

In a semi-closed hydroponic system (Figure 3a), the excessive nutritive solution is collected in a tank or flows directly to the mixer tank, which is continually refilling to

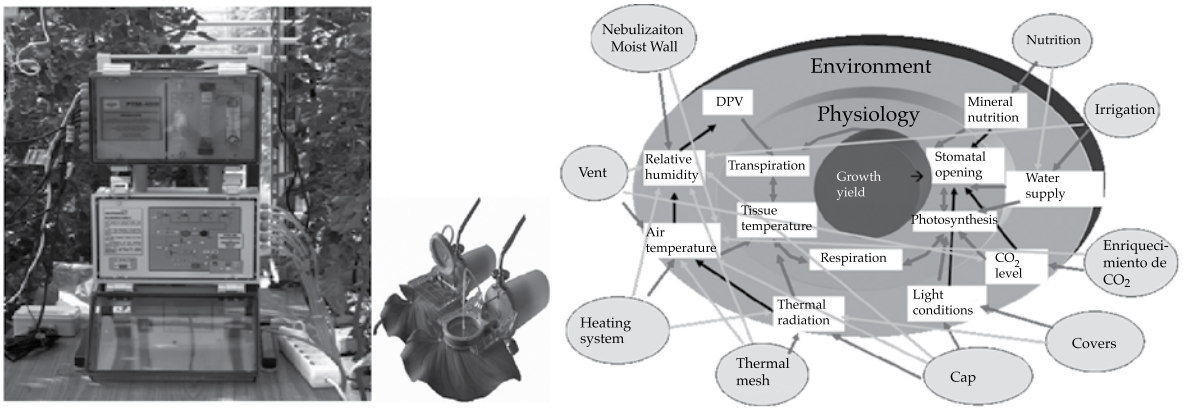

Figure 2. Complexity in control of growth (Schmidt, 2004).

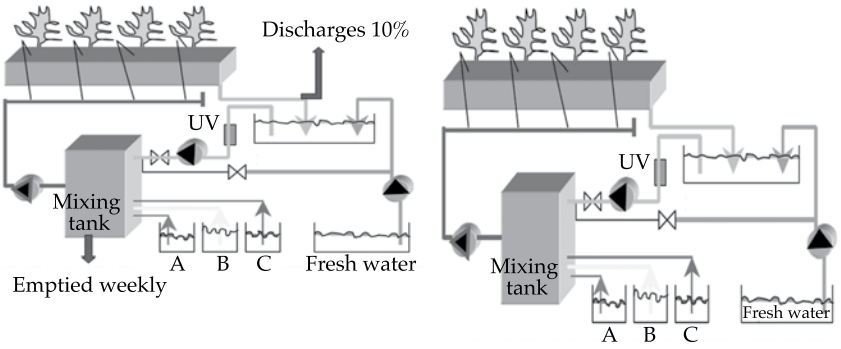

Figure 3. Semi-closed (left) and closed (right) hydroponic system (Polycarpou *et al.*, 2005).

reuse the water for the plants. To avoid an imbalance in the solution, 10% of this water is continuously discharged, and the water in the mixing tank is emptied at determined periods and filled again with fresh water and nutrients. Therefore this is called a semi-closed system.

The above system can be improved considerably by reducing the discharge and thereby conserving water and nutrients, which is known as closed hydroponic system (Figure 3b). The nutritive solution is recycled and the tank is continuously filled with water and the solutions A, B and C.

The above system is based on the fact that plants always use the nutrients they need and let the rest pass through. Therefore, the first wastewater produced is sent to a laboratory for analysis and the amount of each nutrient taken up by the plant is determined. The solution is readjusted accordingly by introducing more or less of each nutrient. The laboratory analysis is performed every week at first, then when the system is well established every one or two months. Using the analysis and the recommendations, the producer adjusts the concentrations of the nutrients A, B and C and the new fertigation formula is programmed into the computer. After a while, the tank will contain the exact nutritional solution required by the plants. This system uses 10 to 50% less water than an open system. The problems created by closed systems include the possible accumulation of Na and Cl, resulting in salinization of the nutritive solution (Bergstrand, 2010). To make the above system even more efficient, in places where there is enough rainfall the water can be collected on the roof of the greenhouse and stored in a tank. This is clean water with low sodium contents, which can be used in closed hydroponic system. In the design and operation of these closed systems, the use of substrates available in the region should be considered to keep costs low.

Semi-closed and Closed Greenhouses

Semi-closed and closed greenhouses are another type of technology that can increase the efficiency of water and energy usage. There is no ventilation in a closed greenhouse and a semi-closed greenhouse has ventilation which is used only when temperatures are very high. Plants can change solar radiation to latent heat (production of water vapor resulting from transpiration of the plants). This decreases the temperature of the leaf and, therefore, the foliage serves as a surface

Figure 4. Condensation system in a semi-closed greenhouse, University of Humboldt, Berlin.

to cool the air in the greenhouse and to absorb heat. Condensation occurs when the temperature inside the greenhouse or of one of its interior surfaces is lower than the dew point temperature (temperature at which water vapor condenses), which decreases humidity while also releasing energy. If the vapor condenses in a heat exchanger, the latent heat again converts into sensible heat. In Holland, it is estimated that 40 to 50% of water used in farming can condense.

The Horticulture Institute of the University of Humboldt, Berlin has a semi-closed greenhouse with corrugated steel pipes on the roof through which cold water circulates. The water from transpiration of plants condenses and is collected in a channel which goes directly to a tank, as seen in Figure 4. This water is reused for fertigation. With the above system, as much as 1.45 l/m^2 was collected per day from July to September 2010.

Conclusions

To produce twice the amount food that will be required in the next 30 years, agriculture will have to increase water use efficiency considerably. In Mexico —a country with low water availability— it is indispensable to not only improve water use efficiency in agriculture but also promote its sustainable use.

Hydroponics is a technology that has resulted in better quality crops with higher yields, as well as more efficient use of water, fertilizers, chemicals and pesticides. This type of system has developed into hydroponic closed recirculation systems which reduce the need for water for crops near evapotranspiration levels. Other types of modern systems include closed and semi-closed greenhouses, which have provided good results in Europe and the United States in terms of conservation of water and energy. In these types of systems, water transpired by plants can be recovered through condensation and used as irrigation water. Combing the above systems, the use of water would be reduced to half or less of the amount transpired by the plants and is thus a promising an innovative option for countries with water scarcity. Nevertheless, it is important to remember that modern technologies that provide large water savings are generally also expensive.

Received: 04/11/2011
Accepted: 25/06/2013

References

ÁLVAREZ, R. Conagua da Impulso al Desarrollo del Campo [en línea]. *Planeta Azul*, 2011. Disponible en *World Wide Web*: http://www.planetaazul.com.mx/site/.

ANTÓN, A., MONTERO, J.I. y MUÑOZ, P. *Necesidades de agua del cultivo de tomate en invernadero. Comparación con el cultivo al aire libre*. IRTA, proyecto de investigación INIA SC00 080 C2. Barcelona, España, 2003. Disponible en *World Wide Web*: http://biblioteca.idict.villaclara.cu/UserFiles/File/CI%20Cultivos%20en%20invernaderos/24.pdf.

BERGSTRAND, K.J. *Approaches for Mitigating the Environmental Impact of Greenhouse Horticulture*. Doctoral Thesis. Acta Universitatis Agriculturae. Swedish University of Agricultural Sciences, Sueciae, 2010.

EUMEDIA. Productividad del agua en cultivos bajo invernadero en la costa mediterránea. *Revista Vida Rural*. Núm. 259, 2007. En *dossier*. Disponible en *World Wide Web*: http://www.vidarural.es/articulos-productividad-del-agua-cultivos-bajo-invernadero-costa-mediterranea/1/458.html.

FERNÁNDEZ, R.E. y CAMACHO, F. *Eficiencia en el uso del agua. Revista Viveros. Universidad de Almería en España, 2005, pp. 86-89*.

FAO. *Protected Cultivation in the Mediterranean Climate. Plant Protection Paper* [on line]. FAO, 1991, pp. 90-317. *World Wide Web*: http://www.scielo.cl/scielo.php?pid=S0365-28072001000400010&script=sci_arttext

PARDOSSI, A., TOGNONI, F., and INCROCCI, L. Mediterranean Greenhouse Technology, the World of Horticulture. *Chronica Horticultural*. Vol. 44, No. 2, 2004.

POLYCARPOU, P., CHIMONIDOU, D., and PAPADOPOULOS, I. Improving Water Use Efficiency in Greenhouse Cultivation in Cyprus. *Options Méditerranéenes*. Series B, No. 57, 2005.

SCHMIDT, U. *Presentación en Curso Internacional de Invernaderos*, Guadalajara, Jalisco, México, 2004.

STANGHELLINI, C. El agua de riego su uso eficiencia y economía. En: Fernández, M., Lorenzo, P., Cuadrado, I. *Mejoría de la eficiencia del agua en cultivos protegidos*. Curso Superior de Especialización. Junta de Andalucía. ISBN 84-88246-21-8, 2003, pp. 25-33.

STANGHELLINI, C. Water Use Efficiency in Tomatos. Practical Hidroponics & Greenhouses. 2010, pp. 52-59.

Institutional Address of the Authors

Dra. Raquel Salazar Moreno
Dr. Abraham Rojano Aguilar
Dr. Irineo Lorenzo López Cruz

Centro de Investigación en Economía y Matemáticas Aplicadas (CIEMA)
Universidad Autónoma Chapingo
Kilómetro 38.5 de la carretera México-Texcoco
56230 Estado de México, México
Teléfono: +52 (5959 9521 500
raquels60@hotmail.com
abrojano@hotmail.com
loci61@hotmail.com

Click here to write the autor

Sunset Tzentzénguaro, Patzcuaro, Michoacan, Mexico.

Photo: Luis E. Rendón.

Discussion

Technical notes and technical articles are open to discussion according to the following guidelines:

- The discussion will be written in the third person.
- The writer of the discussion shall use the term "commentator" when referring to oneself and the term "author" when referring to the one responsible for the technical note or article.
- The discussion shall be sent within 12 months of the last day of the quarter in which the a technical article or note was published.
- The length of the discussion may be extended by written request from the commentator.
- The discussion is to be presented according to the Guide for Collaborators published in this journal (omitting data referring to the length and abstract). In addition, the bibliographical citation of the technical notes or articles to which the discussion refers shall be included.
- The maximum length of the discussion is 4 journal pages (approximately 10 cuartillas, including figures and tables).
- The figures and tables presented by the commentator shall be progressively marked with Roman numbers and when citing those generated by the author the original numeration should be respected.
- The editors will suppress data that does not pertain to the subject of the discussion.
- The discussion will be rejected if it contains topics addressed by other sources, promotes personal interests, is carelessly prepared, raises controversy involving already established facts, is purely speculative or falls outside the purpose of the journal.
- The discussion will be published along with commentaries from the author or authors to which it refers.
- The discussion will be directed by the editor in chief.

Africam Safari Zoo, Puebla, Mexico.

Photo: María Irleth Gama Serrano.

Contributor's guide

The journal ***Tecnología y Ciencias del Agua*** invites specialists to collaborate with original technical articles or notes **related to water, that result from investigations and provide original contributions,** based on the disciplines of hydrology, hydraulics, water management, water and energy, water quality, and physical, biological and chemical sciences as well as political and social sciences, among others, according to the guidelines stated below.

PREPARATION OF THE ARTICLE

FORMAT

Font: Palatino throughout the entire document (body of text, tables and figures).

Font Size: Use 8, 9, 10 and 20 points, according to the following table:

8 points (Palatino)	9 points (Palatino)
• Tables. • Figures. • Acknowledgements.	• Name of authors. • Institution of authors. • Abstract. • *Abstract* and *keywords*. • Institutional address of the authors.
10 points (Palatino)	**20 points capital letters (Palatino)**
• Body of the text. • Title of the work in English.	• Title of the work in Spanish

Line Spacing: double-spaced.

Page Numbers: all pages shall be numbered.

Length

***Technical article*:** **30 pages** (numbered), including figures and tables.
***Technical note*:** **10 pages** (numbered), including figures and tables.

CONTENS

Contens

The article shall present significant contributions to scientific and technological knowledge pertaining to the specialty. It shall be based on finished works or those that have completed a development cycle. It shall show results from a series of experiences over 1 year or more of investigations and be supported by an adequate bibliographical review. **The basic structure of the text shall contain an introduction, the development and the conclusions.** The classic layout is preferable: abstract, introduction, methodology, results, discussion, conclusion and references.

Title

The title, written in Spanish and English, shall be informative and not exceed 12 words.

Abstract

The abstract, **written in Spanish and English**, shall be concise and provide a broad overview of the investigation (objective, method, results and conclusions) without exceeding 250 words.

Key Words

Eight words or key phrases (maximum) shall be provided **in Spanish and English** that facilitate the identification of the information.

Footnotes

Not admitted. The information is to be incorporated into the text.

Acknowledgements

To be included after the text and before the references.

Tables

- One page for each table.
- A list of all the tables cited shall be presented after the references.

Figures

- One page for each figure.
- All the names of the figures shall be included after the tables.
- They should be high-resolution (300 dpi).

Note: When the article is approved by the publication, the author shall send each figure in high-resolution (300 dpi) in JPG format.

References

- The entire bibliography must be referenced in the main body of the text.
- In the case of addressing scientific and technological topics that are common domain, works that denote the knowledge of the authors about the *state-of-art* shall be cited.
- Avoid self-citations to the extent possible
- International ISO-690 and ISO-690-2 standards are to be used as a basis. References to the literature used to develop the document are to be cited with last name of the author and date in parenthesis, for example, (Black, 1989), and ordered alphabetically by last name, ensuring that they are complete.

Examples of references:

Books

Last name of the author and initials in capital letters. Title of the book in capital/small letters and italics. Responsibilities related with the editorial work such as translating and editing. Edition (beginning with the second edition). Publication (city, publisher and year).

Example:

LEVI, E. *Tratado elemental de hidráulica*. Second edition. Jiutepec, Mexico: Instituto Mexicano de Tecnología del Agua, 1996, 303 pp.

When there are two or more authors:

GARCÍA R., E., GONZÁLEZ, R., MARTÍNEZ, P., ATHALA, J. and PAZ-SOLDÁN, G.A. *Guía de aplicación de los métodos de cálculo de caudales de reserva ecológicos en México*. Colección Manuales. Mexico: Convenio SGP-IMTA, 1999, 190 pp.

Titles of works or articles should not be translated. In the event a version exists in Spanish, it shall be indicated at the end of the original reference after the period.

Journals

Last name of the author and initials in capital letters. Title of the article in regular font, capital and small letters. Responsibilities related with the editorial work, such as translating and editing. Publication in capital/small letters and italics. Edition (volume, number, year, pages).

Example:

DÖLING, O.R. y VARAS, E. Operación de sistemas de recursos de agua multipropósito usando un modelo de simulación de procesos. *Ingeniería hidráulica en México*. Vol. XV, no. 2, May-August 2000, pp. 5-18.

Electronic Documents

Last name of the author and initials in capital letters. Title in capital/small letters and italics. Type of media in brackets. Responsibilities related with the editorial work, such as translating and editing (optional). Edition. City of publication. Publisher. Date of publication. Date of last review or update. Date in which the search was conducted in brackets. Series (optional). Notes (optional). Availability and access. Email.

Example:

CARROLL, L. *Alice's adventures in Wonderland* [online]. Textinfo ed. 2.1. Dortmund, Germany. WindSpiel, November 1994 [cited February 10, 1995]. Available in *World Wide Web*: http://www.germany.eu.net/books/carroll/alice.html.

Language

Spanish or English

Separation of numbers and use of decimal points

In *Tecnología y Ciencias del Agua*, the separation between thousands is denoted with a blank space. A decimal point is used to separate whole numbers from fractions. In this regard, refer to *Diccionario panhispánico de dudas*, edited by the Real Academia Española and the Asociación de Academias de la Lengua Española, in 2005, with respect to numeric expressions: "**the Anglo-Saxon use of the period is accepted, normal in some Hispano-American countries…: $\pi = 3.1416$.".**

Delivery of Article

Send the article in *Word* with the name of the authors and institutional address to revista.tyca@gmail.com, with copy to Elizabeth Peña Montiel, elipena@tlaloc.imta.mx.

General Information

The review process will begin once the material is received, during which it is possible that the manuscript could be rejected. If the text is suitable for review, having fulfilled the Editorial Policy and the Editorial Committee having determined so, it will proceed to the review stage.

Depending on the review process, the text may be accepted without changes, with minor changes, with extensive changes or rejected.

Once a work is published, the main author has the right to two journals and ten offprints free of charge.
In there are any questions, please write to Helena Rivas López, hrivas@tlaloc.imta.mx or Elizabeth Peña Montiel, elipena@tlaloc.imta.mx

Editorial Policy

Mission

Disseminate scientific and technical knowledge and advances related to water through the publication of previously unpublished articles and technical notes that provide original contributions.

Our Principles

- Impartiality
- Objectivity
- Honesty

Our Values

- Knowledge
- Experience
- Thematic expertise

Contents

Interdisciplinary, composed of previously unpublished articles and technical notes related to water, that result from research and provide original scientific and technological contributions or innovations, developed based on the fields of knowledge of diverse disciplines.

Topics Covered

Interdisciplinary, related to water, with priority topics in the following knowledge areas:

- Water and energy
- Water quality
- Physical, biological and chemical sciences
- Hydro-agricultural sciences
- Political and social sciences
- Scientific and technological development and innovation
- Water management
- Hydrology
- Hydraulics

Type of Contributions

Technical article: scientific document that addresses and communicates, for the first time, results from a successful investigation or innovation, whose contributions provide and increase current knowledge about the topic of water.

Technical note: text that addresses advances in the field of hydraulic engineering and professional practices in the field of water, while not necessarily making an original contribution in every case it must be a previously unpublished work.

Some of the articles submitted to the review process can result in being published as notes and vice versa. This will occur through a proposal and process of mutual agreement between the authors and the editor responsible for the topic. The article and the note have nearly the same structure (abstract, introduction, methodology, results, discussion, conclusion, references).

Review Process

The journal is governed by a rigorous review process which establishes that each article be analyzed separately by three reviewers who recommend its acceptance, acceptance with minor changes, acceptance with extensive changes, rejection or acceptance as a technical note with the required changes.

At least one of three reviewers will be sought from a foreign institution.

The reviewers may not belong to the same institution as the authors proposing the article for publication.

When the decisions are opposing or inconsistent, the involvement of other reviewers or the members of the Editorial Committee may be requested.

On occasion, the approval of an article will be decided by two reviewers in addition to the opinion of the editor of the corresponding topic or, the editor in chief.

A rejected article will not be accepted for a new review process.

The review process will be performed in such a way that neither the authors nor the reviewers know the names of the other party.

The review process is performed by high-level specialists and experts who are national and internationally renowned in their professional fields and have the ability to reliably evaluate, in a timely manner, the quality as well as the originality of contributions, in addition to the degree of scientific and technological innovation in the topic under which it is submitted for possible publication.

This participation is considered a professional contribution and will be performed as a courtesy.

The reviews have a "Guide for the Reviewer" provided by the journal's Editorial Department.

Final Ruling

The ruling resulting from the review process is not subject to appeal.

Authors

Works are published from authors of any nationality who present their contributions in Spanish; nevertheless, we all accept works in Spanish or English.

Responsibility of the Authors

Submitting a proposal for the publication of an article commits the author not to simultaneously submit it for consideration by other publications. In the event an article has been submitted to another media for eventual publication, the author agrees to do so with the knowledge of the Editorial Department, which will suspend the review process and inform the Editorial Committee of the decision by the authors.

Collaborators whose articles have been accepted will formally cede the copyright to ***Tecnología y Ciencias del Agua***.

The authors are responsible for the contents of the articles.

The author is responsible for the quality of the Spanish used. If the writing is deficient the work will be rejected. ***Water Technology and Sciences*** will only be responsible for the editorial management.

The author commits to making the changes indicated by the editor of the topic in the time frame establish by the editor. In the event these indications are not met, the article will be removed from the review process and be classified as rejected.

The author shall be attentive to resolving the questions and proposals presented by the editors and the editorial coordinator.

Each author shall approve the final printed proofs of their texts.

It is suggested that authors consult the "Guide for Collaborators."

Readers

Academics, investigators, specialists and professionals interested in the analysis, investigation and search for knowledge and solutions to problems related to water.

Reception of Articles

The reception of articles and notes is ongoing.

Time period

Bimonthly, appearing in the second month of the period.

Subscription and Distribution

The journal is distributed through paid and courtesy subscriptions.

Open Access

Water Technology and Sciences, previously ***Hydraulic Engineering in Mexico***, provides a digital version of all the material published since 1985.

Special editions and issues

Water Technology and Sciences will publish special numbers independently or in collaboration with other journals, professional associations or editorial houses with renowned prestige and related to water resources.

In addition, it will publish articles by invitation, acknowledging the professional advances of prominent investigators.

In both cases, the quality of the technical continents and scientific contributions will be reviewed.

Water Technology and Sciences is registered in the following national and international indices and abstracts:

• Thomson Reuters Science Citation Index® (ISI) • Expanded Thomson Reuters Research Alert® (ISI) • Índice de revistas mexicanas de investigación científica y tecnológica del Consejo Nacional de Ciencia y Tecnología (Conacyt) (2013-2018) • Sistema de Información Científica Redalyc (Red de Revistas Científicas de América Latina y El Caribe, España y Portugal), Universidad Autónoma del Estado de México • EBSCO (Fuente Académica Premier NISC; Geosystems, como Marine, Oceanographic and Freshwater Resources) • ProQuest (Cambridge Scientific Abstracts) • Elsevier (Fluid Abstracts: Process Engineering; Fluid Abstracts: Civil Engineering) • CAB Abstracts, CAB International • Latindex (Sistema Regional de Información en Línea para Revistas Científicas de América Latina, el Caribe, España y Portugal), Universidad Nacional Autónoma de México • Periódica (Índice de Revistas Latinoamericanas en Ciencias), Universidad Nacional Autónoma de México • Catálogo Hela (Hemeroteca Latinoamericana), Universidad Nacional Autónoma de México • Actualidad Iberoamericana, CIT-III, Instituto Iberoamericano de Información en Ciencia y Tecnología.

Other Sources

The journal can also be found archived in Google scholar.